

## INFORMATION TO USERS

This manuscript has been reproduced from the microfilm master. UMI films the text directly from the original or copy submitted. Thus, some thesis and dissertation copies are in typewriter face, while others may be from any type of computer printer.

**The quality of this reproduction is dependent upon the quality of the copy submitted.** Broken or indistinct print, colored or poor quality illustrations and photographs, print bleedthrough, substandard margins, and improper alignment can adversely affect reproduction.

In the unlikely event that the author did not send UMI a complete manuscript and there are missing pages, these will be noted. Also, if unauthorized copyright material had to be removed, a note will indicate the deletion.

Oversize materials (e.g., maps, drawings, charts) are reproduced by sectioning the original, beginning at the upper left-hand corner and continuing from left to right in equal sections with small overlaps. Each original is also photographed in one exposure and is included in reduced form at the back of the book.

Photographs included in the original manuscript have been reproduced xerographically in this copy. Higher quality 6" x 9" black and white photographic prints are available for any photographs or illustrations appearing in this copy for an additional charge. Contact UMI directly to order.

# UMI

A Bell & Howell Information Company  
300 North Zeeb Road, Ann Arbor MI 48106-1346 USA  
313/761-4700 800/521-0600



**University of Alberta**

A Comparison of the ICEJAM and RIVJAM Ice Jam Profile Models.

by

Daniel J. Healy



A thesis submitted to the Faculty of Graduate Studies and Research in partial fulfillment of the requirements for the degree of **Master of Science**

in

**Water Resources Engineering**

Department of Civil and Environmental Engineering

Edmonton, Alberta

Fall 1997



National Library  
of Canada

Acquisitions and  
Bibliographic Services

395 Wellington Street  
Ottawa ON K1A 0N4  
Canada

Bibliothèque nationale  
du Canada

Acquisitions et  
services bibliographiques

395, rue Wellington  
Ottawa ON K1A 0N4  
Canada

*Your file* *Votre référence*

*Our file* *Notre référence*

The author has granted a non-exclusive licence allowing the National Library of Canada to reproduce, loan, distribute or sell copies of this thesis in microform, paper or electronic formats.

The author retains ownership of the copyright in this thesis. Neither the thesis nor substantial extracts from it may be printed or otherwise reproduced without the author's permission.

L'auteur a accordé une licence non exclusive permettant à la Bibliothèque nationale du Canada de reproduire, prêter, distribuer ou vendre des copies de cette thèse sous la forme de microfiche/film, de reproduction sur papier ou sur format électronique.

L'auteur conserve la propriété du droit d'auteur qui protège cette thèse. Ni la thèse ni des extraits substantiels de celle-ci ne doivent être imprimés ou autrement reproduits sans son autorisation.

0-612-22602-6

**University of Alberta**

**Library Release Form**

**Name of Author:** Daniel J. Healy

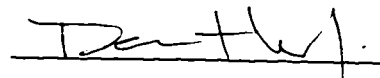
**Title of Thesis:** A Comparison of the ICEJAM and RIVJAM Ice Jam Profile Models.

**Degree:** Master of Science

**Year this Degree Granted:** 1997

Permission is hereby granted to the University of Alberta Library to reproduce single copies of this thesis and to lend or sell such copies for private, scholarly, or scientific research purposes only.

The author reserves all other publication and other rights in association with the copyright in the thesis, and except as hereinbefore provided, neither the thesis nor any substantial portion thereof may be printed or otherwise reproduced in any material form whatever without the author's prior written permission.



Daniel J. Healy

21 Regent Street

Lindsay, ON K9V 3T9

date: 1 OCT 97

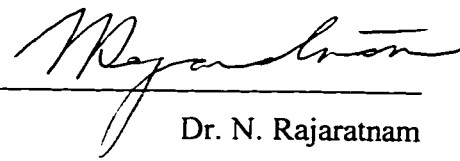
**University of Alberta**

**Faculty of Graduate Studies and Research**

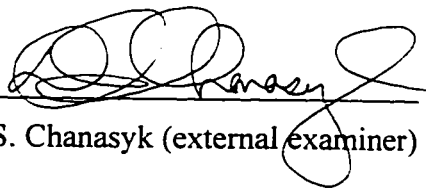
The undersigned certify that they have read, and recommend to the Faculty of Graduate Studies and Research for acceptance, a thesis entitled *A Comparison of the ICEJAM and RIVJAM Ice Jam Profile Models*, submitted by *Daniel J. Healy* in partial fulfillment of the requirements for the degree of *Master of Science in Water Resources Engineering*.



Dr. F.E. Hicks (supervisor)



Dr. N. Rajaratnam



Dr. D.S. Chanasyk (external examiner)

Date: 29 Sept 97

## ABSTRACT

Flooding due to ice jams causes extensive damage along populated rivers in Canada and may result in the loss of life. Numerical models describing ice jam configurations are useful tools for determining their associated flood levels and they provide a means for studying ice jam characteristics which cannot be measured directly in the field. The analytical equations, boundary conditions, solution techniques, and calibration parameters of two ice jam models (RIVJAM and ICEJAM) are examined to assess their suitability as tools for satisfying these objectives. Equivalency between the models' governing equations and solution techniques are illustrated through direct comparison and application to an idealized channel shape. Differences between the models are established through the application to fourteen documented ice jam events which occurred on Canadian Rivers. The relative merits and limitations of these models are outlined and advice on their efficient use is provided.

## ACKNOWLEDGEMENTS

The author would like to thank Spyros Beltaos, a Research Scientist at the National Water Research Institute, who provided invaluable commentary, advice, and technical support throughout this study. His generosity is sincerely appreciated.

The author would like to thank Dr. D.S. Chanasyk and Dr. N. Rajaratnam for committing their time and effort in reviewing this thesis.

The author would also like to acknowledge the academic support from Dr. Peter Steffler who always had an open door and provided valuable feedback to research related inquiries.

The author would like to express appreciation to the following people who provided data that was used during this study: Dr. Sayed Ismail (N.B. Power), Brian Burrel (N.B. Department of Environment), and David Andres and Gary Van Der Vinne of Trillium Engineering and Hydrographics Inc.

This research was funded through an NSERC operating grant to F.E. Hicks and this support is gratefully acknowledged.

The author would especially like to extend gratitude to his supervisor, Dr. Faye Hicks whom provided endless support and encouragement throughout this study. It was a fortunate experience for the author to work with someone of her caliber.



# TABLE OF CONTENTS

|  |    |
|--|----|
| CHAPTER 1.0 INTRODUCTION.....                                    | 1  |
| CHAPTER 2.0 LITERATURE REVIEW.....                               | 5  |
| 2.1 INTRODUCTION.....  | 5  |
| 2.1.1 General.....   | 5  |
| 2.1.2 Season of Formation.....                                   | 6  |
| 2.1.3 Dominant Formation Processes.....                          | 6  |
| 2.1.4 Conditions at the Toe.....                                 | 8  |
| 2.2 EVOLUTION OF THE JAM STABILITY THEORY.....                   | 9  |
| 2.2.1 Kennedy, R.J. (1958, 1962).....                            | 9  |
| 2.2.2 Pariset, E., Hausser, R., and Gagnon, A. (1961, 1966)..... | 10 |
| 2.2.3 Uzuner, M.S., and Kennedy, J.F. (1974, 1976).....          | 13 |
| 2.2.4 Michel, B. (1978).....                                     | 17 |
| 2.2.5 Beltaos, S. (1978, 1979).....                              | 19 |
| 2.2.6 Beltaos, S. (1983).....                                    | 20 |
| 2.3 THE ICEJAM AND RIVJAM MODELS.....                            | 22 |
| 2.3.1 Ice Jam Profiles.....                                      | 22 |
| 2.3.2 The ICEJAM Model.....                                      | 23 |
| 2.3.2.1 Flato, G. and Gerard R. (1986).....                      | 23 |
| 2.3.3 The RIVJAM Model.....                                      | 24 |
| 2.3.3.1 Beltaos, S., Wong, J. (1986).....                        | 24 |
| 2.3.3.2 Beltaos, S. (1988).....                                  | 25 |
| 2.3.3.3 Beltaos, S. (1993).....                                  | 25 |

|   |    |
|---|----|
| CHAPTER 3.0 RIVJAM AND ICEJAM: MODEL FORMULATION AND IMPLEMENTATION .....     | 31 |
| 3.1 INTRODUCTION.....   | 31 |
| 3.2 EQUATION FORMULATIONS .....   | 31 |
| 3.2.1 General.....  | 31 |
| 3.2.2 The RIVJAM formulation .....  | 32 |
| 3.2.2.1 <i>The Jam Stability Equation</i> .....                               | 32 |
| 3.2.2.2 <i>Gradually Varied Flow</i> .....                                    | 34 |
| 3.2.2.3 <i>Frictional Resistance</i> .....                                    | 37 |
| 3.2.3 ICEJAM formulation.....   | 39 |
| 3.2.3.1 <i>The Jam Stability Equation</i> .....                               | 39 |
| 3.2.3.2 <i>Gradually Varied Flow</i> .....                                    | 40 |
| 3.2.3.3 <i>Frictional Resistance</i> .....                                    | 41 |
| 3.4.2 Equivalency of RIVJAM and ICEJAM Formulations .....                     | 41 |
| 3.3 MODEL IMPLEMENTATION.....   | 42 |
| 3.3.1 Introduction .....  | 42 |
| 3.3.2 Boundary and Toe Conditions.....  | 43 |
| 3.3.2.1 <i>Theoretical Boundary Conditions and Solution Progression</i> ..... | 43 |
| 3.3.2.2 <i>Special Considerations at the Ice Jam Toe</i> .....                | 44 |
| 3.3.2.3 <i>ICEJAM Boundary Conditions</i> .....                               | 45 |
| 3.3.2.4 <i>RIVJAM Boundary Conditions</i> .....                               | 46 |
| 3.3.2.4 <i>Implications to Modelled Ice Jam Length</i> .....                  | 46 |
| 3.3.3 Solution Methodology .....  | 47 |
| 3.3.3.1 <i>RIVJAM Solution Methodology</i> .....                              | 47 |
| 3.3.3.2 <i>ICEJAM Solution Methodology</i> .....                              | 47 |
| 3.3.3.3 <i>Similarity of RIVJAM and ICEJAM Solution Methodologies</i> .....   | 48 |
| 3.3.4 Additional Implementation Features .....                                | 50 |
| 3.3.4.1 <i>Flow Through Interstices</i> .....                                 | 50 |

|  |   |     |
|--|---|-----|
| 3.3.4.2  | <i>Geometry Interpolation</i> .....                 | 50  |
| 3.3.5  | Model Input Requirements.....                       | 51  |
| 3.3.5.1  | <i>Introduction</i> .....                           | 51  |
| 3.3.5.2  | <i>RIVJAM Input Requirements</i> .....              | 51  |
| 3.3.5.3  | <i>ICEJAM Input Requirements</i> .....              | 52  |
| 3.4  | MODEL SENSITIVITY.....                              | 52  |
| 3.4.1  | Introduction.....                                   | 52  |
| 3.4.2  | Sensitivity of the RIVJAM model.....                | 57  |
| 3.4.2.1  | <i>Background</i> .....                             | 57  |
| 3.4.2.2  | <i>Boundary Conditions</i> .....                    | 58  |
| 3.4.2.3  | <i>Ice Jam Parameters</i> .....                     | 59  |
| 3.4.2.4  | <i>Channel Geometry</i> .....                       | 66  |
| 3.4.3  | Sensitivity of the ICEJAM Model.....                | 67  |
| 3.4.3.1  | <i>Background</i> .....                             | 67  |
| 3.4.3.2  | <i>Boundary Conditions and Discretization</i> ..... | 67  |
| 3.4.3.3  | <i>Calibration Parameters</i> .....                 | 71  |
| 3.4.3.4  | <i>Channel Geometry</i> .....                       | 74  |
| 3.4.4  | Discussion of Results.....                          | 75  |
| CHAPTER 4.0 MODEL EVALUATION USING DOCUMENTED ICE JAM<br>EVENTS..... |   | 101 |
| 4.1  | GENERAL.....  | 101 |
| 4.2  | DATA COLLATION.....                                 | 101 |
| 4.2.1  | General.....  | 101 |
| 4.2.2  | Data Requirements.....                              | 102 |
| 4.2.3  | Data Sources.....                                   | 103 |
| 4.2.4  | Data Selection and Interpretation.....              | 103 |
| 4.3  | MODELLING APPROACH.....                             | 104 |

|         |   |     |
|---------|---|-----|
| 4.3.1   | Developing Model Familiarity .....                                    | 104 |
| 4.3.2   | The Modelling Process .....   | 104 |
| 4.3.3   | Calibration Criteria .....  | 105 |
| 4.4     | RIGOROUS MODEL INVESTIGATION .....                                    | 105 |
| 4.4.1   | Case Studies Selection .....  | 105 |
| 4.4.2   | Ice Jam with Suspected Grounding - Restigouche River .....            | 106 |
| 4.4.2.1 | <i>ICEJAM Model Application</i> .....                                 | 107 |
| 4.4.2.2 | <i>RIVJAM Model Application</i> .....                                 | 109 |
| 4.4.2.2 | <i>Comparison Between Models</i> .....                                | 112 |
| 4.4.3   | Ice Jam with an Indefinite Length - Thames River .....                | 112 |
| 4.4.3.1 | <i>RIVJAM Model Application</i> .....                                 | 113 |
| 4.4.3.2 | <i>ICEJAM Model Application</i> .....                                 | 115 |
| 4.4.3.3 | <i>Sensitivity of ICEJAM Parameters</i> .....                         | 116 |
| 4.4.3.4 | <i>Equivalency of the Beltaos Mannings Approximation</i> .....        | 116 |
| 4.4.3.5 | <i>Discussion of Results</i> .....                                    | 117 |
| 4.4.4   | Ice Jam with Conflicting Discharge Estimates - Saint John River ..... | 118 |
| 4.4.4.1 | <i>ICEJAM Model Application</i> .....                                 | 119 |
| 4.4.4.2 | <i>RIVJAM Model Application</i> .....                                 | 119 |
| 4.4.4.2 | <i>Discussion of Results</i> .....                                    | 120 |
| 4.4.5   | Interpretations of the Rigorous Model Investigation .....             | 121 |
| 4.4.6   | Calibration Protocol for RIVJAM and ICEJAM .....                      | 122 |
| 4.4.6.1 | <i>ICEJAM Calibration Protocol</i> .....                              | 123 |
| 4.4.6.2 | <i>RIVJAM Calibration Protocol</i> .....                              | 124 |
| 4.5     | VERIFICATION OF CALIBRATION PROTOCOL .....                            | 124 |
| 4.5.1   | Introduction .....  | 124 |
| 4.5.2   | Hay River, near the Town of Hay River .....                           | 128 |
| 4.5.2.1 | <i>Introduction</i> .....   | 128 |
| 4.5.2.2 | <i>Hay River, April 28, 1987</i> .....                                | 129 |
| 4.5.2.3 | <i>Salient Observations</i> .....                                     | 130 |

|          |   |     |
|----------|---|-----|
| 4.5.2.4  | <i>Hay River, April 28, 1992</i> .....  | 131 |
| 4.5.2.5  | <i>Discussion of Results</i> .....  | 133 |
| 4.5.3    | <i>Athabasca River, near Fort McMurray</i> .....  | 133 |
| 4.5.3.1  | <i>Introduction</i> .....   | 133 |
| 4.5.3.2  | <i>Athabasca River, April 19, 1978</i> .....  | 134 |
| 4.5.3.3  | <i>Athabasca River, April 20, 1978</i> .....  | 136 |
| 4.5.3.4  | <i>Athabasca River, April 21, 1978</i> .....  | 138 |
| 4.5.3.5  | <i>Athabasca River, April 29 - May 1, 1979</i> .....                                    | 139 |
| 4.5.3.6  | <i>Athabasca River, April 10, 1984</i> .....  | 140 |
| 4.5.3.7  | <i>Athabasca River, April 14, 1985</i> .....  | 142 |
| 4.5.3.8  | <i>Athabasca River, April 16, 1985</i> .....  | 143 |
| 4.5.3.9  | <i>Athabasca River, April 20, 1986</i> .....  | 145 |
| 4.5.3.10 | <i>Athabasca River, April 22, 1986</i> .....  | 146 |
| 4.7      | DISCUSSION OF RESULTS.....  | 147 |
| 4.7.1    | General.....  | 147 |
| 4.7.2    | Calibrated composite roughness.....   | 147 |
| 4.7.2.1  | <i>Consistency of Calibrated Roughness for Rivers With Multiple Events</i> .....        | 148 |
| 4.7.2.2  | <i>Ice roughnesses deduced using Sabenev's Equation</i> .....                           | 150 |
| 4.7.2.3  | <i>Impact of Choice of Roughness on the Shape of the Computed Ice Jam Profile</i> ..... | 150 |
| 4.7.2.4  | <i>Calibrated Roughness as a Function of Discharge</i> .....                            | 152 |
| 4.7.3    | Validity of Beltaos' Mannings Approximation.....  | 152 |
| 4.7.4    | The Impact of Seepage on Roughness.....   | 153 |
| 4.7.5    | Velocity at the Toe.....  | 154 |
| 4.7.6    | Comparison of Computed Data to Equilibrium Theory.....                                  | 155 |
| 4.7.6.1  | <i>Equilibrium Formulation for Beltaos' friction factor</i> .....                       | 155 |
| 4.7.6.2  | <i>Equilibrium Formulation for Roughness Height</i> .....                               | 156 |

|  |     |
|--|-----|
| 4.7.6.3 <i>Comparison of Beltaos' Friction Factor to Calibrated Case Studies</i> ..... | 157 |
| 4.7.6.3 <i>Comparison of Roughness Height to Calibrated Case Studies</i> .....         | 160 |
| CHAPTER 5.0 CONCLUSIONS AND RECOMMENDATIONS.....                                       | 242 |
| 5.1 VERIFICATION OF THE PHYSICS DESCRIBING ICE JAM MECHANICS .....                     | 242 |
| 5.2 IMPORTANCE OF CARRIER DISCHARGE.....   | 243 |
| 5.3 PRACTICAL APPLICATION OF RIVJAM AND ICEJAM .....                                   | 243 |
| 5.4 RECOMMENDATIONS .....  | 245 |
| REFERENCES .....   | 247 |
| APPENDIX A .....   | 253 |

## LIST OF TABLES

|   |     |
|---|-----|
| Table 3.1 Input parameters for the RIVJAM model. ....                                       | 53  |
| Table 3.2 Input parameters for the ICEJAM model.....  | 54  |
| Table 3.3 Default input parameters for the sensitivity analysis. ....                       | 56  |
| Table 3.4 Typical values of $\mu$ deduced from documented events.....                       | 63  |
| Table 4.1 Calibration results for the Restigouche River. 1988 ice jam event.....            | 126 |
| Table 4.2 Calibration results for the Thames River. 1986 ice jam event.....                 | 127 |
| Table 4.3 Calibration results for the Saint John River. 1993 ice jam event.....             | 127 |
| Table 4.4 Calibration results for the Hay River. 1987 ice jam event.....                    | 131 |
| Table 4.5 Calibration results for the Hay River. 1992 ice jam event.....                    | 132 |
| Table 4.6 Calibration results for the Athabasca River. April 19, 1978 ice jam<br>event..... | 135 |
| Table 4.7 Calibration results for the Athabasca River. April 20, 1978 ice jam<br>event..... | 137 |
| Table 4.8 Calibration results for the Athabasca River. April 21, 1978 ice jam<br>event..... | 138 |
| Table 4.9 Calibration results for the Athabasca River. 1979 ice jam event.....              | 140 |
| Table 4.10 Calibration results for the Athabasca River. 1984 ice jam event.....             | 141 |

|   |     |
|---|-----|
| Table 4.11 Calibration results for the Athabasca River, April 14, 1985 ice jam event.....   | 143 |
| Table 4.12 Calibration results for the Athabasca River, April 16, 1985 ice jam event.....   | 144 |
| Table 4.13 Calibration results for the Athabasca River, April 20, 1986 ice jam event.....   | 145 |
| Table 4.14 Calibration results for the Athabasca River, April 22, 1986 ice jam event.....   | 146 |
| Table 4.15 Summary of roughnesses calibrated by RIVJAM and ICEJAM. ....   | 149 |
| Table 4.16 Summary of roughness, discharge deduced ice roughnesses based on the calibrated composite roughness and the open water bed roughness. .... | 151 |
| Table 4.17(a) Summary of Mannings roughness, discharge, and channel properties for ice jams with equilibrium sections. ....                           | 158 |
| Table 4.17(b) Summary of Beltaos' friction factor, discharge, and channel properties for ice jams with equilibrium sections. ....                     | 159 |



## LIST OF FIGURES

|   |    |
|---|----|
| Figure 2.1 Plan view of stresses acting on a log jam element as described by Kennedy. (1958). .....       | 27 |
| Figure 2.2 Elemental control volume for an ice jam element as described by Uzuner and Kennedy (1976)..... | 28 |
| Figure 2.3 Mohr's circle for lateral stress. ....   | 29 |
| Figure 2.4 Ice jam schematic. ....  | 30 |
| Figure 3.1 Schematic of ice accumulation in the toe region. ....  | 78 |
| Figure 3.2 Comparison of the ICEJAM and RIVJAM results for the trapezoidal channel. ....                  | 78 |
| Figure 3.3. Default runs for sensitivity analysis. ....   | 79 |
| Figure 3.4 Sensitivity of RIVJAM to toe thickness.....  | 80 |
| Figure 3.5 Sensitivity of RIVJAM to $c$ . ....  | 81 |
| Figure 3.6 Sensitivity of RIVJAM to $m_1$ and $m_2$ . ....  | 82 |
| Figure 3.7 Sensitivity of RIVJAM to $K_x$ . ....  | 83 |
| Figure 3.8 Sensitivity of RIVJAM to $\mu$ . ....  | 84 |
| Figure 3.9 Sensitivity of RIVJAM to $\beta_2$ (composite over ice roughness ratio). ....                  | 85 |
| Figure 3.10 Sensitivity of RIVJAM to seepage, $\lambda$ . ....  | 86 |
| Figure 3.11 Sensitivity of RIVJAM to discharge. ....  | 87 |
| Figure 3.12 Sensitivity of RIVJAM to the slope of the slope-line. ....                                    | 88 |
| Figure 3.13 Sensitivity of ICEJAM to cross section spacing. ....  | 89 |
| Figure 3.14 Sensitivity of ICEJAM to thickness at the downstream boundary.....                            | 90 |
| Figure 3.15 Sensitivity of ICEJAM to thickness at the head.....   | 91 |

|   |     |
|---|-----|
| Figure 3.16 Sensitivity of ICEJAM to jam length.....  | 92  |
| Figure 3.17 Sensitivity of ICEJAM to erosion velocity.....  | 93  |
| Figure 3.18 Sensitivity of ICEJAM to roughness.....   | 94  |
| Figure 3.19 Sensitivity of ICEJAM to $K_v$ .....  | 95  |
| Figure 3.20 Sensitivity of ICEJAM to $\mu$ .....  | 96  |
| Figure 3.21 Sensitivity of ICEJAM to discharge.....   | 97  |
| Figure 3.22 Sensitivity of ICEJAM to a change in channel slope.....   | 98  |
| Figure 3.23 Sensitivity of ICEJAM to a change in channel width.....   | 99  |
| Figure 3.24 Sensitivity of ICEJAM to an adverse slope.....  | 100 |
| Figure 3.25 Sensitivity of ICEJAM to a horizontal slope.....  | 100 |
| Figure 4.1 Location of case studies.....  | 161 |
| Figure 4.2 Extent of ice jam and cross section locations for the 1988 Restigouche River ice jam event.....  | 162 |
| Figure 4.3 1988 Restigouche River ice jam as predicted by ICEJAM using Mannings roughness.....  | 163 |
| Figure 4.4 1988 Restigouche River ice jam as predicted by ICEJAM using Mannings roughness, illustrating variation in (a) erosion velocity and (b) thickness at the head.....      | 164 |
| Figure 4.5 1988 Restigouche River ice jam as predicted by RIVJAM using Beltaos' friction factor.....  | 165 |
| Figure 4.6(a) 1988 Restigouche River ice jam as predicted by RIVJAM using Beltaos' Mannings approximation corresponding to equation [3.19].....                                   | 166 |
| Figure 4.6(b) 1988 Restigouche River ice jam as predicted by RIVJAM using Beltaos' Mannings approximation where thickness is set to match the observed data.....                  | 167 |
| Figure 4.7 1988 Restigouche River ice jam as predicted by RIVJAM using Belatos' Mannings approximation, illustrating variation in (a) seepage velocity and (b) toe thickness..... | 168 |
| Figure 4.8 Comparison of predicted ice jam profiles computed by RIVJAM using Beltaos' Mannings approximation and by ICEJAM using Mannings equation.....                           | 169 |

|  |     |
|--|-----|
| Figure 4.9 Extent of ice jam and cross section locaitons for the 1986 Thames River ice jam event. ....   | 170 |
| Figure 4.10(a) 1986 Thames River ice jam as predicted by RIVJAM using Beltaos' friction factor ( $c=0.61$ ). ....  | 171 |
| Figure 4.10(b) 1986 Thames River ice jam as predicted by RIVJAM using Beltaos' friction factor ( $c=0.70$ ). ....  | 172 |
| Figure 4.11 1986 Thames River ice jam as predicted by RIVJAM using Beltaos' Mannings approximation, illustrating limiting value of roughness coefficient, $c$ . ....   | 173 |
| Figure 4.12(a) 1986 Thames River ice jam as predicted by RIVJAM using Beltaos' friction factor. illustrating the effect of seepage where the toe thickness is held constant. ....                                | 174 |
| Figure 4.12(b) 1986 Thames River ice jam as predicted by RIVJAM using Beltaos' friction factor. illustrating the effect of seepage where the toe thickness is varied to achieve a jam of comparable length. .... | 175 |
| Figure 4.13 1986 Thames River ice jam as predicted by ICEJAM for both long and short jam scenarios for (a) a Mannings roughness of 0.070 and (b) a Mannings roughness of 0.055. ....                             | 176 |
| Figure 4.14 1986 Thames River ice jam as predicted by ICEJAM. illustrating sensitivity to (a) $K_x$ and (b) $m$ . ....   | 177 |
| Figure 4.15 1986 Thames River ice jam as predicted by ICEJAM using Beltaos' Mannings approximation. ....   | 178 |
| Figure 4.16 Extent of ice jam for the 1993 Saint John River ice jam event. ....  | 179 |
| Figure 4.17 1993 Saint John River ice jam as predicted by ICEJAM illustrating sensitivity to tow differnet estimated carrier discharges. ....  | 180 |
| Figure 4.18 1993 Saint John River ice jam as predicted by RIVJAM using Beltaos' Mannings approximation. ....   | 181 |
| Figure 4.19 1993 Saint John River ice jam as predicted by RIVJAM using Beltaos' friction factor. ....  | 182 |
| Figure 4.20 Extent of 1987 and 1992 Hay River ice jams and cross section locations. ....   | 183 |
| Figure 4.21 1987 Hay River ice jam as predicted by ICEJAM using Mannings equation. ....  | 184 |

|  |     |
|--|-----|
| Figure 4.22 1987 Hay River ice jam as predicted by ICEJAM using Beltaos' Mannings approximation. ....  | 185 |
| Figure 4.23 1987 Hay River ice jam as predicted by RIVJAM using Beltaos' friciton factor. ....   | 186 |
| Figure 4.24 1987 Hay River ice jam as predicted by RIVJAM using Beltaos' Mannings approximation while adjusting roughness. ....  | 187 |
| Figure 4.25 1992 Hay River ice jam as predicted by ICEJAM using Mannings roughness. ....   | 188 |
| Figure 4.26 1992 Hay River ice jam as predicted by ICEJAM using Beltaos' Mannings approximation. ....  | 189 |
| Figure 4.27 1992 Hay River ice jam as predicted by RIVJAM using Beltaos' friciton factor. ....   | 190 |
| Figure 4.28 1992 Hay River ice jam as predicted by RIVJAM using Beltaos' Mannings approximation with roughness fixed to corresond to the Mannings roughness calibrated by ICEJAM. .... | 191 |
| Figure 4.29(a) Extent of 1978 Athabasca River recorded ice jam events.....   | 192 |
| Figure 4.29(b) Extent of the 1979 Athabasca River recorded ice jam event. ....   | 193 |
| Figure 4.29(c) Extent of the 1984 Athabasca River recorded ice jam event. ....   | 194 |
| Figure 4.29(d) Extent of 1985 Athabasca River recorded ice jam events. ....  | 195 |
| Figure 4.29(e) Extent of 1986 Athabasca River recorded ice jam events.....   | 196 |
| Figure 4.30 Approximate cross section locations on the Athabasca River near Fort McMurray. ....  | 197 |
| Figure 4.30(continued) Cross section locations on the Athabasca River near Fort McMurray. ....   | 198 |
| Figure 4.30(continued) Cross section locations on the Athabasca River near Fort McMurray. ....   | 199 |
| Figure 4.30(continued) Cross section locations on the Athabasca River near Fort McMurray. ....   | 200 |
| Figure 4.30(continued) Cross section locations on the Athabasca River near Fort McMurray. ....   | 201 |

|  |     |
|--|-----|
| Figure 4.31 April 19, 1978 Athabasca River ice jam as predicted by ICEJAM using Mannings equation.....   | 202 |
| Figure 4.32 April 19, 1978 Athabasca River ice jam as predicted by ICEJAM using Beltaos' Manings approximation. ....   | 203 |
| Figure 4.33 April 19, 1978 Athabasca River ice jam as predicted by RIVJAM using Beltaos' friction factor.....  | 204 |
| Figure 4.34 April 19, 1978 Athabasca River ice jam as predicted by RIVJAM using Beltaos' Mannings approximation. ....  | 205 |
| Figure 4.35 April 19, 1978 Athabasca River ice jam as predicted by RIVJAM using Beltaos' Mannings approximation illustrating sensitivity to slope-line slope. .... | 206 |
| Figure 4.36 April 20, 1978 Athabasca River ice jam as predicted by ICEJAM using Mannings equation.....   | 207 |
| Figure 4.37 April 20, 1978 Athabasca River ice jam as predicted by ICEJAM using Beltaos' Manings approximation. ....   | 208 |
| Figure 4.38 April 20, 1978 Athabasca River ice jam as predicted by RIVJAM using Beltaos' friction factor.....  | 209 |
| Figure 4.39 April 20, 1978 Athabasca River ice jam as predicted by RIVJAM using Beltaos' Mannings approximation. ....  | 210 |
| Figure 4.40 April 21, 1978 Athabasca River ice jam as predicted by ICEJAM using Mannings equation.....   | 211 |
| Figure 4.41 April 21, 1978 Athabasca River ice jam as predicted by ICEJAM using Beltaos' Manings approximation. ....   | 212 |
| Figure 4.42 April 21, 1978 Athabasca River ice jam as predicted by RIVJAM using Beltaos' friction factor.....  | 213 |
| Figure 4.43 April 21, 1978 Athabasca River ice jam as predicted by RIVJAM using Beltaos' Mannings approximation. ....  | 214 |
| Figure 4.44 1979 Athabasca River ice jam as predicted by ICEJAM using Mannings equation.....   | 215 |
| Figure 4.45 1979 Athabasca River ice jam as predicted by RIVJAM using Belatos' friction factor. ....   | 216 |
| Figure 4.46 1979 Athabasca River ice jam as predicted by RIVJAM using Belatos' Mannings approximation. ....  | 217 |

|   |     |
|---|-----|
| Figure 4.47 1984 Athabasca River ice jam as predicted by ICEJAM using Mannings equation.....                          | 218 |
| Figure 4.48 1984 Athabasca River ice jam as predicted by ICEJAM using Beltaos' Mannings approximation. ....           | 219 |
| Figure 4.49 1984 Athabasca River ice jam as predicted by RIVJAM using Belatos' friction factor. ....                  | 220 |
| Figure 4.50 1984 Athabasca River ice jam as predicted by RIVJAM using Belatos' Mannings approximation. ....           | 221 |
| Figure 4.51 April 14, 1985 Athabasca River ice jam as predicted by ICEJAM using Mannings equation.....                | 222 |
| Figure 4.52 April 14, 1985 Athabasca River ice jam as predicted by ICEJAM using Beltaos' Mannings approximation. .... | 223 |
| Figure 4.53 April 14, 1985 Athabasca River ice jam as predicted by RIVJAM using Beltaos' friction factor.....         | 224 |
| Figure 4.54 April 14, 1985 Athabasca River ice jam as predicted by RIVJAM using Beltaos' Mannings approximation. .... | 225 |
| Figure 4.55 April 16, 1985 Athabasca River ice jam as predicted by ICEJAM using Mannings equation.....                | 226 |
| Figure 4.56 April 16, 1985 Athabasca River ice jam as predicted by ICEJAM using Beltaos' Mannings approximation. .... | 227 |
| Figure 4.57 April 16, 1985 Athabasca River ice jam as predicted by RIVJAM using Beltaos' friction factor.....         | 228 |
| Figure 4.58 April 16, 1985 Athabasca River ice jam as predicted by RIVJAM using Beltaos' Mannings approximation. .... | 229 |
| Figure 4.59 April 20, 1986 Athabasca River ice jam as predicted by ICEJAM using Mannings equation.....                | 230 |
| Figure 4.60 April 20, 1986 Athabasca River ice jam as predicted by RIVJAM using Beltaos' friction factor.....         | 231 |
| Figure 4.61 April 20, 1986 Athabasca River ice jam as predicted by RIVJAM using Beltaos' Mannings approximation. .... | 232 |
| Figure 4.62 April 22, 1986 Athabasca River ice jam as predicted by ICEJAM using Mannings equation.....                | 233 |

|   |     |
|---|-----|
| Figure 4.63 April 22, 1986 Athabasca River ice jam as predicted by RIVJAM using Beltaos' friction factor.....                                   | 234 |
| Figure 4.64 April 22, 1986 Athabasca River ice jam as predicted by RIVJAM using Beltaos' Mannings approximation. ....                           | 235 |
| Figure 4.65 Discharge versus calibrated composite roughness. ....   | 236 |
| Figure 4.66 Comparison of Mannings $n_o$ to Beltaos' friction factor equivalent to Mannings $n_o$ .....   | 237 |
| Figure 4.67 Ratio of the flow through interstices versus roughness ratio.....   | 238 |
| Figure 4.68 Variation in Beltaos' friction factor, $c$ , where (a) seepage is neglected and (b) seepage is included.....                        | 239 |
| Figure 4.69 Non-dimensional depth versus discharge for (a) Beltaos' friction factor and (b) variation in under ice to composite roughness. .... | 240 |
| Figure 4.70 Non-dimensional depth versus discharge for (a) Mannings roughness and (b) variation in under ice to composite roughness.....        | 241 |

## LIST OF SYMBOLS

- $A_f$  is the area of flow under the ice accumulation;
- $A_j$  is the submerged area of the ice jam;
- $B$  is the width of the underside of the ice;
- $c$  is a coefficient for Beltrami's friction factor;
- $C$  is a Chezy's roughness coefficient;
- $C_i$  is a shear stress coefficient representing cohesion;
- $C_o$  is a shear stress coefficient;
- $f_i$  is a friction factor of the underside of the ice jam;
- $f_o$  is a composite friction factor for the total flow beneath the floating cover;
- $F_o$  is the thrust at the leading edge or *head* of the jam;
- $g$  is the acceleration due to gravity;
- $h$  is the depth of flow below the ice accumulation;
- $H$  is the depth from the water surface to the bed;
- $h_{so}$  is the slope-line depth.



- $H_l$  is the elevation of the energy grade;
- $k_l$  is a coefficient of lateral thrust;
- $k_b$  is the roughness height for the bed influenced portion of flow;
- $k_i$  is the roughness height for the ice influenced portion of flow;
- $k_o$  is the composite roughness height;
- $K_p$  is a passive pressure coefficient;
- $K_v$  is a pressure coefficient analogous to  $K_p$  used by ICEJAM;
- $K_x$  is a coefficient of proportionality between stresses in a jam used by RIVJAM;
- $k_{wood}$  is a sliding coefficient of wood against wood;
- $m_1$  is an exponent for Beltaos' friction factor;
- $m_2$  is an exponent for Beltaos' friction factor;
- $n_b$  is Mannings roughness for the bed influenced portion of the flow;
- $n_i$  is Mannings roughness for the ice influenced portion of the flow;
- $n_o$  is Mannings roughness for the composite flow;
- $p$  is the porosity of the jam;

- $P$  is the force with which the jam upstream is pressing against the jam downstream (as presented by Kennedy, 1958)
- $Q$  is the total discharge flowing under and through the ice accumulation:
- $Q_f$  is the flow under the floating accumulation of ice:
- $Q_p$  is the flow through the voids or (pores) of an ice accumulation:
- $R_i$  is the hydraulic radius of the ice influenced portion of flow:
- $R_o$  is the hydraulic radius corresponding to the composite flow:
- $S_f$  is the slope of the energy grade line:
- $s_i$  is the specific gravity of the ice:
- $S_w$  is the water surface slope;
- $t$  is the thickness of the ice cover;
- $t_{head}$  is the thickness at the head of an accumulation modelled by ICEJAM:
- $t_{toe}$  is the thickness of the solid intact ice at the toe of an accumulation modelled by ICEJAM;
- $t_s$  is the submerged ice thickness;
- $t_{so}$  is the thickness at the downstream boundary (or toe) of an ice accumulation modelled by RIVJAM;
- $I'$  is the average velocity under the ice accumulation;

- $V_{max}$  is the ice erosion velocity;
- $x$  represents the streamwise direction;
- $\alpha$  is the slope of the water surface with respect to the bed.
- $\beta_1$  is a coefficient for jam stability, defined by Beltaos (1993);
- $\beta_2$  is a coefficient for jam stability, defined by Beltaos (1993);
- $\beta_3$  is a coefficient for jam stability, defined by Beltaos (1993);
- $\delta$  is the friction angle (between the ice accumulation and the bank):
- $\phi$  is the shearing angle for the ice accumulation;
- $\gamma_e$  is the effective unit weight of water;
- $\gamma_w$  is the unit weight of water;
- $\eta$  is a non dimensional discharge term;
- $\lambda$  is a seepage velocity coefficient;
- $\mu$  is an ice jam strength parameter;
- $\theta$  is the slope of the water surface with respect to the horizontal;
- $\rho$  is the density of water;
- $\rho_i$  is the density of ice;

$\sigma_x$  is the streamwise stress;

$\sigma_y$  is the thickness averaged transverse stress;

$\sigma_z$  is the averaged vertical stress;

$\tau$  is the shear stress a floating log accumulation investigated by Kennedy, R.J. (1958);

$\tau_b$  is the shear stresses on the bed;

$\tau_i$  is the streamwise shear stress due to the flow of water beneath an ice cover;

$\tau_{xy}$  is the streamwise shear stress due to the applied transverse stress,  $\sigma_y$ ;

$\xi_G$  is a non dimensional discharge term (Gerard. 1988);

$\xi_B$  is a non dimensional discharge term (Beltaos. 1983);

## CHAPTER 1.0 INTRODUCTION

A recent survey conducted by Van Der Vinne, Prowse, and Andres (1996) estimated that damages due to ice jams in Canada average at least \$22 million per year. This is very likely a conservative estimate, given that in Alberta alone, 1997 damage claims related to ice jam flooding in Peace River and Ft. McMurray totaled more than \$9M<sup>1</sup>. Flooding associated with high water levels is typically responsible for the damages caused by ice jams. However, ice jams can also cause damage to river structures (such as bridges) or interfere with navigation (Van Der Vinne, *et al.*, 1996).

Ice jams which occur in populated regions pose the most serious threat as the flood levels can rise to dangerous levels very rapidly. The awesome threat associated with ice jams is well captured by the following excerpt which relates the events recalled by H.J. Moberly, Factor of the Hudson's Bay Co. post at Fort McMurray that occurred on the morning of April 20, 1875 (Moberly and Cameron, 1929):

*"The winter of 1874-75 was a bitter one, with deep snow and never a thaw until April. On the 2<sup>nd</sup> or 3<sup>rd</sup> of that month, however, a further heavy fall of snow was followed by a sudden rise in temperature. The change of weather and the weight of melting snow caused the ice for the 85 mile stretch of rapids above the fort to breakup, and it came down the Athabasca with terrific force. On striking the turn of the stream at the post it blocked the river and drove the ice 2 miles up the Clearwater [River] in piles 40 to 59 feet high. In less than an hour the water rose 57*

---

<sup>1</sup> personal communication, J. Choles, Alberta Environmental Protection, May, 1997

*feet, flooding the whole flat and mowing down trees, some 3 feet in diameter, like grass... ”*

High water levels associated with ice jams often exceed the designated 1:100 year open water flood levels, even though they occur at significantly lower discharge. For example, Beltaos (1995) in commenting on the flood risk map produced by Nova Scotia Department of Environment for the town of Truro, Nova Scotia, noted that *“Upstream of the railway crossing on both the Salmon and North Rivers historical flood levels due to ice jams have frequently exceeded the 1:100-year flood levels shown.”* In addition, at present there is no way to forecast the occurrence of ice jams, and very little that can be done to mitigate their effects once they have formed (Beltaos, 1985).

As with open water floods, good flood plain management requires knowledge of the anticipated flood levels associated with events of a given return period. Because of the complex interactions between the ice and the channel flow which occur during ice jams floods, a frequency analysis on streamflow data is not appropriate. Instead, a physical analysis of the effects of the ice accumulation on flood water levels is required. Over the past three decades efforts have been made to understand the mechanics of ice jams and still their behaviour is far from being fully understood. This is partly because of the fact that an ice jam is a complex phenomenon for which it is nearly impossible to provide an all-encompassing theory which describes their behaviour. Uzuner and Kennedy (1976) expressed the level of complexity of this phenomenon, *“or to be more precise, ensemble of phenomena, [is such] that it is even difficult to frame a concise definition of an ice jam.”* Another very important factor which has limited the advancement of knowledge in the study of ice jams is the inherent danger and logistical difficulties associated with obtaining measurements of even the most fundamental ice jam characteristics (thickness and carrier discharge). Nevertheless, considerable advancements have been made both over the past two decades, as evidenced in the recent publication of the first book dedicated to the topic of ice jams (Beltaos, 1995).

Numerical models describing ice jam configurations have the potential to be extremely useful tools for determining the flood levels that may be expected under varying ice jam conditions. They also have the potential to be useful for studying ice jam characteristics indirectly, through calibration of measured water surface profiles and shear wall data. Also, numerical modelling methods provide an economical means of investigating river ice processes which may further assist in the planning and design of river ice development, management, and control projects.

Currently, there are two generally available (non-proprietary) ice jam profile computational models: RIVJAM and ICEJAM. Both are based on a steady, one-dimensional gradually varied flow approximation, although the numerical solution technique is different in each case. RIVJAM was developed at the National Water Research Institute in Burlington, Ontario, and ICEJAM was developed at the University of Alberta, Edmonton. Based on verbal communication with various consultants, it appears that the ICEJAM model is currently more widely used than RIVJAM, though not necessarily for the right reasons. ICEJAM is relative simple to use, whereas there seems to be a steep learning curve for the RIVJAM model because of numerical sensitivities associated with the solution methodology employed by the RIVJAM model. This is probably because, until recently, the RIVJAM model was considered to be under development and limited documentation for this model was available. A new users' manual is expected to be released this year.

The ICEJAM model was developed as a research tool and there is little documentation on the model past its original presentation in a thesis by Flato (1988) and a conference paper by Flato and Gerard (1986). There have been no further developments for the ICEJAM model since that time, except for the minor modifications introduced during the course of this investigation (to facilitate comparisons between the models). Through personal communication with various consultants it was found that there is considerable interest in the RIVJAM model and its associated capabilities (in particular its ability to account for seepage through the interstices of an ice jam accumulation). Also, the RIVJAM model has undergone

extensive refinements and numerous validations by its developers since its first introduction in 1986. A primary advantage of the RIVJAM model is that it is supported by a national government agency, and users can reasonably expect continued development and support.

The objective of this investigation was to compare these models in a practical sense in order to investigate the similarities and differences between the models, specifically their formulations, solution techniques, and robustness. The intention was to develop insight and awareness which would be useful to potential users of these models, particularly when deciding which model to pursue but also to help flatten the learning curve for those who have previously been discouraged by the lack of familiarity and apparent difficulty in getting these models (particularly RIVJAM) to run. Ancillary objectives of this project included: quantitatively deducing ice jam characteristics through application of these models to a variety of case studies; and, establishing criteria for field investigators collecting ice jam data.

The initial focus of the investigation was to compare the analytical equations, the boundary conditions, and the calibration parameters used by the two models. First, Chapter 2 presents a review of the literature which forms the theoretical basis for these two models as well as the published papers introducing the ICEJAM and RIVJAM models. Similarities between the models' governing equations and solution techniques are examined in detail in Chapter 3, through a direct comparison of the analytical equations. The relative sensitivity of the models' parameters are also illustrated through application to an idealized, prismatic channel. The models' behavior and parameter sensitivity are further explored in Chapter 4, through the application to fourteen case studies documenting ice jam events. Calibration protocols, which expedite the application of both models are developed and tested in Chapter 4, as well. Finally, Chapter 5 presents a summary of the results obtained and recommendations both for potential model users and future research.



## CHAPTER 2.0 LITERATURE REVIEW

### 2.1 INTRODUCTION

#### 2.1.1 General

Ice jams, vary in size and shape in accordance to the prevailing hydraulic, geometric, and meteorological conditions during their development, and the formation processes of ice jams vary depending on these conditions. Due to the variety of "types" of ice jams that are formed as a result of these processes, and the complex nature of this phenomenon, "or to be more precise, ensemble of phenomena... it is difficult even to frame a concise definition of an ice jam" (Uzuner, *et al.*, 1976). In light of the these difficulties, the following represents the most satisfactory definition of an *ice jam*.

*"An ice jam is a stationary accumulation of fragmented ice or frazil that restricts flow."*

(IAHR Working Group on River Ice Hydraulics, 1986).

Ice jams typically form when there is a local reduction in ice transport capacity or when a flux of detached ice floes is arrested for any reason (Beltaos, 1995). The stoppage in ice floes can be relatively dramatic, such as in the case of a breaking front coming to rest within a solid intact ice sheet, or more gradual as in the case of a mass of detached ice floes constricted by a narrowing in the channel. The way in which ice jams form and the prevailing conditions during their genesis give rise to their classification.

The IAHR Working Group on River Ice Hydraulics (1986) proposed a classification system for ice jams. The classification system is governed by four criteria, namely:

the season during which the jam is formed: the dominant formation processes: the spatial extent of the jam: and the state of evolution of the jam at the moment of classification. Common terminology of ice jams focuses on the first two criteria listed above. A closer look at the mechanisms behind their development illustrates the rationale for their classification.

### **2.1.2 Season of Formation**

Ice jams can be distinguished by the season during which they are formed. The *season* (i.e. winter versus spring, or warm weather versus cold) used to identify the "type" of jam relates to the hydraulic and meteorological conditions under which the ice jam was formed. The most common terminology used to distinguish these "types" of jams refers to the time of formation, either freeze-up or break-up. Freeze-up jams, as the name implies, form during the freeze-up period in late fall or early winter and are typically formed from the accumulation of frazil ice or pan ice. These ice jams invariably provide the foundation for the genesis of a solid intact ice cover which is further thickened by thermal processes. Break-up ice jams typically occur during the spring as the ice is broken up mechanically by the hydraulic and buoyant forces of rising waters, resulting from spring runoff.

### **2.1.3 Dominant Formation Processes**

As detached ice floes come to rest at an obstruction, subsequent ice floes will arrive and stop against the upstream edges of the arrested ice floes. The incoming floes experience a downward force and subsequent overturning moment due to flow separation and acceleration effects at the leading edge. When the buoyant forces are large enough to overcome the downward forces due to the momentum and accelerating flow at the leading edge, the individual flows will remain in place, on the surface, arranging themselves to comprise a "juxtaposed" ice cover. The leading edge of the accumulation progresses upstream at a rate which is a direct function of the

supply rate of ice floes. An ice cover forms which for all practical purposes, is of a thickness equal to average thickness of the ice floes comprising the jam.

Thickened ice jams occur when the hydrodynamic forces on the individual ice floes at the leading edge exceed the forces due to buoyancy, causing the ice floe to submerge. These submerged floes may deposit under the floating cover somewhere downstream near the leading edge or they may become entrained in the flow to be carried further downstream under the ice cover. These entrained floes may be deposited under the cover further downstream where lower velocities are encountered or they may reemerge to the surface, downstream of the obstruction.

The dominant formation processes give rise to classical definition of "wide" channel ice jams and of "narrow" channel ice jams first proposed by Pariset, Hausser, and Gagnon (1966). A "narrow" channel ice jam is governed by the hydrodynamic forces at the upstream or "leading" edge of the ice accumulation. As a "narrow" channel ice jam accumulation grows in length (that is to say, as the head of the accumulation propagates upstream), the internal stresses within the ice accumulation grow due to an increased shear on the underside of the ice as the surface area increases, and to the increased downstream component of the weight of the ice jam. The forces are taken up by internal strength of the ice accumulation which is primarily a function of its thickness. When the internal stresses can no longer support the forces due to the shear under the accumulation and the weight of the accumulation, the ice jam will collapse or "shove" in a telescoping manner to form a thicker ice jam which is able to support these applied forces. This forms a different form of ice jam which is known as a "wide" channel ice jam.

"Wide" channel ice jams are typical to break-up and are known to form the most severe types of ice jams in terms of magnitude. These jams are governed by the applied hydraulic and gravitational forces which are offset by the internal strength of the jam. The formulations describing the strength of these types of jams are based on well known soil mechanics theories. This leads to perhaps the most fundamental

assumption behind the development of ice jam mechanics which implies that a mass of detached ice floes can be considered analogous to a cohesionless granular material. The pioneering work on ice jam mechanics by Pariset, *et al.* (1966) base their analysis on the following assumption.

*“The fact that ice jams are formed by a mass of detached floes gives rise to the assumption that the mechanics of the phenomenon are independent of the rheological properties of ice”*

These theories provided the foundation for the formulation of the RIVJAM and ICEJAM numerical models. These theories, which focus on the development of a stability relationship for a cohesionless mass of ice, are described chronologically as they appear in the literature.

#### **2.1.4 Conditions at the Toe**

The *toe* of an ice jam is the downstream limit of the ice accumulation which represents a region more than a specific point or boundary. Little is known about the physical behavior of this region or its exact configuration, other than that it is different than from that of the rest of the jam (Beltaos, *et al.*, 1986). For ice jams of the “wide” channel type, it has been observed in nature that *grounding* may occur at the toe as a result of the ice accumulation coming into contact with the bed due to progressive thickening and shoving of the ice cover. Grounded ice jams are more likely to occur during breakup than at freeze-up because the individual ice floes are typically stronger, the ice accumulation tends to be thicker, and the interstices which allow the passage of flow through a grounded accumulation are larger (Beltaos, 1995).

## 2.2 EVOLUTION OF THE JAM STABILITY THEORY

### 2.2.1 Kennedy, R.J. (1958, 1962)

The earliest theories which attempt to formulate a relationship describing the applied and subsequent resisting forces in an ice jam follow closely to Kennedy's analysis of a pulpwood jam. Kennedy (1958) applied the theories of earth pressure developed by Rankine (an early pioneer in soil mechanics theories who developed a method for determining the earth pressure against a retaining wall (Holtz and Kovacs, 1981)) to an element within a pulpwood log jam that is considered to be in a state of equilibrium. Rankine's theory applies to a soil mass that has just reached a point of shear failure in the context of the plastic equilibrium theory. Plastic equilibrium theory allows for the assumption that the *"stress-strain behavior of the soil can be represented by the rigid-perfectly plastic idealization, in which yielding and shear failure both occur at the same state of stress: unrestricted plastic flow takes place at this stress level"* (Craig, 1992).

Kennedy (1958) considered the stresses acting on an element within the log jam which is at a state of plastic equilibrium or incipient failure. Figure 2.1 illustrates the forces considered in Kennedy's analysis which act on this equilibrium element. If it is assumed that no shear stress is exerted in the horizontal or vertical planes then the vertical, and horizontal stresses can all be considered principle stresses. Kennedy (1962) then assumed an equilibrium element to be in an active state (in terms of Rankine's theory) where the streamwise stress was the major principle stress and the lateral stress (across the river) was the minor principle stress. This implied that displacement of the jam would occur in the vertical direction.

Kennedy's analysis considers a rectangular prismatic channel. By conducting a force balance on the elemental length of a jam depicted in Figure 2.1, Kennedy (1958) arrived at the following relationship describing the forces within a jam:

$$B \frac{dP}{dx} - \tau B + 2k_1 k_{wood} P = 0 \quad [2.1]$$

where:

$P$  “is the force with which the jam upstream is pressing against the jam downstream in a direction parallel with the current”;

$x$  represents the streamwise direction or longitudinal component:

$B$  is the width of the river;

$\tau$  is the shear stress exerted by the flowing water under the floating accumulation:

$k_1$  is the coefficient of lateral thrust; and

$k_{wood}$  “is the sliding coefficient of wood against wood”.

### 2.2.2 Pariset, E., Hausser, R., and Gagnon, A. (1961, 1966)

“The work of Pariset and Hausser (1961) and Pariset, Hausser, and Gagnon (1966), seems to have been a pioneer effort to formulate the problem [of the hydromechanics of floating river ice jams]” (Beltaos, 1978). Through the presentation of their analysis, Pariset, *et al.* (1961, 1966) provide the basis for the classical definition of the “wide” and “narrow” ice jams. The analysis presented assumed an “*ideal rectangular channel of constant shape and roughness*”. The forces described by Pariset, *et al.* (1966) acting within and on an ice cover over a differential length,  $dx$ , and ice thickness,  $t$ , included: the downstream component of weight of the cover in the direction of the water slope,  $F_w$ ; the shear stress on the ice underside caused by the flow of water,  $\tau_i$ ; and the reaction of shear stress at the banks,  $\tau_b$ . Pariset, *et al.* (1966), developed the following relationship describing the balance of the total forces,  $F$ .

$$BdF - (\tau_i + F_w)Bdx + \tau_b dx = 0 \quad [2.2]$$

where  $\tau_b = (C_i + \tan \phi k_1 F)l$ . They then wrote:

$$\frac{BdF}{dx} + 2l(C_i + \tan \phi k_1 F) - \tau_i B - F_w B = 0 \quad [2.3]$$

where:

$\phi$  is the shearing angle for the ice accumulation; and

$C_i$  a constant describing the cohesion of the ice accumulation.

They then integrated equation [2.3] to give:

$$F = \frac{B}{2k_1 \tan \phi} (\tau_i + F_w) - \frac{C_i l}{k_1 \tan \phi} - A e^{-\frac{2k_1 \tan \phi x}{B}} \quad [2.4]$$

where:

$$A = \frac{B}{2k_1 \tan \phi} (\tau_i + F_w) - \frac{C_i l}{k_1 \tan \phi} - F_o \quad [2.5]$$

and  $F_o$  is the thrust at the leading edge or *head* of the jam.  $F_o$  is considered to be the boundary condition at the upstream edge of the jam (i.e. at  $x = 0$ ). Pariset, *et al.* (1966) considered two cases that might apply to equation [2.4], and by doing so introduced the classical definition of "narrow" and "wide" ice jams. The two cases presented, describe the limiting conditions on equation [2.4], where  $A$  is either negative or positive.

For the first case, where  $A$  is negative, they stated that the maximum thrust is expected to occur at  $x = 0$  with magnitude of  $F_o$ , and hence the maximum thrust occurs at the leading edge (i.e.  $F_i = F_o$ ). They also implied that the forces due to the weight of the jam,  $F_w$ , and the shear stress underneath the ice,  $\tau_i$ , are negligible in

comparison to the hydrodynamic forces at the leading edge and that these forces are readily accepted by the banks. Based on this they developed criteria for stability at the leading edge of the accumulation. These and similar criteria are summarized by Uzuner, *et al.* (1974).

The second case outlined by Pariset, *et al.* (1966) describes the so called wide jam scenario where the coefficient  $A$  in equation [2.4] is positive. They showed that the total thrust acting on the jam increases in the downstream direction, approaching a maximum or limit defined as,

$$F_{\max} = \frac{B}{2k_1 \tan \phi} (\tau_i + F_w) - \frac{C_1 l}{k_1 \tan \phi} \quad [2.6]$$

Next, Pariset, *et al.* (1966) suggested that the ice cover will shove and then thicken to increase the internal forces,  $F_i$ , necessary to resist the applied forces. Pariset, *et al.* (1966) employed concepts similar to Rankine's earth pressure theory relating the streamwise stress to vertical stress (which account for gravitational and buoyant forces acting on the ice) such that the internal resistance in the streamwise direction,  $F_i$ , will approach the "probable" value of,

$$F_i = \rho_i \left( 1 - \frac{\rho_i}{\rho} \right) \frac{gt^2}{2} \tan^2 \left( 45 + \frac{\phi}{2} \right) \quad [2.7]$$

where the  $\tan^2 \left( 45 + \frac{\phi}{2} \right)$  term is analogous to a passive pressure coefficient,  $K_p$ , used in Rankine's earth pressure theory. By equating the applied external forces,  $F_{\max}$ , to the internal resistance,  $F_i$ , they obtained:

$$\frac{B}{2k_1 \tan \phi} (\tau_i + F_w) - \frac{C_1 l}{k_1 \tan \phi} = \rho_i \left( 1 - \frac{\rho_i}{\rho} \right) \frac{gt^2}{2} K_p \quad [2.8]$$

To simplify this relationship, Pariset, *et al.* (1966) introduced the jam strength coefficient,  $\mu$ , expressed as:



$$\mu = k_1 K_p \tan \phi \quad [2.9]$$

where  $k_1$  and  $K_p$  are functions of  $\phi$ . Pariset. *et al.* (1966) went on to state that  $k_1$  is less than or equal to one “depending on the active or neutral state of the granular mass of ice.”

By substituting equation [2.9] into equation [2.8] they wrote:

$$\rho_i \left(1 - \frac{\rho_i}{\rho}\right) \frac{gt^2}{2} = \frac{B}{2\mu} (\tau_i - F_w) - \frac{C_i t}{\mu} \quad [2.10]$$

These relationships described by Pariset. *et al.* (1961, 1966) provided the foundation for current ice jam theory. An “analytical” classification of sorts based on river “width” is also suggested.

### 2.2.3 Uzuner, M.S., and Kennedy, J.F. (1974, 1976)

In studying the hydraulics and mechanics of river ice jams, Uzuner. *et al.* (1974) provided a foundation for the development of a theoretical model for river ice jams, which was later developed into a mathematical model for the equilibrium reach and upstream transition portion of an ice jam (Uzuner, *et al.*, 1976).

Uzuner. *et al.* (1976) considered an element within a floating mass of ice as depicted in Figure 2.2, and then conducted a force balance on the element in the streamwise,  $x$ , direction to get.

$$\frac{\partial}{\partial x} (\sigma_x t) - \frac{\partial}{\partial y} (\tau_{xy} t) - \tau_i \cos \left( \frac{\rho_i}{\rho} \frac{\partial \alpha}{\partial x} \right) - \rho_i g t \sin(\theta + \alpha) = 0 \quad [2.11]$$

where:

$\sigma_x$  is the streamwise stress:

$\tau_{xy}$  is the streamwise shear stress due to the applied transverse stress,  $\sigma_y$ :

$t$  is the thickness of the ice cover;

$\tau_i$  is the streamwise shear stress due to the flow of water beneath the cover:

$\rho_i$  is the density of ice;

$\rho$  is the density of water:

$\theta$  represents the slope of the water surface with respect to the horizontal; and

$\alpha$  represents the slope of the water surface with respect to the bed.

Uzunur, *et al.* (1974) limited their analysis to the case where the slope of the water surface with respect to the bed was considered much less than the slope of the water surface with respect to the horizontal (i.e.  $\alpha \ll \theta$  which led to  $\frac{\rho_i}{\rho} \frac{\hat{\alpha}}{\hat{\alpha}} \cong 1$ ), and

therefore, wrote equation [2.11] as:

$$\frac{\hat{c}}{\hat{\alpha}} (\sigma_x t) - \frac{\hat{c}}{\hat{\alpha}} (\tau_{xy} t) - \tau_i - \rho_i g t \sin(\theta) = 0 \quad [2.12]$$

Here the first term represents the downstream component of the internal stress, the second term represents the reaction at the banks, the third term represents the shear due to the flow of water under the ice cover, and the last term represents the streamwise force due to the weight of the jam.

By considering the ice jam to be laterally uniform, they wrote,

$$\frac{\hat{c}}{\hat{\alpha}} (t, \tau_i) = 0 \quad [2.13]$$

which simplifies the integration of equation [2.12].

Before integrating equation [2.12], Uzuner, *et al.* (1974) found expressions for  $\sigma_x$  and  $\tau_{xy}$  as functions of ice jam thickness,  $t$ . Uzuner, *et al.* postulated that the behavior of a mass of fragmented ice is related to the under ice shear stress,  $\tau_i$ , and the internal strength, represented by both  $\sigma_x$  and  $\tau_{xy}$ . They expected the ice cover to remain intact until critical values or limits of  $\sigma_x$  and  $\tau_{xy}$  were exceeded at which point the cover would instantaneously fail and reconfigure to a new thickness adequate to support the external loads reflected in  $\tau_i$ . Uzuner, *et al.* (1974) went on to state “*that the cover will not thicken by this process until its strength is exceeded; that is t will not be dependent on the loading until the onset of failure.*” This concept is not unlike the theories of Rankine for earth pressure described by Craig (1992), which “*considers the state of stress in a soil mass when the condition of plastic equilibrium is reached.*” Uzuner, *et al.*'s (1976) analysis is therefore limited to critical states or conditions of incipient failure.

Uzuner, *et al.* (1976) stated that the vertical stresses,  $\sigma_z$ , in a floating mass of fragmented ice are a result of the downward component of weight of the ice and the resisting upward thrust due to buoyancy. These forces are as depicted in Figure 2.2. The vertical stress is expected to reach a maximum at the phreatic surface:

$$\sigma_z = t \left( 1 - \frac{\rho_i}{\rho} \right) (1 - p) \rho_i g \cos \theta \quad [2.14]$$

The vertically average stress was written by Uzuner, *et al.* (1976) as:

$$\bar{\sigma}_z = \frac{t}{2} \left( 1 - \frac{\rho_i}{\rho} \right) (1 - p) \rho_i g \cos \theta; \quad [2.15]$$

while the effective unit weight of the cover was defined as:

$$\gamma_e = \frac{1}{2} \left( 1 - \frac{\rho_i}{\rho} \right) (1 - p) \rho_i g \cos \theta. \quad [2.16]$$

Therefore, Uzuner, *et al.* (1976) wrote the vertical average stress as:

$$\bar{\sigma}_z = \gamma_e t \quad [2.17]$$

Applying Rankine's passive pressure theory, Uzuner, *et al.* (1976) defined the streamwise stress as:

$$\sigma_x = k_x \bar{\sigma}_z \quad [2.18]$$

Next, Uzuner, *et al.* (1976) defined the critical value for the lateral shear stress,  $\tau_{xy}$ , as:

$$\tau_{xy_{max}} = C_o \bar{\sigma}_z + C_i \quad [2.19]$$

Where  $C_o$  is a shear stress coefficient, and  $C_i$  is the cohesive intercept.

When applying the traditional Mohr-Coulomb concepts, the coefficients  $C_o$  and  $C_i$  describe a stress-dependent component and a stress-independent component, respectively (Holtz and Kovacs, 1981). The equivalent representation of equation [2.19] on a Mohr's circle diagram is illustrated in Figure 2.3 where  $C_o$  is taken to be equal to  $\tan\phi$ . Uzuner, *et al.* (1976) highlighted the likelihood of  $C_o$ ,  $C_i$  and  $k_x$  as being strain-rate dependent, but treated them as constants in their analysis.

For the straight prismatic channel case, Uzuner, *et al.* (1976) stated that the shear stress exerted by the flow under the ice cover,  $\tau_i$  is uniformly distributed across the stream while the transverse shear strength within the cover,  $\tau_{xy}$ , varies linearly in the transverse direction. For a symmetric channel the transverse shear strength within the cover,  $\tau_{xy} = 0$  at the channel centerline, increasing to a maximum at the banks. They defined this transverse shear stress relationship as:

$$\tau_{xy} = -\frac{2y}{B} \tau_{xy_{max}} \quad [2.20]$$

where  $y$  is the transverse distance from the channel centerline. They expected that shear failure would occur at its maximum value, corresponding to the banks.

Next, Uzuner, *et al.* (1976) substituted equations [2.17], [2.18], [2.19], and [2.20] into equation [2.12] to obtain:

$$\frac{\partial}{\partial x}(k_x \gamma_e t) - \frac{\partial}{\partial y} \left[ \frac{-2y}{B} (C_o \gamma_e t + C_i) \right] - \tau_i - \rho_i g t \sin \phi = 0 \quad [2.21]$$

Integrating equation [2.21] (see Uzuner, *et al.*, 1974) while: denoting  $k_x$  by a passive pressure coefficient,  $K_p$ ; defining the slope of the water surface,  $\sin \phi$ , by  $S_w$ ; and assuming  $\tau_i$  and  $t$  to be invariant in the transverse direction, they wrote:

$$\frac{dt}{dx} = \frac{\tau_i}{2K_p \gamma_e} + \frac{\rho_i g S_w - 2C_i}{2K_p \gamma_e} - \frac{C_o t}{K_p B} \quad [2.22]$$

Equation [2.22] can be described as a jam stability equation which applies to the "wide" channel type jam under steady state conditions at incipient failure.

#### 2.2.4 Michel, B. (1978)

With a focus on ice jams during break-up, Michel (1978) identified three major *categories of factors* which govern their formation: "*the resistance of the continuous cover, the importance of the flood wave, and the morphology of the river bed.*" The "resistance" of the cover described by Michel refers to the strength or state of the intact ice cover prior to break-up. Ultimately, the intact cover is fragmented as a result of hydrodynamic forces. The relative magnitude of these forces dictates the nature of the fragmented ice which potentially contributes to an ice jam. Two types of break-up are then described by Michel on this basis. The first is a *dynamic* or *premature* break-up, where a relatively strong and competent intact ice cover is fragmented by a large sudden discharge (high hydrodynamic forces). The second type refers to a *thermal* or *mature* break-up, where a very weak, thermally decayed or *rotten* ice cover is fragmented by very moderate discharges (low hydrodynamic

forces). The severity of the winter or ice generation period also plays a role in defining the nature of the ice prior to break-up. In the end however, it is essentially the hydrodynamic forces which govern the nature of the fragmented ice contributing to an ice jam.

The intent of this report is to build on those theories where the behaviour of a mass of detached floes (which are assumed cohesionless) is considered analogous to the behaviour of soil. However, it is important to note that cohesion does exist in ice jams to a varying degree depending on the type of jam. The effects of cohesion in an ice jam were raised when Michel (1978) questioned the validity of the Mohr-Coulomb concept as it applies to ice jam mechanics. Essentially, Michel (1978) stated that the Mohr-Coulomb relationship does not apply for all ice jams because ice floes can not be considered analogous to soil due to the re-freezing processes that can occur in a fragmented mass of ice, in particular for frazil ice and freeze-up jams. For example, for freeze-up jams, the majority of the strength can be provided by a thin layer of ice forming between the ice floes. Michel's (1978) intent was not to discourage the use of these soil mechanics concepts for break-up jams where temperature effects are less predominant, but only to make this point clear.

The processes of re-freezing are complex and are related primarily to temperature. These processes are further complicated by the inclusion of pressure effects introduced at the interface between detached floes. However, for "wide" channel jams during breakup, these effects are considered negligible (Beltaos, 1978).

### **2.2.5 Beltaos, S. (1978, 1979)**

Early work presented by Beltaos (1978, 1979) provided a comparison of the ice jam mechanics theories developed by Pariset, *et al.* (1966) and Uzuner, *et al.* (1976). Beltaos rewrote the following versions of the jam stability equations under steady state and equilibrium conditions of these authors as.

$$\mu\rho_i\left(1-\frac{\rho_i}{\rho}\right)\frac{gt^2}{2}=\frac{B}{2}(\tau_i+\rho_i gS_w t)-C_i t \quad [2.23]$$

and.

$$C_o(1-p)\mu\rho_i\left(1-\frac{\rho_i}{\rho}\right)\frac{gt^2}{2}=\frac{B}{2}(\tau_i+\rho_i gS_w t)-C_i t \quad [2.24]$$

where equations [2.23] and [2.24] represent the theories presented by Pariset. *et al.* (1966) and Uzuner. *et al.* (1976), respectively. By direct comparison. Beltaos (1978, 1979) found coincidence between these two equations when,

$$\mu=C_o(1-p). \quad [2.25]$$

This generally accepted version of  $\mu$  (Ashton. 1986) is a variation on the original definition of  $\mu$ . (equation [2.9]) Pariset. *et al.* (1966). in which all variables describing  $\mu$  were functions of the internal angle of resistance.  $\phi$ .

Through observation of ice jams in the field. Beltaos (1978) attempted to quantify the jam strength parameter  $\mu$ . The nature of real ice jams does not allow for the direct measurement of this parameter (both from a safety and logistical perspective).

Perhaps the value in adopting a parameter such as  $\mu$ . is that it allows one to lump various unknown parameters (e.g.  $\phi$ ,  $k_1$ ,  $K_p$ ,  $C_o$ . and  $p$ ) together in the hopes of better quantifying the overall process (Ashton. 1986). Beltaos (1978, 1979) attempted to measure  $\mu$  indirectly through the substitution of more easily quantifiable parameters into a simplified version of Pariset. *et al.*'s (1966) equilibrium equation. His general approach was to approximate the under ice shear stress as.

$$\tau_i=\rho g S_w R_i \quad [2.26]$$

where  $R_i$  is the hydraulic radius of the ice influenced portion of flow, and then substitute this relationship into Pariset, *et al.*'s (1966) jam stability equation [2.23] to give:

$$\mu = \left[ \frac{S_w B}{t} \left( 1 + \frac{\rho R_i}{\rho_i t} \right) - \frac{2C_i}{\rho_i g t} \right] \left( \frac{1}{1 - \rho_i / \rho} \right) \quad [2.27]$$

Beltaos (1978) found during the analysis of an ice jam on the Smoky River an ice jam that the term associated with the cohesion,  $C_i$ , was very small in comparison to the first term in the square brackets of equation [2.27]. By neglecting this cohesion term and setting  $\rho_i / \rho = 0.92$ ,  $\rho = 1000 \text{ kg/m}^3$ , and  $g = 9.81 \text{ m/s}^2$ . Beltaos rewrote equation [2.27] as:

$$\mu = 12.5 \frac{S_w B}{t} \left( 1 + \frac{R_i}{0.92t} \right) \quad [2.28]$$

For the field investigations considered by Beltaos (1978), values for  $\mu$ , computed using equation [2.28], ranged from 0.9 to 2.2. Methods for determining the hydraulic radius of the ice portion of flow,  $R_i$ , are described by Beltaos (1978).

### 2.2.6 Beltaos, S. (1983)

Adding to his earlier work on the analysis of the hydraulics of flow under an ice jam, Beltaos (1983) stated that the composite roughness,  $f_o$ , for the flow under an ice jam is:

$$f_o = \frac{f_i + f_b}{2} \quad [2.29]$$

where the subscripts  $i$  and  $b$  denote the ice influenced and bed influenced portions of flow, respectively. A new relationship describing the composite roughness of the flow under an ice accumulation was also introduced by Beltaos (1983) which was based on Nezhikhovskiy's (1964) interpretation of field data collected from freeze-up



ice jams in the former Soviet Union. From the work of Nezhikhovskiy (1964). Beltaos (1983) suggested the following empirical, logarithmic relationship for roughness which expanded beyond Nezhikhovskiy's suggestion that the roughness of the ice jam increased linearly with thickness:

$$f_i = \left[ 1.1.6 + 2 \log \left( \frac{R_i}{d_{i,84}} \right) \right]^2 \quad [2.30]$$

where  $d_{i,84}$  is the roughness value that exceeds 84% of the representative set of individual roughness values. Beltaos (1983) deduced the following empirical relationship for  $d_{i,84}$  using Nezhikhovskiy's field data:

$$d_{i,84} = 1.43 \left\{ 1 - e^{[-0.734(t-0.15)]} \right\} \quad [2.31]$$

Beltaos (1983) plotted  $d_{i,84}$  against thickness,  $t$ , and found the resulting curve to be similar in shape to the roughness-thickness relationship for log jams, presented by Kennedy, R.J. (1958). These roughness relationships provided the basis for Beltaos' friction factor which is used by the RIVJAM model.

Beltaos (1983) reiterated the complexities and inherent unpredictability associated with an ice jam, which makes it impossible to generate an all encompassing theory with respect to their analysis. However, he stated that the general acceptance towards the analysis of equilibrium ice jams as a solution to worse case scenarios, in the context of high water stages, appeared reasonable. Consequently, Beltaos (1983) developed a non-dimensional depth versus discharge relationship based on an equilibrium form of the jam stability equation ([2.23] without the cohesion term) where he assumed the depth of flow,  $h$ , under a jam to be:

$$h = \left[ \frac{q}{\sqrt{\frac{4gS_w}{f_o}}} \right]^{2/3} \quad [2.32]$$

where  $q$  is the unit discharge per width of the ice jam. By substituting equation [2.32] into the equilibrium jam stability equation [2.23] and neglecting the cohesion,  $C_i$ , Beltaos (1983) obtained (after some algebra):

$$t = \frac{WS_w}{2\mu(1-s_i)} \left\{ 1 + \left[ 1 + \frac{(2f_o)^{1/3} \mu(1-s_i)}{s_i} \left( \frac{f_i}{f_o} \right) \left( \frac{q^2}{gS_w} \right)^{1/3} \right]^{1/2} \right\} \quad [2.33]$$

From this relationship, Beltaos (1983) introduced the first non-dimensional depth versus discharge relationships for equilibrium ice jams. Beltaos (1983) used this relationship to plot idealized non-dimensional depth versus discharge curves to non-dimensional depth versus discharge values for ice jams observed in the field, and found that the observed data from equilibrium ice jams fell on or near these curves, and that the non-equilibrium ice jam data fell below the theoretical curves.

## 2.3 THE ICEJAM AND RIVJAM MODELS

### 2.3.1 Ice Jam Profiles

Break-up ice jams have been observed in the field and a "typical" idealized profile describing these ice jams commonly appears in the literature. The ICEJAM and RIVJAM one-dimensional numerical models compute ice jam profiles which resemble this profile. Figure 2.4 represents a schematic of the expected shape an ice jam would take given an adequate supply of fragmented ice under steady state

conditions. This type of profile could be expected to occur under the "wide" channel conditions described previously by Pariset, *et al.* (1966), and can be divided into four distinct regions: the *upstream transition*; an *equilibrium section*; the *downstream transition*; and a *toe region*. For limited supplies of ice, the ice jam depicted in Figure 2.4 may not achieve an equilibrium section.

The jam stability equation is applicable over the downstream transition, the equilibrium section, and the portion of the upstream transition which behaves as a "wide" channel ice jam. Often the upstream limit of this section is comprised of juxtaposed ice or hydraulically thickened ice which behaves according to the "narrow" channel jam criteria. Little is known about the toe region to date. However, the usual assumptions inherent in the jam stability relationships described above are not applicable in this region, due to the added resistance provided by the intact ice, and where grounded accumulations occur, contact of the ice accumulation with the bed.

### 2.3.2 The ICEJAM Model

#### 2.3.2.1 Flato, G. and Gerard R. (1986)

Flato and Gerard (1986) developed a computer program (ICEJAM) to solve a jam stability equation similar to that developed by Uzuner, *et al.* (1976) along with a gradually varied flow equation. The model was designed to compute the water surface and thickness profiles of a "wide" cohesionless non-equilibrium ice jam. In their model, the equations are solved using an iterative procedure where the solution to the gradually varied flow equation progresses in the upstream direction and the jam stability equation is solved by progressing in the downstream direction. A floating toe configuration is assumed and the model computes a characteristically linear shape through the toe region which is governed by a user-specified ice erosion criterion. Flato, *et al.* (1986) evaluated the model through application to a prismatic, rectangular channel which approximated the Mackenzie River at Norman Wells.

This model was developed as a research tool and was part of a M.Sc. thesis written by Greg Flato in the Department of Civil Engineering, University of Alberta. Flato's thesis, *Calculation of Ice Jam Profiles* (1988), and the conference paper by Flato, *et al.* (1986) represent the only publicly available documentation on this model. There has been no evolution of the ICEJAM model since its development, but the model continues to be used by other investigators (Gerard, Jasek, and Hicks 1992; Andres, 1996; Demuth, Hicks, Prowse, and McKay, 1996).

### 2.3.3 The RIVJAM Model

#### 2.3.3.1 Beltaos, S., Wong, J. (1986)

At about the same time the ICEJAM model was being developed, the numerical algorithms for the RIVJAM model were first being introduced by Beltaos and Wong (1986). Beltaos and Wong (1986) noted that the previous research had "*concentrated on predicting ice jam thickness and stage in the equilibrium reach [of an ice jam] with a satisfactory measure of success*". Beltaos and Wong (1986) combined the theories introduced by Pariset, *et al.* (1966) and Uzuner, *et al.* (1976) with equations of motion to develop three first-order differential equations and then solved them numerically. In addition, Beltaos and Wong (1986) developed a relationship to describe the flow through the interstices between ice floes, to allow for grounded ice accumulations.

The three differential equations developed were functions of three unknowns, namely: the slope of the water surface,  $S_w$ ; the submerged thickness of ice,  $t_s$ ; and the depth of flow below the ice cover,  $h$ . The numerical solution progressed only in the downstream direction, starting at equilibrium conditions to compute the ice jam profile for the downstream transition. Beltaos and Wong (1986) applied this numerical algorithm to two case studies (the Thames River, Ontario, and the Athabasca River, Alberta) and concluded that the application of the model "*resulted in plausible findings with regard to grounding of ice jams*".

### 2.3.3.2 *Beltaos, S. (1988)*

The non-dimensionalized depth versus discharge relationships developed by Beltaos (1983) were applied to a documented ice jam event which occurred on the Thames River, Ontario, in 1986, and Beltaos (1988) estimated that the jam strength parameter,  $\mu$ , was either 1.20 or 1.34 for this event, depending on the assumed value for roughness. Beltaos (1988) also investigated the decrease in the thickness downstream of the toe, and found that for the Thames River event it could be approximated by a linear relationship. "*Favorable weather conditions*" caused the January, 1986 Thames River ice jam event to freeze in place which enabled transverse thickness measurements to be taken at various locations along the length of the jam. Beltaos found that "*the thickness of the jam exhibited large variability across the river but without consistent trends*" and stipulated that "*in a crude way, this finding justified the theoretical assumption of lateral uniformity*" (Beltaos, 1988). This suggested that the one-dimensional analysis used by RIVJAM is justifiable.

### 2.3.3.3 *Beltaos, S. (1993)*

By approximating the slope of the water surface to the friction slope and neglecting changes in velocity heads, Beltaos (1993) reduced the three partial differential equations developed previously (Beltaos, and Wong 1986) into two first order partial differential equations. A one-dimensional model (RIVJAM) which assumes a "wide" cohesionless ice jam under steady state conditions was developed to solve these equations numerically. These first order equations were solved using a Runge-Kutta solution technique in a numerical subroutine called DVERK which was obtained from the Mathematical and Statistics Library (1980).

A major addition to the formulation of these equations was the inclusion of seepage through the interstices of the ice jam into the continuity equation. This allowed for the RIVJAM model to "predict" grounded toe conditions. The model computed in either the upstream or downstream directions from a known thickness and water level. This model was applied to three case studies (Thames River, 1986; Restigouche

River, 1988; and Rushoon River, 1989) and it was found that the RIVJAM model provided "*reasonably good predictions of the configuration of* [the ice jams it was applied to], *with appropriate choices of the model parameters*" (Beltaos, 1988). Beltaos indicated that the model was still in the testing phase and that more field data would assist in the development of the model and that the use of the model "*in a predictive mode should rely on prior calibration*" (Beltaos, 1988).

Until just recently, the 1988 paper represented the most current publicly available documentation for the RIVJAM model. A users manual for the RIVJAM model is expected to be released from the National Water Research Institute, Burlington, Ontario, this year. The evolutionary development of the RIVJAM model has been documented in the literature and has been tested against various case studies. The RIVJAM model is supported by the Federal government and is intended for practical use.

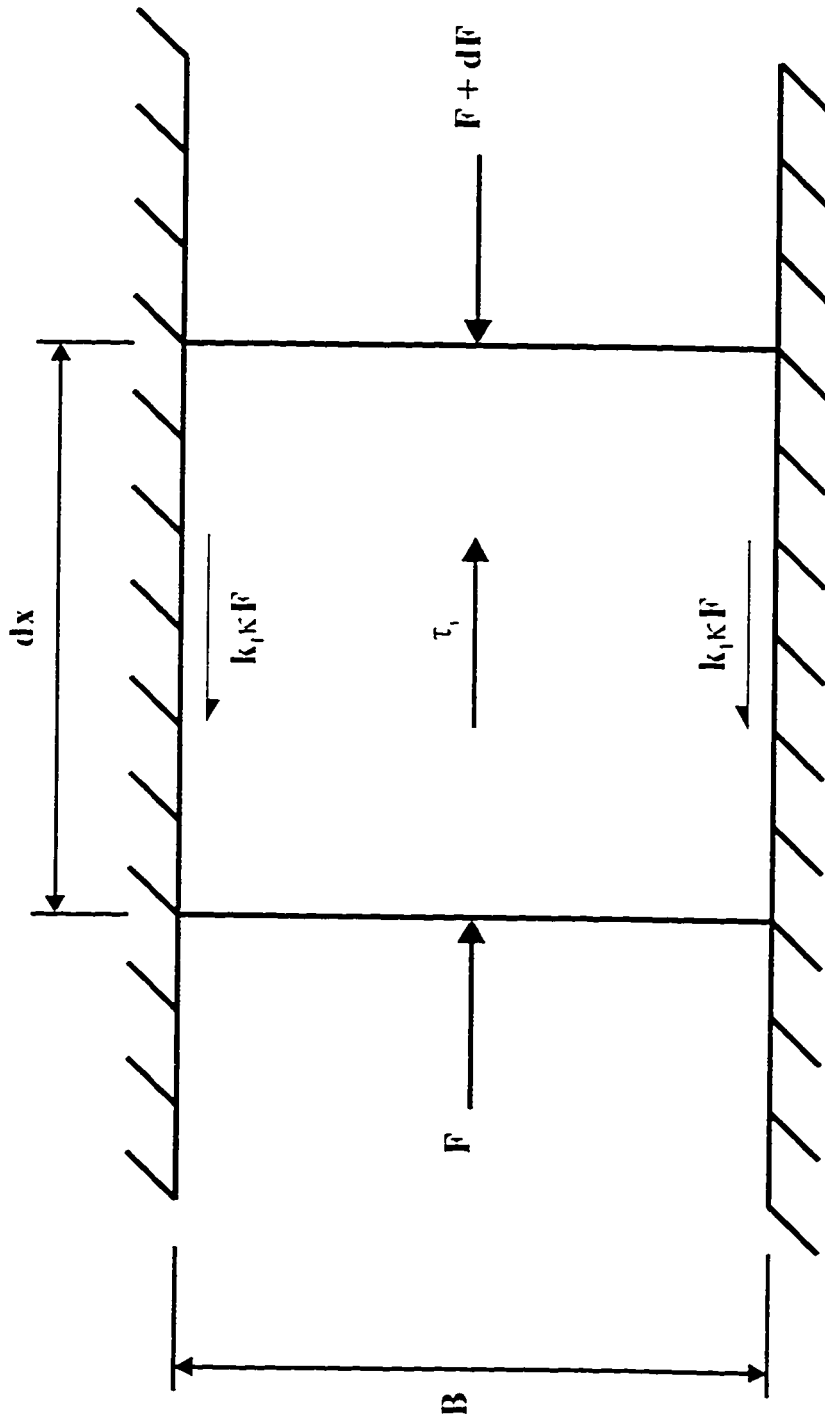


Figure 2.1 Plan view of stresses acting on a log jam element as described by Kennedy, (1958).

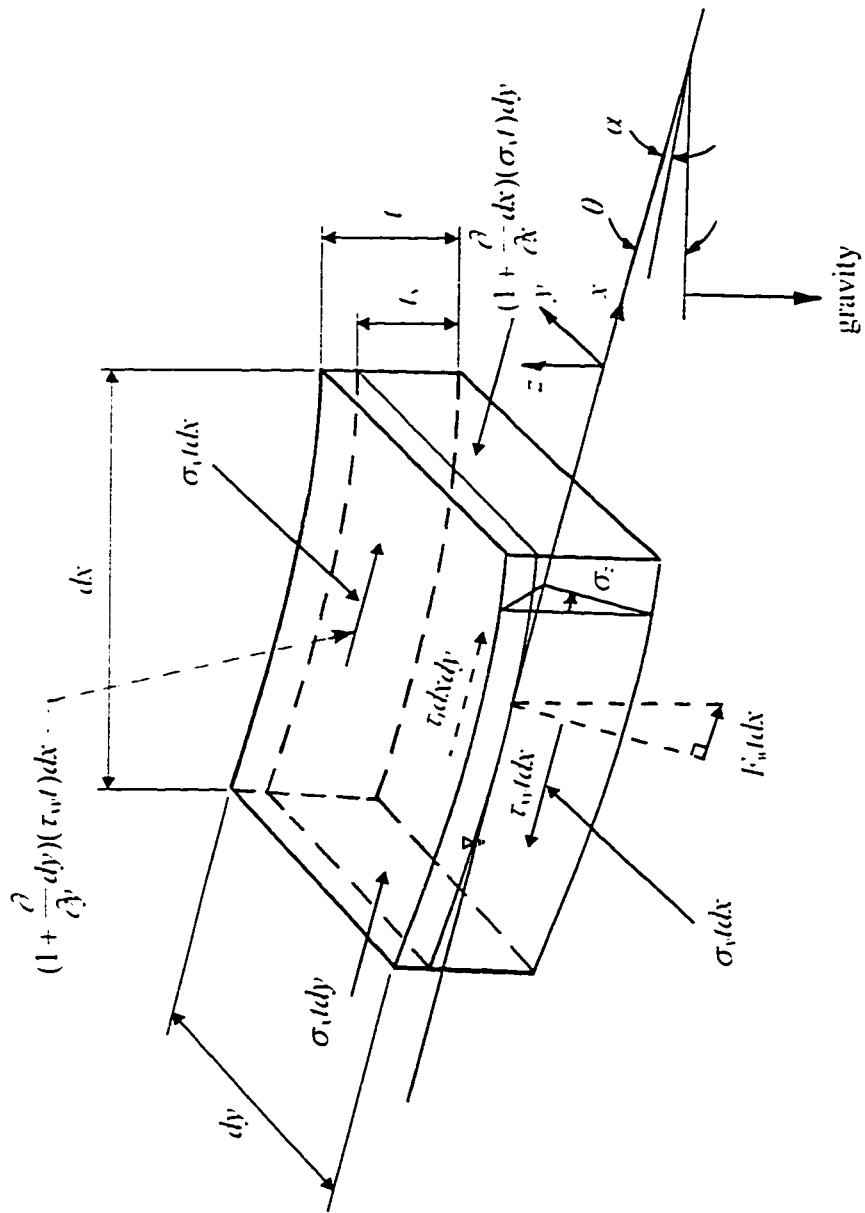


Figure 2.2 Control volume for an ice jam element as described by Uzuner and Kennedy (1976).



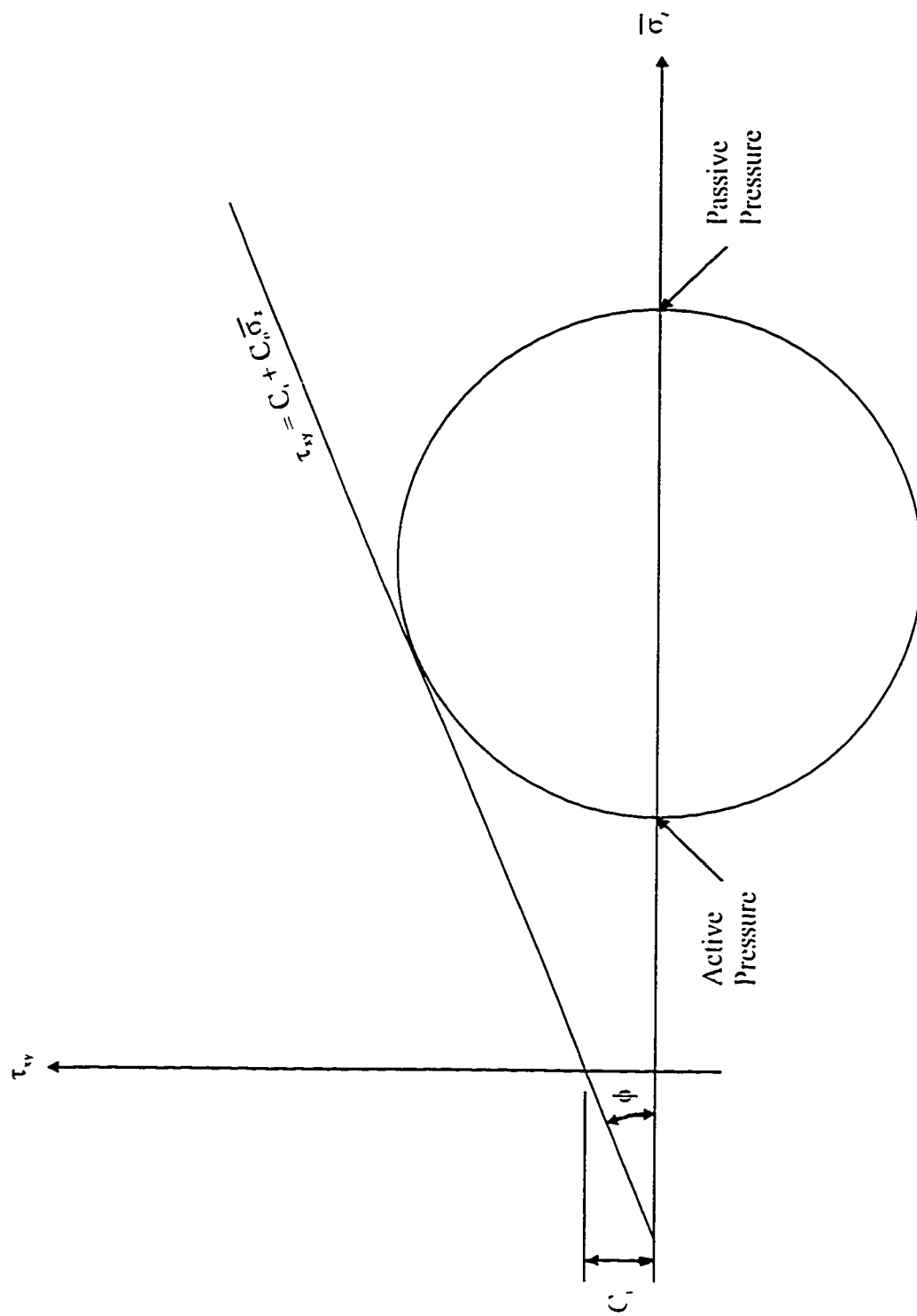


Figure 2.3 Mohr's circle for lateral stress.

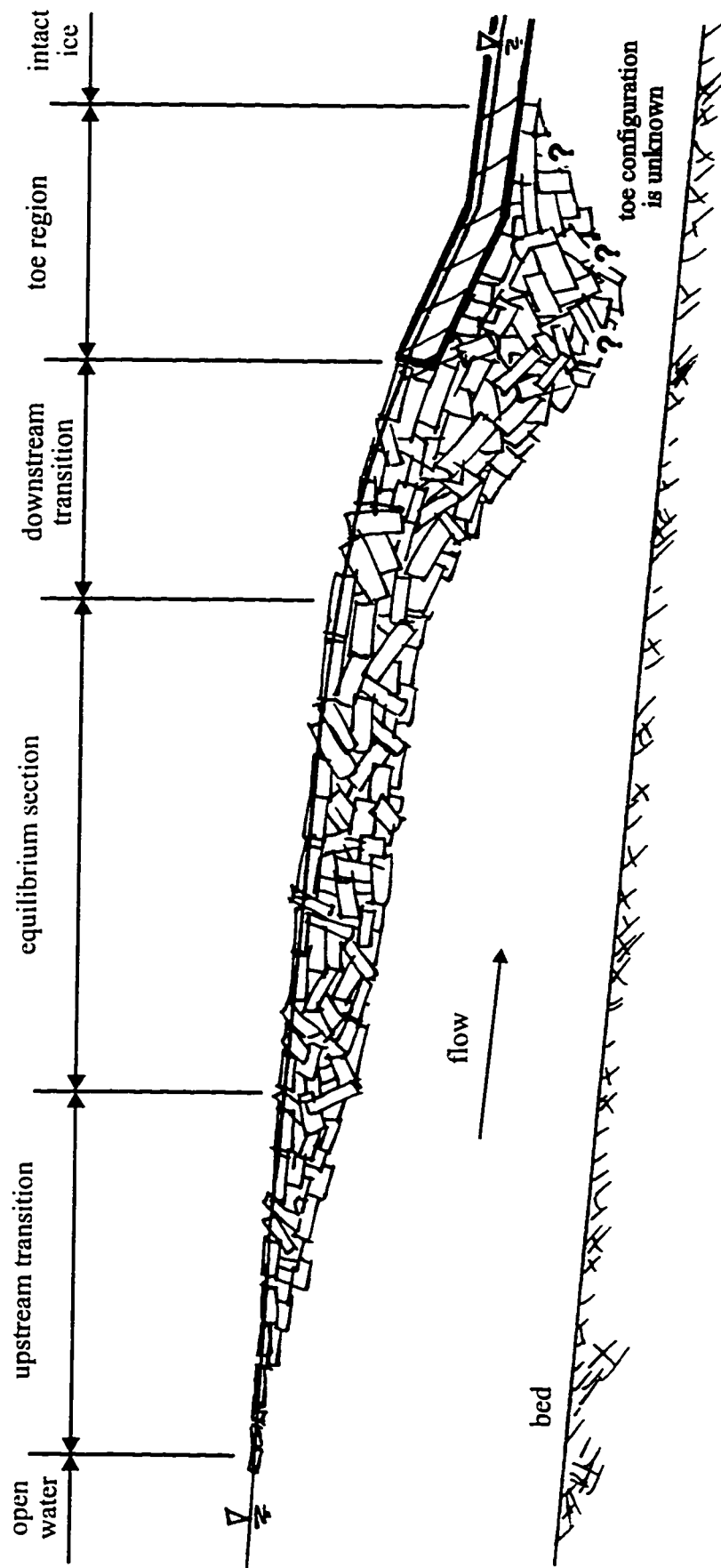


Figure 2.4 Ice jam schematic.

## CHAPTER 3.0 RIVJAM AND ICEJAM: MODEL FORMULATION AND IMPLEMENTATION

### 3.1 INTRODUCTION

A complete description of the formulation and implementation of the ICEJAM and RIVJAM numerical models provided a foundation for their direct comparison. After establishing the equivalency between the models formulations, the implementation features of these models was explored, while highlighting the similarities and differences between the models. A sensitivity of the boundary conditions, ice jam parameters, and channel geometry was also investigated.

### 3.2 EQUATION FORMULATIONS

#### 3.2.1 General

Chapter 2 provided a brief description of the development of the RIVJAM and ICEJAM numerical models and indicated the basis for their formulations. RIVJAM and ICEJAM use similar forms of the jam stability equation which was developed by previous investigators (Pariset, *et al.*, 1966; Uzuner, *et al.*, 1976), however, their gradually varied flow equations and methods for computing frictional resistance differs slightly. A detailed description of the models' formulations, which highlights their similarities and differences, is presented below to provide the basis for their direct comparison.

### 3.2.2 The RIVJAM formulation

The RIVJAM model (Beltaos, *et al.*, 1986; Beltaos, 1988, 1993) computes the longitudinal variation in ice thickness and water surface profile for a cohesionless, wide channel ice jam. RIVJAM also accounts for seepage through the fragmented ice cover which allows for flow through grounded accumulations of ice. The model combines the calculation of the longitudinal variation in jam thickness with the analysis of one dimensional, gradually varied flow under steady state conditions for open channels, resulting in a system of two ordinary differential equations: the first representing a relationship for jam stability; and the second representing a gradually varied flow approximation.

#### 3.2.2.1 The Jam Stability Equation

Through manipulation of the jam stability relationships developed by Uzuner, *et al.* (1976), Beltaos, *et al.* (1986) derived the following form of the jam stability equation:

$$\frac{dt_s}{dx} = \beta_1 \left[ \beta_2 \frac{f_o Q^2}{4gh^2 t_s} + S_w \right] - \beta_3 \frac{t_s}{B} \quad [3.1]$$

where:

$t_s$  is the submerged ice thickness;

$f_o$  is the composite friction factor for the flow under the jam;

$Q$  is the discharge flowing under the jam;

$S_w$  is the water surface slope;

$B$  is the width of the underside of the ice; and

$x$  represents the streamwise direction.

The three dimensionless coefficients,  $\beta_1$ ,  $\beta_2$  and  $\beta_3$ , are defined as:

$$\beta_1 = \frac{s_i^2 \gamma_w}{2 K_x \gamma_e} \quad [3.2]$$

$$\beta_2 = \frac{f_i}{2 f_o} \quad [3.3]$$

$$\beta_3 = \frac{C_o}{K_x} \quad [3.4]$$

where:

$s_i$  is the specific gravity of ice:

$\gamma_w$  is the unit weight of water:

$K_x$  is a coefficient of proportionality between the compressive "strength" of the jam and the thickness averaged, effective, vertical stress caused by buoyancy:

$C_o$  is a shear stress coefficient:

$f_i$  is the friction factor of the underside of the ice jam;

$f_o$  is the composite friction factor for the total flow beneath the floating cover; and

$\gamma_e$  is the effective unit weight of water, defined as:

$$\gamma_e = \frac{1}{2} \left( 1 - \frac{\rho_i}{\rho} \right) (1 - p) \rho_i g \cos \theta \quad [3.5]$$

where:

$\rho_i$  is the density of ice;

$\rho$  is the density of water:

$p$  is the porosity of the jam:

$g$  is the acceleration due to gravity: and

$\theta$  is the angle, degrees, of the downstream component of the weight of the jam with the horizontal. (This is a relatively small angle, so that  $\cos \theta \cong 1$ )

### 3.2.2.2 *Gradually Varied Flow*

For conservation of mass, which also accounts for flow through the voids, Beltaos, *et al.* (1986) specified that:

$$Q = Q_f + Q_p \quad [3.6]$$

where:

$Q$  is the total flow through the ice jam:

$Q_f$  is the flow under the floating accumulation of ice: and

$Q_p$  is the flow through the interstices within the ice accumulation.

Beltaos, *et al.* (1986) developed the following relationship to describe the flow through the interstices:

$$Q_p = \lambda A_j \sqrt{S_w} \quad [3.7]$$

where

$\lambda$  is a coefficient describing the flow through the voids in the ice cover; and

$A_j$  is the submerged cross sectional area of the ice jam.

For conservation of momentum under steady state conditions, Beltaos (1988) wrote:

$$S_w - \frac{\tau_i + \tau_b}{\rho gh} = - \frac{V^2}{Bgh} \frac{d(A_f)}{dx} \quad [3.8]$$

where:

$\tau_i$  is the shear stress on the ice underside;

$\tau_b$  is the shear stress on the bed;

$h$  is the depth of flow below the ice accumulation;

$V$  is the average velocity under the ice accumulation; and

$A_f$  is the area of flow under the ice accumulation.

Beltaos (1988) found the term on the right hand side of equation [3.8] to be less than 6% of  $S_w$  for a documented ice jam event on the Thames River and, therefore, neglected this term to approximate the surface water slope to:

$$S_w = \frac{\tau_i + \tau_b}{\rho gh} \quad [3.9]$$

In earlier work, Beltaos (1986) had defined the combined shear forces on the bed and the ice as:

$$\tau_i + \tau_b = \frac{f_o}{4} \rho V^2 \quad [3.10]$$

Combining equations [3.7], [3.9], and [3.10], Beltaos (1997) obtained the following approximation to the surface water slope:

$$S_w = \left[ \frac{Q}{A_f \sqrt{\frac{4}{f_o} g \frac{A_f}{B} + \lambda A_f}} \right]^2 \quad [3.11]$$

The elevation of the energy grade,  $H_T$ , at any point along an ice jam is:

$$H_T = z + h + t_s + \frac{V^2}{2g} \quad [3.12]$$

where  $z$  is the distance from the bed to a specified datum.

From this, the slope of the energy grade line,  $S_f$  (also known as the friction slope), for a gradually varied flow can then be written as:

$$S_f = -\frac{d}{dx}(H_T) = -\frac{d}{dx}\left(z + h + t_s + \frac{V^2}{2g}\right) \quad [3.13]$$

By definition, the slope of bed,  $S_o$ , is:

$$S_o = -\frac{dz}{dx} \quad [3.14]$$

By combining equations [3.13] and [3.14], neglecting the velocity head term in equation [3.13], and by approximating the water surface slope to the friction slope (i.e.  $S_w \cong S_f$ ), Beltaos, *et al.* (1986) wrote:

$$\frac{dh}{dx} = S_o - S_w - \frac{dt_s}{dx} \quad [3.15]$$

Substitution of equation [3.11] into equations [3.1] and [3.15], respectively, gives:

$$\frac{dt_s}{dx} = \beta_1 \left[ \beta_2 \frac{f_o Q^2}{4gh^2 t_s} + \left[ \frac{Q}{A_f \sqrt{\frac{4}{f_o} g \frac{A_f}{B} + \lambda A_j}} \right]^2 \right] - \beta_3 \frac{t_s}{B} \quad [3.16]$$



$$\frac{dh}{dx} = S_o - \frac{dt_s}{dx} - \left[ \frac{Q}{A_f \sqrt{\frac{4}{f_o} g \frac{A_f}{B} + \lambda A_f}} \right]^2 \quad [3.17]$$

All of the unknown terms in Equations [3.16] and [3.17] can be expressed in terms of  $t_s$  and  $h$ , and they represent the two ordinary differential equations which are solved by the RIVJAM model.

### 3.2.2.3 Frictional Resistance

Beltaos' composite friction factor,  $f_o$ , is based on an empirical relationship developed by Nezhikhovskiy (1964) who analyzed field data collected from freeze-up ice accumulations in the former Soviet Union. Beltaos (1993) writes this friction factor relationship as:

$$f_o = ct_i^{m_1} h^{-m_2} \quad [3.18]$$

where  $c$  is a dimensionless coefficient, and  $m_1$  and  $m_2$  are exponents.

This relationship indicates that the composite roughness pertaining to the flow under an ice jam is a function of the jam thickness and depth of flow beneath the cover. Details supporting the structure of equation [3.18] are presented by Beltaos (1997).

Beltaos (1989) suggested in an unpublished *quasi* users manual that, when the exponents  $m_1$  and  $m_2$  are set to zero and one third, respectively, equation [3.28] can be related to Mannings roughness as follows:

$$n_o = 0.10\sqrt{c} \quad [3.19]$$

To derive this relationship, Beltaos equated the friction slopes defined by Chezy's and Mannings equations in the following manner. First consider Chezy's equation written as:

$$V = C\sqrt{R_o S_f} \quad [3.20]$$

where:

$C$  is Chezys roughness coefficient; and

$R_o$  is the hydraulic radius corresponding to the composite flow, in m.

By defining Chezys  $C$  in terms of the friction factor,  $f_o$ , as:

$$C = \sqrt{\frac{8g}{f_o}} \quad [3.21]$$

so that the friction slope for Chezys equation becomes:

$$S_f = \frac{f_o V^2}{8gR_o} \quad [3.22]$$

the friction slope for Mannings equation is:

$$S_f = \frac{V^2 n_o^2}{R_o^{4/3}} \quad [3.23]$$

Combining Equations [3.22] and [3.23] gives:

$$n_o^2 = \frac{f_o R_o^{1/3}}{8g} \quad [3.24]$$

For wide ice covered rectangular channels, it is common to assume that the hydraulic radius is approximately equal to half of the hydraulic depth which is exactly equal to half of the depth of flow. Using this, equation [3.24] can be approximated by:

$$n_o^2 = \frac{f_o \left(\frac{h}{2}\right)^{1/3}}{8g} \quad [3.25]$$

By substituting Beltaos' friction factor (equation [3.18]) into equation [3.25],  
Mannings roughness can be written as:

$$n_o = \sqrt{\frac{ct_s^{m_1} h^{1/3}}{8g2^{1/3} h^{m_2}}} \quad [3.26]$$

Substituting  $9.806 \text{ m/s}^2$  for  $g$ , setting  $m_1 = 0$ , and  $m_2 = 1/3$ , Manning roughness can be approximated by:

$$n_o \cong 0.100586\sqrt{c} \quad [3.27]$$

Rounding to two decimal places gives equation [3.19] which applies for rectangular channels.

### 3.2.3 ICEJAM formulation

The ICEJAM model (Flato, *et al.*, 1986; Flato, 1988) was developed to calculate the thickness and water surface profiles for a cohesionless, wide channel ice jam with a floating toe (Flato, *et al.*, 1986). For this floating toe configuration, the "seepage" through the interstitial spaces in the ice cover is neglected (Flato, *et al.*, 1986). The model computes the longitudinal variation in ice jam thickness together with the one dimensional, steady, gradually varied flow, resulting in a system of two ordinary differential equations.

#### 3.2.3.1 The Jam Stability Equation

The development of the jam stability equation in ICEJAM closely follows those theories presented by Pariset, *et al.* (1966) and in particular, Uzuner, *et al.* (1976). However, the shear stress at the banks is treated in a slightly different manner than presented by Uzuner, *et al.* (1976). Flato, *et al.* (1986) defined the shear stress at the banks,  $\tau_o$ , as,

$$\tau_o = \sigma_y \tan \delta \quad [3.28]$$

where:

$\sigma_y$  is the thickness averaged transverse stress; and

$\delta$  is the angle of friction in degrees between the ice accumulation and the bank.

They also used the relationship between the streamwise and transverse stress presented by Pariset, *et al.* (1966):

$$\sigma_y = K_{xy} \sigma_x \quad [3.29]$$

where  $K_{xy}$  is an empirical lateral stress coefficient that is less than or equal to one.

Using Mohr's circle, Flato, *et al.* (1986) showed that:

$$K_{xy} = \frac{1 - \sin^2 \phi}{1 + \sin^2 \phi} \quad [3.30]$$

where  $\phi$  is the shearing angle in degrees.

Approximating  $\delta$  with  $\phi$ , and using Equations [3.28] and [3.29], Flato, *et al.* (1986)

developed the following form of the jam stability equation:

$$\frac{dt}{dx} = \frac{\tau_i}{2K_v \gamma_e t} + \frac{\rho_i g S_w}{2K_v \gamma_e} - \frac{K_{xy} t \tan \phi}{B} \quad [3.31]$$

where:

$t$  is the ice thickness; and

$K_v$  is a passive pressure coefficient following Rakine's theory of earth pressure.

### 3.2.3.2 Gradually Varied Flow

For the gradually varied flow analysis, Flato (1988) uses Chezys equation [3.20] and defines Chezys roughness,  $C$ , as:

$$C^2 = g \left[ 2.5 \ln \left( \frac{R_o}{k_o} \right) + 6.2 \right]^2 \quad [3.32]$$

Substituting equation [3.32] into Chezy's equation gives for the friction slope:

$$S_f = \frac{d}{dx}(H_f) = \frac{V^2}{\left[ 2.5 \ln \left( \frac{R_o}{k_o} \right) + 6.2 \right]^2 g R_o} \quad [3.33]$$

where  $k_o$  is the composite roughness height, in m. Equations [3.31] and [3.33] are two first order differential equations which are solved by the ICEJAM model.

### 3.2.3.3 Frictional Resistance

As is evident in equation [3.33], the ICEJAM model utilizes an absolute roughness height,  $k_o$ , to represent the resistance to flow. This composite roughness height,  $k_o$ , represents the combined roughness of the ice underside,  $k_i$ , and of the bed,  $k_b$ . The ICEJAM model uses the following Sabenev's relationship to calculate composite roughness:

$$k_o = \left[ \frac{k_i^{1/4} + k_b^{1/4}}{2} \right]^4 \quad [3.34]$$

## 3.4.2 Equivalency of RIVJAM and ICEJAM Formulations

The jam stability equation developed by Beltaos, *et al.* (1986) for the RIVJAM model can be rearranged to:

$$\frac{dt}{dx} = \frac{\tau_i}{2K_x \gamma_e t} + \frac{\rho_i g S_w}{2K_x \gamma_e} - \frac{C_{of}}{K_x B} \quad [3.35]$$

The jam stability equation for the ICEJAM model is rewritten here for comparison:

$$\frac{dt}{dx} = \frac{\tau_i}{2K_v \gamma_e t} + \frac{\rho_i g S_w}{2K_v \gamma_e} - \frac{K_{xy} t \tan \phi}{B} \quad [3.36]$$

Coincidence between equations [3.35] and [3.36] is found when  $\frac{K_x}{K_v} = 1$ ,  $K_v K_{xy} = 1$  and  $\tan \phi = C_o$ . As parameters such as  $C_o$ ,  $K_x$ ,  $K_v$ ,  $p$ , and  $\phi$  are difficult to measure directly in the field, it has become generally accepted to group such parameters together into one single jam strength parameter. This parameter, generally referred to as  $\mu$ , was first introduced by Pariset, *et al.* (1966), and has often been used to describe the relative strength of ice accumulations. Its value, obtained indirectly from documented ice jams, has been found to range from 0.6 to 3.5, with values between 0.8 and 1.2 considered most realistic (Ashton, 1986; Beltaos, 1983). Flato, *et al.* (1986) and Beltaos, *et al.* (1986) presented their definitions of  $\mu$ , respectively, as:

$$\mu = K_v K_{xy} \tan \phi (1 - p) . \quad [3.37]$$

and

$$\mu = C_o (1 - p) . \quad [3.38]$$

Again, coincidence between equations [3.35] and [3.36] can be found through substitution of the corresponding definitions of  $\mu$ , provided these definitions of  $\mu$  are considered equivalent.

### 3.3 MODEL IMPLEMENTATION

#### 3.3.1 Introduction

This section is designed to present in a detailed manner, the methods used by the models to implement their formulations described above. The objective of both models is to compute an ice jam profile given information on channel geometry, discharge, roughness, and ice jam characteristics. They both solve similar forms of

the jam stability and gradually varied flow equations using numerical approximations to differential equations. Although the solutions obtained by both models are similar, the means by which they are solved are different. A detailed presentation of the solution techniques used by the models and the impact of varied input to each model is investigated to establish more concretely, *how these models are similar*, and *how these models are different*.

### **3.3.2 Boundary and Toe Conditions**

#### ***3.3.2.1 Theoretical Boundary Conditions and Solution Progression***

Both models require two boundary conditions for their respective solutions of the jam stability and gradually varied flow equations. Flato, *et al.* (1986) suggested that the physics inherent in equations [3.31] and [3.33] would imply that an iterative solution which solves the gradually varied flow equation in the upstream direction and the jam stability equation in the downstream direction would be most appropriate.

*“As is familiar from regular open channel hydraulics, for a [subcritical flow] the appropriate location for the necessary initial condition for [the gradually varied flow equation] is at a downstream control... However, from the physics of the problem it is evident that the appropriate initial condition for [the jam stability equation] is at the upstream end of the accumulation”* (Flato, *et al.*, 1986).

This would imply that the appropriate boundary conditions for the problem would be a known downstream water level and a known upstream ice thickness. Although the validity of the former boundary condition is well established in the open channel flow literature, no proof of the assertion that the jam stability equation should proceed from a known upstream boundary condition has been developed to date. However, empirical evidence supporting Flato, *et al.* (1986) assertion has been presented by Zufelt (1996) based on results from his unsteady flow ice jam modelling efforts.

*"This study found, however, that well behaved solutions only occurred for integration in the downstream direction, given a thickness relation for the upstream boundary "* (Zufelt, 1996).

### **3.3.2.2 Special Considerations at the Ice Jam Toe**

In considering the application of these models, it is important to note that some of the basic assumptions inherent within the jam stability equation no longer apply within the toe region. More specifically, the downward thrust is no longer absorbed solely by the resistance at the banks. Much of the resistance is supplied by the obstruction (solid intact ice sheet) or by portions of the bed (in particular for grounded accumulations). Also, for a grounded accumulation, where the ice floes are in direct contact with the bed, the thickness averaged vertical stress is no longer due to buoyancy alone (the usual assumption).

Figure 3.1 depicts a schematic of the toe region and suggests the existence of a downstream limit for the region in which the jam stability equation applies (interface A-A). The RIVJAM model does not attempt to compute downstream of point A-A, where additional frictional resistance becomes available at the bottom of the ice sheet, leading to a gradual decrease and disappearance of the rubble thickness. Though Figure 3.1 depicts a "floating toe" condition, grounding (characterized by a jam thickness that extends to the river bed) may occur at or upstream of A-A. In such cases, RIVJAM will only compute as far downstream as the point of grounding. The ICEJAM model, on the other hand, stipulates that all ice jams have a floating toe, and computes the entire profile by making the following two assumptions.

1. There is a region under the sheet ice where the thickness decreases in such a manner that the flow velocity under the rubble is equal to a user-specified value, the "erosion" velocity as discussed below (the rubble thickness is now less than would be dictated by the stability equations [3.1, 3.31]).
2. The solid intact ice sheet compensates for the reduction in strength of the accumulation due to a decrease in thickness by the reactive force normal to the



vertical face of the intact ice sheet and by additional frictional resistance between the underside of the intact ice cover and ice rubble.

These assumptions in ICEJAM result in a characteristically linear water surface profile downstream of point A-A, joined rather abruptly to the curved, M-2 type of profile that prevails upstream of A-A.

A floating toe configuration is assumed by ICEJAM and the toe configuration is approximated by assuming that the thickness is governed by an "erosion velocity",  $V_{max}$ , which is the maximum velocity the accumulation at the toe can withstand before individual floes are swept downstream. This approach assumes that no scour will occur on the bed. As mentioned previously, when this erosion velocity is exceeded, the flow depth below the cover is increased through the reduction of the computed ice jam thickness using the jam stability equation, so as to reduce the velocity to  $V_{max}$ . Thus the cover is effectively floated upwards to accommodate the flow. When the velocity determined below the cover is less than  $V_{max}$ , the usual form of the jam stability equation, coupled with a gradually varied flow equation, is used to compute the jam profile. The location at which the  $V_{max}$  criterion is no longer exceeded corresponds to interface A-A in Figure 3.1, and can usually be recognized by a distinct change in slope of the computed water surface profile.

### **3.3.2.3 ICEJAM Boundary Conditions**

The two boundary conditions which must be specified for the ICEJAM model simulation, are the ice thickness at the upstream end of the ice accumulation and the thickness of the solid intact ice at the boundary downstream of the toe, consistent with the theoretical considerations presented by Flato, *et al.* (1986). The water level at this boundary is calculated automatically by ICEJAM through a simple uniform flow depth calculation based on the user-specified thickness of the intact ice cover downstream of the jam. The user can also override this automated feature and set this downstream water level to a specified elevation. This water level represents the initial condition used for the solution of the gradually varied flow equation. The

thickness at the upstream end of the accumulation is used to approximate the initial ice jam thickness profile and provides the initial condition required for the computation of the ice jam thickness, progressing in the upstream direction using the jam stability equation.

#### ***3.3.2.4 RIVJAM Boundary Conditions***

The RIVJAM model also requires two input boundary conditions: the flow depth and the thickness of the ice at the starting point of the calculations which is typically at the downstream end of the modelled accumulation. The downstream starting point does not necessarily have to be located at the furthest downstream point where the jam stability equation applies (interface A-A in Figure 3.1). However, it should not be downstream of this point, as discussed earlier. For most applications or calibrations to measured data, it is recommended that the downstream boundary be set to match a measured or known water level upstream or at interface A-A.

#### ***3.3.2.4 Implications to Modelled Ice Jam Length***

The difference in the required boundary conditions for the two models means that the size (or the length) of the modelled ice jam is controlled differently in each case. Since the ICEJAM model requires a specified thickness and corresponding water level downstream of the toe and an ice thickness at the head of the accumulation, the length of the jam is essentially predetermined by the user. In the RIVJAM model both boundary conditions are specified at the downstream point in the modelled reach (which may, in fact, be within the ice jam as mentioned earlier). Therefore, for the RIVJAM model, the volume of ice (and therefore the length of the accumulation) is controlled primarily by the thickness specified at the (downstream) starting point. Essentially this means that the length of the jam is an “output” in RIVJAM if this downstream thickness is known. If this point is at the jam toe, then the thickness is generally an estimate which is adjusted to produce a jam of the correct size.

For the RIVJAM model, the “equilibrium jam” (theoretically, an infinitely long jam of constant thickness except near the toe and head) profile can be determined by specifying increasing ice thicknesses at the toe until the model “blows up”, (i.e. produces a continuously diverging solution). Then the equilibrium jam profile is that produced by the maximum toe thickness which provides a physically realistic ice jam profile.

### **3.3.3 Solution Methodology**

#### ***3.3.3.1 RIVJAM Solution Methodology***

As discussed earlier, the RIVJAM model is based on a gradually varied flow approximation which neglects the gradient in the velocity head term (equation [3.17]). This simplified gradually varied flow equation is coupled with the ice jam stability equation [3.16] providing a system of two equations for the unknown ice thickness and flow depth which are solved together using a Runge-Kutta solution sub-routine obtained from the International Mathematical and Statistical Libraries (1980). This explicit technique facilitates the simultaneous solution of equations [3.16] and [3.17] as all of the unknowns can be expressed in terms of only two variables, specifically the submerged ice thickness,  $t_s$ , and depth of flow below the cover,  $h$ . The RIVJAM model has been set up such that the user can choose for the calculations to proceed in either the upstream or the downstream direction (Beltaos, 1993). However, as discussed above, it is not theoretically correct to compute the solution of a subcritical gradually varied flow profile in the downstream direction as subcritical flow is controlled from downstream. Therefore, it is recommended that the RIVJAM option to compute ice jam profiles in the downstream direction not be selected.

#### ***3.3.3.2 ICEJAM Solution Methodology***

In the ICEJAM model a sequential, iterative solution of the ice jam stability and gradually varied flow equations is employed (equations [3.31] and [3.33]). The accumulation thickness along the entire length of the ice jam is initially assumed to be

equal to the upstream boundary thickness specified by the user, and a gradually varied flow profile is calculated progressing in the upstream direction from a known downstream water level. Using the water surface profile just calculated, the ice jam stability equation [3.31] is then solved by stepping from the head of the jam to the toe, computing the thickness required to satisfy jam stability without regard to the depth of flow and consequently the under ice *erosion* velocity,  $V_{max}$ . This new ice thickness configuration is then used to compute a new gradually varied flow profile stepping in the upstream direction. During this computational “sweep”, the depth of flow that corresponds to the ice jam thickness that was computed during the previous downstream “sweep” is checked against the minimum depth of flow required to satisfy the maximum allowable erosion velocity criteria. If this criteria is not satisfied the ice thickness is reduced to satisfy the erosion velocity constraint.

*“It is presumed that the streamwise resistance lost by this reduction in thickness can be provided by the solid ice sheet, and the shear between the accumulation and the underside of the solid ice...Hence the end of the solid ice must be near the section where no reduction in the accumulation thickness is required to satisfy the erosion velocity constraint...In other words, the thickness in the downstream transition region is governed by [the jam stability equation] while that in the toe region is governed by the gradually varied flow profile and the [maximum allowable] erosion velocity” (Flato, et al., 1986).*

This iterative process is repeated until the solution converges to a user specified tolerance. In order to facilitate convergence of the solution, an under-relaxation approach is employed after the fifth iteration which limits the change in the magnitude of ice jam thickness to one third of that just computed between iterations.

### **3.3.3.3 Similarity of RIVJAM and ICEJAM Solution Methodologies**

Although the equivalency of the two jam stability *equation formulations* has been established, it was desirable to determine whether the different solution

methodologies and boundary conditions had any significant impact on the results obtained with the two models. To overcome the slight differences that were expected to occur due to the different interpolation techniques used by each model for a natural (irregular) channel, an idealized channel was used. It was based on the Restigouche River case study, as the Restigouche River is considered "*representative of northern Canadian conditions, i.e. large streams subjected to a single breakup event each year... The stream size, though moderate by comparison to that of the Mackenzie or the Peace, combines with its considerable slope to produce very thick ice jams and serious flooding*" (Beltaos and Burrell, 1990). A trapezoidal channel with a constant base width of 150 m, a 2:1 side slope, and a bed slope of 0.0008 was used. The discharge for these tests was set to 300 m<sup>3</sup>/s which was close to the recorded discharge for the 1988 ice jam event on the Restigouche River (Beltaos, and Burrell (1990). To ensure that only the effects of the solution methodology and boundary conditions were being compared, the ICEJAM model was modified to accept RIVJAM's jam stability equation [3.1]. As the models handle the toe conditions differently, the downstream boundary for both models had to be adjusted so as to match the furthest downstream point where the jam stability equation governed (interface A-A in Figure 3.1). This was done by first running the ICEJAM model and examining the computed velocities to determine the most downstream point where the velocity was below  $V_{max}$ , and hence the point where the ice jam stability equation took over the calculations. The ice thickness and flow depth computed by the ICEJAM model at this location were then used as the input boundary conditions for the RIVJAM model. As the flow equations used in ICEJAM do not account for seepage, the seepage coefficient,  $\lambda$ , for RIVJAM was set to zero. Because the ICEJAM simulation requires that the upstream ice thickness be specified as a boundary condition, the upstream ice thickness computed from the RIVJAM simulation then had to be used as an input to the ICEJAM model to determine the final profile for comparison to the RIVJAM model's test results.

Figure 3.2 presents the toe region of the profiles obtained by this method. The results obtained for the two solution methodologies are quite close. The maximum difference in computed ice thickness computed between the two models was 2.1% and the maximum difference in depth was 0.5%. This indicates that the simplification to the gradually varied flow analysis in the RIVJAM model is justified (at least in this case) and that the decoupled solution used in the ICEJAM model is not a disadvantage.

### 3.3.4 Additional Implementation Features

#### 3.3.4.1 Flow Through Interstices

Prior to laboratory investigations conducted by Wong, Beltaos, and Krishnappan (1985) and the analysis of Beltaos, *et al.* (1986) described herein, the seepage through the fragmented ice accumulation was assumed to be negligible. However, this assumption leads to implausibly large or even infinite flow velocities where the jam is so thick that it is partly or fully grounded. As grounded jams are known to occur naturally, especially near the toe, Beltaos sought to describe the flow through the interstitial spaces of the rubble, which would represent the main portion of the discharge through the toe region of a grounded accumulation. The relationship used to describe the flow through the voids, developed by Beltaos, *et al.* (1986) is written again as:

$$Q_p = \lambda A_j \sqrt{S_w} \quad [3.7]$$

#### 3.3.4.2 Geometry Interpolation

No interpolation of channel geometry or cross section properties is provided in the ICEJAM model. Therefore, the spatial discretization is dependent upon the location of the input cross sections. This is a limiting feature in practical applications as the spacing between surveyed cross sections is seldom adequate in terms of the spatial discretization required to resolve the computed profile. Therefore, for this study a

preprocessing program (Appendix A) was developed to calculate interpolated cross sections from the available surveys which could then be used as input to the ICEJAM model.

The addition of interpolated cross sections to RIVJAM's input file is not necessary as the model automatically interpolates between the cross sections given in the input file.

*"The step length of computation,  $\Delta x$ , is selected automatically, based on user-specified tolerances for the changes in  $t_s$  and  $h$ "* (Beltaos, 1997). The cross section properties are then interpolated linearly between sections by the solution routine, allowing the spatial discretization to be refined in regions where solution variables are changing rapidly.

### **3.3.5 Model Input Requirements**

#### ***3.3.5.1 Introduction***

Details on the format requirements for the input files required by RIVJAM are available in a users manual which is expected to be published this year (1997). Formats for the input files required by the ICEJAM model (along with sample input data files) are provided in a Masters thesis by Greg Flato (1988). Essentially, both models require parameter input information and channel geometry information.

#### ***3.3.5.2 RIVJAM Input Requirements***

The RIVJAM model requires two data files: the first file being a cross section data input file; and the second being a parameter input file. The original version of RIVJAM requires the cross sectional data to be in a standard HEC-2 file format, while the most recent version of RIVJAM, which utilizes a so called "user-friendly" DOS shell interface, requires the cross sectional data to be in a slightly different format. The solution techniques of both versions are identical, however it was found to be more expedient to use the original version for the analysis. The parameter input file includes: the boundary condition parameters; the input parameters required to

solve the jam stability and gradually varied flow equations; and the convergence criteria parameters required by the Runge-Kutta solution algorithm. A descriptive list of the boundary conditions, and input parameters of primary importance included in the RIVJAM input file is provided in Table 3.1.

### ***3.3.5.3 ICEJAM Input Requirements***

The ICEJAM model requires a single data file which includes both parameter and cross sectional data. This input file includes: the boundary condition parameters: the input parameters required to solve the jam stability and gradually varied flow equations; and a parameter for convergence criteria. A descriptive list of the boundary conditions, and input parameters of primary importance included in the ICEJAM input file is illustrated in Table 3.2.

## **3.4 MODEL SENSITIVITY**

### **3.4.1 Introduction**

Many of the input parameters required by these two models are difficult, if not impossible, to quantify based on field measurements. Direct measurement techniques do not exist for many of the ice jam characteristics, and also because it is often unsafe to make direct measurements on river ice jams. For these reasons, it was desirable to carry out a sensitivity analysis on the various input parameters in order to determine which could reasonably be left constant during calibration efforts, effectively reducing the number of calibration parameters. This sensitivity analysis also afforded the opportunity to develop an understanding of the relative behaviour of these two models, and to establish the relative importance of physical versus numerical sensitivity, in the case of the RIVJAM model.



Table 3.1 Input parameters for the RIVJAM model.

| Symbol        | Parameter                         | Description   |
|---------------|-----------------------------------|---|
| $Q$           | discharge ( $m^3/s$ )             | Total discharge beneath and through the ice accumulation.   |
| $C_o$         | internal strength coefficient     | Analogous to Mohr Coloumb internal friction constant which is equivalent to $\mu/(1-p)$ .   |
| $K_x$         | internal strength coefficient     | Coefficient of proportionality between the compressive strength of the jam and the thickness averaged, effective, vertical stress caused by buoyancy. |
| $s_i$         | specific gravity of ice           | Specific gravity of ice.  |
| $\gamma$      | unit weight of water ( $N/m^3$ )  | Unit weight of water.   |
| $p$           | porosity                          | Porosity of the ice accumulation which is assumed equivalent above and below the phreatic surface.  |
| $\lambda$     | seepage parameter ( $m \cdot s$ ) | Constant used to determine the flow through the interstices.  |
| $\beta_2$     | ice to bed roughness ratio        | Equivalent to the friction factor of the underside of the jam divided by twice the composite friction factor, $f_i/(2f_o)$ .                          |
| $c$           | hydraulic resistance coefficient  | Semi-empirical friction factor coefficient used to define the composite friction factor, $f_o$ .  |
| $m_1$         | hydraulic resistance exponent     | Semi-empirical friction factor exponent used to define the composite friction factor, $f_o$ .   |
| $m_2$         | hydraulic resistance exponent     | Semi-empirical friction factor exponent used to define the composite friction factor, $f_o$ .   |
| $x_{so}$      | starting point of computation     | First computational node used for computation.  |
| <i>SLOPEO</i> | slope of slope-line               | Slope of the slope-line which passes through the first station identified in the cross section input file.  |
| $t_{so}$      | submerged ice jam thickness (m)   | Boundary condition for first computational node.  |
| $h_{so}$      | slope-line depth (m)              | Boundary condition for first computational node.  |

NOTE: Parameters are dimensionless unless otherwise stated.

Table 3.2 Input parameters for the ICEJAM model.

| Symbol     | Parameter                                      | Description   |
|------------|--|---|
| $Q$        | discharge ( $m^3/s$ )                          | Total discharge beneath the ice accumulation.   |
| $\tan\phi$ | tangent of the shearing angle, $\phi$          | Coefficient that is analogous to Mohr Coloumb internal friction constant, $C_o$ .   |
| $K_v$      | internal strength coefficient                  | Coefficient of proportionality between the compressive strength of the jam and the thickness averaged, effective, vertical stress caused by buoyancy (analogous to the passive pressure coefficient used in Rankine's theory).  |
| $K_{xy}$   | internal lateral stress coefficient            | Empirical lateral stress coefficient taken to be less than or equal to one (as defined by Pariset, <i>et al.</i> (1966)).   |
| $\rho_i$   | ice density ( $kg/m^3$ )                       | Density of ice.   |
| $p$        | porosity                                       | Porosity of the ice accumulation which is assumed equivalent above and below the phreatic surface.  |
| $k_b$      | roughness height (m)                           | $k$ which applies to the bed influence portion of the flow.   |
| $k_i$      | roughness height (m)                           | $k$ which applies to the ice influenced portion of the flow.  |
| WLTD       | water elevation at the downstream boundary (m) | The user specified downstream boundary condition for the elevation of the water level at the first computational node (solid intact ice sheet), when set to zero this elevation is automatically calculated based on a simple normal depth computation based on $l_{ioe}$ . |
| $V_{max}$  | maximum under ice velocity (m/s)               | The maximum user specified average under ice velocity.  |
| $l_{ioe}$  | thickness of intact ice at d/s boundary (m)    | Boundary condition for first computational node which represents conceptually, the thickness of the intact solid ice sheet at the downstream limit of the jam.  |
| $l_{head}$ | thickness of ice at the head (m)               | Boundary condition for the ice thickness at the head of the jam   |

NOTE: Parameters are dimensionless unless otherwise stated.

The sensitivity analysis was designed to investigate three categories of model input, specifically: boundary conditions; ice jam parameters; and channel geometry. The idealized trapezoidal channel, used to illustrate the similarities between the two models' solution methodologies, was again used for this sensitivity analysis. Only those parameters which would be varied during a calibration effort were varied.

It was considered desirable to consider a similar "default ice jam" for both models and for the various friction slope equations investigated. A non-equilibrium jam was selected for the analysis, as it was found that the model results exhibited greater sensitivity for non-equilibrium jams than for equilibrium jams. It was not possible to achieve completely identical ice jams by the various methods because of model sensitivity to the choice of friction equation and solution methodology. Therefore, a series of runs was first conducted to establish "default ice jams" based on the criteria that jam length and ice volume should be as consistent as possible. A set of "default parameters" were established for both models to provide a baseline for comparison of the effect of each parameter's variation. These default parameters, listed in Table 3.3, were selected based on ranges of values observed in the field or corresponded to values recommended by the models' developers. Figure 3.3 illustrates the three "default jam" profiles computed by ICEJAM and RIVJAM using these default parameters. The first ice jam profile, computed with the RIVJAM model using Beltaos' friction factor, had a computed ice volume of 810,000 m<sup>3</sup>. The second ice jam profile, computed with the ICEJAM model using the Chezy equation, had a computed ice volume of 830,000 m<sup>3</sup>. The third and final ice jam profile, computed with the ICEJAM model using Mannings equation, had a computed ice volume of 750,000 m<sup>3</sup>.

Table 3.3 Default input parameters for the sensitivity analysis.

| RIVJAM default parameters |                         |                               | ICFJAM default parameters |                       |  |
|---------------------------|-------------------------|-------------------------------|---------------------------|-----------------------|--|
| Symbol                    | Default Value           | Description                   | Symbol                    | Default Value         | Description  |
| $Q$                       | 330 m <sup>3</sup> /s   | discharge                     | $Q$                       | 330 m <sup>3</sup> /s | discharge  |
| $C_o$                     | 1.67                    | internal strength coefficient | $\tan\phi$                | 1.67                  | tan of shearing angle  |
| $K_x$                     | 10                      | internal strength coefficient | $K_v$                     | 10                    | internal strength coefficient  |
| $s_i$                     | 0.92                    | specific gravity of ice       | $K_{sy}$                  | 0.10                  | internal strength coefficient  |
| $\gamma$                  | 9.806 kN/m <sup>2</sup> | unit weight of water          | $\rho_i$                  | 920 kg/m <sup>3</sup> | density of ice   |
| $P$                       | 0.4                     | porosity                      | $p$                       | 0.4                   | porosity   |
| $\lambda$                 | 1.75 m/s                | seepage velocity              | $V_{max}$                 | 1.50 m/s              | erosion velocity   |
| $\beta_2$                 | 0.5                     | roughness ratio, $f_1/2f_o$   | $n_b$                     | 0.045                 | bed roughness  |
| $c$                       | 0.40                    | friction factor coefficient   | $n_i$                     | 0.045                 | ice roughness  |
| $m_1$                     | 1                       | friction factor exponent      | $k_b$                     | 1.20 m                | bed roughness  |
| $m_2$                     | 1                       | friction factor exponent      | $k_i$                     | 1.20 m                | ice roughness  |
| <i>SLOPEO</i>             | 0.0008                  | slope of the slope-line       | <i>WLTD</i>               | 0                     | specifies auto-calculation of water level at the downstream boundary |
| $l_{so}$                  | 3.20 m                  | thickness at the toe          | $l_{toe}$                 | 1.00 m                | thickness of intact ice at the toe                                   |
| $h_{so}$                  | 1.70 m                  | slope line depth              | $l_{head}$                | 0.10 m                | thickness of ice at the head   |

In order to quantify the effects of parameter variation in this sensitivity analysis, the computed flow depth under the ice jam and the computed ice thickness values were compared at a representative point within the jam. When expressed as percentages, these variations were referenced to the largest computed values at this representative section (i.e. based on the results for the parameter value which produced the largest computed depth and ice jam thickness at the specified representative location).

### **3.4.2 Sensitivity of the RIVJAM model**

#### ***3.4.2.1 Background***

As discussed earlier, when the toe thickness of an ice jam is known, the ice jam length is essentially an output of the RIVJAM model. However, practically speaking, it is not generally possible to measure the toe thickness and, therefore, the toe thickness becomes an additional calibration parameter for a known ice jam length and water surface profile. During this investigation it was observed that the changes due to parameter variation observed in the ice jam profiles computed by RIVJAM reflected both the sensitivity of the numerical algorithm used to solve the coupled equations *and* the sensitivity of the physics inherent in the jam stability and flow equations. The former was reflected in variations in the computed length of ice jam (for a given toe thickness) while the latter was evident in cases of an ice jam of consistent length.

Both types of model sensitivity were investigated here. First, to illustrate the sensitivity attributable to RIVJAM's numerical solution technique, the effects of parameter variation on the computed jam profile were examined without adjusting the jam toe thickness (an adjustment which is required to maintain a consistent jam size). Then, in order to gain a greater understanding of the physical sensitivity, the toe thickness was adjusted so as to maintain a jam of comparable length to the "default" jam.

### 3.4.2.2 *Boundary Conditions*

In addition to the toe thickness, the RIVJAM model requires the water elevation at the downstream boundary. This elevation is defined by the sum of the submerged toe thickness,  $t_{so}$ , and the vertical distance from the bottom of ice to the slope-line (slope-line depth),  $h_{so}$ . For applications to documented events, this water elevation is either known or is specified, therefore, during calibration through adjustment of the toe thickness, the slope-line depth is adjusted accordingly to maintain the specified water elevation.

#### *Downstream Ice Thickness, $t_{so}$*

Although the user may start the computations at any point within an ice jam where the water level and ice thickness are known, the most common location for this downstream boundary is at the jam toe. Therefore, for convenience, this boundary condition is referred to as the toe thickness in this discussion.

Beltaos (1997) stated that *“increasing values of toe thickness... will result in longer and thicker jams, until an equilibrium reach is formed,”* and that at *“this point the solution becomes asymptotic and very small changes in [toe thickness] will result in large changes in the length of the jam”*. These expectations were reflected in this sensitivity analysis as Figure 3.4 illustrates. In this example, an increase in toe thickness from 2.0 m to 4.0 m, caused the jam to lengthen from 2500 m to 6500 m (or by 2.6 times) and raised the overall water surface profile throughout the jam.

In some cases, as expected from Beltaos' model description cited above, it was observed that a small change in toe thickness (in the order of centimeters) would cause a very large change in the computed jam length (in the order of kilometers). This reflects numerical sensitivity, which is attributable to the solution methodology, or more specifically, as Beltaos (1997) described, the *“structure of the system of equations being solved by the model is such that there is a limiting value of [the toe thickness] which will produce an infinitely long jam”*. This numerical effect is also

illustrated in Figure 3.4 where a further increase in toe thickness to 4.8 m. caused the solution to continuously diverge or to “blow-up”. In this case, the specified toe thickness has clearly exceeded the limiting value of toe thickness which would produce an equilibrium jam.

### 3.4.2.3 Ice Jam Parameters

*Roughness Parameters,  $c$ ,  $m_1$  and  $m_2$*

Beltaos’ composite friction factor equation [3.18]:

$$f_o = ct_s^{m_1} h^{-m_2} \quad [3.18]$$

is a function of the flow depth,  $h$ , and the submerged ice thickness,  $t_s$ . Beltaos (1997) suggested the following values for  $m_1$ ,  $m_2$  and  $c$ . For jams where the average thickness is less than about 3 m he recommended  $m_1 = m_2 = 1$  and  $c = 0.40$  to  $0.60$ . Based on inconclusive available information on very thick jams, Beltaos (1997) presented a “best guess” that for ice jams greater than 3 m in thickness, ice jam roughness dependence on jam thickness decreases to the point where  $m_1$  should be set to zero. Keeping  $m_2$  at 1 leads to a practical range of  $c$  of 1.00 to 1.70 (Beltaos, 1997). As discussed earlier, in section 3.2, Mannings equation can be approximated using  $m_1 = 0$  and  $m_2 = 1/3$ . Finally, setting both  $m_1$  and  $m_2$  to zero results in a constant friction factor, equal to  $c$ .

For this sensitivity analysis, the constants  $c$ ,  $m_1$ , and  $m_2$ , were adjusted individually to illustrate both their relative sensitivity and their impact on the overall shape of the computed profile. Throughout calibration of the case study events (reported in Chapter 4) using Beltaos’ friction factor equation ( $m_1 = m_2 = 1$ ),  $c$  was found to vary between 0.10 and 0.50. As stated above Beltaos (1997) found  $c$  to vary between 0.40 to 0.60 for most of his model applications. Based on these findings  $c$  was varied between 0.20 and 0.50 in this sensitivity analysis.

Figure 3.5(a) illustrates the impact on the computed water surface profile for changes in  $c$ , with no adjustments to the boundary conditions. (Note that to reduce clutter the thalweg, indicated by a thick black line below the computed profiles, will not be labeled in this and subsequent figures). For a  $c$  of 0.20 a 3.4 km non-equilibrium ice jam profile was computed by the RIVJAM model. Increasing  $c$  to 0.50 both lengthened and thickened the computed ice jam profile beyond equilibrium causing the computed ice jam profile to diverge (or “blow up”).

Figure 3.5(b) illustrates the impact of changes in  $c$  on the computed water surface profile, while adjusting the toe thickness to maintain a jam of relatively constant length. It was found that the computed water surface stage increased as  $c$  increased and that water surface slope near the toe region became steeper with an increase in  $c$ . To maintain a consistent length in the computed ice jam profiles while reducing the roughness  $c$  from 0.50 to 0.20, the toe thickness had to be reduced from 3.78 m to 1.50 m. At station 12000 m, the difference in the computed flow depth for the two roughnesses was approximately 1 m or 20% and the difference in the computed jam thickness was approximately 0.20 m or 14%.

The effects of varying the exponents in equation [3.18] were investigated for the three scenarios discussed above, specifically: Beltaos’ friction factor equation ( $m_1 = m_2 = 1$ ); thick jam cases ( $m_1 = 0, m_2 = 1$ ); and, for Mannings approximation ( $m_1 = 0, m_2 = 1/3$ ). Figure 3.6 illustrates the results of the sensitivity analysis for these three combinations of exponents (or friction factor formulations). Figure 3.6(a) illustrates the impact on varying the exponents where the toe thickness is held constant. This figure indicates that the model is sensitive to the type of friction factor formulation. For Beltaos’ friction factor (represented by the solid black line) the “default” jam described in Figure 3.3 is reproduced. For the thick jam case (represented by the dotted black line), the computed ice jam profile began to diverge near station 11000 m. Using Beltaos’ Mannings approximation (represented by the fine black line) the computed length of the ice jam profile was approximately 2 km shorter than the default jam. The model is sensitive to the choice in friction factor



formulation when the toe thickness is held constant. Figure 3.6(b) presents the results where the thickness at the toe was adjusted to maintain an ice jam of comparable length to the default jam. The three variations on the friction factor produce ice jam profiles of distinct shape. Beltaos' friction factor formulation (represented by the solid black line) is used as a reference for the other two friction factor variations. Using a friction factor corresponding to a thick jam (represented by the black dotted line) the computed ice jam profile appeared to be characteristically linear over the computed length (near the downstream portion in particular). The computed water surface profile underestimated the computed default jam profile near the toe region (approximately 7% at station 10500) and overestimated the water surface elevation at the head by approximately 9%. Using a Mannings approximation (represented by the fine black line), it was found that the computed water surface profile was greater than the default jam over its entire length. The computed thickness was approximately 25% thicker near the middle of the computed profile (station 12500 m) and computed water level at the head was approximately 24% higher than that computed by the default jam (Beltaos' friction factor). In general, it was observed that Beltaos' friction factor produced thinner ice jams with flatter slopes near the head than computed by the other two methods. Also, Mannings approximation produced higher water surface profiles than either Beltaos' friction factor or the thick jam friction factor formulation.

#### *Passive Pressure Coefficient $K_x$*

The sensitivity of  $K_x$  could only be demonstrated through the generation of a non-equilibrium jam, since inspection of the jam stability equation reveals that  $K_x$  drops out of the relationship for equilibrium conditions (i.e. when  $dt/dx=0$ ). Beltaos (1995) reported that:

*“Laboratory experiments by Cheng and Tatinclaux (1977) and Uzuner, et al. (1974) indicated that  $K_x$  is between 7 and 10. The only field data set that is amenable to an analysis for  $K_x$ , indicated that the product*

$K_x(1-p)$  was between 5 and 6. If  $p$  is assumed equal to 0.4, then  $K_x \approx 8 - 10$  (Beltaos, 1988).”

Beltaos (1997) stated that “RIVJAM applications on more recent case studies seem to suggest a value of 12. Thus, the recommended range is 10-12, with the upper limit being the most likely value.” Based on this information, it was considered reasonable to assume that  $K_x$  may range between 8 and 12 for natural ice jam events and therefore these values were used for testing the sensitivity of  $K_x$ .

Figure 3.7 illustrates the results of this sensitivity analysis. Figure 3.7(a) illustrates the impact of changing  $K_x$  without adjusting the toe thickness. It was found that increasing  $K_x$  from 8 to 12 caused an increase in the length of the computed ice jam profile from 13.7 km to 15.2 km. Figure 3.7(b) illustrates the impact of changing  $K_x$  while adjusting the toe thickness so as to achieve a computed jam profile of consistent length. Here, an increase in  $K_x$  caused the computed water surface profile to drop only slightly. At the near midpoint of the longitudinal profile (station 12500 m) the difference in the computed flow depth was 0.20 m (a change of approximately 3% at this location), and the difference in the computed ice jam thickness was 0.16 m (a change of approximately 11% at this location).

Based on these results it was concluded that the computed jam profile was not very sensitive to changes in  $K_x$  within the range of 8 to 12, in terms of physical *behaviour*. However, RIVJAM’s numerical sensitivity to this parameter is significant.

#### *Jam Strength Parameter, $\mu$*

The jam strength parameter  $\mu$  reflects the combination of two input parameters for the RIVJAM model, specifically  $C_o$  and  $p$  as defined previously in equation [3.38]:

$$\mu = C_o(1 - p). \quad [3.38]$$

They are generally combined in practical applications because of the fact that it is difficult to determine them separately from field measurements (Ashton, 1985). For

this same reason.  $\mu$  was investigated in this sensitivity analysis rather than considering the sensitivity of  $C_o$  and  $p$  separately.

Table 3. 4 presents typical values of  $\mu$  deduced from documented ice jams. These are comparable to the values obtained in laboratory investigations (Uzuner, *et al.*, 1976). Beltaos (1978, 1983) indirectly deduced values of  $\mu$  for 12 documented ice jams where ice thickness was unknown, and obtained values of  $\mu$  ranging mostly between 0.8 and 1.3, with extreme values as low as 0.6 and as high as 3.5. Based on all of the available data, a generally accepted range for  $\mu$  is 0.8 to 1.2. Therefore, these values were used for the sensitivity analysis of  $\mu$ .

Table 3. 4 Typical values of  $\mu$  deduced from documented ice jams.

| Investigator           | $\mu$      | Site                    |
|------------------------|------------|-------------------------|
| Calkins, 1983          | 1.2 to 1.3 | New England states, USA |
| Neill and Andres, 1984 | 0.9        | Peace River, Canada     |
| Beltaos, 1988          | 1.2 to 1.3 | Thames River, Canada    |

As Figure 3.8 shows, model results display both a physical and a numerical sensitivity to  $\mu$ . Figure 3.8(a) illustrates the numerical sensitivity by presenting the computed ice jam profile results for varying  $\mu$  when the boundary conditions are fixed. In this example, an increase in  $\mu$  from 0.8 to 1.2 caused an increase in jam length from 3.3 km to 8.0 km. Figure 3.8(b) illustrates the physical sensitivity of the RIVJAM model to  $\mu$  by presenting the computed ice jam profile for varying  $\mu$  when the toe thickness is adjusted so as to maintain a consistent jam length. In this case, an

increase in  $\mu$  from 0.8 to 1.2 caused an overall decrease in the water surface profile and a decrease in accumulation thickness. It also flattened the water surface slope in the vicinity of the toe. The difference in the computed flow depths at station 11000 m was 0.45 m, or approximately 7%. The difference in the computed thickness was 0.24 m, or approximately 12% at this location.

#### *Ratio of Ice Roughness to Composite Roughness, $\beta_2$*

The ratio of ice roughness to twice the bed roughness ( $\beta_2$ , as defined in equation [3.3]) was investigated in this sensitivity analysis. Based on the range of values suggested by Beltaos (1997), the values tested were 0.4 and 0.6.

Figures 3.9 (a) and (b) illustrate the numerical and physical sensitivity of the RIVJAM model to this parameter, respectively. In Figure 3.9(a), which illustrates the impact of changing  $\beta_2$  without adjusting the boundary conditions, it is seen that an increase in the friction factor ratio,  $\beta_2$ , from 0.4 to 0.6 shortened the length of the jam from 5.9 km to 3.4 km. Figure 3.9(b) illustrates the physical effects of changing  $\beta_2$  by adjusting the toe thickness so as to achieve a computed jam profile of consistent length. As the friction factor ratio was increased it was found that the both the computed water surface profile and the required thickness near the toe increased. The difference between the computed flow depth at station 12000 m was 0.34 m (approximately 5%) and the difference in the computed thicknesses was 0.20 m (approximately 12%).

#### *Seepage Parameter, $\lambda$*

The seepage parameter,  $\lambda$ , was adjusted between 0.5 m/s and 3.0 m/s which exceeds the range of 1.0 to 2.5 m/s suggested by Beltaos (1997). Figure 3.10(a) illustrates the impact of changing  $\lambda$  without adjusting the input toe thickness. Here, an increase in  $\lambda$  from 0.5 to 3.0 m/s increased the length of the jam only slightly from 4.0 km to 4.6 km. Figure 3.10(b) illustrates the impact of changing  $\lambda$  while adjusting the toe

thickness so as to achieve a computed jam profile of consistent length. As  $\lambda$  was increased it was found that there was little change to the computed water surface profile. The difference in the computed flow depths at station 11500 m was 0.08 m (approximately 1%) and the difference in the computed thickness was 0.04 m (approximately 2%). For this particular case, the computed profiles appeared insensitive to changes in  $\lambda$ , both physically and numerically. Using equation [3.7] the flow through the voids at the toe was computed for each case. When the toe thickness was held constant the flow through the voids was 10% for  $\lambda = 0.5$  m/s. and 39% for  $\lambda = 3.0$  m/s. When the toe thickness was adjusted to maintain the same length of ice jam, the flow through the voids was 12% for  $\lambda = 0.5$  m/s. and 34% for  $\lambda = 3.0$  m/s. An increase in the seepage velocity resulted in an increase in the percent of flow passing through the voids, as would be expected. Seepage effects were apparent during the analysis of this particular ice jam, which was not grounded, and the seepage would be expected to become even more important for grounded ice jams.

#### *Discharge, $Q$*

Discharge was examined in this sensitivity analysis, as it is often unknown or only estimated for documented ice jam events. This is due to the dynamic nature of and dangerous conditions produced by ice jams, as it is difficult to obtain direct measurements of the discharge under such conditions and open water rating curves are inapplicable under ice affected conditions.

For this analysis, the default discharge was first increased and then decreased by 10% to investigate the sensitivity due to a change in discharge within a percent range that would correspond to a plausible range of error corresponding to discharge estimates on real events. The results are presented in Figure 3.11. Figure 3.11(a) illustrates the impact of changing discharge without adjusting the boundary conditions. Here, an increase in discharge from 300 m<sup>3</sup>/s to 360 m<sup>3</sup>/s shortened the length of the jam from 5.5 km to 3.5 km. Figure 3.11(b) illustrates the impact of changing discharge while adjusting the initial thickness so as to achieve a computed jam profile of comparable

length. As expected, a discharge increase was reflected in an increase in computed depths. The difference in the computed flow depths at station 12500 m was 0.40 m (or approximately 8%) and the difference in the computed thickness was 0.03 m (approximately 2%).

The importance of the numerical sensitivity for this parameter is noted as reasonable deductions on the physical response of an ice jam due to an increase in discharge can be made. The computed water surface profile would be expected to increase with an increase in discharge. It is also expected that the length of the jam would be more dependent on the available volume of ice contributing to the jam and not so dependent on discharge (as is implied by Figure 3.11(a)).

#### **3.4.2.4 Channel Geometry**

##### *Slope-Line Slope, SLOPEO*

The slope-line passes through the lowest bed elevation or thalweg of the first cross section in the input file. Cross section properties are interpolated linearly along lines parallel to this slope-line. Beltaos (1997) states that the “*model output is rather insensitive to the slope of the slope-line, so that a horizontal line would generally be an adequate choice, provided the inputted cross sections are not too far apart.*” It was decided to examine the sensitivity of this parameter because unstable solutions were obtained when calibrating some of the case studies (discussed in Chapter 4) for which cross sections were widely spaced.

To exaggerate the effect of the slope of the slope-line on modelling results, the cross section spacing was set to 5 km for the idealized trapezoidal channel for these sensitivity tests. Figure 3.12 shows that when the slope of the slope-line was set to zero, the solution (which is stepping upstream) first began to diverge and then the computations were arrested. Figure 3.12 also illustrates that the computations stop when the computed bottom of ice profile intersects the slope-line (which occurs for the example case where the slope-line slope of 0.0002).

Based on these results, and the fact that “large” cross section spacing is a relative circumstance, it is recommended that RIVJAM users use a slope-line slope which approximates the bed slope rather than a horizontal line, in order to avoid solution failures of the type illustrated in Figure 3.12.

### **3.4.3 Sensitivity of the ICEJAM Model**

#### ***3.4.3.1 Background***

The gradually varied flow equations used by the ICEJAM model use Chezys equation where Chezys  $C$  is approximated by a logarithmic relationship which includes roughness height,  $k_o$ . The roughness of both the bed and the underside of the ice are represented by  $k_b$  and  $k_i$ , respectively, and are expressed in meters. The composite roughness,  $k_o$  is calculated by ICEJAM using Sabenev’s equation [3.34].

It was desirable to have a model which used Mannings roughness as it is a more familiar form of roughness, in particular for river engineering applications. Consequently, the ICEJAM model was modified by the author to accept Mannings roughness.

The roughness in the Chezys relationship is a function of the depth and varies over the computational reach, while roughness for the Mannings relationship is independent of depth and does not vary over the computational reach. Therefore, both the Chezys roughness and Mannings roughness options for ICEJAM were investigated during the sensitivity analysis.

#### ***3.4.3.2 Boundary Conditions and Discretization***

##### *Discretization*

As described previously, the ICEJAM model relies on the inputted cross sections for the discretization used by the solution. Cross section spacing becomes particularly important in the downstream transition of the ice jam where properties of the

computed ice jam profile are changing rapidly. It was necessary to illustrate the importance of cross section spacing and, therefore, was included in the sensitivity analysis.

For the analysis on the idealized trapezoidal channel, the cross section spacing was varied from 25 m spacing to 400 m spacing. Figure 3.13 illustrates the impact on the computed water surface profile for the varied cross section spacing. Both Figure 3.13(a) and Figure 3.13(b) indicate that the cross section spacing is particularly important in the downstream transition of the ice jam. The 25 m cross section spacing provides adequately fine discretization, while 400 m cross section spacing for both the Manning and Chezy roughness calculations did not. Figure 3.13(b) also indicated that the cross section spacing was more sensitive when using the Chezy's roughness computation than when using the Mannings roughness computation for this particular analysis. Flato (1986) also illustrated the importance of cross section spacing, in particular near the toe region.

#### *Thickness at the Downstream Boundary, $t_{toe}$*

The thickness at the downstream boundary is intended to represent physically, the thickness of the intact ice at the toe. This boundary thickness was adjusted between 0.25 m and 1.50 m which bracket a reasonable range of ice thicknesses that might be expected to form on Canadian rivers over an average winter.

Figure 3.14 shows that an increase in the thickness at the downstream boundary caused a shift in the interface A-A (described previously as the point at which the jam stability equation governs) downstream. For the Mannings roughness computation (Figure 3.14(a)), interface A-A was moved downstream by 175 m when thickness at the downstream boundary was increased from 0.25 m to 1.50 m. For the Chezy's roughness computation (Figure 3.14(b)), interface A-A was moved downstream by 100 m when thickness at the downstream boundary was increased from 0.25 m to 1.50 m. For both cases, the change in the thickness at the downstream boundary appeared to have no visual impact on the overall computed jam profile further on



upstream of interface A-A where the jam stability equation governed (at roughly station 11000 m).

It was concluded that the ICEJAM model was insensitive to the specific thickness at the downstream boundary, upstream of interface A-A, however, the computed length of the toe region is affected by the choice of this parameter.

#### *Thickness at the Head, $t_{head}$*

The thickness at the head was adjusted between 0 m and 1.50 m to illustrate its impact on the computed water surface profile. Figure 3.15 illustrates that a change in the thickness at the head appears to have no visual impact on the computed jam profile near the downstream portion of the jam. The impact on the computed water surface profile through an adjustment in the thickness at the head was similar for both the Mannings roughness computation (Figure 3.15(a)) and the Chezy's roughness computation (Figure 3.15(b)).

This parameter can also be used to represent the thickness at a point downstream of the head (its intended location), and when used in this manner, it may become an important calibration parameter if this thickness is not already known.

#### *Ice Jam Length*

Although the length of the accumulation is not a specified boundary condition per se, it is a user specified constraint which forces the length of the computed ice jam to correspond to the first and last cross sections in the input file. The last cross section in the input file represents the furthest upstream computational node. The length is essentially predetermined by the user and therefore, can be considered in an abstract sense, to be a boundary condition. The length of the jam was adjusted from 2000 m to 6000 m for this analysis.

Figure 3.16 illustrates that an increase in the length of the jam caused an increase in the computed water surface profiles for both the Mannings and Chezy's runs. This

increase in water surface elevation was not quantified in this case as the length of jams are site specific and *typical values* for jam lengths did not apply. The intent is to demonstrate the general effect due to varying the jam length. It was concluded that the specified length becomes an important calibration parameter when the length of the ICEJAM being modelled is unknown.

#### *Maximum Under Ice or Erosion Velocity, $V_{max}$*

The erosion velocity,  $V_{max}$ , provides a means of computing the thickness profile through the toe region as discussed previously. It was considered to be a boundary condition as it simply dictates where the jam stability equation governs or rather defines the location of interface A-A. Throughout the case studies  $V_{max}$  was adjusted to provide the best fit to measured data irrespective of what may be considered to be a reasonable range of values for erosion velocities and  $V_{max}$  was found to range between (1.0 m/s to 2.5 m/s) and these values were used for the analysis.

Figure 3.17 clearly indicates the impact of the *erosion* velocity on the location of interface A-A. The general trend illustrated by Figure 3.17 is, that as  $V_{max}$  decreases, the region governed by  $V_{max}$  lengthens and extends further upstream. For the Mannings roughness computation where  $V_{max} = 1.0$  m/s this region extends to roughly 1 km in length (Figure 3.17(a)), while for the Chezy's roughness computation the region extends roughly 0.5 km (Figure 3.17(b)). Figure 3.17(b) also illustrates that for a relatively high  $V_{max}$  (2.5 m/s in this case) an unrealistic shape in the computed ice jam profile is exhibited near the toe.

The values of *erosion* velocity tested in this analysis should be interpreted in a relative sense as the impact of this parameter on the computed water surface slope varies depending on the hydraulics and channel geometry specific to the study under investigation. That is to say, that an *erosion* velocity of 2.5 m/s may result in a computed water surface profile that is unrealistic under one scenario (as was the case for this particular analysis) and a realistic water surface profile in another scenario (as

was found later during the case studies). The general trend however, is that when  $V_{max}$  is increased, the computed length of the downstream transition decreases.

It should be noted that this criteria simply provides a way for the computation to pass through the toe region (where the configuration is unknown) to a point where the jam stability equation governs (i.e. within the downstream transition). Flato (1988) acknowledged the limitations associated with this characteristically linear approximation of the toe region and noted that it may not be representative to conditions observed in the field.

### 3.4.3.3 Calibration Parameters

#### *Roughness*

Both Mannings composite roughness,  $n_o$ , and Chezys composite roughness height,  $k_o$ , were investigated in the sensitivity analysis. The composite Mannings roughness was varied between 0.030 and 0.060 (representing a plausible range of roughness for flows under ice jams) and the Chezys roughness height was varied between 0.30 m and 3.0 m. A Chezys roughness height of 0.30 m was selected as the lower bound as it loosely corresponds to a Mannings roughness of 0.030 according to the following Strickler's type relationship described by Henderson (1965):

$$n_o = \frac{k_o^{1/6}}{8.41\sqrt{g}} \quad [3.39]$$

The upper bound for  $k_o$  corresponding to  $n_o = 0.060$  would have been approximately 15.6 m, which definitely exceeds the depth of flow for the "default" jam. This upper bound was therefore abandoned and a roughness height of 3.0 m was selected as this approached, but did not exceed, the depth of flow.

Figure 3.18 illustrates the impact of roughness on the computed water surface profile. Figure 3.18(a), representing the Mannings roughness computation, indicated that an increase in  $n_o$  increased the overall computed thickness and water surface profile. At

station 12000 m. the water surface profile increased by 1.52 m (21%) and the thickness increased by 0.37 m (17%).

Figure 3.18(b), representing the Chezys roughness computation, indicated that an increase in  $k_o$  also increased the overall computed thickness and water surface profile. At station 12000 m, the water surface profile increased by 1.65 m (22%) and the thickness increased by 0.30 m (15%).

It was therefore deduced that the computed water surface profile was sensitive to changes in roughness, within plausible ranges of roughness and therefore, is considered an important calibration parameter.

#### *Coefficient. $K_v$*

As explained previously in the sensitivity analysis of  $K_x$  used by RIVJAM, it was necessary to investigate the sensitivity of  $K_v$  (a passive pressure coefficient) used in ICEJAM for a non-equilibrium jam and  $K_v$  was varied from 8 to 12 (corresponding to the range tested on  $K_x$ ) for analysis.

Figure 3.19 illustrates that the computed water surface profile was not very sensitive to changes in  $K_v$  for the range of values tested. An increase in  $K_v$  from 8 to 12 caused a slight decrease in the computed water surface profile, corresponding to a decrease in the computed ice jam thickness. It is also interesting to note that the computed bottom of ice profiles differed by less than 1% for both the Mannings and the Chezys roughness calculations.

For the Mannings roughness calculation (Figure 3.19(a)), the water surface profile decreased by 0.32 m (5%) and the thickness decreased by 0.29 m (13%) at station 12000 m. For the Chezys roughness calculation (Figure 3.19(b)), the water surface profile decreased by 0.12 m (2%) and the thickness decreased by 0.16 m (8%) at station 12000 m.

It was concluded that the computed ice jam profile was not very sensitive to changes in  $K_v$ , within the range of tested values (8 to 12).

#### *Coefficient. $\mu$*

As is the case for the RIVJAM model,  $\mu$  is not a direct input parameter for the ICEJAM model, however, it can be deduced from equation [3.37]. For the same reasoning outlined during the analysis of the RIVJAM model, the coefficient  $\mu$  was adjusted between 0.8 and 1.2.

Figure 3.20 illustrates the sensitivity of the computed water surface profile to changes in  $\mu$ . As  $\mu$  was increased from 0.8 to 1.2 the computed water surface profile decreased and the jam thickness also decreased. For the Mannings roughness calculation (Figure 3.20(a)), the water surface profile decreased by 0.35 m (5%) and the thickness decreased by 0.21 m (10%) at station 12000 m. For the Chezy's roughness calculation (Figure 3.20(b)), the water surface profile decreased by 0.34 m (5%) and the thickness decreased by 0.20 m (10%) at station 12000 m.

#### *Discharge. $Q$*

As for the RIVJAM sensitivity analysis, the discharge was adjusted to investigate its impact on the computed water surface profile. The discharge was adjusted between 300 m<sup>3</sup>/s and 360 m<sup>3</sup>/s. It was found that an increase in discharge caused an increase in the computed water surface elevation.

Figure 3.21 presents the results for an increase in discharge from 300 m<sup>3</sup>/s to 360 m<sup>3</sup>/s. For the Mannings roughness calculation (Figure 3.21(a)), the water surface profile increased by 0.44 m (7%) and the thickness increased by 0.10 m (5%) at station 12000 m. For the Chezy's roughness calculation (Figure 3.21(b)), the water surface profile increased by 0.39 m (6%) and the thickness increased by 0.07 m (7%) at station 12000 m.

#### **3.4.3.4 Channel Geometry**

The equivalency between ICEJAM and RIVJAM had already been established and to avoid the difficulties associated with the inherent numerical sensitivity of the RIVJAM model, it was decided to use ICEJAM to test the impact of channel geometry on the computed ice jam profile.

Using the Mannings roughness, all input parameters were fixed to the default values listed previously in Table 3.3 and only the slope or width of the channel was adjusted to investigate its impact on the shape of the jam profile. The four different scenarios were investigated during the analysis were: a change in channel slope; a change in channel width; an adverse channel slope; and a horizontal channel slope.

The intent was illustrate the general impact of these changes on the computed ice jam profile, and the assessment of this analysis justified only a qualitative description of these impacts. Figure 3.22 illustrates the impact of an abrupt change in channel slope on the computed ice jam profile. Figure 3.22(a) illustrates the computed ice jam profile for the case where the channel slope changes from 0.0002 to 0.0008 (moving in the downstream direction). Proceeding from the head towards the toe, it was observed that the thickness of the ice jam profile increased when the slope increased. Figure 3.22(b) shows the reverse effect, when the channel slope (moving downstream) was decreased from 0.0008 to 0.0002 (i.e. the computed thickness decreased).

Figure 3.23 illustrates the impact of a change in channel width on the computed ice jam profile. Figure 3.23(a) indicates that the computed thickness decreases as the channel width decreases and Figure 3.23(b) indicates that the computed thickness increases as the computed width increases.

Figure 3.24 illustrates the impact of an adverse slope on the computed ice jam thickness. It was observed that the thickness decrease over the region where the

adverse slope was encountered. This appears reasonable as lower velocities (which implies lower shear stress on the ice underside) would be expected in this region.

Lastly, the effect of a section with a horizontal slope within the computational reach was investigated. It was found that the ICEJAM model would not run for this scenario and Figure 3.25 illustrates the profile of the bed that was used to investigate this scenario. The observed effect of a horizontal bed within the computational reach served primarily as a warning to potential users to not add horizontal channel sections within the computational reach.

#### 3.4.4 Discussion of Results

Based on the analysis of the physical sensitivity of the RIVJAM model, it was deduced that the computed water surface profile and ice jam thickness are particularly sensitive to the input toe thickness and specified ice jam roughness. Model results also display sensitivity to the carrier discharge, but are considerably less sensitive to the jam seepage parameter,  $\lambda$ , at least for the hypothetical case considered here. Physically, the *computed water surface profile* is also somewhat sensitive to changes in the input roughness ratio and the jam strength parameter,  $\mu$ , but not to variations in the coefficient,  $K_x$ . The *computed ice jam thickness* appears to be relatively insensitive to variations in the passive pressure coefficient, roughness ratio, and the jam strength parameter.

It was found during the analysis of the ICEJAM model that shape of the computed ice jam profile can be considered sensitive to the boundary condition parameters when the location of the head and toe are not known. The ICEJAM model appeared to be most sensitive to roughness, somewhat sensitive to the jam strength parameter  $\mu$ , and least sensitive to variations in the passive pressure coefficient,  $K_v$ .

The erosion velocity,  $V_{max}$ , was found to serve as a useful means of progressing from the downstream boundary (solid intact ice) to the point where the jam stability

equation governs. The length of the computed toe region is dependent on the specified erosion velocity and it was found that for *high* values an unrealistic shape in the ice jam profile was computed. A value of erosion velocity for which this occurs can not be specified at this point, as the computed shape of the toe region is also dependent on the prevailing hydraulic and geometric conditions which vary from case to case.

The analysis of the numerical sensitivity of the RIVJAM model has illustrated that the computed length of the jam (and therefore the volume of ice in the accumulation) is relatively sensitive to the input toe thickness and *all* of the specified ice jam characteristics (roughness, passive pressure coefficient, roughness ratio, and the jam strength parameter). The computed ice jam length is also fairly sensitive to the carrier discharge and, though to a much lesser extent, to the jam seepage parameter,  $\lambda$  (at least for the hypothetical case considered here).

This sensitivity in the ice jam length computed by the RIVJAM model is not considered a limitation, since it may possibly facilitate the consideration of predictive, or hypothetical, situations somewhat more readily than the ICEJAM model (for which the user must specify the ice jam length *a priori*). However, when either model is used in a prediction capacity the following advice from Beltaos (1997) should be heeded:

*"In practical applications, every effort should be made to determine the maximum ice volume that can accumulate within a jam. Even where this has to be done conservatively, knowledge of the ice volume greatly increases the confidence in the model predictions because of the attendant reduction in sensitivity."*

*"In practice therefore, the common problem will be to predict the configuration of an ice jam for given channel bathymetry and flow, so as to match an independently determined ice volume in the jam."*



Despite the fact that the length of the ice jam is essentially an output of the RIVJAM model, when analyzing documented ice jams for cases where the toe thickness is unknown, the ice jam length must be known. In this case, and in all applications of the ICEJAM model, the user must pay special attention to the observed length of jam and in particular not confuse the observed head of the ice accumulation with the actual head of the ice jam, since there is always the possibility that a “*surface layer of juxtaposed ice flows*” (Beltaos, 1997) may be present upstream of the ice jam. Since the toe thickness of an ice jam is seldom known with confidence (due to the inherent difficulties in measuring it accurately), the length of the jam can be considered required information for the application of either model to the problem of deducing ice jam parameters from documented ice jam events. Furthermore, the nature of the physical sensitivity of the models suggests that, at least in some instances, calibration will be more sensitive to the ice roughness than to either  $\mu$  or  $K_x$ . Where, in addition, discharge is unknown and must be estimated during the calibration procedure, it may be impractical to attempt to determine precise values for  $\mu$  or  $K_x$ .

The interpretations developed through the sensitivity analysis on the idealized (prismatic) channel are refined in Chapter 4 which presents a detailed investigation of the behaviour of these models for a variety of documented events.

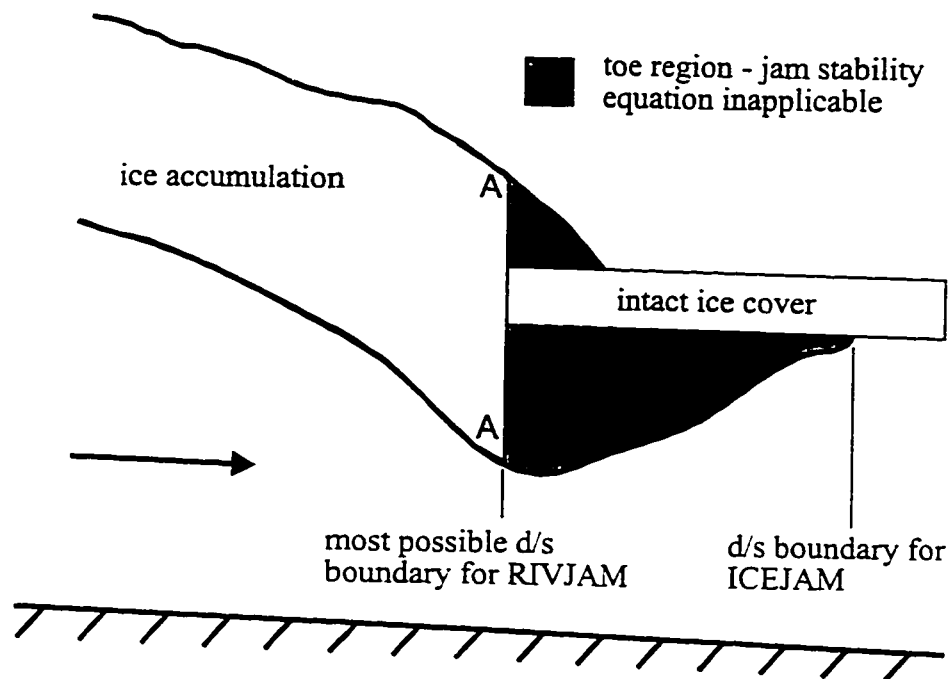


Figure 3.1. Schematic of ice accumulation in the toe region.

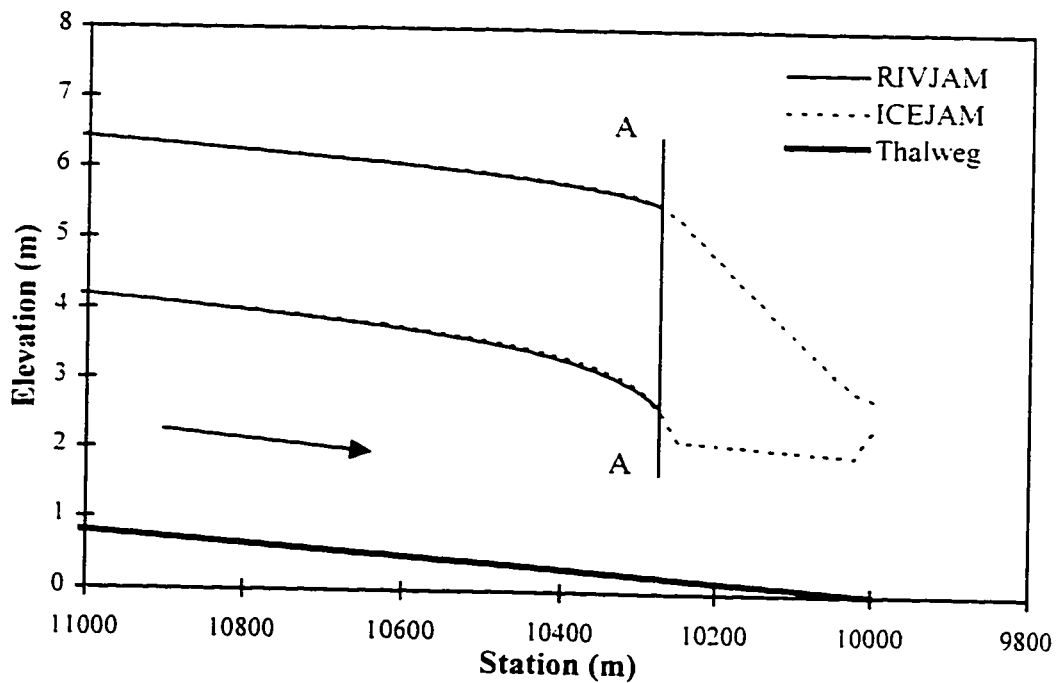


Figure 3.2. Comparison of ICEJAM and RIVJAM results for the trapezoidal channel.

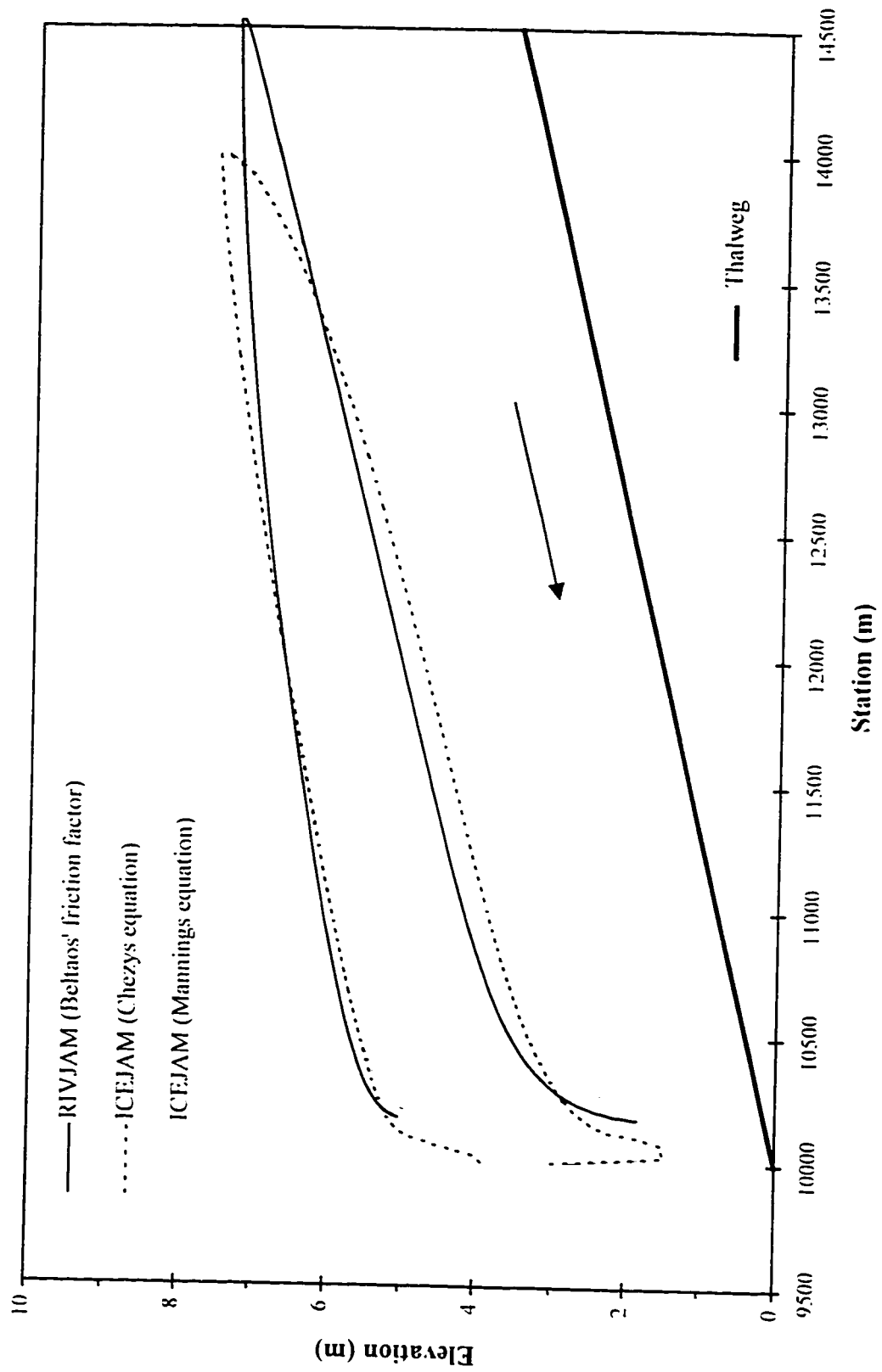


Figure 3.3. Default runs for sensitivity analysis.

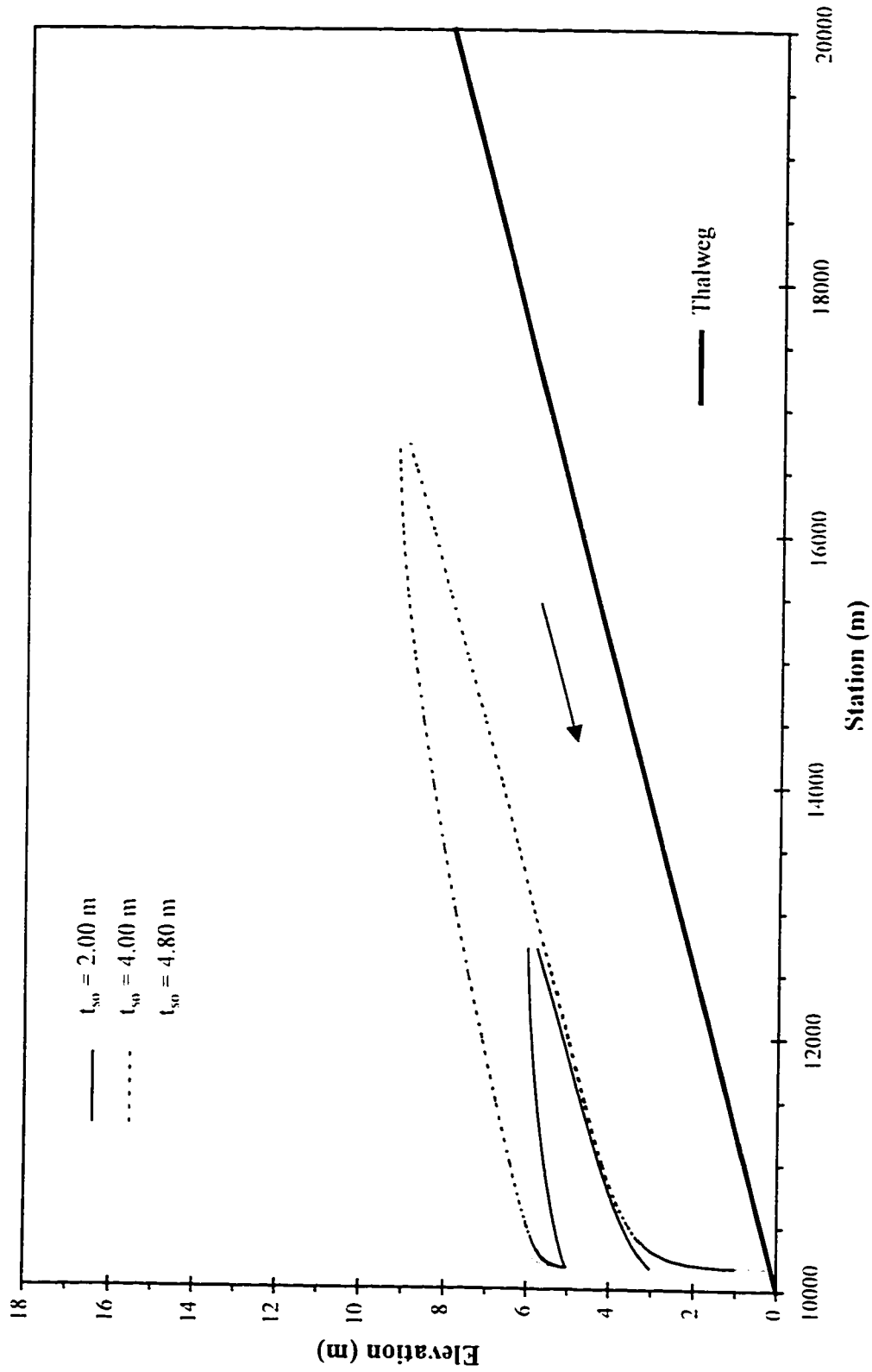


Figure 3.4. Sensitivity of RIVIAM to toe thickness.

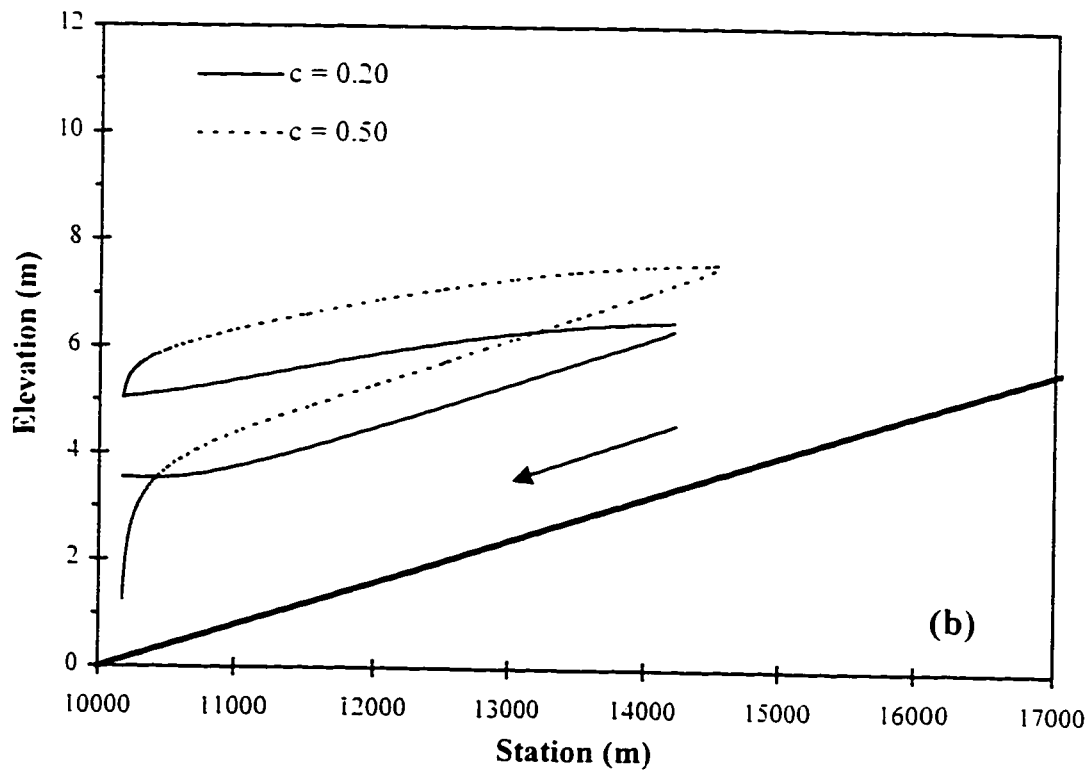
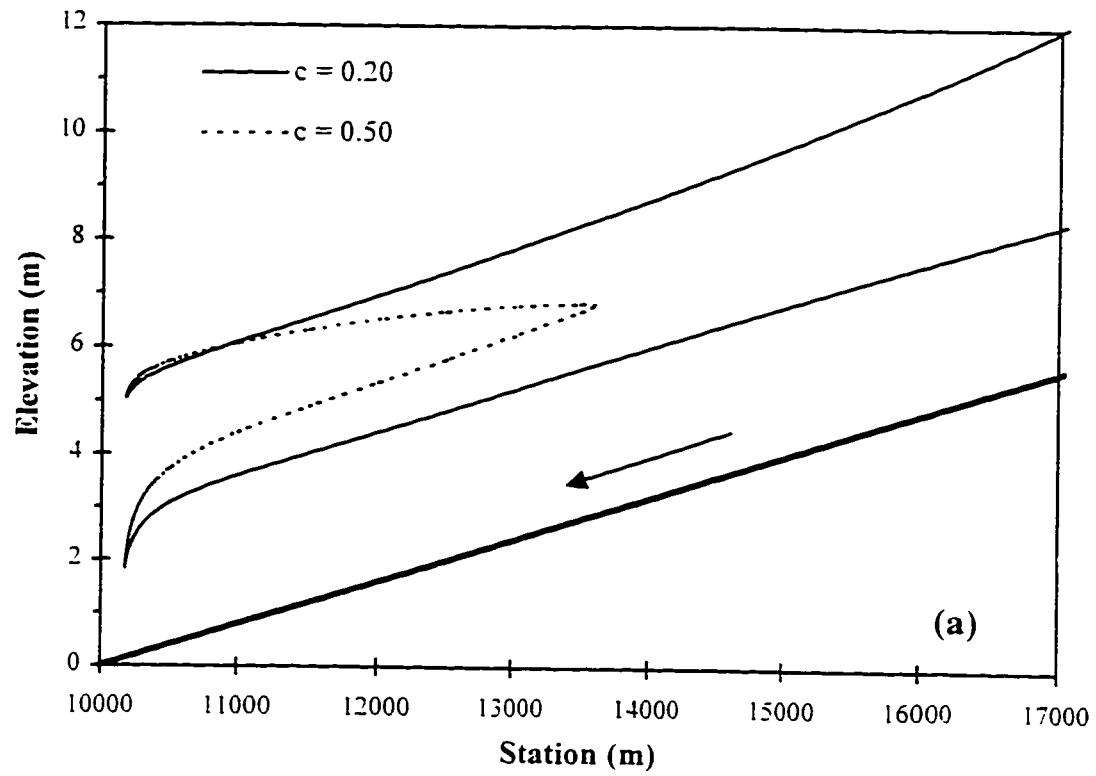


Figure 3.5. Sensitivity of RIVJAM to  $c$  for (a) constant toe thickness and (b) consistent ice jam length.

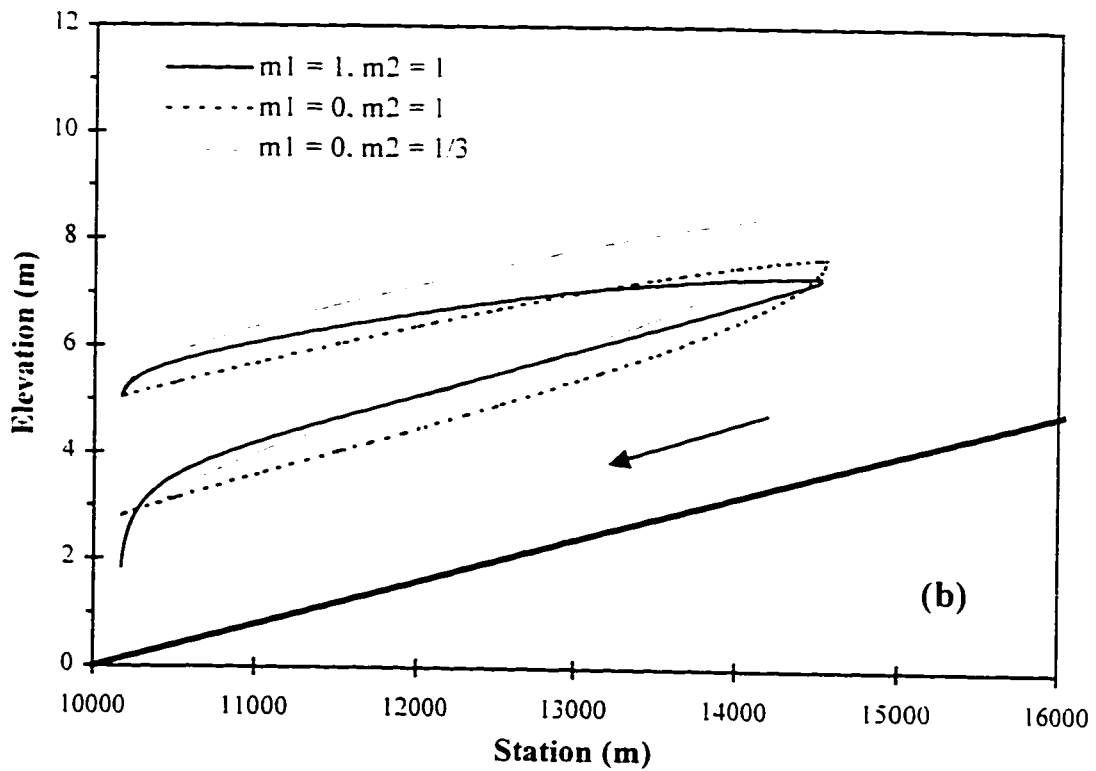
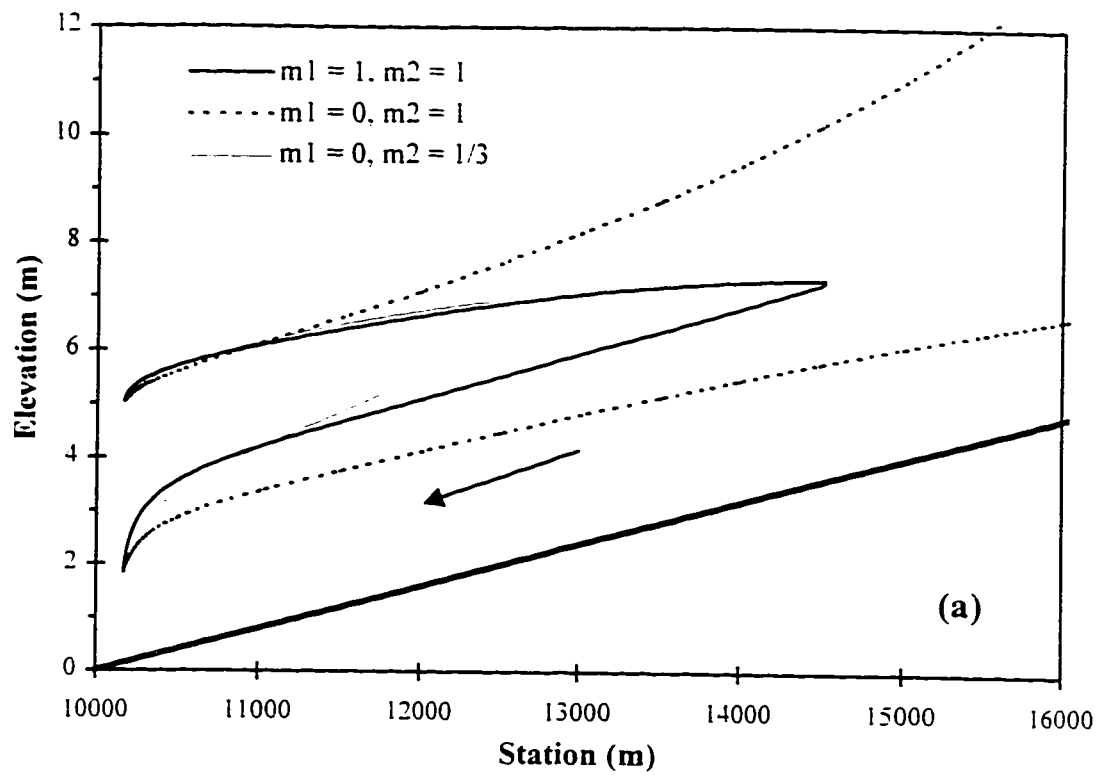


Figure 3.6. Sensitivity of RIVJAM to  $m_1$  and  $m_2$  for (a) constant toe thickness and (b) constant ice jam length.

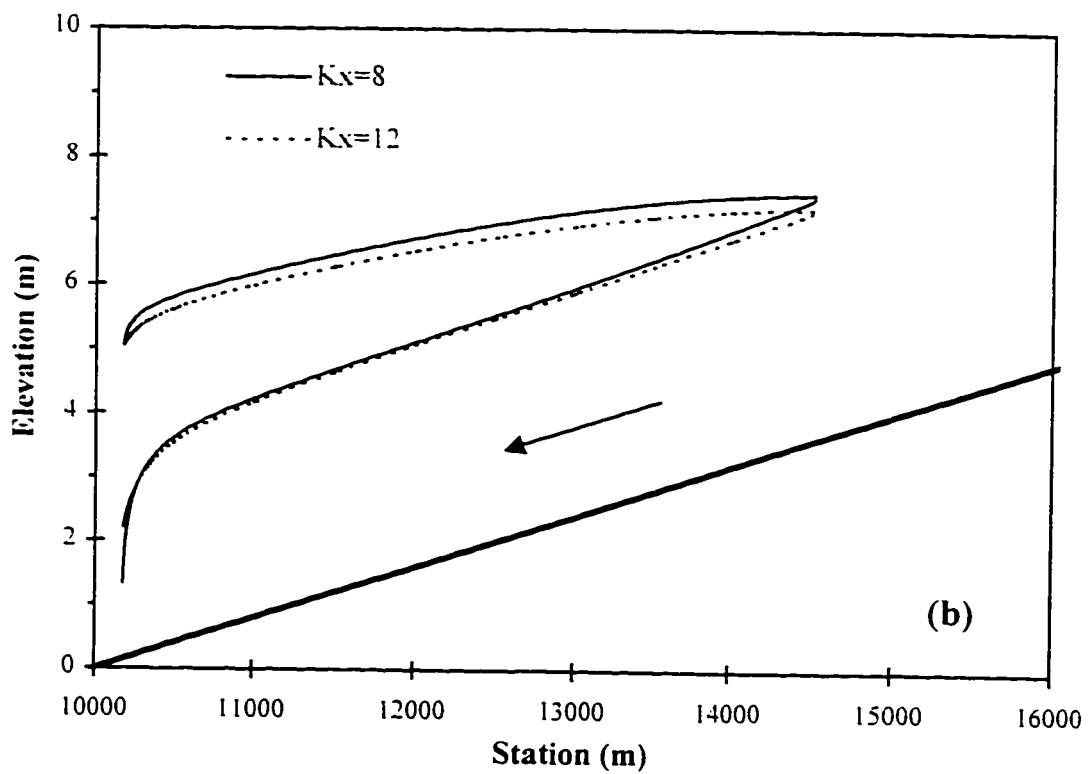
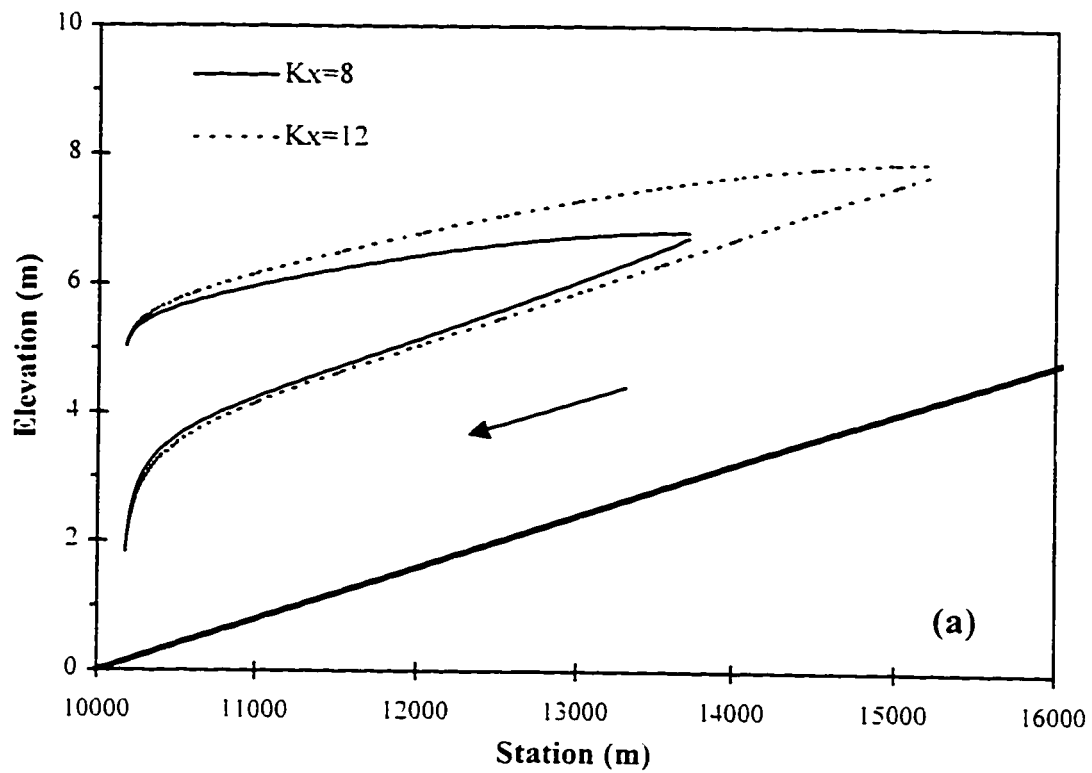


Figure 3.7. Sensitivity for RIVJAM to  $K_x$  for (a) constant toe thickness and (b) consistent ice jam length.

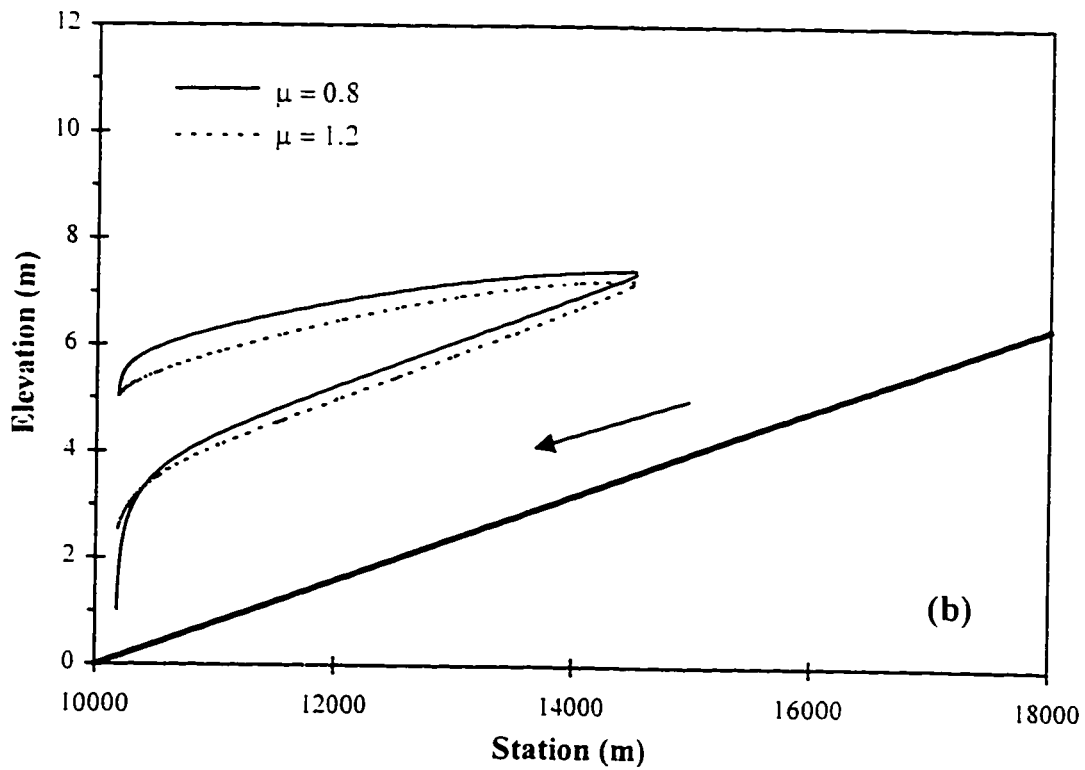
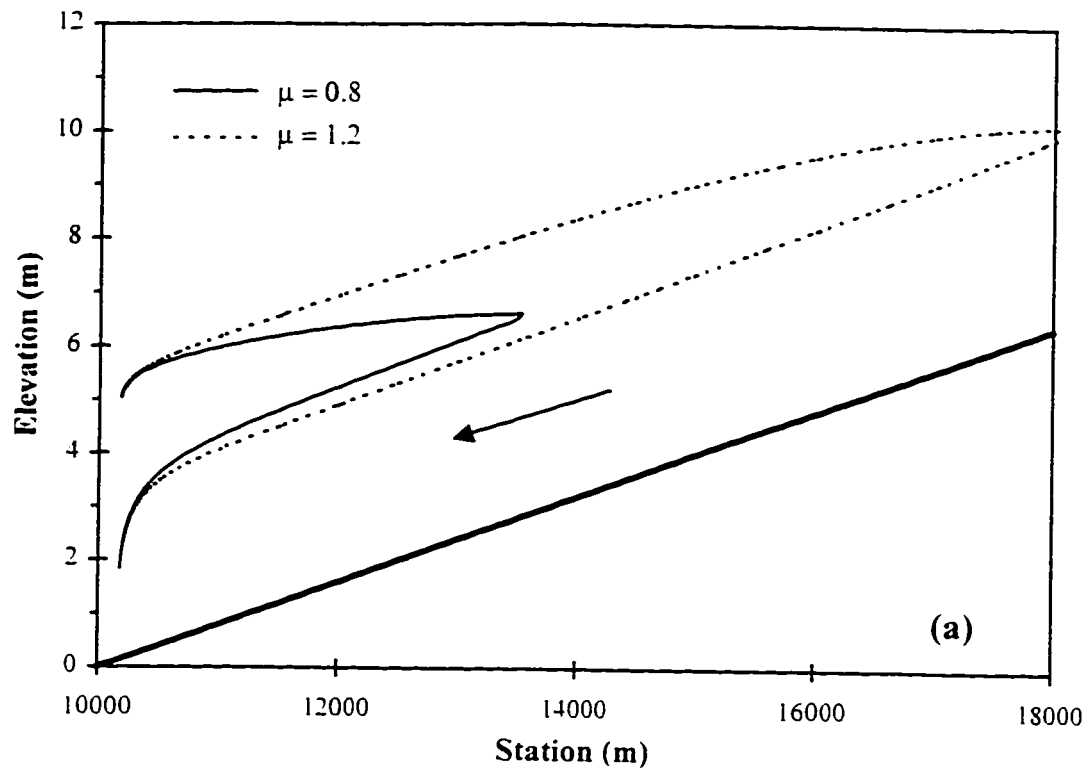


Figure 3.8. Sensitivity of RIVJAM to  $\mu$  for (a) constant toe thickness and (b) consistent ice jam length.



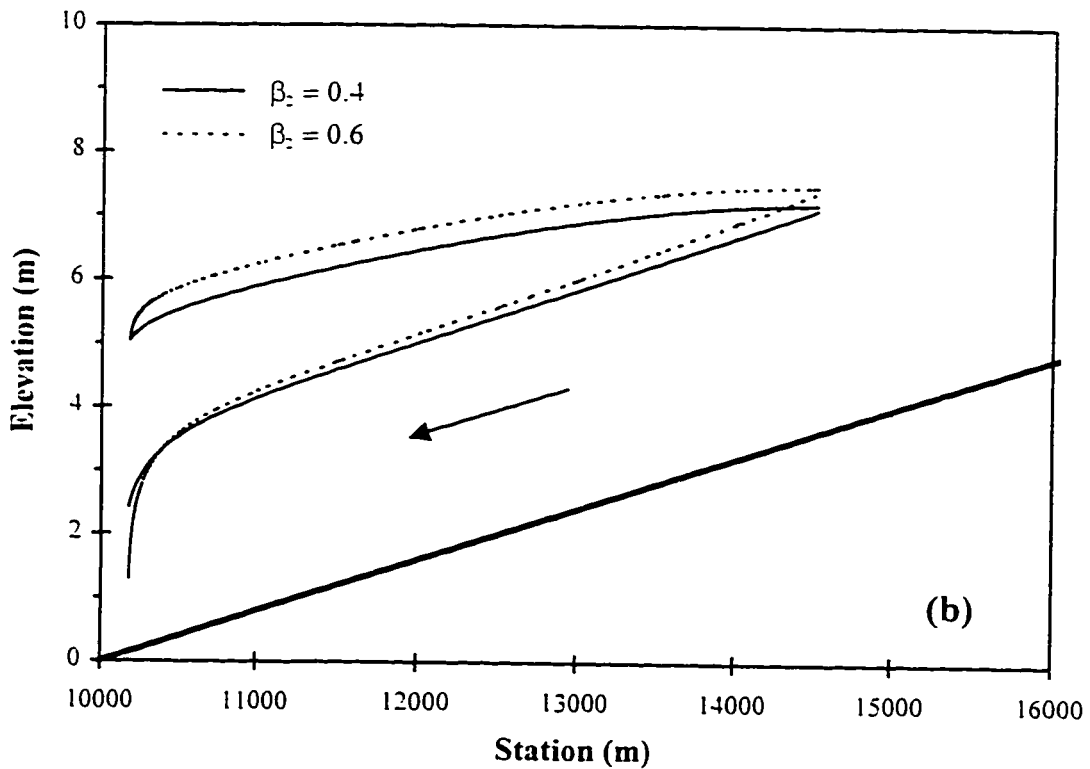
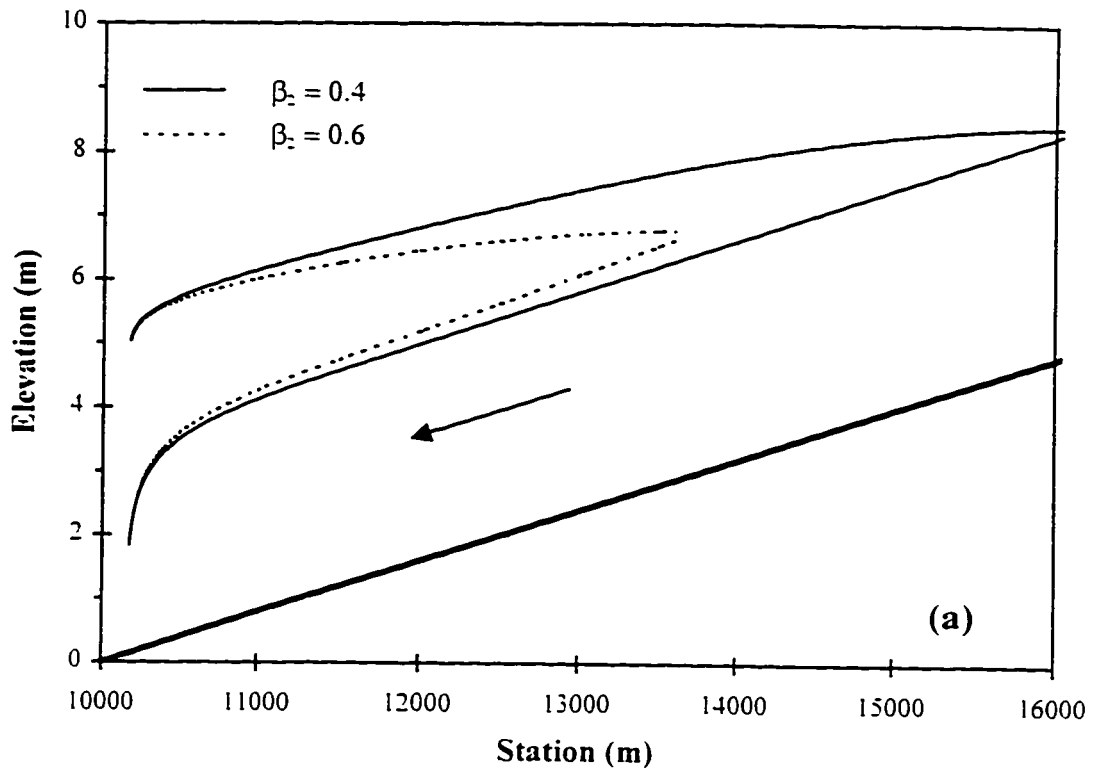


Figure 3.9. Sensitivity of RIVJAM to  $\beta_2$  for (a) constant toe thickness and (b) consistent ice jam length.

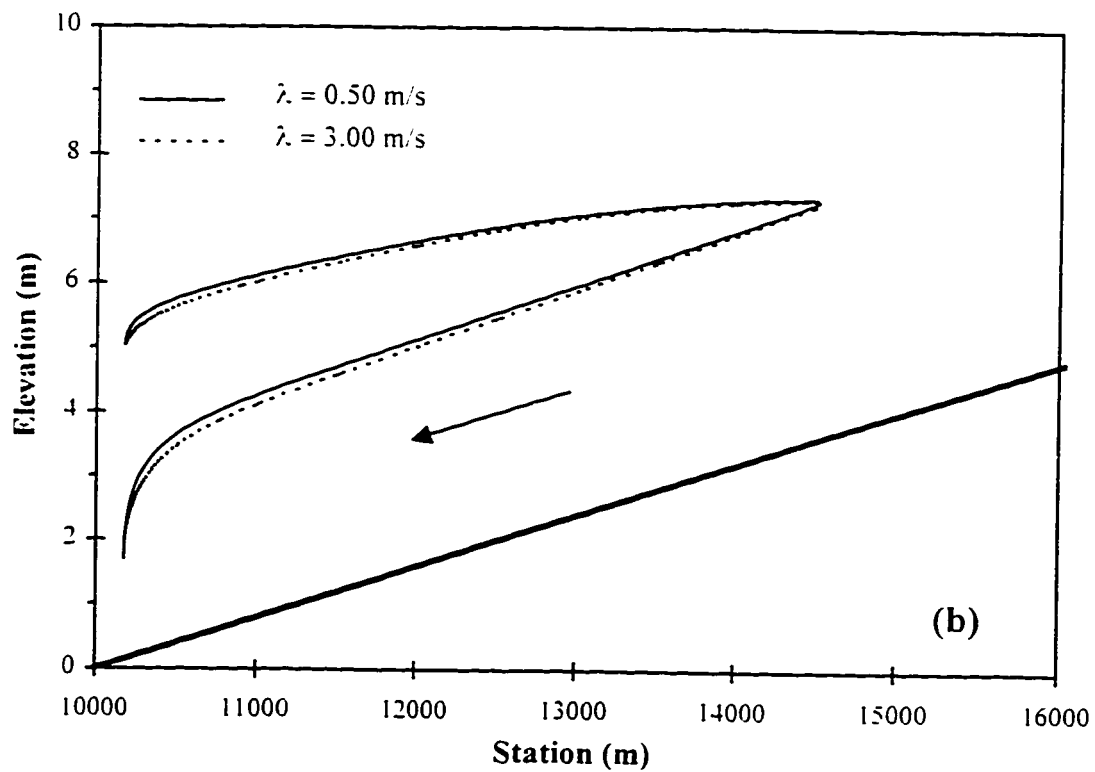
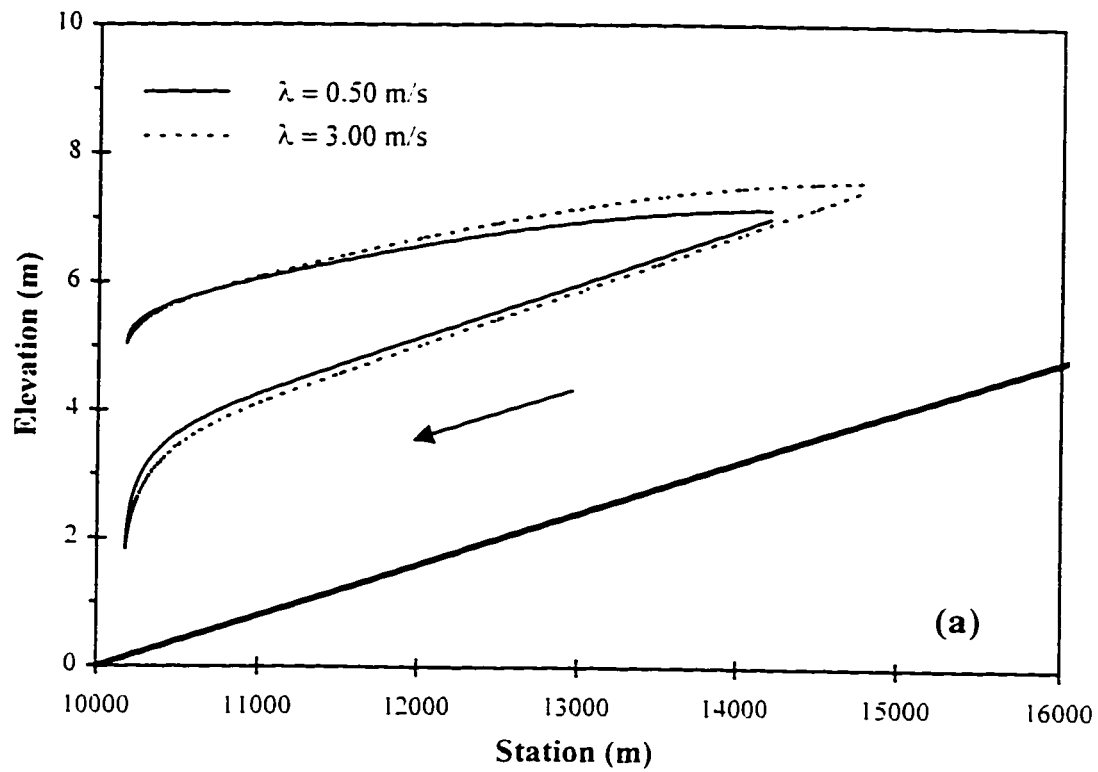


Figure 3.10. Sensitivity of RIVJAM to  $\lambda$  for (a) constant toe thickness and (b) consistent ice jam length.

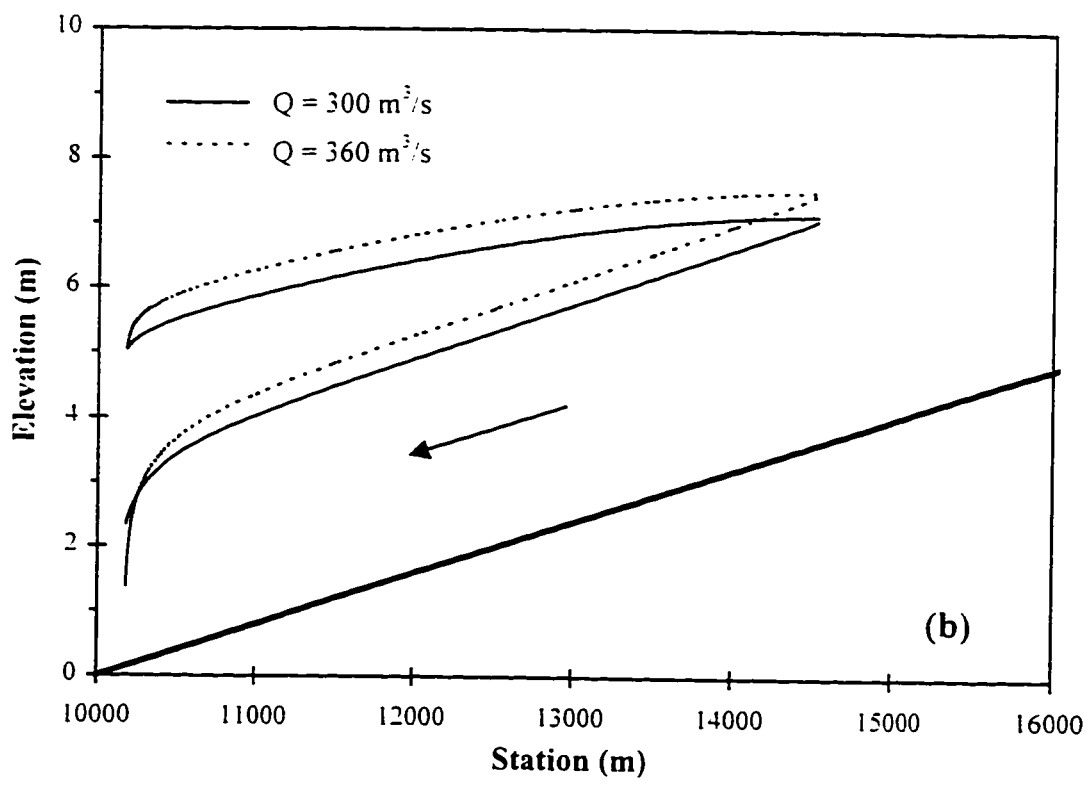
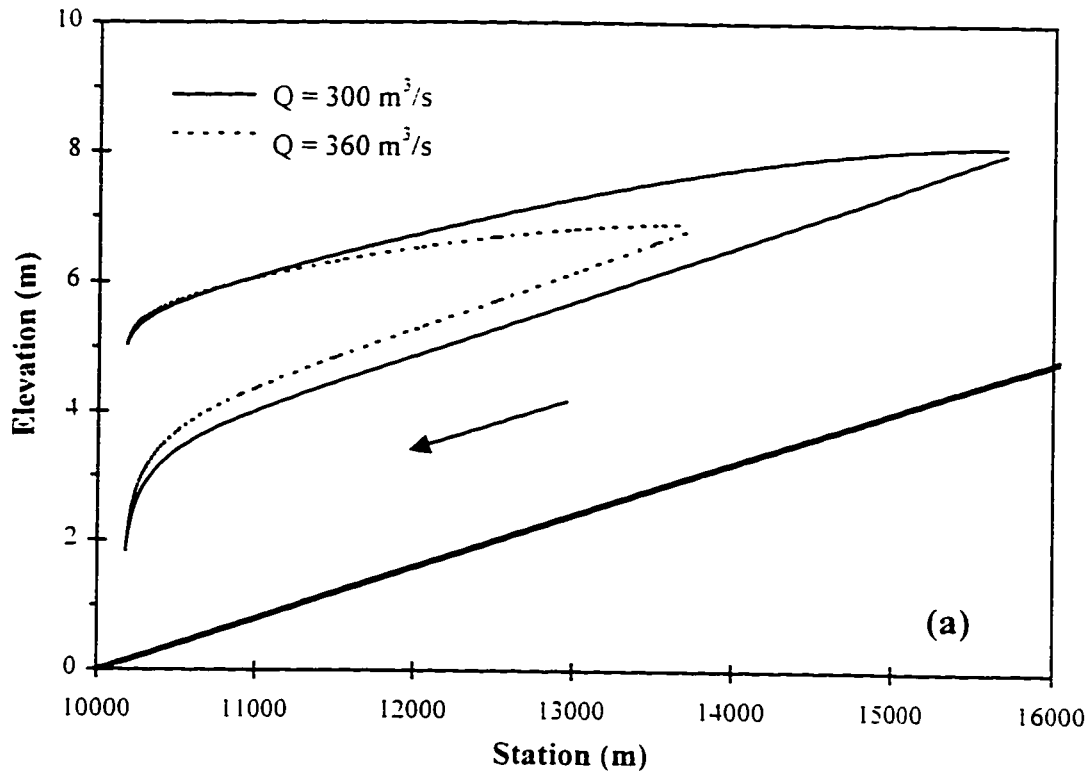


Figure 3.11. Sensitivity of RIVJAM to  $Q$  for (a) constant toe thickness and (b) consistent ice jam length.

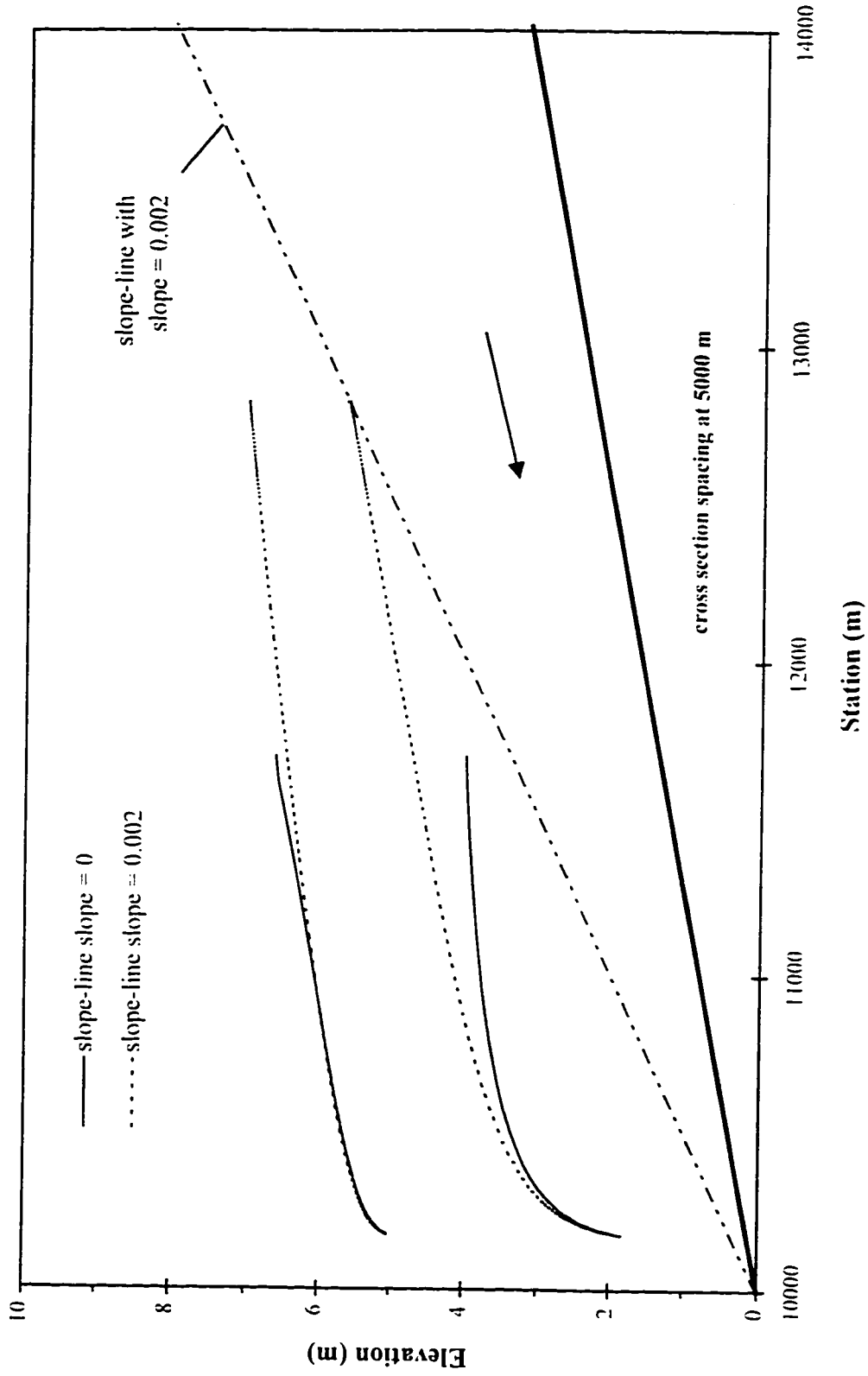


Figure 3.12. Sensitivity of RIVJAM to slope-line slope.

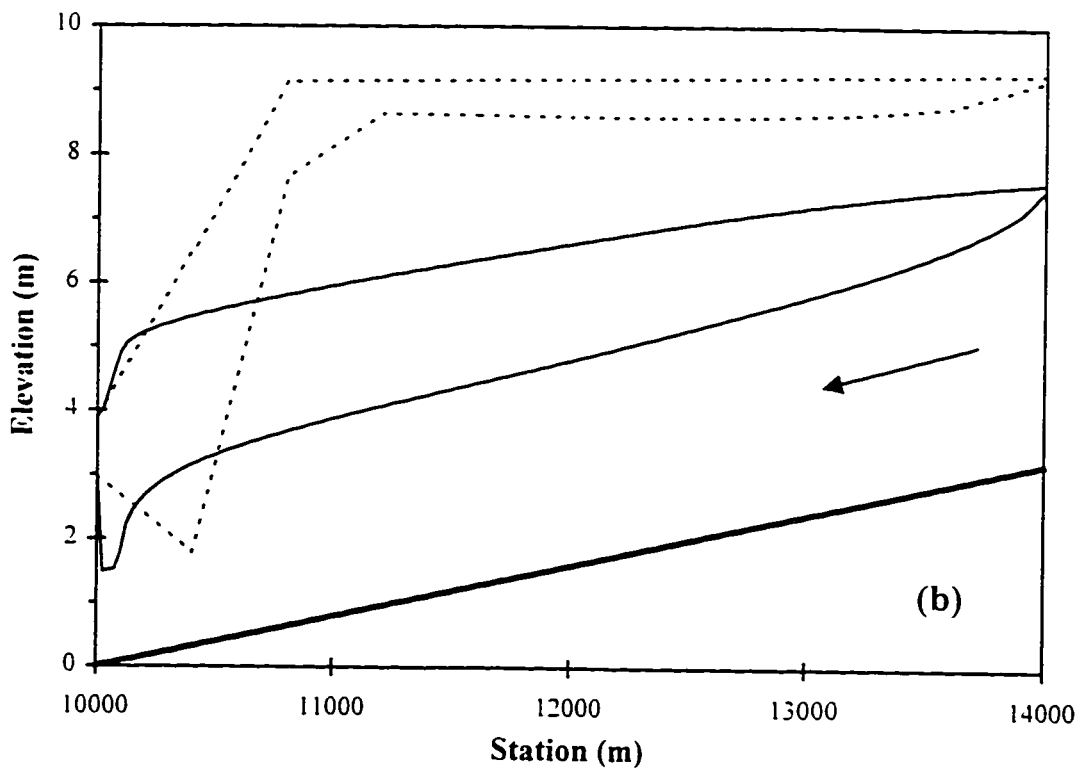
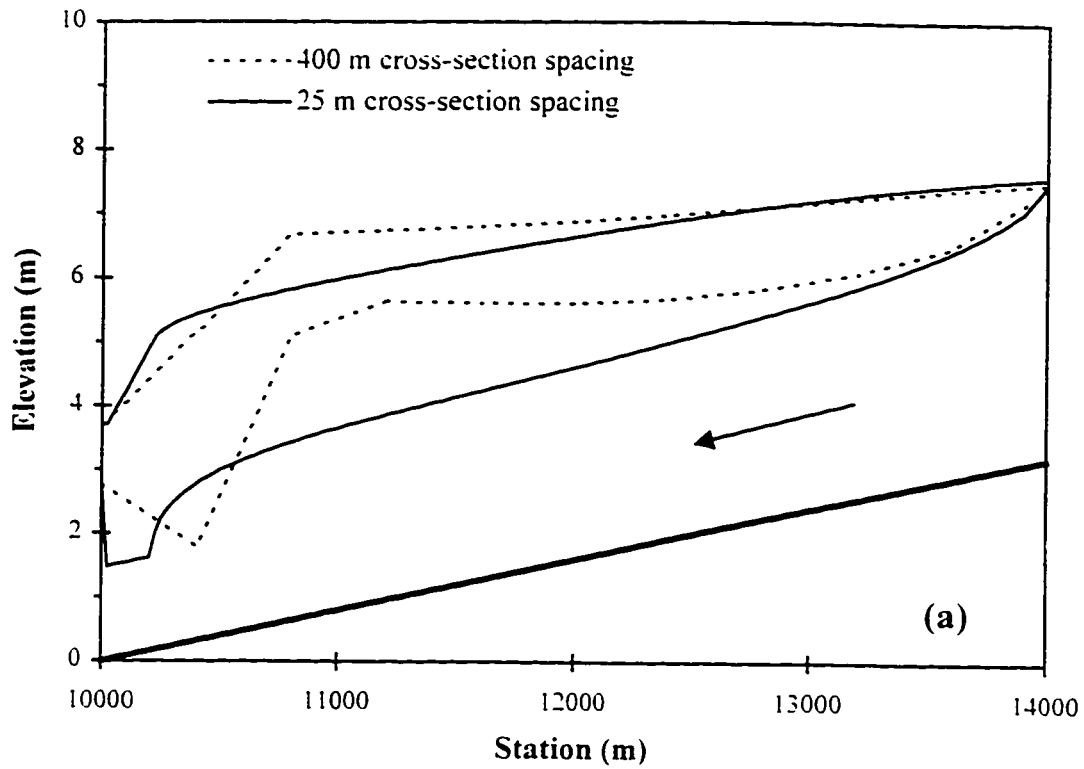


Figure 3.13. Sensitivity of ICEJAM to cross section spacing using (a) Manning's roughness, and (b) Chezy's roughness.

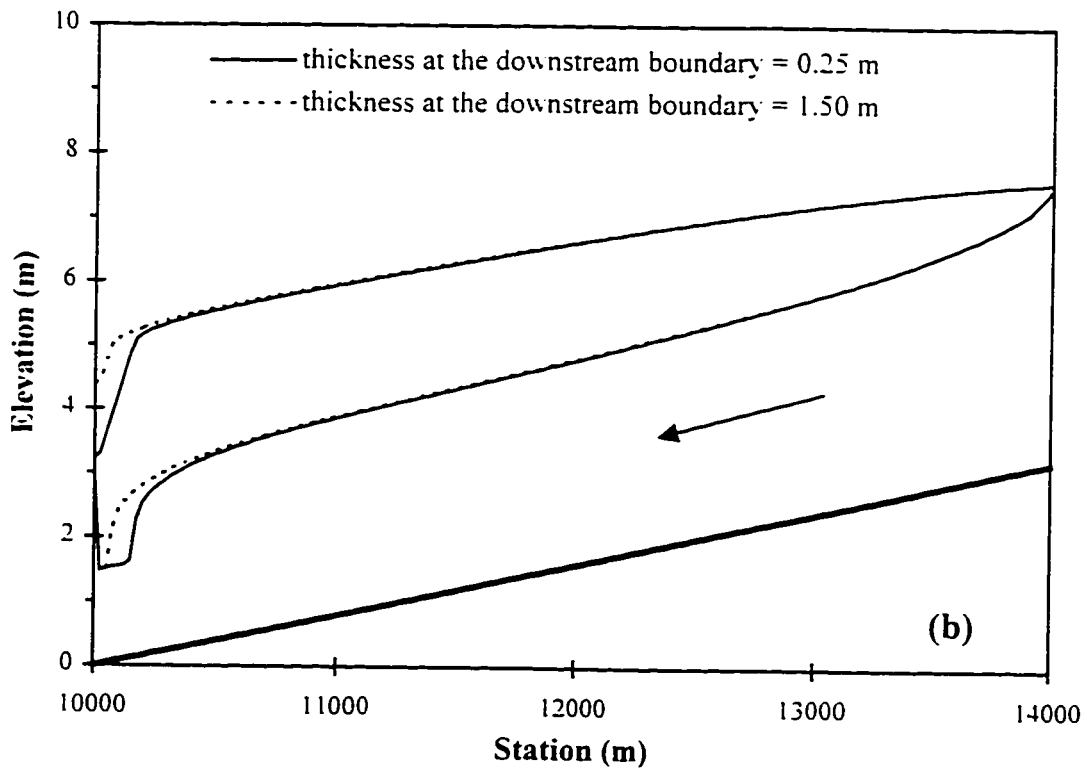
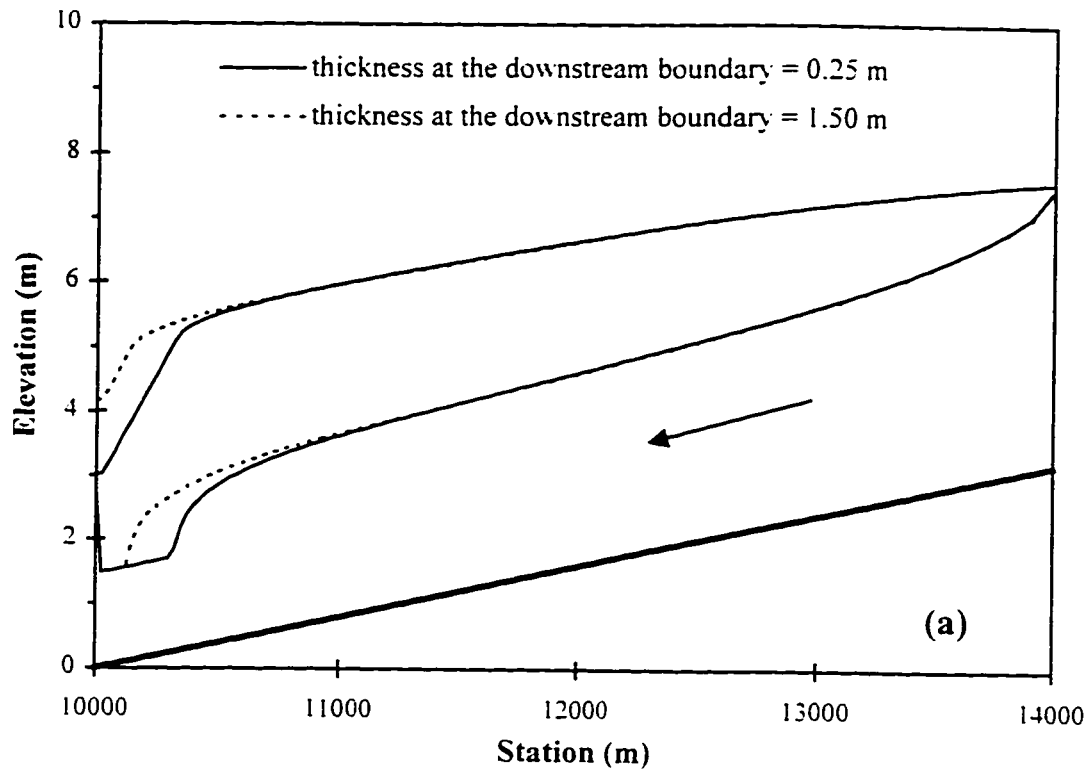


Figure 3.14. Sensitivity of ICEJAM to thickness at the downstream boundary for (a) Mannings roughness, and (b) Chezy's roughness.

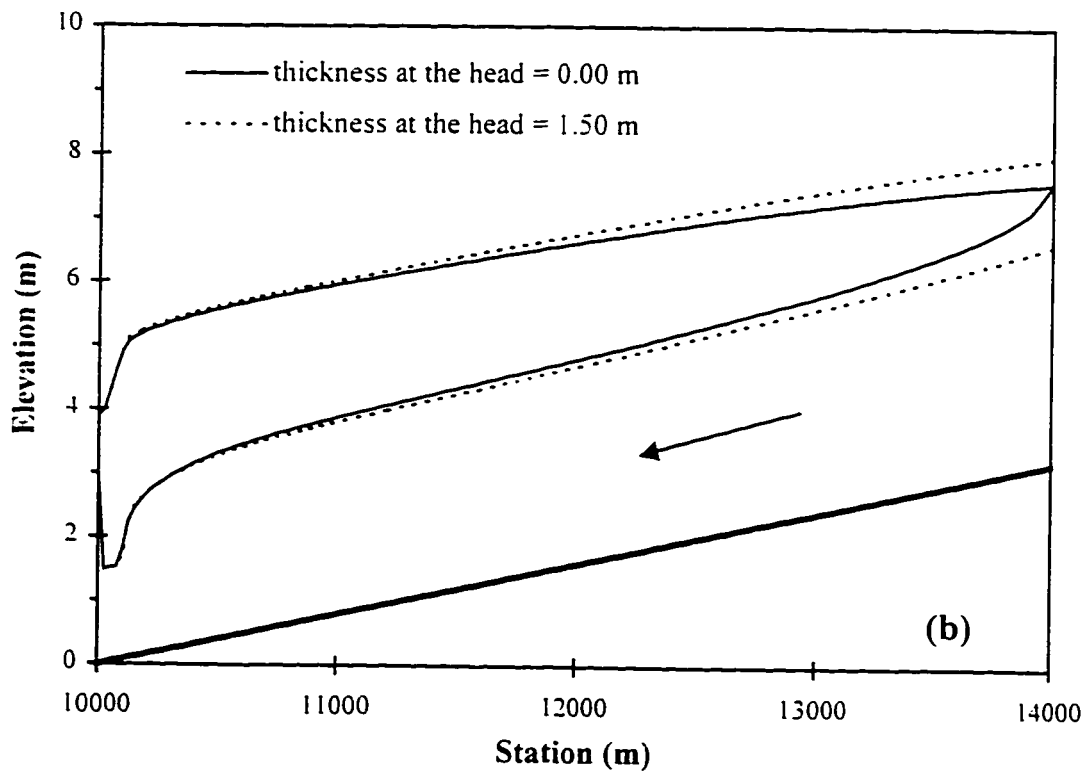
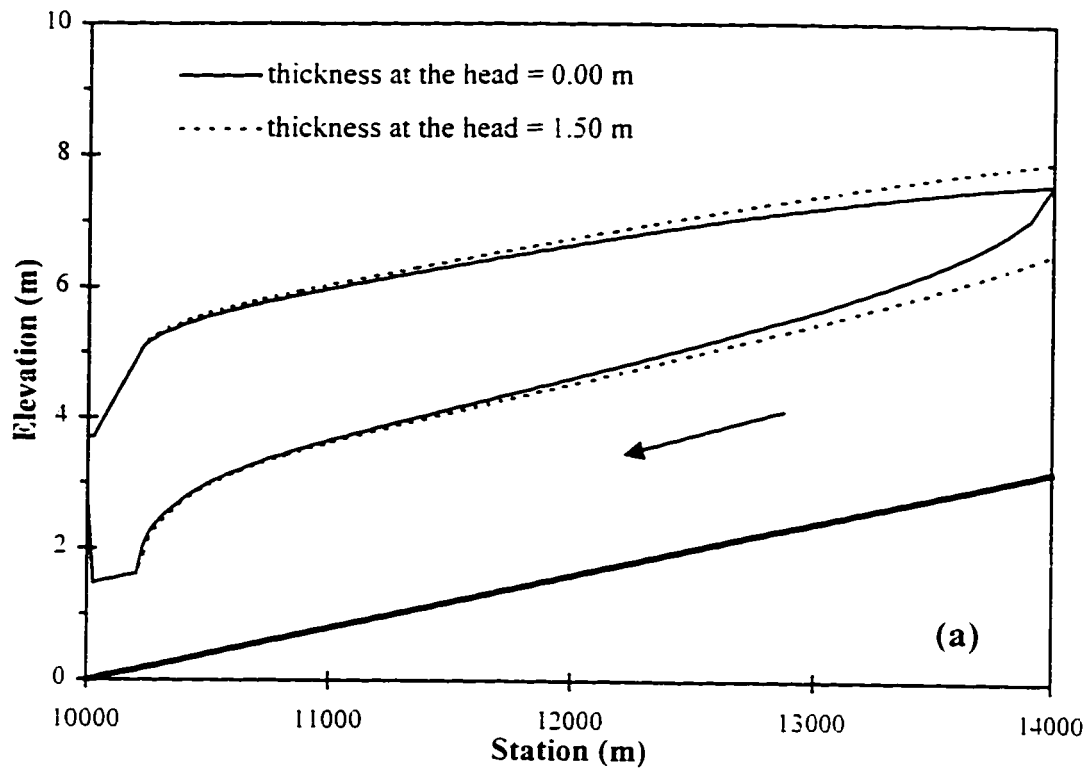


Figure 3.15. Sensitivity of ICEJAM to the thickness at the head for (a) Mannings roughness, and (b) Chezy's roughness.

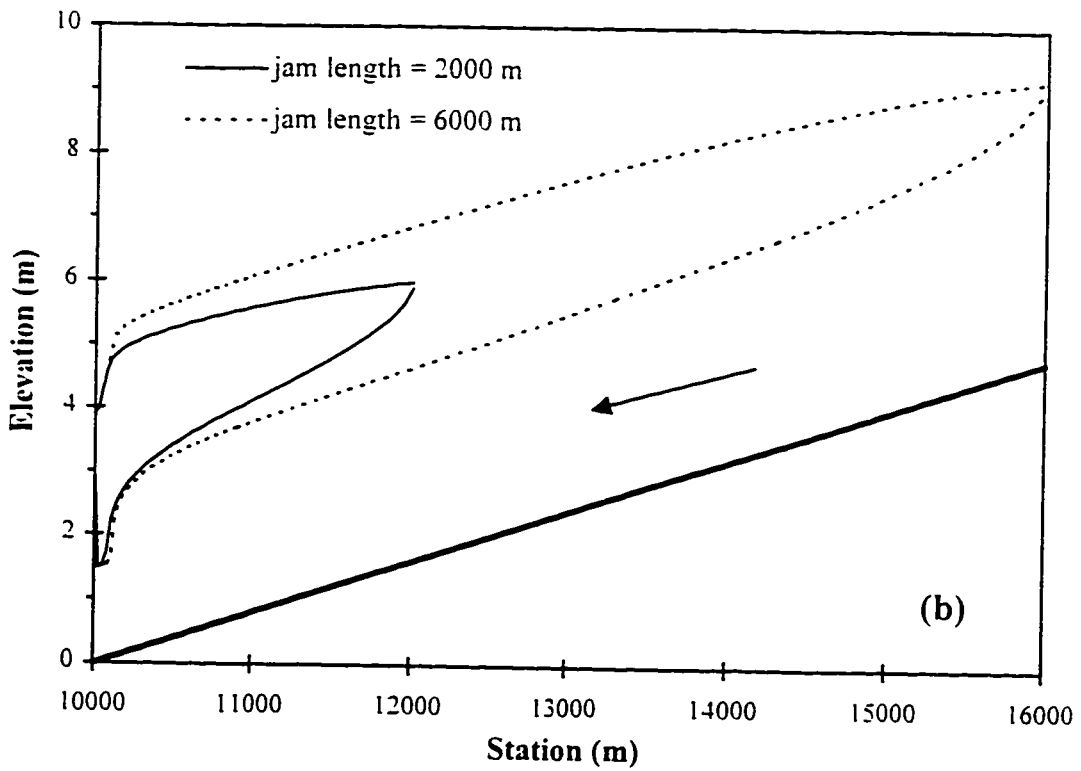
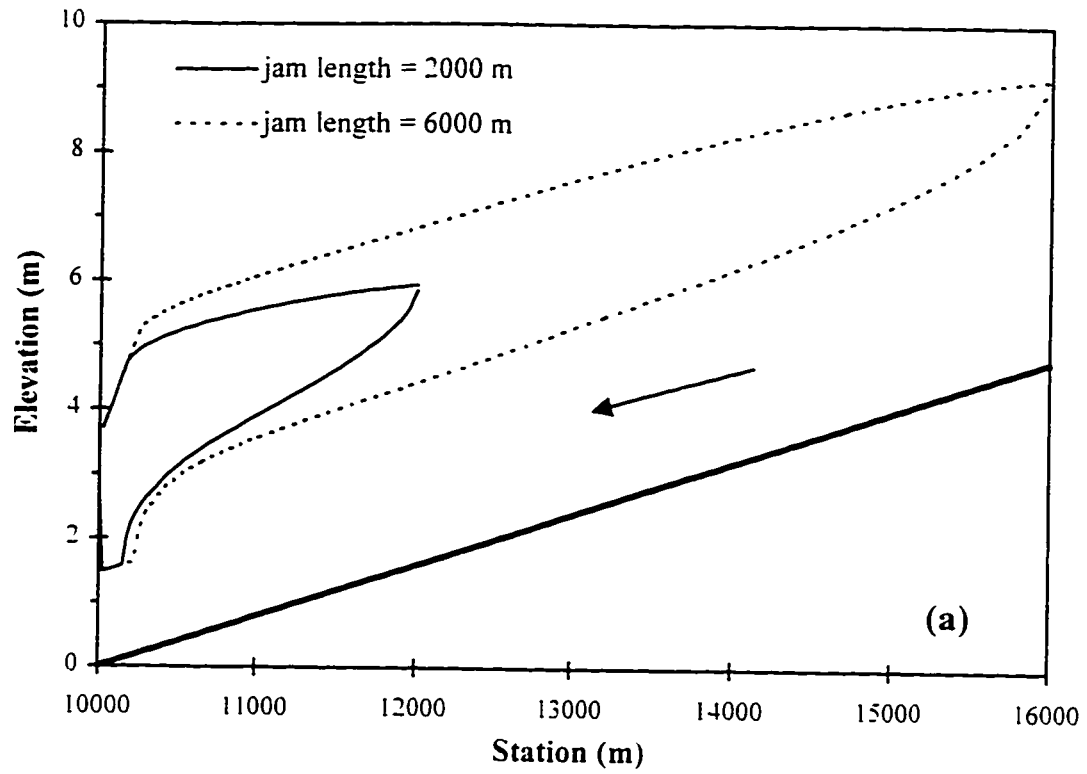


Figure 3.16. Sensitivity of ICEJAM to jam length for (a) Manning's roughness, and (b) Chezy's roughness.



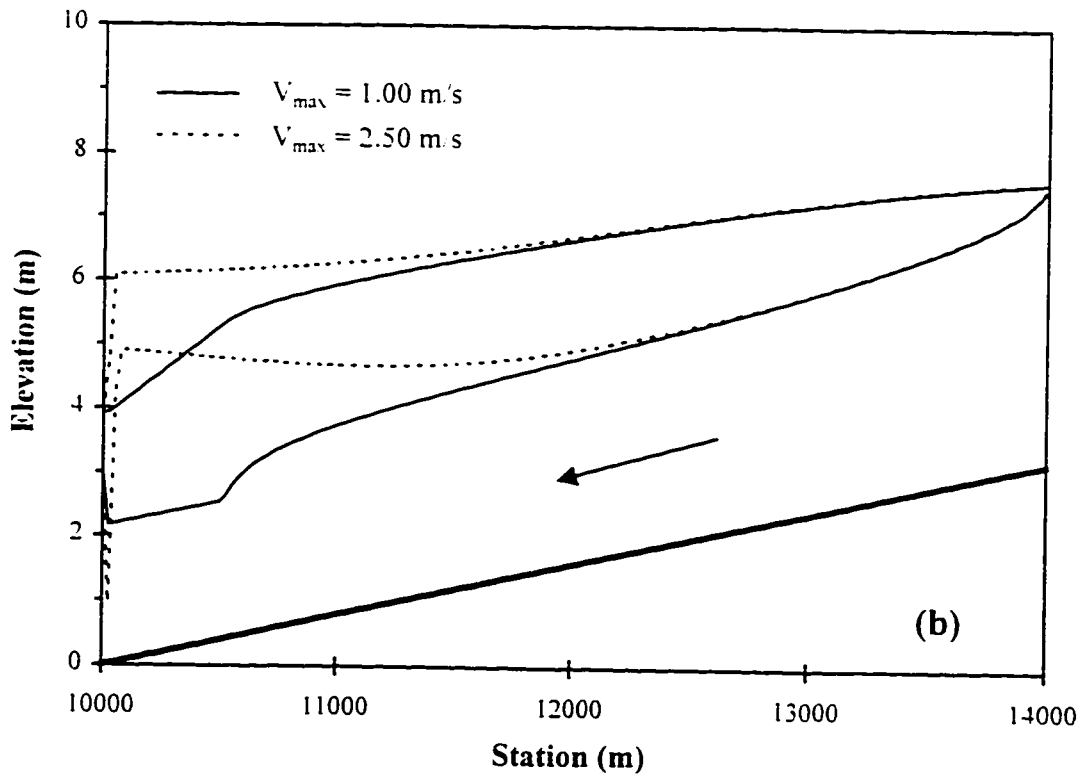
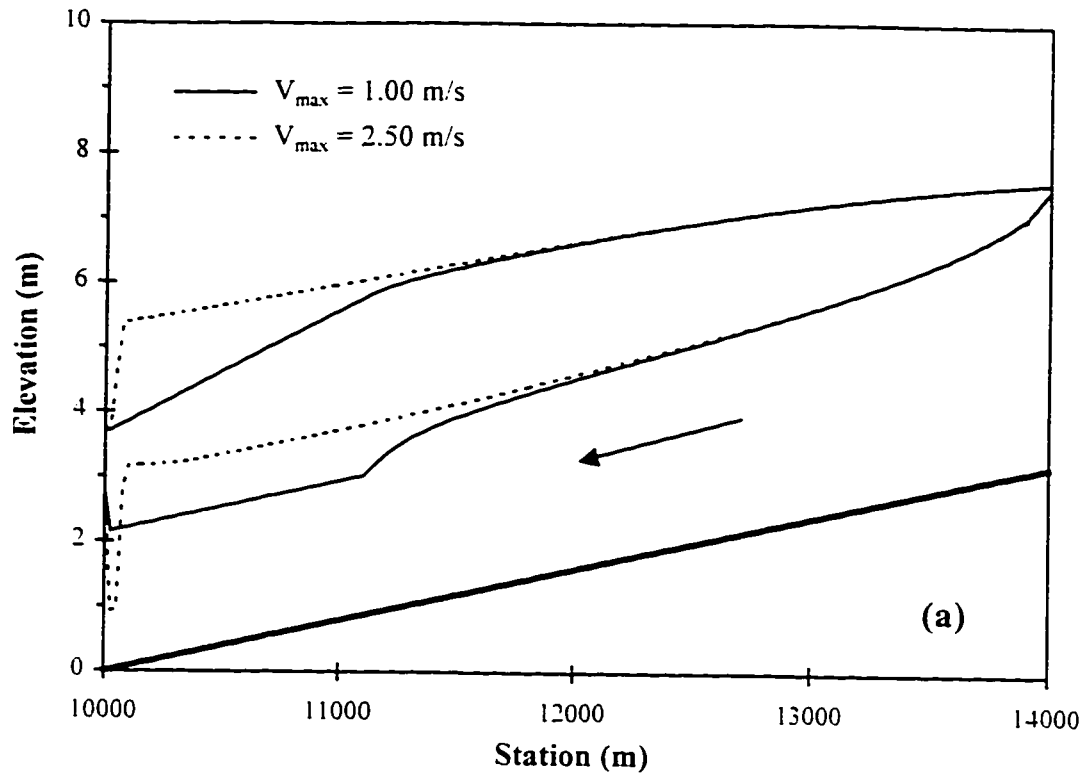


Figure 3.17. Sensitivity of ICEJAM to erosion velocity for (a) Mannings roughness, and (b) Chezy's roughness.

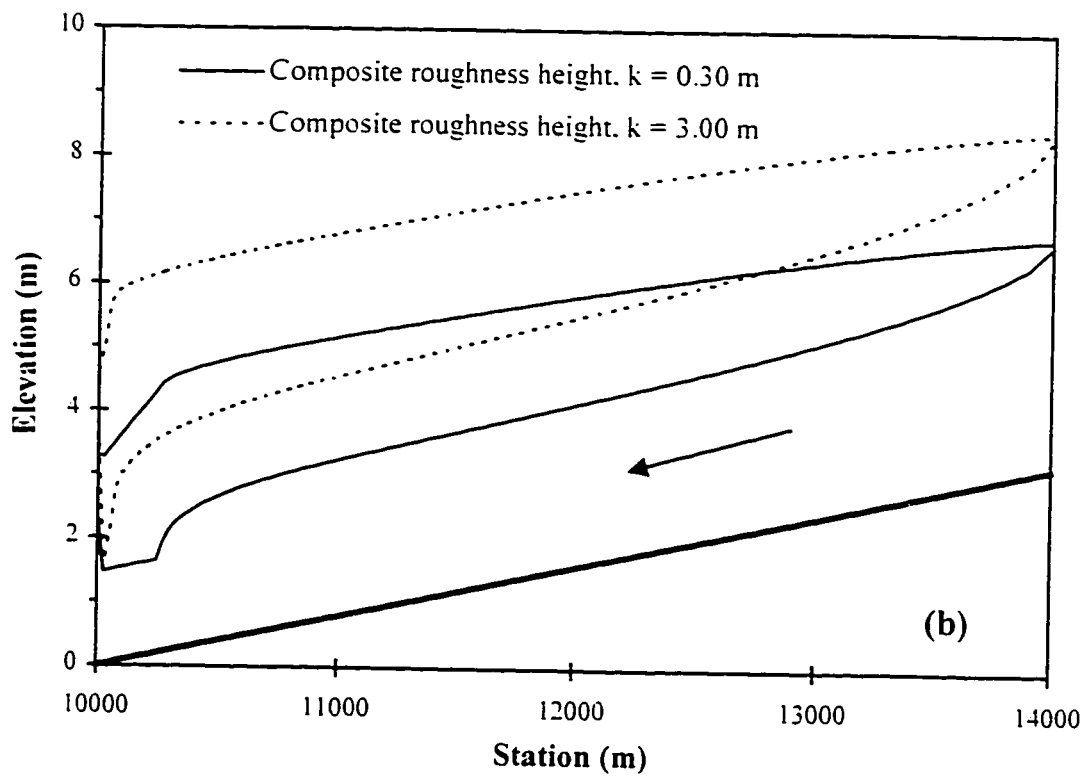
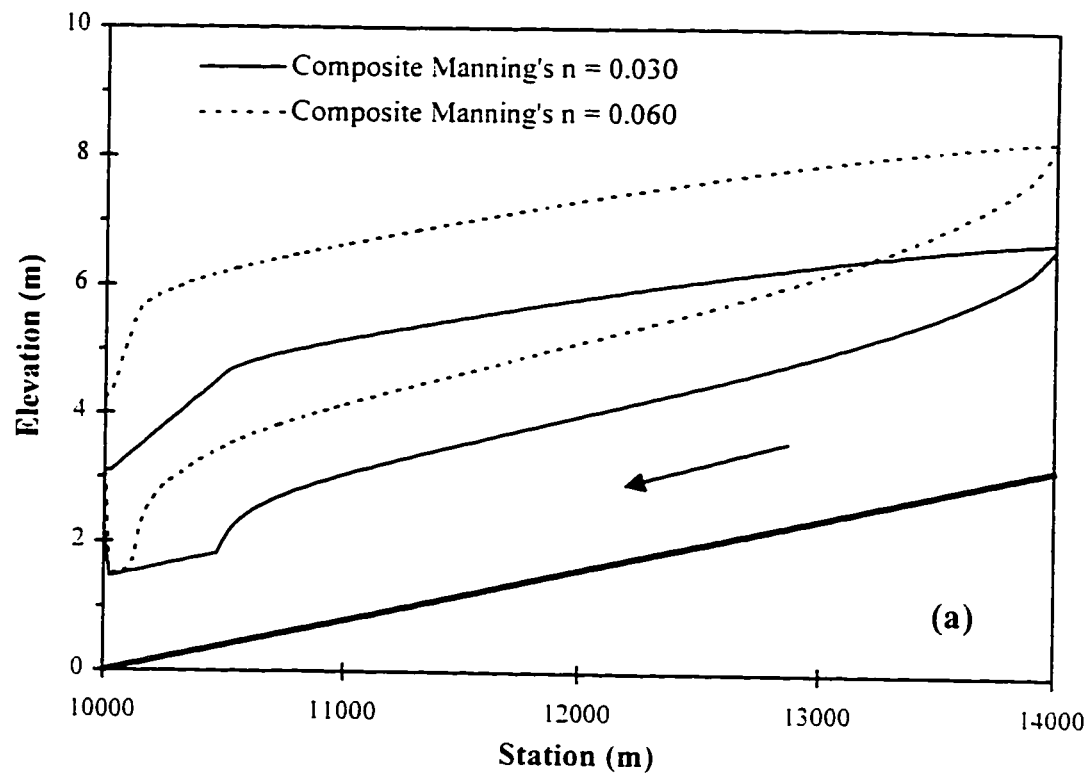


Figure 3.18. Sensitivity of ICEJAM to roughness for (a) Mannings roughness, and (b) Chezy's roughness.

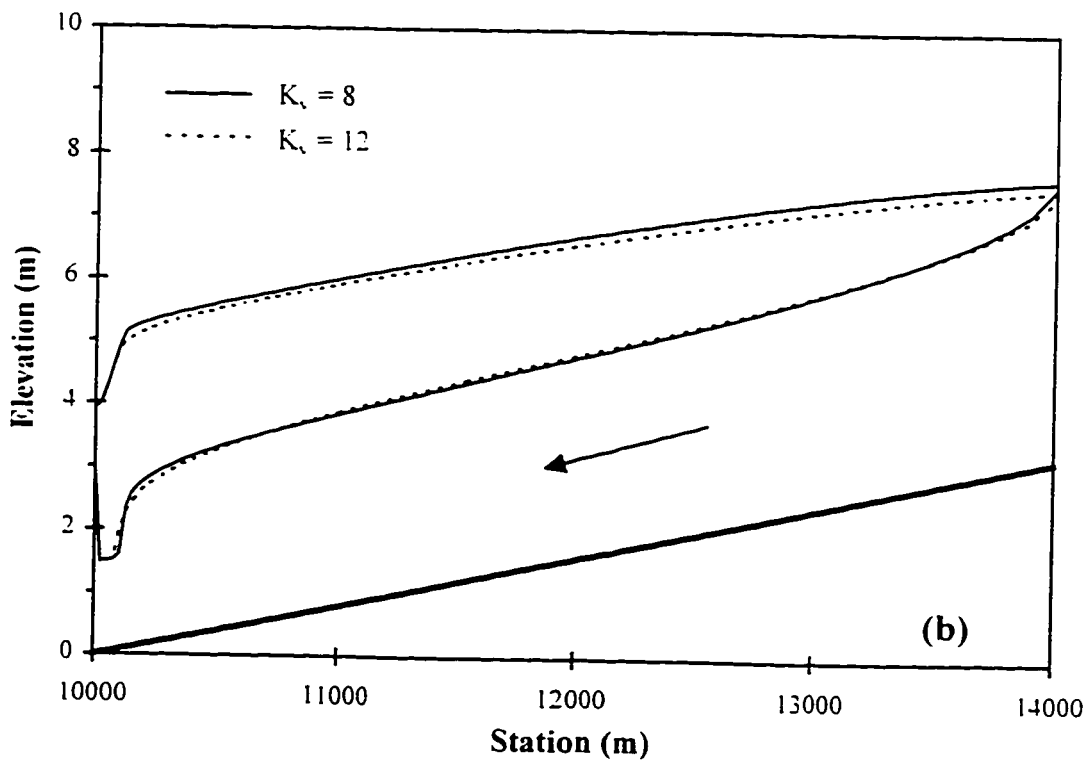
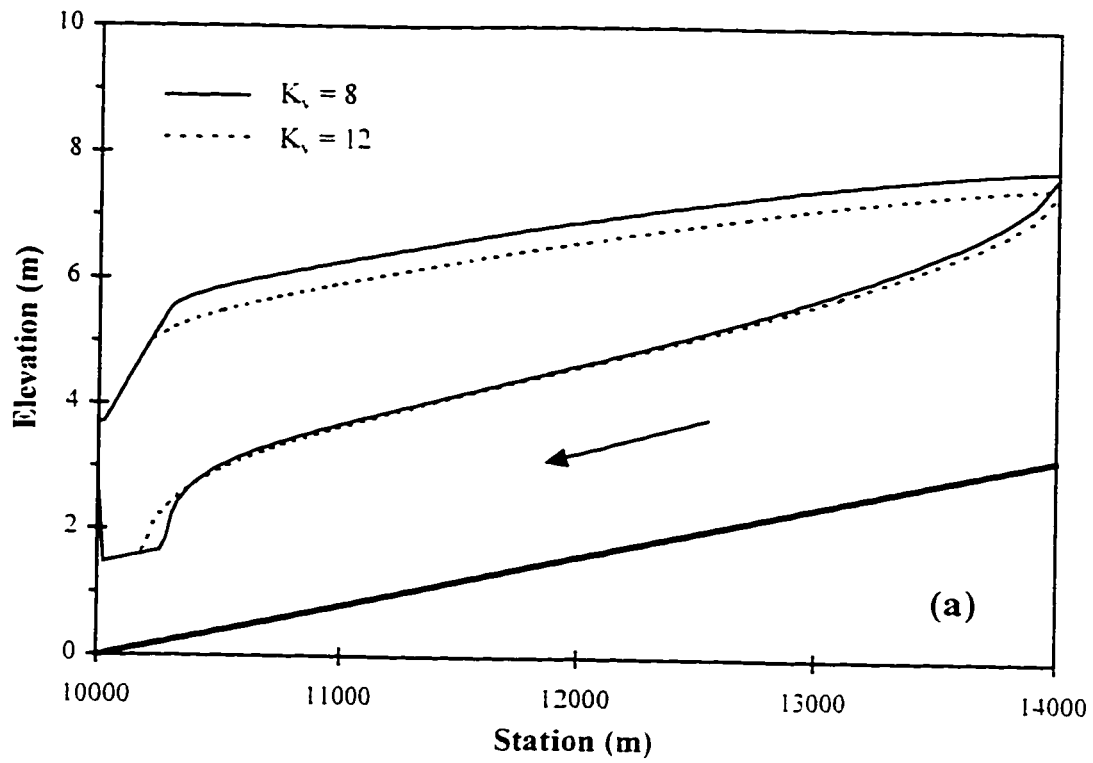


Figure 3.19. Sensitivity of ICEJAM to  $K_s$  for  
 (a) Manning's roughness, and (b) Chezy's roughness.

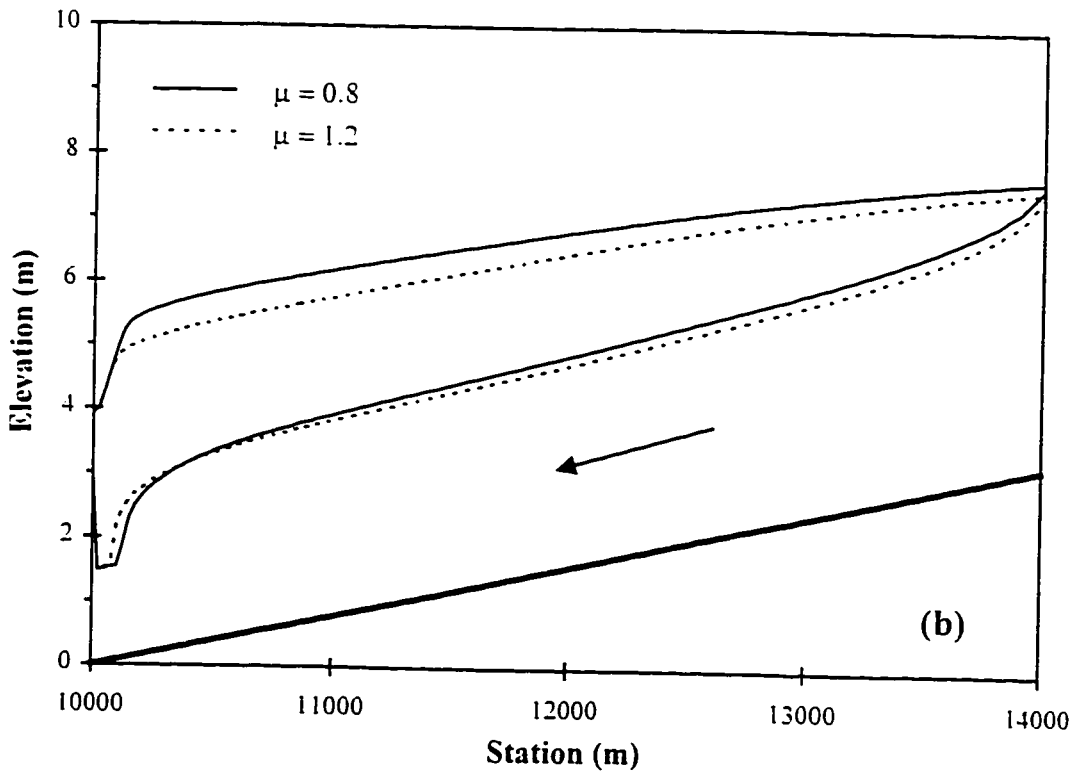
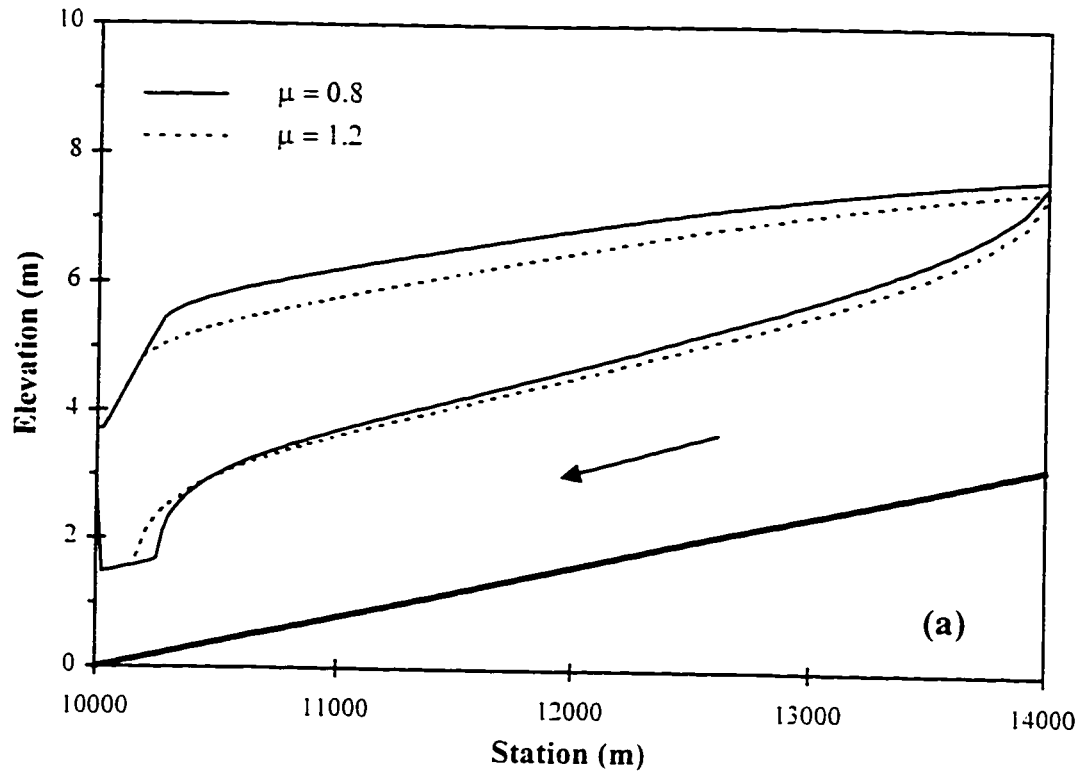


Figure 3.20. Sensitivity of ICEJAM to  $\mu$  for (a) Manning's roughness, and (b) Chezy's roughness.

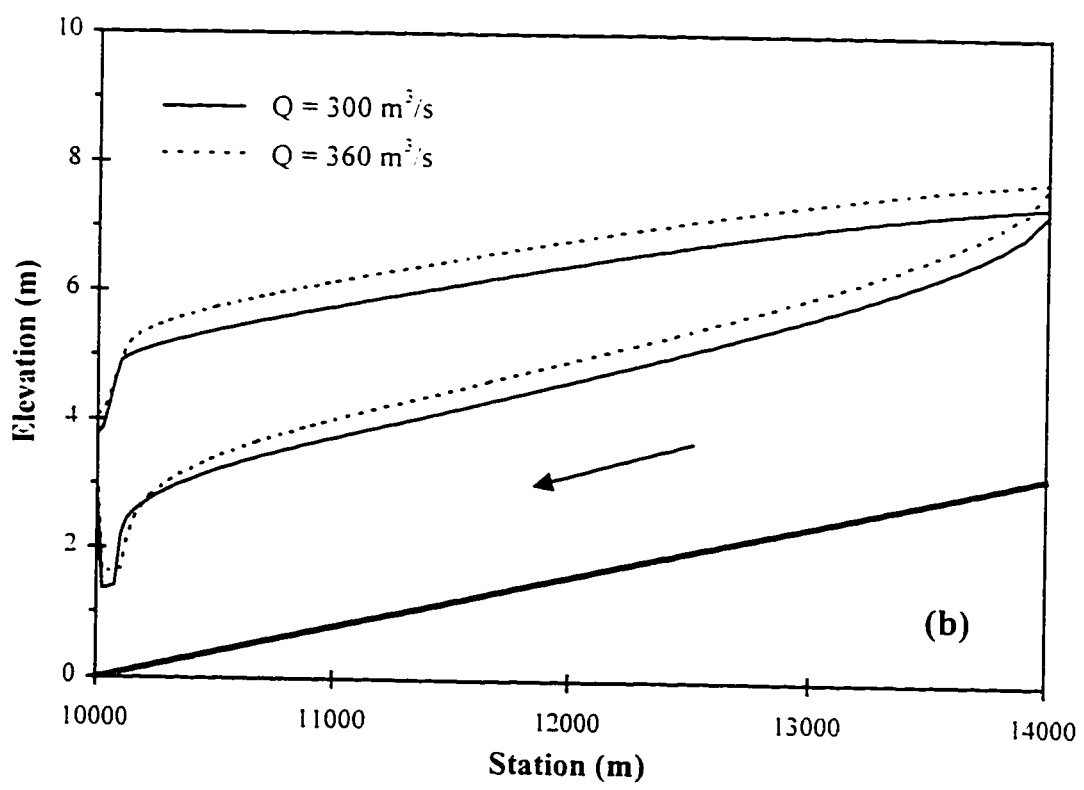
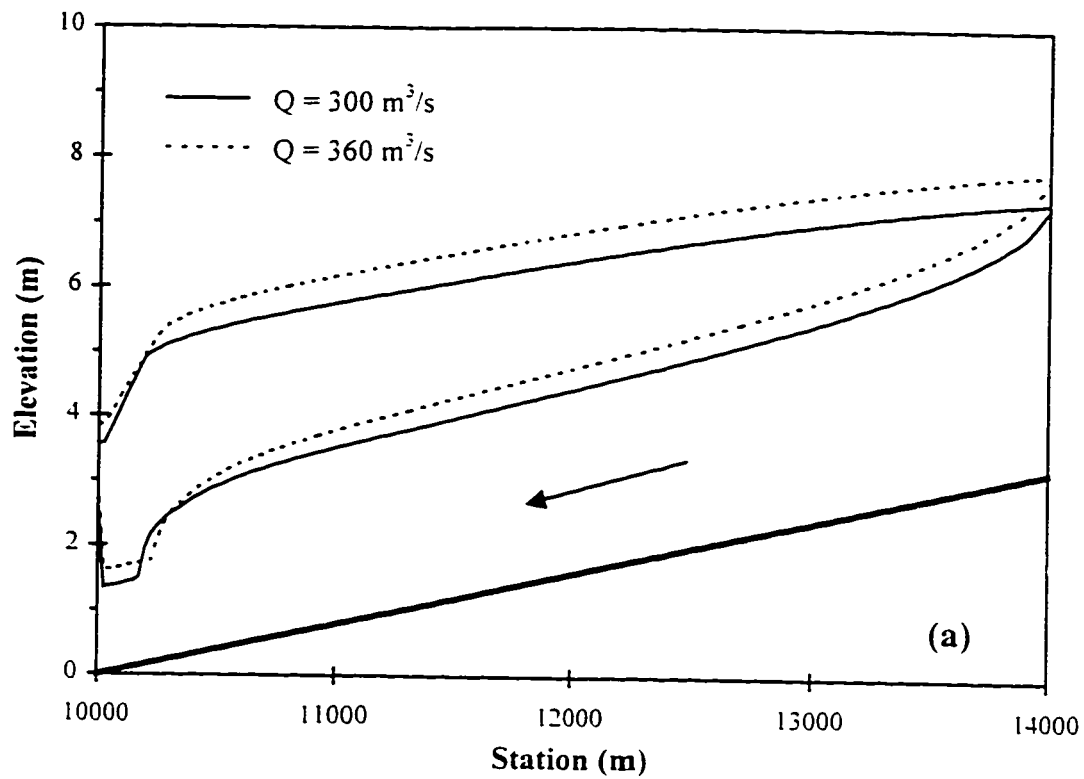


Figure 3.21. Sensitivity of ICEJAM to  $Q$  for (a) Mannings roughness, and (b) Chezy's roughness.

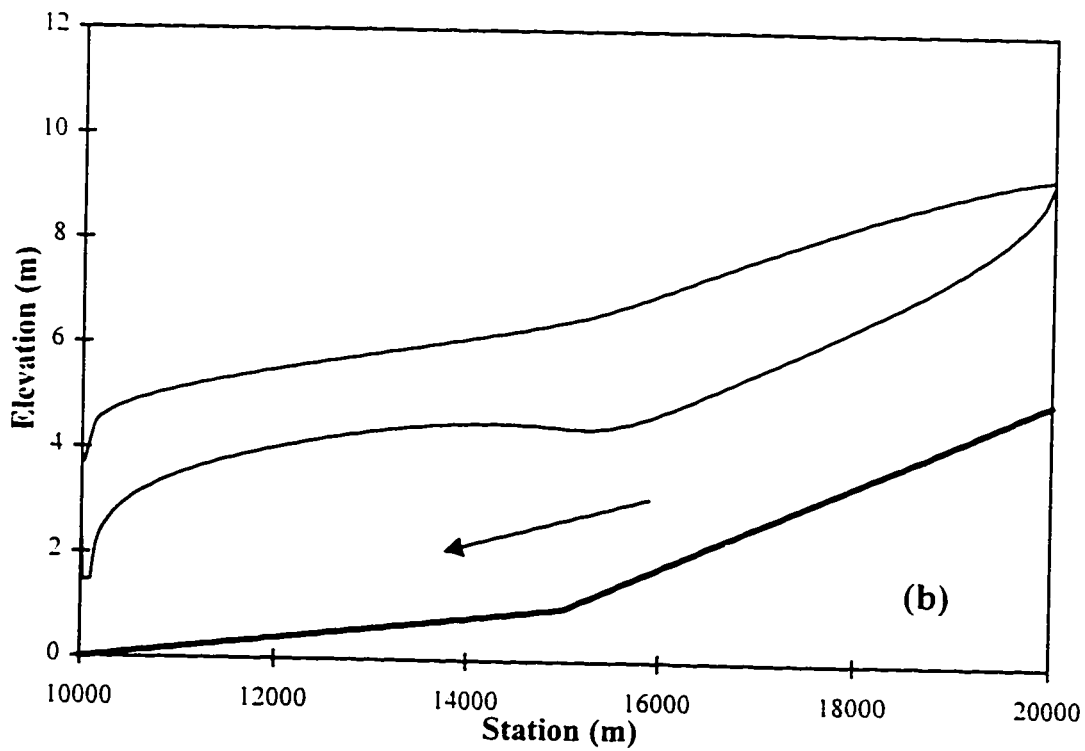
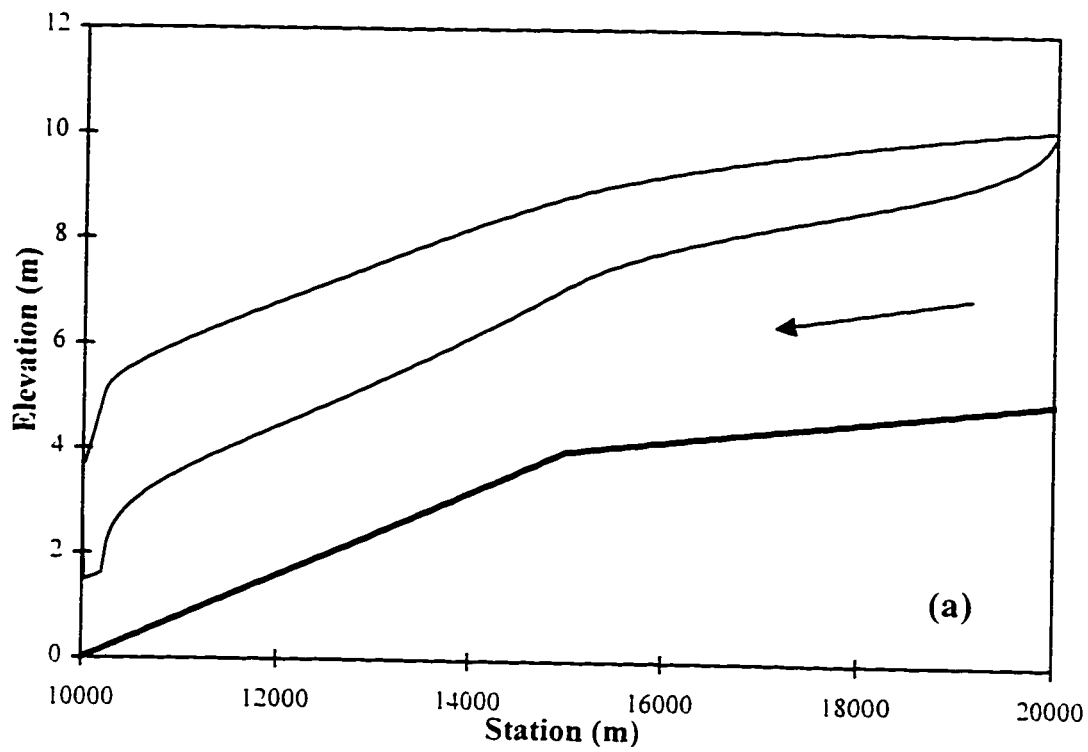


Figure 3.22. Sensitivity of ICEJAM to a change in channel slope for (a) 0.0002 to 0.0008, and (b) 0.0008 to 0.0002

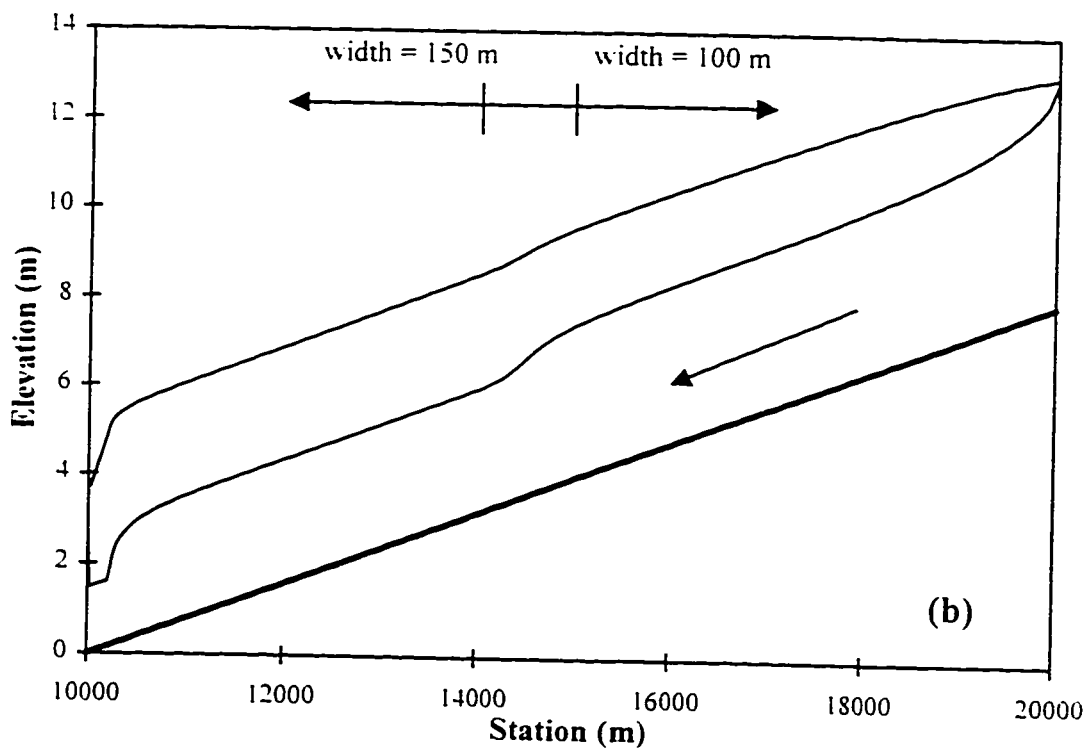
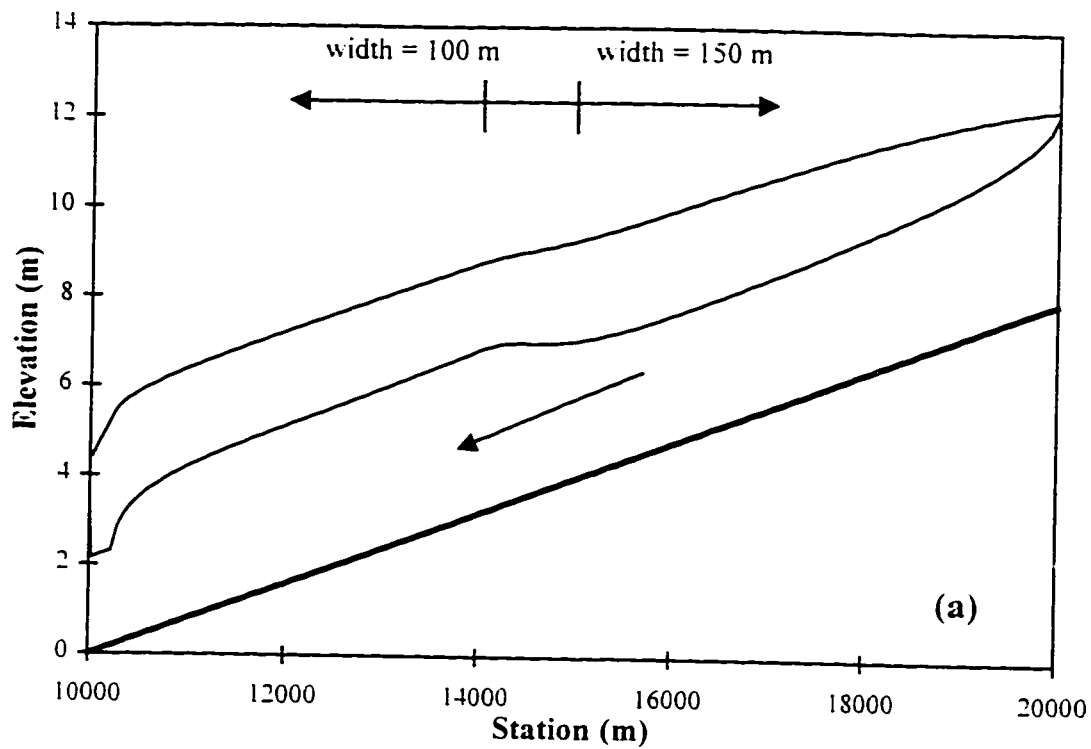


Figure 3.23. Sensitivity of ICEJAM to a change in channel width for (a) 150 m to 100 m wide, and (b) 100 m to 150 m wide

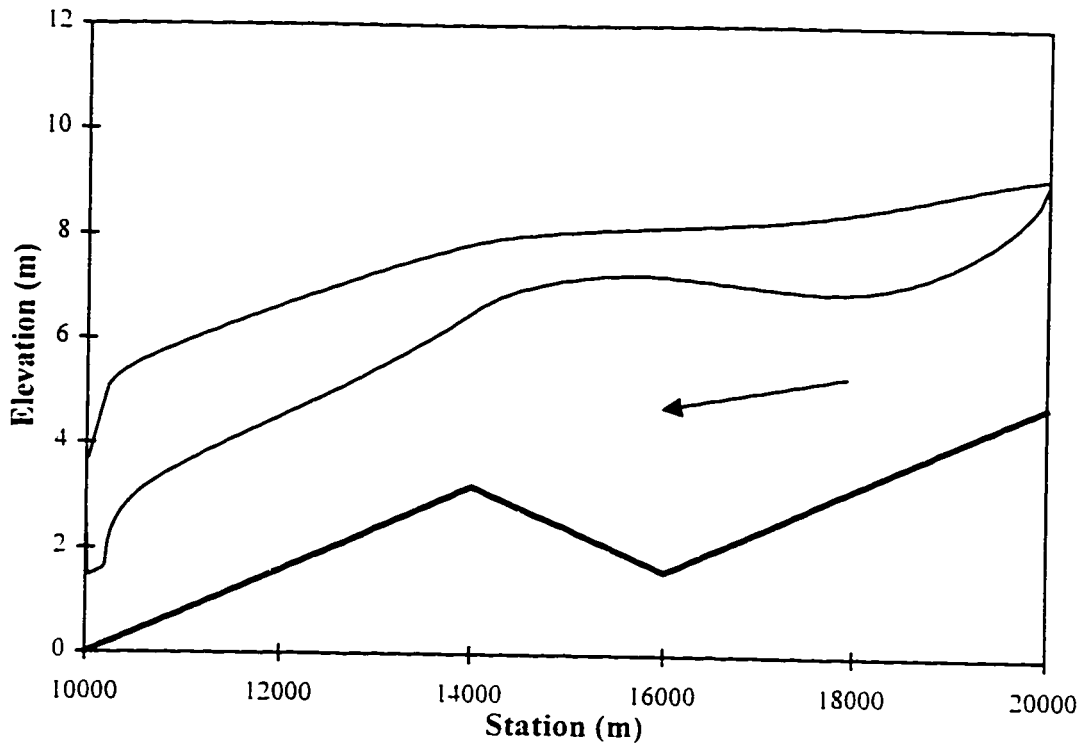


Figure 3.24. Sensitivity of ICEJAM to an adverse slope.

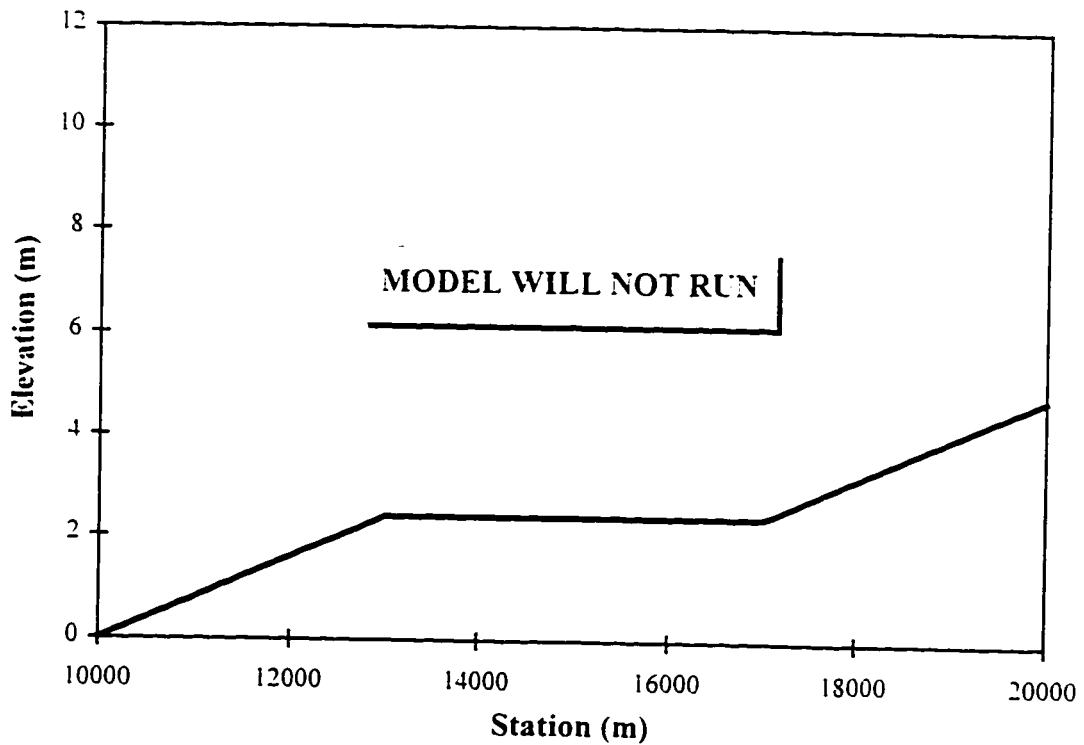


Figure 3.25. Sensitivity of ICEJAM to a horizontal slope.



## CHAPTER 4.0 MODEL EVALUATION USING DOCUMENTED ICE JAM EVENTS

### 4.1 GENERAL

The objectives of the numerical modelling portion of the study were: to investigate the ice jam profile models through their application to documented ice jam events; to develop a standard protocol for their efficient use; to evaluate the quality of the data available for the case studies; and to gain some general insight on the characteristics of the ice jams under study.

Figure 4.1 illustrates the site locations of those documented ice jam events used for this study. These documented ice jam events occurred on: the Restigouche and Saint John Rivers, in New Brunswick; the Thames River near Chatham, Ontario; the Hay River at the town of Hay River in the North West Territories, and the Athabasca River near Fort McMurray, Alberta.

### 4.2 DATA COLLATION

#### 4.2.1 General

It was not feasible to collect data directly in the field in part due to a lack of resources and in terms of confidence in being able to collect a complete set of data for analysis. Ice jam events are unpredictable and identifying exactly where and when one might occur is an unrealistic goal. Even after selecting a reach of river where ice jam events are known to occur, it is possible that an ice jam event would not have occurred (as

would be the case for a thermal breakup) or the jam might not have been of the wide channel type defined by Pariset, *et al.* (1966). Therefore, the data used in this study were collated from previously documented events available in the literature. An analysis based on a data set that contained several documented ice jam events was preferred over an analysis which relied solely on a single data set. Through application to fourteen documented events obtained from the literature, the models were tested against a variety of hydraulic and geometric conditions.

A data report providing a complete summary of the data, and methods used for its reduction and interpretation, describing the documented ice jam events investigated in this study is currently under development (Healy, 1997).

#### **4.2.2 Data Requirements**

The first task of the data collation phase was to identify the data required to investigate the models' behaviour through their application to documented events. Based on the models' required input and computed output it was determined that the following data was needed to achieve the objectives of this investigation: cross sectional data to describe the geometry of the river; measured data describing the observed ice jam profile; and knowledge of the carrier discharge corresponding to the observed ice jam profile. Of course, geometric data and documented ice jam profile data must be referenced to a common datum. Given this required information, an ice jam profile could then be computed and compared to the observed ice jam profile. Ideally, the observed ice jam profile data would clearly identify both the water surface profile and the bottom of ice profile (thickness profile) along the entire length of the jam, extending from below the toe to above the head. Also, an ideal set of data would identify the location of the obstruction at the toe (typically a solid intact ice sheet) and the upstream limit of the ice accumulation governed by the wide jam criteria defined by Pariset, *et al.* (1966).

### **4.2.3 Data Sources**

Potentially suitable documented ice jam events were identified from journal papers, conference papers, and published technical reports. The journal and conference papers did not provide the minimum amount of data required for the analysis (typically cross sectional data was missing). Therefore, the authors of these papers were contacted to request additional data, where available.

Government agencies provided the most complete data, in the published reports on ice jam documentation. The data used for this study were mostly obtained from the following sources: the National Water Research Institute in Burlington Ontario; New Brunswick Department of the Environment, N.B. Power; the Alberta Research Council; the Department of Civil and Environmental Engineering, University of Alberta; and Trillium Engineering and Hydrographics Inc., Edmonton. The specific sources used for each event are cited in this report as the data are presented.

### **4.2.4 Data Selection and Interpretation**

Only those documented events which provided the required data were selected for use in this investigation. These were events where there was adequate cross sectional, jam profile, and discharge data available. Usually this data required conversion to a format which was compatible with the models.

A considerable amount of time was invested in the data collation process since much of the data (in particular the data from the Alberta Research Council) were available only in graphical form. These data were digitized and then input into file formats compatible with the models. This process involved transferring graphs onto tracing paper (to obtain a clear and sharp image free of annotation clutter), and then scanning them into an image file on a personal computer. Next, these computer images were digitized using the Sigma Scan<sup>c</sup> software package to obtain numeric data which could then be collated into a usable form for the models.

In some cases the cross sections were not referenced to a common datum or were referenced only to a measured (open water) surface profile. For these cases a datum was established by interpolating between known sections that were referenced to a common datum.

## **4.3 MODELLING APPROACH**

### **4.3.1 Developing Model Familiarity**

Application of these models to reproduce documented ice jam events was not always straightforward. Therefore, it was first necessary to develop a general familiarity with the models. This allowed for the development of a standard, effective approach to the modelling process. To achieve this, the models were applied to several of the case studies using the cross sectional data and discharge corresponding to the particular documented ice jam event under investigation. The computed profiles generated by the models were then plotted with the measured profile data to facilitate a visual comparison. Model input parameters were then adjusted for computation of different profiles and observations were made as to how well the computed profiles matched the observed data. Through an extensive trial and error process, a general familiarity with the models was gained and an intuition about the impact of each parameter on the computed profile was developed.

### **4.3.2 The Modelling Process**

To develop a more scientific approach to the modelling process, a rigorous investigation of the models was conducted through application to selected case studies for which more comprehensive data was available. Through this investigation, a standard modelling protocol was developed. This protocol was then tested against the remaining case studies to assess and refine the protocol and to explore any trends in ice jam roughness or other ice jam characteristics using a standardized method.

### **4.3.3 Calibration Criteria**

ICEJAM and RIVJAM were calibrated for all 14 recorded ice jam events, to investigate their behaviour and their relative sensitivity to input parameters. The models were calibrated to measured data given a priori information on discharge and boundary conditions. The measured data consisted of water surface and bottom-of-ice elevations located along (horizontally) the length of the documented ice jam. Roughness was adjusted manually for each event to provide the best visual fit between simulated and measured data.

For each calibration, the computed water surface profile was matched to the measured one. The best visual fit constituted a computed water surface profile that represented the best visual average through the measured data points. Mannings  $n$  was adjusted to the nearest 0.005; for Beltaos' friction factor,  $c$  was adjusted to the nearest 0.01.

## **4.4 RIGOROUS MODEL INVESTIGATION**

### **4.4.1 Case Studies Selection**

Three case studies were selected for detailed analysis and rigorous model investigation. The first was an ice jam which occurred on the Restigouche River in New Brunswick on April 6, 1988. This particular case study was selected primarily because the documented configuration near the ice jam toe suggested extensive grounding and, since the ICEJAM model does not consider flow through interstices, it provided a good opportunity to examine the importance of this capability to modelling grounded ice jams, in addition to the models' general sensitivity to input conditions.

The second case study selected was an ice jam documented by Beltaos and Moody (1986) which occurred on the Thames River in Ontario on February 26, 1986. This event was selected because during this study it was found that the documented length

of the jam disagreed noticeably with the computed length produced by the RIVJAM model in some cases. This event proved to be a challenging problem for both models, in particular, because it was an event where the two models could be made to produce either very similar, or very different results.

The third case study selected was an ice jam documented by Beltaos, Burrell, and Ismail (1994) which occurred on the Saint John River in New Brunswick on April 14, 1993. This event was selected as there were two different carrier discharge estimates, obtained by different methods, both of which were considered to be quite reasonable. This case study highlights the difficulty in obtaining reliable discharges for ice jam events and provided a means of investigating the importance of obtaining accurate discharges to successful model application.

#### **4.4.2 Ice Jam with Suspected Grounding - Restigouche River**

Figure 4.2 presents a general location plan of the Restigouche River and cross section locations used for the analysis along the reach of interest. The Restigouche River extends from its headwaters in the Chaleur Uplands in northern New Brunswick and flows in a generally easterly direction to the border between Quebec and New Brunswick. It then follows the border downstream of its confluence with the Patapedia River to its mouth which empties into Chaleur Bay. Chaleur Bay is shared by Quebec to the north and New Brunswick to the south. The reach of interest for this study extends from the entrance of Upsalquitch River downstream to its confluence with the Matapedia River.

The ice jam, documented by Beltaos and Burrell (1990, see also: Beltaos and Burrell, 1996), formed initially on April 5, 1988, and was enlarged by incoming ice on April 6, 1988. Water surface profiles were measured through the resulting accumulation on April 6, 7 and 8. On April 6, the ice jam was observed to be approximately 18 km long, extending from its toe near Babcock Brook to its head near Brandy River. This ice jam profile remained relatively stable for approximately two days, and the data

obtained over these days produced “near coincident” profiles, therefore, steady state conditions could reasonably be assumed. The approximate bottom of the jam was estimated from shear wall data obtained on April 10, after the ice jam’s release and the data obtained suggested that “*the jam was practically grounded at the toe*” (Beltaos and Burrell, 1990).

The discharge could not be measured during the period the jam was documented. However, Beltaos and Burrell (1990) reported a good match to the measured data using RIVJAM with a discharge of 330 m<sup>3</sup>/s. This discharge was used in the application of the models during the investigation.

#### ***4.4.2.1 ICEJAM Model Application***

For the ICEJAM runs, frictional resistance was calculated based on Mannings equation. The three main reasons for selecting Mannings composite roughness,  $n_o$ , to compute frictional resistance over Chezy’s composite roughness (expressed in terms of a roughness height,  $k_o$ ), to compute frictional resistance were:

1. Those who study river engineering applications and processes are familiar with Mannings roughness and absolute values of Mannings roughness possess physical meaning to these investigators.
2. For flows under ice covers, and in particular for very rough under ice surfaces (which are common to ice jams), the roughness height used for Chezy’s roughness computations may approach or even exceed the depth of flow.
3. The connection between Mannings roughness and Beltaos’ friction factor described in equation [3.19] could be tested through the analysis.

#### ***Roughness Calibrations***

For the first ICEJAM calibration  $K_x$  was set to 10,  $\mu$  was set to 1.0, and the *erosion* velocity,  $V'_{max}$ , was set to 2.00 m/s. Mannings composite roughness was then adjusted

to provide the best visual fit to the observed data describing the ice jam profile shape. In addition, the thickness at the upstream boundary of the computed profile,  $t_{so}$  (corresponding to the most upstream surveyed cross section, station 26410 m), was adjusted to an equilibrium thickness, as this was observed to be an equilibrium ice jam and the observed location of the head was approximately 12 km upstream from station 26410 m (Beltaos and Burrell, 1990).

Figure 4.3 illustrates the computed ice jam profile compared to the recorded data for a calibrated composite Mannings roughness of 0.070. The computed water surface profile gave a good overall visual fit to the observed water surface data with a only slight overestimation near the toe (approximately 2% of the observed depth). The computed thickness profile matched the observed thickness implied by the shear wall data reasonably well over the computed length of the jam with the exception of the toe region where the computed thickness underestimated the observed data by approximately 20%. Although the thickness of the upstream boundary is usually associated with the head of the computed ice jam, it has been demonstrated here that this boundary may correspond to some point within the jam.

It was intended to investigate the ICEJAM model where the roughness was calculated using Beltaos' friction factor. However the model would not compute an ice jam profile for this particular case study. In an attempt to get the model to run, every single model input parameter was adjusted within, above, and below reasonable ranges, and yet the ICEJAM model would still not run. However, it was found that for several of the subsequent case studies the ICEJAM model would run using Beltaos' friction factor to compute roughness.

#### *Sensitivity to Boundary Conditions*

For this case study, the impact of ICEJAM's boundary conditions on the computed ice jam profile for a documented event was investigated. Figure 4.4(a) presents the results obtained in the toe region of the ice jam with the ICEJAM model for a calibrated composite Mannings  $n_o$  of 0.070, with values of *erosion* velocity,



$V_{max} = 1.00, 1.50$  and  $2.00$  m/s. Note that for  $V_{max} = 1.00$  m/s, the break in the water surface profile (corresponding to interface A-A, Figure 3.2) is about 0.5 km upstream of where the edge of the sheet ice cover was observed in the field (personal communication, Spyros Beltaos) which is obviously unrealistic. Based on these runs, it appeared that values of *erosion* velocity between 1.50 and 2.00 m/s would be expected to provide reasonable results for this event.

Figure 4.4(b) illustrates the effect of varying the thickness at the upstream boundary, or “head”, on the computed jam profile and ice volume. As this boundary thickness is decreased, the computed thickness near the head is reduced and the computed water surface profile drops. However, the influence of this upstream ice thickness diminishes in the downstream direction. It is important to note that without knowledge of the location of the head of the ice jam or of the thickness of the ice at some point within the ice jam upstream of the toe region, the specified thickness at the upstream boundary becomes an important calibration parameter.

#### 4.4.2.2 RIVJAM Model Application

##### *Roughness Calibrations*

Figure 4.5 illustrates the computed results obtained using RIVJAM. Again  $K_x$  was set to 10 and  $\mu$  was set to 1.0. The initial thickness,  $t_{so}$ , was set to match the observed shear wall data and the roughness was then adjusted to provide the best visual fit to the observed data. This was achieved using Beltaos’ friction factor,  $f_o$ , where both  $m_1$  and  $m_2$  were set to one, and adjusting  $c$ . Setting the seepage velocity  $\lambda$ , to 1.75 m/s it was found that  $c = 0.64$  provided the best fit to the measured water level data.

Comparing the computed ice jam profiles presented in Figure 4.3 and 4.5 for ICEJAM and RIVJAM, respectively, it is seen that the models compute nearly identical water surface profiles but RIVJAM computes a slightly thinner ice jam overall (a difference of only roughly 8% within the equilibrium reach). It is significant to note that RIVJAM produced the proper ice thickness at the head of the

ice jam (approximately the equilibrium thickness) as an output, whereas this is a required input for the ICEJAM model. This is important in terms of the relative suitability of these models to predictive rather than analytical applications.

The next step was to investigate the validity of the relationship described by equation [3.19]:

$$n_o = 0.10\sqrt{c} \quad [3.19]$$

where Mannings roughness is expressed in terms of Beltaos' roughness coefficient,  $c$ . Figure 4.6 illustrates the results using Beltaos' Mannings approximation for which the seepage was set to zero (for equivalency between the models). Figure 4.6(a) presents the ice jam profile computed by RIVJAM with the roughness coefficient,  $c$ , set to 0.49 (which based on equation [3.19] corresponds to ICEJAM's calibrated Mannings  $n_o$  of 0.070). Here, by adjusting only the toe thickness to achieve the best possible fit to the observed data, it is seen that the computed water surface profile underestimated the observed data over the entire computed length of the ice jam. Further increasing of the toe thickness caused the model to "blow up".

Figure 4.6(b) illustrates the results for an alternative approach in which the toe thickness was held constant at the observed value and the roughness coefficient,  $c$ , was adjusted to give the best fit to the observed data. The resulting  $c$  was 0.64 (corresponding to a Mannings  $n_o = 0.080$ ).

It is significant that the calibration shown in Figure 4.6(b), based on the known toe thickness and Beltaos' Manning approximation ( $m_1 = 0$  and  $m_2 = 1/3$ ), produced the same value of  $c$  as shown in Figure 4.5, obtained using the friction factor equation ( $m_1 = m_2 = 1$ ) and the known toe thickness, as this implies that the friction factor is relatively independent of the ice thickness for this case. This supports Beltaos' (1997) assertion of this independence for the ice jams of thickness greater than about 3 m (as is the case here).

### *Sensitivity to the Seepage Velocity*

The analysis conducted on the trapezoidal channel suggested that seepage was a relatively insensitive parameter when the jam length was kept nearly constant through adjustment of the toe thickness,  $t_{so}$ . However, the hypothetical ice jam studied during the analysis of the trapezoidal channel, was not grounded at the toe whereas for the Restigouche River event, the documented configuration near the toe for the suggested extensive grounding. Since the toe thickness for this event was known, this event provided a good opportunity to examine the importance of the seepage velocity,  $\lambda$ , which is important since the ICEJAM model does not consider flow through interstices.

Figure 4.7(a) illustrates the sensitivity of the RIVJAM model to variations in the seepage velocity,  $\lambda$ , for a constant toe thickness of 5.26 m. As was observed in analysis of the trapezoidal channel, an increase in seepage velocity with no adjustment to the boundary conditions, caused an increase in both the length and thickness of the computed ice jam profile. Based on these results, values of seepage velocity between 1.70 and 2.00 m/s were found to provide a reasonable match for this particular data set, which illustrates that the value of  $\lambda = 1.75$  m/s used in the initial runs was an appropriate choice (Figure 4.5).

### *Sensitivity to Toe Thickness*

It is important to note that the thickness values based on the shear wall data represent estimates of the exact thickness, since the sensitivity analysis on the trapezoidal channel suggested that adjustments to the specified toe thickness can be expected to have a noticeable impact on the computed ice jam profile. Figure 4.7(b) illustrates the effect of varying the toe thickness,  $t_{so}$ , on the computed jam profile for a seepage velocity of 1.70 m/s and the previously calibrated roughness using Beltaos' Mannings approximation. As the Figure shows, the toe thickness specified by the user can produce very different jam profiles and, therefore, this boundary condition acts as one

of the major calibration parameters for the RIVJAM model when the toe thickness is unknown.

#### **4.4.2.2 Comparison Between Models**

Figure 4.8 depicts a close-up of the toe region comparing the results from ICEJAM (erosion velocity = 2.00 m/s) and RIVJAM (toe thickness = 5.26 m, as observed). Both models provide a reasonable and comparable simulation of the water surface profile. Although the RIVJAM model appears slightly better at capturing the profile of the underside of the ice cover near the toe it should be remembered that the thickness at the most downstream point is a specified input boundary condition for the RIVJAM model. To improve ICEJAM's performance in the toe area of this grounded jam, it was necessary to stipulate a rather high value for erosion velocity (2.00 m/s).

The upstream boundary thickness required by ICEJAM was slightly less sensitive than the downstream boundary thickness required by RIVJAM. However, the apparent sensitivity in the downstream thickness observed during the application of RIVJAM model, was likely due to *numerical* sensitivity as opposed to *physical* sensitivity as was demonstrated during the analysis of the trapezoidal channel.

The calibrated Beltaos' Mannings approximation overestimated the Mannings roughness that was calibrated using the ICEJAM model. However, this could have been due to the large thickness of this jam, as discussed earlier (effect of ice jam thickness being small). Also, when Beltaos' Mannings approximation was forced to correspond to the Mannings roughness calibrated by ICEJAM, the best possible computed water surface profile did not capture the observed shape of the ice jam and underestimated the observed water surface profile data.

#### **4.4.3 Ice Jam with an Indefinite Length - Thames River**

Figure 4.9 shows the location of the documented Thames River ice jam event and the locations of the cross sections over the reach under investigation. The Thames River

is located in southwestern Ontario and flows primarily southwards through Chatham to empty into Lake St. Claire at the town of Lighthouse. Winter jams occur on this river as periods of above freezing temperatures and rain are not uncommon during the coldest months of the year. This case study represents a jam which formed as a result of a period of warm weather combined with rain which raised the water level in the river causing the ice to break up and move downstream (Beltaos and Moody 1986).

This winter ice jam on the Thames River in Ontario, which was documented by Beltaos and Moody (1986), formed as a result of the release of an upstream ice jam during the evening of January 22, 1986. High water marks were photographed in the newly formed jam were photographed during the morning of January 23. after cold weather had returned and conditions had stabilized. Subsequently, a solid ice layer formed over the ice jam making it safe to collect thickness measurements. Based on the consistency between ice thickness measurements taken within the same section of the jam on February 4 and February 25, 1986, it was assumed that the jam thickness did not change over the period during which the measurements were taken (January 23 to February 26, 1986).

Using the Water Survey of Canada gauge record at Thamesville (gauge 02GE003), and estimating the time of travel between the gauge and the jam sites to be 12 hours, Beltaos (1988) estimated the discharge to be 290 m<sup>3</sup>/s. This discharge of 290 m<sup>3</sup>/s along with jam strength constants  $\mu$  and  $K_x$  at 1.0 and 10, respectively, were used in the application of both models to this case study.

#### ***4.4.3.1 RIVJAM Model Application***

Figure 4.10 presents the ice jam profiles computed by RIVJAM using Beltaos' friction factor where seepage velocity was set to 1.75 m/s. Figure 4.10(a) illustrates the computed ice jam profile where the thickness at the toe was fixed to 2.20 m (which roughly corresponded to the observed shear wall data), and the roughness coefficient,  $c$ , was adjusted to provide the best fit to the observed data. It was found that for a  $c$  of 0.61 the best overall visual fit to the recorded data could be achieved.

The observed water surface profile appeared to be underestimated slightly along the middle and upstream portions of the jam.

Figure 4.10(b) presents the ice jam profile computed by RIVJAM where both the thickness at the downstream boundary and the roughness coefficient,  $c$ , were adjusted freely (without regard to the shear wall data) to provide the best fit. It was found that a better overall fit could be achieved with  $c = 0.70$  and a thickness at the toe,  $t_{so} = 2.90$  m, which represents a slight overestimation of the thickness indicated by the shear wall data. Visually, this calibration (using  $c = 0.70$  and  $t_{so} = 2.90$  m) provided a better overall fit to the observed data than the previous calibration shown in Figure 4.10(a) (for  $c = 0.61$  and  $t_{so} = 2.20$  m).

Figure 4.11 presents the computed ice jam profile generated by the RIVJAM model using Beltaos' Mannings approximation, where the seepage velocity was set to zero. For this run, the thickness at the toe was fixed to correspond to the shear wall data (i.e.  $t_{so} = 2.20$  m), and the roughness was adjusted to provide the best overall fit to the observed data. The roughness coefficient,  $c = 0.367$ , was the limiting value which provided the best overall fit to the observed data as the computed ice jam profile diverged for a  $c = 0.367$ . A computed jam length which exceeded the length indicated in Figure 4.11 could not be achieved without obtaining a divergent solution.

It was noted that a longer and thinner ice jam profile was computed by RIVJAM using Beltaos' friction factor (with seepage set to 1.75 m/s) than by using Beltaos' Mannings approximation (with seepage set to 0 m/s). It was decided to verify that this effect was due to the method of calculating frictional resistance and not due to the inclusion of seepage. Figure 4.12 illustrates the results computed by RIVJAM using Beltaos' friction factor ( $c = 0.70$ ) where seepage velocity,  $\lambda$ , is varied from 0 to 1.75 m/s. Figure 4.12(a) shows the computed results where the toe thickness is not adjusted and only the seepage velocity is varied. For a seepage velocity of 0 m/s (represented by the black dotted line) the length of the jam decreased by approximately 2.6 km, although, the general shape of the profile was consistent with

that computed using a seepage velocity,  $\lambda = 1.75$  m/s (represented by the solid black line). Figure 4.12(b) shows the computed results where the roughness,  $c$  was adjusted to 0.6635 to maintain a jam of comparable length and the seepage was again varied. Setting the seepage velocity to zero (represented by the black dotted line) RIVAJM computed a nearly coincident ice jam profile as was computed with a seepage velocity,  $\lambda = 1.75$  m/s (represented by the solid black line). These results suggested that the long and thin shape exhibited by Figure 4.10 is due to the method for computing frictional resistance (i.e. Beltaos' friction factor) and not due to the inclusion of seepage.

#### ***4.4.3.2 ICEJAM Model Application***

During the RIVJAM calibration using Beltaos' Mannings approximation (Figure 4.11), it was found that the computed location of the head (station 34585 m) was approximately 8 km downstream of the documented location of the head observed by Beltaos and Moody (1986). Given the short jam length which was computed by the RIVJAM model, two scenarios were considered for the ICEJAM investigation. In the first scenario, a short jam length, corresponding to the length described by the RIVJAM run (i.e. head at station 34585 m), was assumed. In the second scenario, it was assumed that the head was at the location reported by Beltaos and Moody (1986) (i.e. head at station 42000). In both scenarios, the thickness at the head was set to 0.30 m (as Beltaos and Moody (1986) noted the average ice floe thickness ranged from 0.20m to 0.30m), the erosion velocity was set to 2.00 m/s, and Mannings roughness was adjusted in an attempt to match the computed profile to the measured data.

Figure 4.13(a) depicts the computed profiles for both the short and long jam scenarios resulting from a calibrated Mannings roughness,  $n_o = 0.070$ , which matched the recorded profile data within the downstream portion of the jam. As the figure illustrates, the short jam reproduces the measured profile adequately. However, the computed water levels in the upstream portion of the long jam were well above the

measured data (by approximately 1 m). Figure 4.13(b) depicts the computed profile for the long jam where a calibrated Mannings  $n_o = 0.055$  matched the recorded profile data within the upstream portion of the jam. However as the figure also illustrates, this approach did not adequately capture the jam profile in the vicinity of the toe. Based on these results, it was concluded that the shorter jam was more consistent with the measured data.

#### ***4.4.3.3 Sensitivity of ICEJAM Parameters***

The shape of the observed and computed ice jam profiles suggested that this ice jam event was not of the equilibrium type. This provided a good opportunity to test the sensitivity of the coefficients  $K_x$  and  $\mu$  for a documented ice jam event. Figure 4.14 presents the results of this sensitivity analysis conducted using the ICEJAM model where Mannings roughness was used to compute frictional resistance.  $K_x$  was varied from 8 to 12, and  $\mu$  was varied from 0.8 to 1.2. Figure 4.14(a) illustrates the impact of varying  $K_x$  on the computed ice jam profile. The maximum differences in the computed thickness and water levels for this range of  $K_x$  values were 0.23 m (17%) and 0.08 m (1%), respectively. Figure 4.14(b) illustrates the impact of varying  $\mu$  on the computed ice jam profile. The maximum differences in the computed thickness and water levels for this range of  $\mu$  were respectively, 1.11 m (36%) and 0.37 m (5%).

#### ***4.4.3.4 Equivalency of the Beltaos Mannings Approximation***

It was decided to investigate the relationship between Mannings  $n_o$  and Beltaos friction coefficient,  $c$ , (equation [3.19]) for this case study again using RIVJAM. Figure 4.15 illustrates the results using RIVJAM with Beltaos' Mannings approximation and seepage velocity set to zero. The roughness coefficient,  $c$ , was forced to 0.3025 (corresponding to  $n = 0.055$ , which was calibrated previously by the ICEJAM model) and the toe thickness was adjusted without regard to the shear wall data to provide the best overall fit to the measured data. It was found that for this roughness the computed water surface profile underestimated the observed data in the



middle portion of the jam, while the calibrated thickness at the downstream boundary of 1.87 m gave a reasonable match to the recorded shear wall data.

#### **4.4.3.5 Discussion of Results**

The results obtained using Mannings roughness to compute frictional resistance indicated that the upstream limit associated with the “wide” jam criteria was at approximately station 34585 m. The results obtained using Beltaos’ friction factor indicated that this upstream limit extended to station 37000 m. In both cases the head associated with a “wide” jam criteria underestimated the length of the jam observed by Beltaos and Moody (1986) in the field (station 42000 m). It is possible that upstream of somewhere between stations 35000 and 37000 m, the ice jam may have behaved more like the “narrow” type described by Pariset, *et al.* (1966). This deduction is consistent with the qualitative description of the ice jam event provided by Beltaos (1988), and with the very low thickness that was measured in the last few kilometers of the jam. It is important to point out that re-freezing was likely during this event, and may explain why the jam did not collapse from a narrow jam and maintain its thin profile over its length.

For the ICEJAM runs it was evident that some prior knowledge as to the location of the upstream limit of the ice jam (behaving as a “wide” channel jam) was required. It is unlikely that this location could have been easily identified, had not the initial RIVJAM runs suggested its possible location. This would indicate that the requirement for the user to input the ice jam length might be considered a disadvantage of the ICEJAM model. Alternatively, it could be considered an indication of the importance of supplemental descriptive data and good judgment in the interpretation of field data to the proper use of models of this type.

During this particular case study, it was also discovered that a longer and thinner jam, exhibiting a flatter water surface profile near the head could be achieved using Beltaos’ friction factor to compute frictional resistance than could be achieved using

Mannings and that this effect was not a result of the inclusion of seepage through the jam voids.

#### **4.4.4 Ice Jam with Conflicting Discharge Estimates - Saint John River**

Figure 4.16 shows the location of the documented Saint John River ice jam event. The Saint John River originates from the base of Little Saint John Lake in the State of Maine and flows primarily east to the border between Canada and the United States. The river follows the border and then turns south through province of New Brunswick to empty into the Bay of Fundy at Saint John, New Brunswick. The reach under investigation for this study extends between Edmunston and Grand Falls.

Major jamming started on April 11, 1993 and on the evening of that day, a jam above Fort Kent released and ran downstream. On April 12, this ice combined with ice arriving from reaches further upstream of Fort Kent, accumulated near Ste-Anne to form a major jam which remained in place for approximately two days. Water surface data was obtained over the length of the jam on April 13 and 14 and shear wall data was obtained after the jam's release. Beltaos, *et al.* (1994) provide a description of the ice jam event and these investigators made available to the author cross sectional and observed water surface profile data. Shear wall data was digitized from a figure presented in the conference paper by Beltaos, *et al.* (1994).

The event documented on April 13 was not included in the analysis as discharge varied widely over that day (1500 to 5000 m<sup>3</sup>/s). Nearly steady flow was observed on April 14 and two discharge estimates were available which had been determined by equally acceptable methods. The two estimates were noticeably different and therefore, provided a good opportunity to investigate the impact of variable discharge on model application.

Water Survey of Canada gauges below Fish River near Fort Kent (WSC 01AD002) and at Grand Falls (WSC 01AF002) recorded stream flow data during this event and on the morning of April 14, 1993, after clearing of ice, four additional gauges began

to record stream flow data on tributaries along the reach of interest at: Madawaska River; Iroquois River; Rivier Verte (Green River); and Grande River. Using the hourly stream flow data obtained at these gauges, the flows were routed downstream using an unsteady hydraulic flood routing model based on the St. Venant equations to generate a hydrograph at the toe of the ice jam. The methods used to generate this hydrograph are outlined by Hicks, McKay, and Shabayek (1997). The computed discharge corresponding to the documented ice jam event on April 14 was 2250 m<sup>3</sup>/s by this method.

Additional stream flow estimates were obtained from estimated inflows to the Grand Falls power plant which were based on simple stage, storage and outflow relationships. Discharge estimates obtained by this method were found to vary slightly until the latter part of the day on April 14 and up until the ice jam's release where the discharge was estimated to be approximately 3000 m<sup>3</sup>/s.

#### ***4.4.4.1 ICEJAM Model Application***

Figure 4.17 presents the ice jam profiles computed by ICEJAM using Mannings roughness, values of  $K_v = 10$ , and  $\mu = 1.0$ . The two discharge estimates of 2250 and 3000 m<sup>3</sup>/s. Roughness was then adjusted to achieve the best possible fit to the observed data in each case. For a discharge of 2250 m<sup>3</sup>/s a Mannings roughness of  $n_o = 0.040$  provided the best fit to the observed water levels and location of the head of the jam. Holding the roughness, and all other parameters constant, the discharge was then set to 3000 m<sup>3</sup>/s causing the computed ice jam profile to increase by nearly 2 m. Using a discharge of 3000 m<sup>3</sup>/s, the roughness was then adjusted to  $n_o = 0.030$  to provide the best fit to the observed data.

#### ***4.4.4.2 RIVJAM Model Application***

Figure 4.18 illustrates the computed results obtained using RIVJAM where  $K_x$  was set to 10,  $\mu$  was set to 1.0, the seepage velocity,  $\lambda$ , was set to 0 m/s, and Beltaos' Mannings approximation was used to calculate frictional resistance. First the

roughness was forced to correspond to the Mannings roughness calibrated by ICEJAM ( $n_o = 0.040$ ) using equation [3.19], and the toe thickness was adjusted to achieve a computed length equal to that observed. Here the computed water surface profile was underestimated over the entire length of the jam. Then the roughness coefficient,  $c$ , was adjusted to 0.25 (corresponding to  $n_o = 0.050$ ) to provide the best overall fit to the observed data.

Figure 4.19 shows the computed ice jam profile generated by RIVJAM using Beltaos' friction factor where seepage velocity was set to 1.75 m/s. It was found that the best fit to the observed water level data could be achieved by setting the toe thickness,  $t_{so}$  to 5.80 m, and the roughness coefficient,  $c$  to 0.28. However, this run overestimated the observed length of the ice jam by approximately 11 km. Next, roughness was held constant and the toe thickness was adjusted to,  $t_{so} = 4.00$  m to generate an ice jam profile which matched the observed length of the jam. Although the computed location of the head matched the documented location of the head, the computed water surface profile underestimated the observed data near the head by approximately 2.0 m. For the final run of this series, the toe thickness calibrated in the first run was used and the roughness coefficient,  $c$ , was increased to 0.38 to match the computed location of the head to the observed location. The computed water surface profile underestimated the observed water level data near the head by approximately 1 m (which is half of the error computed in the previous calibration).

#### ***4.4.4.2 Discussion of Results***

During this case study the application of the ICEJAM model using different discharges (both of which were obtained by accepted methods) produced noticeably different results. The results of this case study suggested that discharge is a sensitive input parameter and it also underlined the importance of obtaining reliable discharge estimates if these models are to be used to investigate ice jam characteristics such as roughness. This remains one of the key difficulties in studying ice jams, given the unsteady nature of the flow both spatially and temporally.

During the application of the RIVJAM model computations using Beltaos' friction factor again produced longer and thinner jams. In addition it was found for this particular case study that using Mannings roughness produced better results than using Beltaos' friction factor.

#### **4.4.5 Interpretations of the Rigorous Model Investigation**

The following conclusions were drawn from the results obtained during the rigorous investigation of the ICEJAM and RIVJAM models:

1. In the absence of ice jam toe thickness data, the thickness at the downstream boundary becomes an important calibration parameter in the RIVJAM model. The ICEJAM model is less sensitive to estimates of the specified thickness at the upstream boundary (at the head of the accumulation) as gradients in the solution are typically much larger near the toe than near the head.
2. For the documented ice jam events studied in this rigorous analysis with the ICEJAM model, the computed water surface profile appears to be relatively insensitive to the coefficients  $\mu$  or  $K_x$  within the ranges suggested in the literature. Therefore, it would seem that, for practical application of the models, it is reasonable to set these coefficients to values which represent the average of the range of suggested values in the literature (i.e.  $\mu = 1.0$  and  $K_x = 10$ ). Although variations in these parameters have been shown to produce widely varying ice jam lengths with the RIVJAM model, it is unlikely that this numerical sensitivity has the potential to contribute to the refinement of the values deduced for these parameters with models of the type.
3. Although the assumed toe configuration used in the ICEJAM model provides a useful expedient to make the transition to the jam stability equation, it is important to note that the resulting shape is not entirely consistent with natural occurrences, particularly when the toe is grounded.

4. The jam stability equation used for computation by the ICEJAM and RIVJAM models is based on the assumptions of a wide channel jam as defined by Pariset *et al.* (1966). However, during field observations, the documented head of a jam often identifies the leading edge of the entire ice accumulation. Much of the ice downstream of the identified location of the head could have simply been juxtaposed ice or the accumulation might have thickened under the narrow jam criteria defined by Pariset, *et al.* (1966). Therefore, some judgment may be required to define the most upstream point or true “head” of the ice jam profile computed by the models. As was found during the Thames River case study, the model RIVJAM model may assist in interpreting the location of this upstream limit or “head”.
5. To obtain similar results between the models, a larger roughness is required when using Beltaos’ Mannings approximation for RIVJAM than when using Mannings roughness for ICEJAM. Similarly, it was found that computed water surface profiles generated by RIVJAM (using Beltaos’ Mannings approximation, where roughness was forced to match a Mannings roughness calibrated by the ICEJAM model) underestimated the computed water surface profile generated by ICEJAM. This suggests that the relationship described by equation [3.19] was not applicable to the case studies investigated during the rigorous model investigation.
6. The models’ results are sensitive to discharge and reliable discharge estimates are essential for examining ice jam characteristics through the application of these models to documented events.

#### **4.4.6 Calibration Protocol for RIVJAM and ICEJAM**

Based on the results of the rigorous investigation, protocols to be used for the application of the ICEJAM and RIVJAM models to documented events were developed. The protocols suggest default values to be used for parameters which exhibited low physical sensitivity and outline an effective and expedient procedure

for application of the models to documented events. These calibration protocols employ the same default values used for the trapezoidal channel analysis, and outline the general procedure for model calibration to observed data. These protocols were verified during the application of the models to the remaining case studies.

#### **4.4.6.1 ICEJAM Calibration Protocol**

The following steps outline the suggested steps to be used when calibrating the ICEJAM model to a documented ice jam event.

1. Choose the location of the upstream and downstream boundaries based on the documented ice jam profile data and set all default parameters to those suggested during the trapezoidal analysis (i.e.  $K_v = 10$ , and  $\mu = 1.0$  by setting  $K_{\text{ty}} = 0.10$ ,  $\tan\phi = 1.67$ , and  $p = 0.4$ , (see Table 3.3)).
2. Allow the model to calculate the water level for the most downstream computational node (i.e. set  $WLTD = 0$ ) and compute the water surface profile using an initial guess for roughness.
3. Adjust roughness until the computed ice jam profile provides best overall fit to the observed data.
4. “Fine tune” the shape of the computed profile to match the observed data near the toe by adjusting the location of the downstream boundary and the specified *erosion velocity* (note that adjustments to *erosion velocity* do not have a big impact on the computed profile further upstream of the toe region). If required, adjust the roughness slightly to achieve a closer match to the observed data.

As was discovered during the Thames River case study, the length of the jam may require shortening to a length which is governed by the “wide” jam criteria defined by Pariset *et al.* (1966).

#### **4.4.6.2 RIVJAM Calibration Protocol**

The following steps outline the suggested steps to be used when calibrating the RIVJAM model to a documented ice jam event.

1. Select the location of the first computational node to correspond with the location of a known or measured water level and determine the vertical distance from the known elevation at this location to the elevation of the slope-line. This vertical distance represents the sum of the submerged thickness,  $t_{so}$ , and the distance from the bottom of the ice to the slope-line (slope-line depth),  $h_{so}$ .
2. Select an initial guess for roughness and set all default parameters to those suggested during the trapezoidal analysis (i.e.  $\lambda = 1.75$  m/s,  $K_x = 10$ , and  $\mu = 1.0$  by setting  $C_o = 1.67$ , and  $p = 0.4$ . (see Table 3.3)).
3. Where observed thickness data is available, set the thickness at the toe to match the recorded data and adjust roughness to the best overall fit of the computed ice jam profile to the recorded profile data. Where thickness data is not available, adjust both  $t_{so}$  and  $h_{so}$  through a trial and error approach to achieve the best match to the observed data.

### **4.5 VERIFICATION OF CALIBRATION PROTOCOL**

#### **4.5.1 Introduction**

The standard protocol developed from the rigorous model investigation was tested against the remaining case studies. A brief description of the results was noted for each case study below. To avoid unnecessary repetition in the text, the results obtained for each case study are summarized in tabular form.

For each case study, various methods were used to compute frictional resistance. These methods were selected to provide a means of comparison between the methods



and to investigate any trends in roughness for the various case studies. The following model runs were implemented for each case study.

1. ICEJAM where Mannings roughness is adjusted to provide the best fit to the observed data.
2. When possible, ICEJAM using Beltaos' Mannings approximation where the roughness coefficient,  $c$ , is adjusted to provide the best fit to the observed data.
3. RIVJAM using Beltaos' friction factor and seepage,  $\lambda$ , set to 1.75 m/s, where both the roughness coefficient,  $c$ , and the toe thickness are adjusted to provide the best overall fit to the observed data. When shear wall data is available, the toe thickness is set to correspond to the observed thickness at the toe and roughness is adjusted to provide the best fit.
4. Same as *run 3* above with seepage,  $\lambda$ , set to 0 m/s. Using the calibrated toe thickness from run 3, adjust only roughness,  $c$ , to achieve a near identical ice jam profile as to that computed in run 3.
5. RIVJAM using Beltaos' Mannings approximation, where the roughness coefficient,  $c$ , is set to correspond to the Mannings roughness calibrated by ICEJAM (run 1) using equation [3.19], seepage velocity is set to zero, and the toe thickness is adjusted to provide the best overall fit to the observed data.
6. When adequate toe thickness data are available, RIVJAM using Beltaos' Mannings approximation, where the toe thickness is set to correspond with the observed data, seepage velocity is set to zero, and the roughness coefficient,  $c$ , is adjusted to provide the best overall fit to the observed data.

A brief description of the documented ice jam event is provided for each case study below and only the salient observations are discussed. The results obtained during the application of the models to each case study are summarized at the end of this chapter.

As the results of the calibrations of the three case studies considered during the rigorous investigation are relevant to the ultimate discussions, they are presented first. Tables 4.1 to 4.3 summarize the results obtained during the investigation of the Restigouche River, Thames River, and Saint John River, respectively.

The ICEJAM model would not run using Beltaos' friction factor for the case studies in the rigorous analysis (as discussed previously), although it was found to run during some of the subsequent case studies. It is not known why the model would not run for these particular case studies. Every effort was made to get the model to run through parameter variation and these attempts proved to be unsuccessful. The text "*WOULD NOT RUN*" is included in the table for runs where the ICEJAM model would not run to indicate that this particular run was not ignored. For the cases where there was not adequate shear wall data indicating the toe thickness (which was required for run 6) the text "*SHEAR WALL DATA NOT AVAILABLE*" is added.

During the calibrations using ICEJAM, the automated feature for computing the water level (which is calculated assuming uniform flow) was used so that the computed value could be compared to the observed. Also, the figures corresponding to *run 4* are not included in this report as they were calibrated to produced identical profiles as those from *run 3*.

Table 4.1 Calibration Results for the Restigouche River, 1988 ice jam event.

| Run Number | Figure | Model  | Erosion                    | Seepage  | Roughness |                      |
|------------|--------|--------|----------------------------|----------|-----------|----------------------|
|            |        |        | Velocity                   | Velocity | <i>c</i>  | <i>n<sub>o</sub></i> |
| 1          | 4.3    | ICEJAM | 2.00 m/s                   | -        | -         | 0.070                |
| 2          | -      | ICEJAM | <b>MODEL WOULD NOT RUN</b> |          |           |                      |
| 3          | 4.5    | RIVJAM | -                          | 1.75 m/s | 0.64      | -                    |
| 4          | ^      | RIVJAM | -                          | 0 m/s    | 0.515     | -                    |
| 5          | 4.6    | RIVJAM | -                          | 0 m/s    | 0.49      | 0.070*               |
| 6          | 4.7    | RIVJAM | -                          | 0 m/s    | 0.64      | 0.080*               |

\* equivalent Mannings roughness based on equation [3.19]

^ same profile as computed in Run 3.

Table 4.2 Calibration Results for the Thames River. 1986 ice jam event.

| Run Number | Figure  | Model  | Erosion             | Seepage  | Roughness |                      |
|------------|---------|--------|---------------------|----------|-----------|----------------------|
|            |         |        | Velocity            | Velocity | <i>c</i>  | <i>n<sub>o</sub></i> |
| 1          | 4.13(a) | ICEJAM | 2.00 m/s            | -        | -         | 0.055                |
| 2          | -       | ICEJAM | MODEL WOULD NOT RUN |          |           |                      |
| 3          | 4.10    | RIVJAM | -                   | 1.75 m/s | 0.70      | -                    |
| 4          | ^       | RIVJAM | -                   | 0 m/s    | 0.6635    | -                    |
| 5          | 4.15    | RIVJAM | -                   | 0 m/s    | 0.3025    | 0.055*               |
| 6          | 4.11    | RIVJAM | -                   | 0 m/s    | 0.366     | 0.061*               |

\* equivalent Mannings roughness based on equation [3.19]

^ same profile as computed in Run 3.

Table 4.3 Calibration Results for the Saint John River. 1993 ice jam event.

| Run Number | Figure | Model  | Erosion             | Seepage  | Roughness |                      |
|------------|--------|--------|---------------------|----------|-----------|----------------------|
|            |        |        | Velocity            | Velocity | <i>c</i>  | <i>n<sub>o</sub></i> |
| 1          | 4.17   | ICEJAM | 2.50 m/s            | -        | -         | 0.040                |
| 2          | -      | ICEJAM | MODEL WOULD NOT RUN |          |           |                      |
| 3          | 4.19   | RIVJAM | -                   | 1.75 m/s | 0.38      | -                    |
| 4          | ^      | RIVJAM | -                   | 0 m/s    | 0.2725    | -                    |
| 5          | 4.18   | RIVJAM | -                   | 0 m/s    | 0.16      | 0.040*               |
| 6          | 4.18   | RIVJAM | -                   | 0 m/s    | 0.25      | 0.050*               |

\* equivalent Mannings roughness based on equation [3.19]

^ same profile as computed in Run 3.

## **4.5.2 Hay River, near the Town of Hay River**

### ***4.5.2.1 Introduction***

Figure 4.20 shows the location of Hay River and a detailed plan of the study area and cross section locations. The area of study is located in the town of Hay River and the focus of the investigation was on the east channel. Hay River originates from Hay Lake in the northwestern corner of Alberta and flows northwards to its mouth on the southwestern shore of Great Slave Lake, North West Territories. The Hay River splits from its main channel around Vale Island in the town of Hay River with the main portion of the flow (roughly two thirds) passing through the east channel (Gerard and Stanley, 1988).

Two separate ice jam events, recorded on April 28, 1987, and April 28, 1992 were investigated during this study. The first event was documented by Gerard and Stanley (1988) and the data for the second event was obtained from Andres (1996). Both of these ice jam events formed accumulations which extended from within the east channel to upstream beyond the split into the main channel. As the discharge through the main and east channels would have been different and because ICEJAM and RIVJAM can only model a constant discharge, only the downstream portion of both events which was contained in the east channel were modelled. The discharge used for both events ( $420 \text{ m}^3/\text{s}$  for the 1987 event and  $605 \text{ m}^3/\text{s}$  for the 1992 event) corresponded to discharge estimates for the east channel provided in a report from Trillium Engineering and Hydrographics Inc. (1996). The estimates for flow through the east channel were based on recorded water levels obtained at a Water Survey of Canada gauge (WSC 07OB008, located upstream of the town of Hay River on the North West Territories/Alberta border) and measured water levels at the bridge located in the east channel (using a stage discharge curve for open water and “fully developed” ice jam conditions developed by Stanley, (1988)).

For both the 1987 and 1992 recorded ice jam events, the thickness at the upstream boundary (corresponding to the most upstream surveyed cross section in the east channel, station 5700) was not known, since the observed location of heads for both of these events were located upstream of the east-west channel split in the main channel. Therefore, for the RIVJAM model no comparison between the computed and observed locations of the head could be made for these case studies. For the ICEJAM model the thickness was set to provide the best fit to the observed water level at station 5700 m.

#### ***4.5.2.2 Hay River, April 28, 1987***

Gerard and Stanley (1988) provided a detailed description of the events surrounding the 1987 break up and documented ice jam. On April 25, 1987 an ice jam formed approximately 4 km upstream of the east-west channel split and on April 26, 1987 two major movements within this ice jam were observed. The first occurred at 16:20 h where the ice pushed downstream into both the east and west channels with a temporary toe location formed in the east channel just downstream of the split (just upstream of station 5700 m). At 17:50 h the second movement caused the ice jam to push further downstream into the east channel where the toe stopped near station 2450 m. This jam remained in place for the next few days where little movement of the ice jam was observed in the east channel and therefore, steady state conditions could reasonably be assumed. There was movement observed near the head of the ice accumulation which was located approximately 5 km upstream of the east-west channel split. Water elevations were recorded along the jam in the east channel on the morning of April 28, 1987.

Table 4.4 summarizes the computed results (illustrated in Figures 4.21 to 4.24) obtained using the standardized protocol for the application of the models to this ice jam event. For the ICEJAM runs the thickness at the head (station 5700 m) was set to 1.00 m which was close to thickness computed by the RIVJAM model runs (1.20 m). All of the runs computed using both models were found to provide good visual fits to

the observed water level data upstream of station 2500 m. The RIVJAM model was started at the measured water level just upstream of station 2500 m. It was not clear, based on the available data, where the downstream limit of the jam stability equation was (interface A-A, Figure 3.2) so the RIVJAM runs were started at the measured water level near station 2500 m, since it was certain that this point would be upstream of this interface.

#### ***4.5.2.3 Salient Observations***

Figure 4.21 presents the results computed by ICEJAM using Mannings roughness and a calibrated Mannings roughness of 0.050. It was found that water level at the downstream boundary computed by ICEJAM overestimated the observed data by approximately 1.30 m. However, upstream of this point the remaining water levels were represented well by the computed profile. As was mentioned previously, the computed water elevation at the downstream boundary is based on a normal depth calculation (which implies uniform flow) and inspection of the bed indicates a mild slope changing to a less mild slope which would cause the flow to accelerate (which obviously could not be considered uniform).

Figure 4.22 presents the results computed by ICEJAM using Beltaos' Mannings approximation. It was found that a value of roughness,  $c$  of 0.27 (which translates to a Mannings roughness of 0.052 using equation [3.19]) provided the best fit to the measured water level data. For this run the computed water level at the downstream boundary was, again, approximately 1.30 m.

Figure 4.23 presents the results computed by RIVJAM using Beltaos' friction factor. It was found that a roughness coefficient,  $c$  of 0.35 provided the best overall fit to the measured data. It is important to note that the  $c$  calibrated using Beltaos' friction factor (which is a function of depth and ice thickness) does not relate to Mannings roughness. The computed water surface profile, as compared to those computed by ICEJAM, was found to overestimate the water surface slightly near the middle of the jam and underestimate the measured water level data near station 5700 m, and that the

computed thickness over the length of the jam was less than that computed using Mannings roughness.

Figure 4.24 presents the results computed by RIVJAM using Beltaos' Mannings approximation where the roughness was forced to correspond to the Mannings roughness calibrated by the ICEJAM model (using equation [3.19]). It was found that the computed profile only slightly underestimated the computed water surface profile generated using ICEJAM (Figure 4.21). However, for all practical purposes, both of these computed profiles can be considered equally good.

Shear wall data was not recorded for this ice jam event and therefore run 6 could not be implemented.

*Important!* To reduce repetition, only the salient observations that differ from those found in this case study will be noted in subsequent case studies.

Table 4.4 Calibration Results for the Hay River, 1987 ice jam event.

| Run Number | Figure | Model  | Erosion                              | Seepage  | Roughness |        |
|------------|--------|--------|--------------------------------------|----------|-----------|--------|
|            |        |        | Velocity                             | Velocity | $c$       | $n_o$  |
| 1          | 4.21   | ICEJAM | 1.75 m/s                             | -        | -         | 0.050  |
| 2          | 4.22   | ICEJAM | 1.75 m/s                             | -        | 0.27      | 0.052* |
| 3          | 4.23   | RIVJAM | -                                    | 1.75 m/s | 0.35      | -      |
| 4          | ^      | RIVJAM | -                                    | 0 m/s    | 0.222     | -      |
| 5          | 4.24   | RIVJAM | -                                    | 0 m/s    | 0.25      | 0.050* |
| 6          | -      | RIVJAM | <b>SHEAR WALL DATA NOT AVAILABLE</b> |          |           |        |

\* equivalent Mannings roughness based on equation [3.19]

^ same profile as computed in Run 3.

#### 4.5.2.4 Hay River, April 28, 1992

The data used for the 1992 Hay River ice jam event (both water level and discharge data) was obtained from a report provided by Trillium Hydrographics Inc.

(Andres 1996). This report however, had no description of the events leading up to the 1992 ice jam event, and no description of this event could be found in the literature. It was decided to include this event for the analysis, because reliable data was available and a lack of knowledge describing the chronology of events surrounding this ice jam did not detract from the objectives of this case study, which were to apply the models using a standardized protocol to recorded data.

As was the case for the 1987 Hay River ice jam event, the thickness at the upstream limit of the computational reach (station 5700 m) was set to correspond to an equilibrium thickness (for the ICEJAM runs) or was calibrated to correspond to an equilibrium thickness (for the RIVJAM runs). The discharge used in the east channel for this case study (taken from the report by Trillium Hydrographics Inc., 1996) was 605 m<sup>3</sup>/s.

Table 4.5 Calibration Results for the Hay River, 1992 ice jam event.

| Run Number | Figure | Model  | Erosion Velocity                     | Seepage Velocity | Roughness |                      |
|------------|--------|--------|--------------------------------------|------------------|-----------|----------------------|
|            |        |        |                                      |                  | <i>c</i>  | <i>n<sub>o</sub></i> |
| 1          | 4.25   | ICEJAM | 2.00 m/s                             | -                | -         | 0.045                |
| 2          | 4.26   | ICEJAM | 2.00 m/s                             | -                | 0.25      | 0.050*               |
| 3          | 4.27   | RIVJAM | -                                    | 1.75 m/s         | 0.30      | -                    |
| 4          | ^      | RIVJAM | -                                    | 0 m/s            | 0.26      | -                    |
| 5          | 4.28   | RIVJAM | -                                    | 0 m/s            | 0.2025    | 0.045*               |
| 6          | -      | RIVJAM | <b>SHEAR WALL DATA NOT AVAILABLE</b> |                  |           |                      |

\* equivalent Mannings roughness based on equation [3.19]

^ same profile as computed in Run 3.

Table 4.5 summarizes the computed results (illustrated in Figures 4.25 to 4.28) obtained using the standardized protocol for the application of the models to this ice jam event. Both ICEJAM and RIVJAM underestimated the recorded water levels between stations 3500 and 4500 m, by approximately 0.20 and 0.80 m, respectively.



It is not clear why the observed water levels are underestimated over this reach. However, the fact that both models gave relatively consistent results over this portion of the jam would suggest that the difference is due to inadequate resolution of the channel geometry in this reach. For this event the water elevation at the downstream boundary computed by ICEJAM approximated the observed water level data well. Also, when Beltaos' Mannings approximation was set to correspond to the Mannings roughness calibrated by ICEJAM, the computed water surface profile underestimated the observed water levels more than all other runs (Figure 4.28).

#### ***4.5.2.5 Discussion of Results***

The 1987 and 1992 ice jam events documented on the Hay River occurred over the same reach of river. It was noted that when these events were calibrated independently, the roughness associated with the two events was very similar. The calibrated Mannings roughness for the two events were 0.050 for the 1987 event and 0.045 for the 1992 event. The calibrated roughness coefficient,  $c$ , using Beltaos' friction factor was 0.35 for the 1987 event and 0.30 for the 1992 event. The roughness was slightly lower for the 1992 event than for the 1987 event (as indicated by two different methods for computing frictional resistance), as might be expected, given that the discharge for the 1992 event ( $605 \text{ m}^3/\text{s}$ ) was greater than the discharge for the 1987 event ( $420 \text{ m}^3/\text{s}$ ).

### **4.5.3 Athabasca River, near Fort McMurray**

#### ***4.5.3.1 Introduction***

Figure 4.29 illustrates the location of observed ice jam events on the Athabasca River near Fort McMurray that were used for this study. The Athabasca River stretches from its head waters in the mountains of Jasper National Park northeast across the province of Alberta to its delta into Lake Athabasca. The reach of interest for this study extends from approximately Long Rapids to just downstream of Fort McMurray, which is situated at the confluence of the Athabasca and Clearwater

Rivers. Figure 4.30 shows the locations of the cross sections used for the Athabasca River case studies.

The need to study and document ice jam events on large Alberta rivers was identified during the early nineteen seventies and “*in 1974, the Transportation and Surface Water Engineering Division of Alberta Research Council initiated a long term research program to observe and document breakup in selected river reaches in Alberta... The first year’s results were reported by Gerard, 1975*” (Beltaos, 1978). For this first year of record, no data was available for analysis on the Athabasca River as “*breakup at this location was missed and the formation of the ice jam was not observed*” (Gerard, 1975).

The available documented ice jam data for the Athabasca River found by the author was for the years 1977, 1978, 1979, 1983, 1984, 1985, 1986, and 1987. The events from years 1977 and 1987 were not included in this analysis as reliable discharge estimates were not available for these years. Cross sections of the reach used for the analysis were obtained from Alberta Research Council, Surface Water Engineering (ARC-SWE) reports printed in the years 1977, 1978, 1983, 1984, 1985, and 1987. Jam profile data was obtained from the reports corresponding to the year of the event under study. The data was obtained from figures in these reports and was digitized and then converted to a useable format required by the models.

#### ***4.5.3.2 Athabasca River, April 19, 1978***

During the spring of 1978 a jam formed with its toe located at MacEwan Bridge, Fort McMurray. It was observed that by “*roughly 20:00 hours 19<sup>th</sup> April [1978] a stable ice jam had been formed upstream of MacEwan Bridge*” (Doyle and Andres, 1978). Profile data on this jam was obtained through areal observations over a period of three days (April 19 - 21). The jam evolved over this period into three distinct jams which were recorded. The first distinct jam was recorded on April 19, 1978. The discharge used for the analysis of this event was 1200 m<sup>3</sup>/s.

Through direct observations of the toe at MacEwan Bridge, it was deduced that the jam was not grounded (Doyle, *et al.*, 1978). Ice floes in the jam were observed to range from 0.7 m to 1.2 m thick. The observed location of the head was not reported by Doyle, *et al.* (1978) for this event and therefore the comparison of the computed location versus the observed location could not be made.

Table 4.6 summarizes the computed results (illustrated in Figures 4.31 to 4.34) obtained using the standardized protocol for the application of the models to this ice jam event. All calibrations provided a good visual fit to the observed data, with the exception of two observed water levels between stations 310000 and 318000 m. These points were ignored during the calibration process as they were thought to not be consistent with the rest of the observed data. In addition, recorded data points which indicated an adverse water slope were ignored during the calibration process. Doyle, *et al.* (1978) indicated that 9 km and further upstream of MacEwan Bridge, errors in water level estimates could be in excess of 1.0 m. These "suspect" data points are more than 9 km upstream of MacEwan Bridge and they fall below the computed water surface profile by approximately 1.9 m.

Table 4.6 Calibration Results for the Athabasca River, April 19, 1978 ice jam event.

| Run Number | Figure | Model  | Erosion                              | Seepage  | Roughness |                      |
|------------|--------|--------|--------------------------------------|----------|-----------|----------------------|
|            |        |        | Velocity                             | Velocity | <i>c</i>  | <i>n<sub>o</sub></i> |
| 1          | 4.31   | ICEJAM | 2.00 m/s                             | -        | -         | 0.045                |
| 2          | 4.32   | ICEJAM | 2.00 m/s                             | -        | 0.25      | 0.050*               |
| 3          | 4.33   | RIVJAM | -                                    | 1.75 m/s | 0.16      | -                    |
| 4          | ^      | RIVJAM | -                                    | 0 m/s    | 0.13      | -                    |
| 5          | 4.34   | RIVJAM | -                                    | 0 m/s    | 0.2025    | 0.045*               |
| 6          | -      | RIVJAM | <b>SHEAR WALL DATA NOT AVAILABLE</b> |          |           |                      |

\* equivalent Mannings roughness based on equation [3.19]

^ same profile as computed in Run 3.

### *Observations on the Sensitivity of RIVJAM to cross section spacing*

During the initial applications of the RIVJAM model to this event, it was found that the solutions were diverging beyond approximately station 301000 m. Through many trial and error approaches, it was found that the model simply could not compute an ice jam profile which matched the observed data beyond this point. It was then suspected that there were some instabilities inherent in the solution technique due to the automated interpolation procedure. As Beltaos (1997) notes, the RIVJAM program automatically iterates between surveyed cross sections based on the user defined slope of the slope-line (*SLOPEO*). For these initial runs *SLOPEO* had been set to zero. In order to obtain a stable solution that would not diverge, two different approaches were explored. The first approach was to increase the slope-line slope from zero to a value that followed the slope of the channel bed, and the second approach was to manually add interpolated cross sections to the data file between stations 300300 and 312250 m (which were approximately 12 km apart) while maintaining a slope-line slope of zero.

Figure 4.35 illustrates impact of the choice of slope-line slope and the addition of interpolated cross sections on the computed ice jam profile. For the case where the slope-line slope is set to zero and there are no interpolated cross sections added between stations 300300 and 312250 m, the computed profile diverged. Adjusting the slope-line slope, to roughly follow the slope of the bed (0.001) the solution, again, diverged. However, when the slope of the slope-line was left at zero and interpolated cross sections were added at 150 m intervals between stations 300300 and 312250 m, reasonable results were obtained. Therefore, for the remaining Athabasca case studies, interpolated cross sections were added between these stations to ensure a convergent solution.

#### **4.5.3.3 Athabasca River, April 20, 1978**

The ice jam documented on April 19, 1978 evolved over the next day thickening and shoving into a shorter jam (Doyle, *et al.*, 1978). The toe remained in the same place

over the next two days and water level profiles were obtained again on the mornings of April 20, and April 21, 1978. The discharge estimated for April 20, 1978 was estimated between 1000 and 1200 m<sup>3</sup>/s. For this investigation the discharge was taken to be 1000 m<sup>3</sup>/s as the discharge used for the calibration of the previous event was 1200 m<sup>3</sup>/s and the recorded water level data suggested that the jam had reduced in size which would indicate a lesser discharge than for the April 19 event.

Table 4.7 summarizes the computed results (illustrated in Figures 4.36 to 4.39) obtained using the standardized protocol for the application of the models to this ice jam event. For the calibrations by both RIVJAM and ICEJAM the computed location of the head was calibrated (RIVJAM) or set (ICEJAM) to closely match the observed location of the head. Again, there were suspect data points within the same region as the 19 April 1978 ice jam event. These points were ignored during the calibration process and the computed water surface profiles were calibrated to match the data within the downstream portion of the jam which was indicated to be more accurate (Doyle *et al.*, 1978).

Table 4.7 Calibration Results for the Athabasca River. April 20, 1978 ice jam event.

| Run Number | Figure | Model  | Erosion                              | Seepage  | Roughness |                      |
|------------|--------|--------|--------------------------------------|----------|-----------|----------------------|
|            |        |        | Velocity                             | Velocity | <i>c</i>  | <i>n<sub>o</sub></i> |
| 1          | 4.36   | ICEJAM | 2.00 m/s                             | -        | -         | 0.040                |
| 2          | 4.37   | ICEJAM | 2.00 m/s                             | -        | 0.20      | 0.045*               |
| 3          | 4.38   | RIVJAM | -                                    | 1.75 m/s | 0.12      | -                    |
| 4          | ^      | RIVJAM | -                                    | 0 m/s    | 0.095     | -                    |
| 5          | 4.39   | RIVJAM | -                                    | 0 m/s    | 0.16      | 0.040*               |
| 6          | -      | RIVJAM | <b>SHEAR WALL DATA NOT AVAILABLE</b> |          |           |                      |

\* equivalent Mannings roughness based on equation [3.19]

^ same profile as computed in Run 3.

It was found that the runs using RIVJAM and ICEJAM gave a reasonable match to the observed water level data downstream of the “suspect” data points (i.e. downstream of approximately station 305000m). No other salient observations in addition to those described for the 1987 Hay River event were found.

#### 4.5.3.4 Athabasca River, April 21, 1978

Water levels were recorded again on the morning of April 21, 1978 when the jam was observed to have shortened and discharge dropped to approximately 900 m<sup>3</sup>/s (Doyle *et al.*, 1978). This discharge was used for the application of the models to this case study.

Table 4.8 summarizes the computed results illustrated in Figures 4.40 to 4.43. The documented profile for this event was very similar to the profile documented on April 20, 1978 with only a slight drop in water level along the length of the jam. It was found that the same calibrated Mannings roughness applied for this event as for the April 20, 1978 event, which implies that the reduction in discharge was the reason for lower water surface profile on April 21, 1978. All runs computed water surface profiles which provided a good fit to the observed data downstream of approximately station 305000 m.

Table 4.8 Calibration Results for the Athabasca River, April 21, 1978 ice jam event.

| Run Number | Figure | Model  | Erosion                       | Seepage  | Roughness |                      |
|------------|--------|--------|-------------------------------|----------|-----------|----------------------|
|            |        |        | Velocity                      | Velocity | <i>c</i>  | <i>n<sub>o</sub></i> |
| 1          | 4.40   | ICEJAM | 2.00 m/s                      | -        | -         | 0.040                |
| 2          | 4.41   | ICEJAM | 2.00 m/s                      | -        | 0.20      | 0.045*               |
| 3          | 4.42   | RIVJAM | -                             | 1.75 m/s | 0.15      | -                    |
| 4          | ^      | RIVJAM | -                             | 0 m/s    | 0.12      | -                    |
| 5          | 4.43   | RIVJAM | -                             | 0 m/s    | 0.16      | 0.040*               |
| 6          | -      | RIVJAM | SHEAR WALL DATA NOT AVAILABLE |          |           |                      |

\* equivalent Mannings roughness based on equation [3.19]

^ same profile as computed in Run 3.

#### ***4.5.3.5 Athabasca River, April 29 - May 1, 1979***

A total of three ice jams were observed in the vicinity of Fort McMurray during the 1979 break up on the Athabasca River. The first ice jam that formed just upstream of Fort McMurray was observed to be very dynamic and remained in place for less than one day. The release of this first ice jam contributed to the formation of two other ice jams downstream. A minor ice jam formed downstream of MacEwan Bridge in Fort McMurray and a major ice jam formed with its toe at MacEwan Bridge just upstream of the minor jam. These major and minor ice jams remained in place for approximately three days (April 30 - May 1) and water level measurements obtained over these days indicated little change in the ice jam profile, suggesting steady state conditions. A detailed description of these events is provided by Doyle and Andres (1979) and their estimated discharge for this event was 1150 m<sup>3</sup>/s.

The observed water level data for this event was referenced to an open water surface profile and had to be interpreted to correspond to a datum common to that of the cross sections. Only the data which could be reduced to this common datum were considered in this calibration. The data collected between April 29 and May 1, 1979 was assumed to correspond to one event since little change in the ice jam profile was observed over this period, and also because the scatter in the data made it difficult to determine if there were three distinct ice jams corresponding to the days they were documented.

Table 4.9 summarizes the computed results illustrated in Figures 4.44 to 4.46. For the ICEJAM runs, the length of the jam was made to correspond to the observed location of the head and for the RIVJAM runs the calibrated location of the head slightly over estimated the observed location of the head. Given the scatter in the data, it was considered that both models provided a reasonable fit to the observed data.

Table 4.9 Calibration Results for the Athabasca River, 1979 ice jam event.

| Run Number | Figure | Model  | Erosion Velocity              | Seepage Velocity | Roughness $c$ | Roughness $n_o$ |
|------------|--------|--------|-------------------------------|------------------|---------------|-----------------|
| 1          | 4.44   | ICEJAM | 2.00 m/s                      | -                | -             | 0.050           |
| 2          | -      | ICEJAM | MODEL WOULD NOT RUN           |                  |               |                 |
| 3          | 4.45   | RIVJAM | -                             | 1.75 m/s         | 0.35          | -               |
| 4          | ^      | RIVJAM | -                             | 0 m/s            | 0.28          | -               |
| 5          | 4.46   | RIVJAM | -                             | 0 m/s            | 0.25          | 0.050*          |
| 6          | -      | RIVJAM | SHEAR WALL DATA NOT AVAILABLE |                  |               |                 |

\* equivalent Mannings roughness based on equation [3.19]

^ same profile as computed in Run 3.

Figure 4.46 illustrates the results computed by RIVJAM using Beltaos' Mannings approximation adjusted to match the Mannings roughness calibrated by ICEJAM. To obtain the best possible fit to the observed data, the toe thickness had to be adjusted so that the computed bottom of ice was near the observed water levels and the computed water surface profile near middle of the ice jam was underestimated more than by the previous ICEJAM run (Figure 4.44).

#### 4.5.3.6 Athabasca River, April 10, 1984

On April 10, 1984, moving ice from upstream progressed downstream at a celerity of 2.6 m/s pushing through the solid ice cover at Fort McMurray and eventually came to rest just downstream of Horse River at 22:40 h. The resulting ice jam remained in place for roughly 2 hours. Complete documentation of this ice jam, during its relatively short "stable" period, was not possible due to darkness. Data for the downstream portion of the jam was collected on the following morning based on the height of shear walls left behind after the jam's release. Water levels in the upstream portion of the jam were "*determined photographically using the gauges established for that purpose*" (Andres and Rickert, 1985). The discharge for this event was estimated from gauge records at MacEwan Bridge and downstream of Fort



McMurray. The “most reasonable” estimate for discharge during this event was 640 m<sup>3</sup>/s (Andres, *et al.*, 1985).

Table 4.10 summarizes the computed results illustrated in Figures 4.48 to 4.50. The observed location of the head was near station 306000 m (1 km upstream of the maximum value in the plots). However, it was found that reasonable fits to the observed data could not be achieved when the computed location of the head agreed with the observed location. Instead, the calibrations for this case study were carried out so as to provide the best fit to the observed water level and bottom of ice profiles as priority over producing the correct length. It was found that a computed head location near station 303200 m (2.8 km downstream of the observed location) provided the best results for ICEJAM. RIVJAM computed the location of the head approximately 600 m upstream near station 303800 m (2.2 km downstream of the observed location).

Table 4.10 Calibration Results for the Athabasca River, 1984 ice jam event.

| Run Number | Figure | Model  | Erosion  | Seepage  | Roughness |                      |
|------------|--------|--------|----------|----------|-----------|----------------------|
|            |        |        | Velocity | Velocity | <i>c</i>  | <i>n<sub>o</sub></i> |
| 1          | 4.47   | ICEJAM | 1.25 m/s | -        | -         | 0.075                |
| 2          | 4.48   | ICEJAM | 1.25 m/s | -        | 0.60      | 0.077*               |
| 3          | 4.49   | RIVJAM | -        | 1.75 m/s | 0.75      | -                    |
| 4          | ^      | RIVJAM | -        | 0 m/s    | 0.65      | -                    |
| 5          | 4.50   | RIVJAM | -        | 0 m/s    | 0.5625    | 0.075*               |
| 6          | 4.50   | RIVJAM | -        | 0 m/s    | 0.5625    | 0.075*               |

\* equivalent Mannings roughness based on equation [3.19]

^ same profile as computed in Run 3.

It was found that ice jam profiles computed by both ICEJAM and RIVJAM provided equally good fits to the observed water level data. The ICEJAM runs and the RIVJAM run using Beltaos’ Mannings approximation gave a better average fit to the observed thickness data than the RIVJAM model using Beltaos’ friction factor.

However, as Figure 4.49 illustrates, the RIVJAM run using Beltaos' friction factor provided a better fit to the measured thickness data near station 299000 m and 300000 m. In addition the furthest upstream measured water level is captured best by this run. These observations were consistent with the previous runs, which was that Beltaos' friction factor tends to compute longer and thinner ice jam profiles.

#### **4.5.3.7 Athabasca River, April 14, 1985**

On April 14, 1985, moving ice came to rest just upstream of Mountain Rapids at 11:20 h and "*an extremely stable jam formed... and [discharge] estimates could readily estimated*" (Andres, *et al.*, 1985). This ice jam remained in place until at least 20:00 h, April 18, 1987, (the time of the last observation). Upon the subsequent release of the ice jam, evidence of grounding at the toe was observed. Ice jam profiles were documented using areal reconnaissance (helicopter flights) to document different "states" of the ice jam during its observed lifetime. The first documented water surface profile was obtained during the ice jam's peak stage on April 14, 1985, while the second profile was taken at a lower and more stable water level on April 16, 1985. Shear walls approximately 4 m thick were left behind near the head of the first ice jam when the ice jam collapsed to a shorter length on April 16. Andres *et al.* (1985) estimated that the discharge corresponding to the April 14, 1987 profile was 1400 m<sup>3</sup>/s.

Table 4.11 summarizes the computed results for the calibration runs illustrated in Figures 4.51 to 4.54. It was found during the calibration of both models that the observed thickness near the upstream limit of the observed water level data could not be reproduced by either model. If the thickness of the computed ice jam profile was made to correspond to the observed thickness (approximately 4 m) the observed water levels would be grossly overestimated. Therefore, during the calibration of the models to the observed data, the documented thickness near station 328000 m was ignored.

Table 4.11 Calibration Results for the Athabasca River. April 14, 1985 ice jam event.

| Run Number | Figure | Model  | Erosion                              | Seepage  | Roughness |                      |
|------------|--------|--------|--------------------------------------|----------|-----------|----------------------|
|            |        |        | Velocity                             | Velocity | <i>c</i>  | <i>n<sub>o</sub></i> |
| 1          | 4.51   | ICEJAM | 2.25 m/s                             | -        | -         | 0.030                |
| 2          | 4.52   | ICEJAM | 2.25 m/s                             | -        | 0.10      | 0.032 <sup>*</sup>   |
| 3          | 4.53   | RIVJAM | -                                    | 1.75 m/s | 0.10      | -                    |
| 4          | ^      | RIVJAM | -                                    | 0 m/s    | 0.08      | -                    |
| 5          | 4.54   | RIVJAM | -                                    | 0 m/s    | 0.09      | 0.030 <sup>*</sup>   |
| 6          | -      | RIVJAM | <b>SHEAR WALL DATA NOT AVAILABLE</b> |          |           |                      |

<sup>\*</sup> equivalent Mannings roughness based on equation [3.19]

<sup>^</sup> same profile as computed in Run 3.

All runs provided a good overall fit to the observed water level data. However, the thickness at the upstream end of the modelled portion of the reach underestimated the observed shear wall data. Andres, *et al.* (1985) make no comment on this thickness data which appears to be suspect.

It is interesting to note that the toe thickness for Beltaos' friction factor calibrated using RIVAJAM (Figure 4.53) suggests grounding (as was reported) while the calibrated toe thickness using Beltaos' Mannings approximation (Figure 4.54) did not. This implied that the location of grounding using Beltaos' Mannings approximation was further downstream than that indicated by Beltaos' friction factor. Since there was no toe thickness data it was difficult to explore this observation any further.

#### 4.5.3.8 Athabasca River, April 16, 1985

After the April 14, 1985 ice jam had collapsed, a shorter ice jam remained in place which shared the same toe location as the previous ice jam. Recorded water level data was obtained from areal photographs on April 16, 1985, after the shortened jam

had become relatively stable. The discharge estimated for this event was 620 m<sup>3</sup>/s (Andres, *et al.*, 1985).

Table 4.12 summarizes the computed results illustrated in Figures 4.55 to 4.58. For the calibrations of ICEJAM and RIVJAM, the computed location of the head was forced to correspond to the observed location of the head. Below station 324000 m it was found that the computed water surface profiles generated by both models matched the observed data well, although it was found that the RIVJAM model using Beltaos' friction factor provided the best fit to the observed data near the middle of the jam. However, water elevations at the head computed by all model runs were at a higher elevation than the recorded water elevation upstream at station 328100 m. This implied an adverse water surface slope between these two points. For the RIVJAM run using Beltaos' friction factor (Figure 4.57) this difference was less noticeable. The RIVJAM model using Beltaos' friction factor produced the best results for this particular case study.

Table 4.12 Calibration Results for the Athabasca River, April 16, 1985 ice jam event.

| Run Number | Figure | Model  | Erosion   | Seepage  | Roughness |                      |
|------------|--------|--------|---|----------|-----------|----------------------|
|            |        |        | Velocity  | Velocity | <i>c</i>  | <i>n<sub>o</sub></i> |
| 1          | 4.55   | ICEJAM | 2.25 m/s  | -        | -         | 0.045                |
| 2          | 4.56   | ICEJAM | 2.25 m/s  | -        | 0.25      | 0.050*               |
| 3          | 4.57   | RIVJAM | -   | 1.75 m/s | 0.50      | -                    |
| 4          | ^      | RIVJAM | -   | 0 m/s    | 0.32      | -                    |
| 5          | 4.58   | RIVJAM | -   | 0 m/s    | 0.2025    | 0.045*               |
| 6          | -      | RIVJAM | <b>SHEAR WALL DATA NOT AVAILABLE AT THE TOE</b> |          |           |                      |

\* equivalent Mannings roughness based on equation [3.19]

^ same profile as computed in Run 3.

#### 4.5.3.9 Athabasca River, April 20, 1986

The toe of the 1986 ice jam was observed to be near the mouth of Parsons Creek, approximately 7 km downstream of MacEwan Bridge on April 19, 1986. The ice jam had stabilized by April 20, 1986, at which time the profile of the jam was documented by ground surveys at accessible points, and also by oblique photographs taken from the air. Malcovish, Andres and Mostert (1988) provide a more detailed description of the events surrounding this ice jam and they estimated the discharge for the April 20, 1986 ice jam to be 620 m<sup>3</sup>/s.

Table 4.13 summarizes the computed results illustrated in Figures 4.59 to 4.61. For this event, computed ice jam profiles were generated so as to correspond to the observed location of the head. It was found that both that RIVJAM model using Beltaos' friction factor and ICEJAM model using Mannings roughness produced the best results. RIVJAM using Beltaos' Mannings approximation (fixed to correspond to the Mannings roughness calibrated using ICEJAM) underestimated the data over the entire length of the jam. In all cases the models did not capture the measured water level near station 291000 m.

Table 4.13 Calibration Results for the Athabasca River, April 20, 1986 ice jam event.

| Run Number | Figure | Model  | Erosion Velocity                     | Seepage Velocity | Roughness |                      |
|------------|--------|--------|--------------------------------------|------------------|-----------|----------------------|
|            |        |        |                                      |                  | <i>c</i>  | <i>n<sub>o</sub></i> |
| 1          | 4.59   | ICEJAM | 1.25 m/s                             | -                | -         | 0.050                |
| 2          | -      | ICEJAM | <b>MODEL WOULD NOT RUN</b>           |                  |           |                      |
| 3          | 4.60   | RIVJAM | -                                    | 1.75 m/s         | 0.32      | -                    |
| 4          | ^      | RIVJAM | -                                    | 0 m/s            | 0.25      | -                    |
| 5          | 4.61   | RIVJAM | -                                    | 0 m/s            | 0.25      | 0.050*               |
| 6          | -      | RIVJAM | <b>SHEAR WALL DATA NOT AVAILABLE</b> |                  |           |                      |

\* equivalent Mannings roughness based on equation [3.19]

^ same profile as computed in Run 3.

#### 4.5.3.10 Athabasca River, April 22, 1986

On April 22, 1986 the ice jam which had originally formed on the April 19, 1986, had dropped in elevation slightly and this new profile was documented. It was noted that the observed location of the head had remained near the same location as the ice jam documented previously on April 20, 1986. The discharge for this ice jam event was estimated to be 300 m<sup>3</sup>/s (Malcovish, *et al.*, 1988).

Table 4.14 summarizes the computed results illustrated in Figures 4.62 to 4.64. As was found for the April 20, 1986 event, the computed water surface profiles and location of the head generated by both the ICEJAM and RIVJAM models provided a good fit to the observed data. The measured data for this event is very limited and it is difficult to comment on any comparisons between the computed and the observed data. However, it was found that even though the computed shape of the jam was very irregular, the RIVJAM and ICEJAM models produced very similar results.

Table 4.14 Calibration Results for the Athabasca River, April 22, 1986 ice jam event.

| Run Number | Figure | Model  | Erosion Velocity                      | Seepage Velocity | Roughness <i>c</i> | Roughness <i>n<sub>o</sub></i> |
|------------|--------|--------|---------------------------------------|------------------|--------------------|--------------------------------|
| 1          | 4.62   | ICEJAM | 1.00 m/s                              | -                | -                  | 0.045                          |
| 2          | -      | ICEJAM | <b>MODEL WOULD NOT RUN</b>            |                  |                    |                                |
| 3          | 4.63   | RIVJAM | -                                     | 1.75 m/s         | 0.27               | -                              |
| 4          | ^      | RIVJAM | -                                     | 0 m/s            | 0.18               | -                              |
| 5          | 4.64   | RIVJAM | -                                     | 0 m/s            | 0.2025             | 0.045*                         |
| 6          | -      | RIVJAM | <b> SHEAR WALL DATA NOT AVAILABLE</b> |                  |                    |                                |

\* equivalent Mannings roughness based on equation [3.19]

^ same profile as computed in Run 3.

## 4.7 DISCUSSION OF RESULTS

### 4.7.1 General

The calibration protocols developed during the rigorous model investigation were tested against eleven documented ice jam events on the Hay and Athabasca Rivers. It was found that by following these protocols, the models could be successfully applied to these case studies producing computed ice jam profiles which gave good visual fits to the observed water level data. The calibrated composite roughness values obtained during both the rigorous models investigation and the verification phase portions of this study were compared under various scenarios to try and define if there were any definite trends between these roughnesses. The importance of seepage as it relates to roughness was also investigated.

Table 4.15 presents a summary of the calibrated roughnesses for each event obtained using ICEJAM and RIVJAM. The calibrated values for roughness included in this table are: Mannings roughness calibrated using ICEJAM,  $n_o$ ; Beltaos' Mannings approximation calibrated using ICEJAM and RIVJAM,  $n_o^*$ ; and Beltaos' friction factor calibrated using RIVJAM (represented by the roughness coefficient,  $c$ ). In addition, the calibrated erosion velocity,  $V_{max}$ , used by ICEJAM, and the average velocity of the flow underneath the ice at the toe,  $V_f$ , computed by RIVJAM, are included in this table for comparison.

### 4.7.2 Calibrated composite roughness

The composite Mannings roughness calibrated by ICEJAM ranged between 0.030 to 0.075 for all of the fourteen events investigated during this study. The range of roughnesses represented by Beltaos' friction factor coefficient,  $c$ , was 0.10 to 0.75. Little is known about typical values for  $c$ . However, as discussed earlier, Beltaos (1997) suggested that for ice jams where the average thickness is less than about 3 m

$c$  typically ranges between 0.40 to 0.60 and that values as low as 0.20 have been encountered during RIVJAM applications.

#### ***4.7.2.1 Consistency of Calibrated Roughness for Rivers With Multiple Events***

The Hay and the Athabasca Rivers were the only two rivers with multiple documented ice jam events. Two separate events which occurred along the same reach of Hay River were investigated, and it was found that the calibrated composite Mannings roughnesses were 0.045 and 0.050, where the lower roughness was associated with the higher discharge. This tendency is physically reasonable since Mannings roughness would be expected to decrease as discharge increases.

For the Athabasca River case studies, composite Mannings roughness values ranged between 0.040 and 0.050 with the exceptions of the April 14, 1985 event (where Mannings composite roughness was 0.030) and the 1984 event (where the Mannings composite roughness was 0.075). It was also found that, for the 1985 ice jam, the roughness increased from 0.030 to 0.045 when the ice jam evolved as the discharge dropped from 1400 m<sup>3</sup>/s to 640 m<sup>3</sup>/s (a reduction of more than 50%). In contrast with the trends observed for the 1985 events on the Athabasca and events on the Hay River, during the 1978 Athabasca River events the roughness was found to *decrease* as the discharge decreased (by 25%). It is possible that the relatively lower reduction in discharge during the 1978 Athabasca River events from 1200 m<sup>3</sup>/s to 900 m<sup>3</sup>/s did not have as big an impact on the roughness for this case study. However, it is more plausible that the underside of the ice jam became less rough over the three days that it remained in place, especially since this jam was observed to remain very stable with little change in water levels over the three day period it was observed. Over the three days the jam remained in place, the underside of the ice jam would have been smoothed by incoming warm water.



Table 4.15 Summary of roughnesses calibrated by RIVJAM and ICEJAM

| Event                           | Discharge<br>(m <sup>3</sup> /s) | ICEJAM calibrated roughness |               |           | RIVJAM calibrated roughness |                    |                       |                 |
|---------------------------------|----------------------------------|-----------------------------|---------------|-----------|-----------------------------|--------------------|-----------------------|-----------------|
|                                 |                                  | $n_0$                       | $n_0^*$       | $V_{max}$ | $n_0^*$                     | $C_{\lambda=1.75}$ | $V_{f(\lambda=1.75)}$ | $C_{\lambda=0}$ |
| Restigouche River, 1988         | 330                              | 0.070                       | would not run | 2 m/s     | 0.08                        | 0.64               | 0.24 m/s              | 0.515           |
| Thames River, 1986              | 290                              | 0.055                       | would not run | 2 m/s     | 0.061                       | 0.70               | 1.09 m/s              | 0.6635          |
| Saint John River, 1993          | 2250                             | 0.040                       | would not run | 2.5 m/s   | 0.05                        | 0.38               | 1.95 m/s              | 0.2725          |
| Hay River, 1987                 | 420                              | 0.050                       | 0.050         | 1.75 m/s  | no data                     | 0.35               | 0.64 m/s              | 0.222           |
| Hay River, 1992                 | 605                              | 0.045                       | 0.050         | 2 m/s     | no data                     | 0.30               | 0.91 m/s              | 0.26            |
| Athabasca River, April 19, 1978 | 1200                             | 0.045                       | 0.050         | 2 m/s     | no data                     | 0.16               | 0.97 m/s              | 0.13            |
| Athabasca River, April 20, 1978 | 1000                             | 0.040                       | 0.045         | 2 m/s     | no data                     | 0.12               | 0.90 m/s              | 0.095           |
| Athabasca River, April 21, 1978 | 900                              | 0.040                       | 0.045         | 2 m/s     | no data                     | 0.15               | 1.08 m/s              | 0.12            |
| Athabasca River, 1979           | 1150                             | 0.050                       | would not run | 2 m/s     | no data                     | 0.35               | 1.35 m/s              | 0.28            |
| Athabasca River, 1984           | 640                              | 0.075                       | 0.077         | 1.25 m/s  | 0.075                       | 0.75               | 0.38 m/s              | 0.65            |
| Athabasca River, April 14, 1985 | 1400                             | 0.030                       | 0.032         | 2.25 m/s  | no data                     | 0.10               | 1.75 m/s              | 0.08            |
| Athabasca River, April 16, 1985 | 620                              | 0.045                       | 0.050         | 2.25 m/s  | no data                     | 0.50               | 0.73 m/s              | 0.32            |
| Athabasca River, April 20, 1986 | 455                              | 0.050                       | would not run | 1.25 m/s  | no data                     | 0.32               | 0.48 m/s              | 0.25            |
| Athabasca River, April 22, 1986 | 300                              | 0.045                       | would not run | 1 m/s     | no data                     | 0.27               | 0.37 m/s              | 0.18            |

\*Converted from Beltaos Mannings approximation ( $n_0 = 0.10c^{1/2}$ )

#### ***4.7.2.2 Ice roughnesses deduced using Sabenev's Equation***

Table 4.16 presents values for under ice roughness deduced using Sabenev's equation for Mannings roughness, where the under ice roughnesses,  $n_i$ , were developed from the composite roughness values calibrated with the ICEJAM model, as well as reported open water bed roughnesses for the reaches investigated. It is acknowledged that the Sabenev's equation was derived based on some relatively limiting assumptions (Uzuner, 1975). Also, the under ice bed roughness would be expected to be different from that under open water conditions for the same discharge, and finally the discharges under consideration here are different than those for which the open water bed roughnesses were determined. Nevertheless, this approach represents the state-of-the-art in current practice and at least gives the reader a feel for the plausible range of ice roughnesses which might occur in nature.

Some of the values obtained in this manner (0.099 and 0.111 for example) are intuitively, unrealistically high. The primary factors that are suspect in contributing to these erroneous values include: poor estimates for discharge; inappropriate bed roughness values used in the Sabenev's equation; and the inapplicability of the assumptions inherent in Sabenev's equation.

#### ***4.7.2.3 Impact of Choice of Roughness on the Shape of the Computed Ice Jam Profile***

During the calibration of the models to the documented events, it was found that Mannings roughness and Beltaos' friction factor produced ice jam profiles of different shapes. Beltaos' friction factor was found to produce ice jam profiles that were longer and thinner with flatter slopes near the head than those computed using Mannings roughness. In some cases (the Saint John River, for example) it was found that Mannings roughness was better at capturing the measured data, while in others (Thames, River) Beltaos' friction factor produced better results. Therefore it could not be said that either method for computing frictional resistance was consistently

Table 4.16 Summary of deduced ice roughnesses based on calibrated composite roughness and open water bed roughness.

| Event                           | $n_o$ | $n_b$ | Source for estimate of open water bed roughness                     | * $n_i$ |
|---------------------------------|-------|-------|---|---------|
| Restigouche River, 1988         | 0.070 | 0.032 | Beltaos and Burrell (1990)  | 0.099   |
| Thames River, 1986              | 0.055 | -     | none available  | -       |
| Saint John River, 1993          | 0.040 | 0.020 | Hicks, McKay, and Shaybayek   | 0.056   |
| Hay River, 1987                 | 0.050 | 0.029 | Gerard, Hicks, and Jasek (1990) - converted from $k_{bed} = 0.20$ m | 0.067   |
| Hay River, 1992                 | 0.045 | 0.029 | Gerard, Hicks, and Jasek (1990) - converted from $k_{bed} = 0.20$ m | 0.059   |
| Athabasca River, April 19, 1978 | 0.045 | 0.025 | Kellerhals, Neill, and Bray (1972); Andres (1985)                   | 0.061   |
| Athabasca River, April 20, 1978 | 0.040 | 0.025 | Kellerhals, Neill, and Bray (1972); Andres (1985)                   | 0.053   |
| Athabasca River, April 21, 1978 | 0.040 | 0.025 | Kellerhals, Neill, and Bray (1972); Andres (1985)                   | 0.053   |
| Athabasca River, 1979           | 0.050 | 0.025 | Kellerhals, Neill, and Bray (1972); Andres (1985)                   | 0.070   |
| Athabasca River, 1984           | 0.075 | 0.025 | Kellerhals, Neill, and Bray (1972); Andres (1985)                   | 0.111   |
| Athabasca River, April 14, 1985 | 0.030 | 0.025 | Kellerhals, Neill, and Bray (1972); Andres (1985)                   | 0.035   |
| Athabasca River, April 16, 1985 | 0.045 | 0.025 | Kellerhals, Neill, and Bray (1972); Andres (1985)                   | 0.061   |
| Athabasca River, April 20, 1986 | 0.050 | 0.025 | Kellerhals, Neill, and Bray (1972); Andres (1985)                   | 0.070   |
| Athabasca River, April 22, 1986 | 0.045 | 0.025 | Kellerhals, Neill, and Bray (1972); Andres (1985)                   | 0.061   |

\* ice roughness is deduced from Sabanevs equation based on the calibrated composite roughness,  $n_o$ , and the reported bed roughness,  $n_b$

better than the other. It was also verified on the Thames River case study that different shape computed by Beltaos' friction factor, as compared to that obtained with Mannings equation, was not due to the inclusion of seepage.

#### **4.7.2.4 Calibrated Roughness as a Function of Discharge**

Figure 4.65 presents a graph of the calibrated composite Mannings roughness,  $n_o$ , for the fourteen case studies as a function of discharge. Here a trend towards decreasing roughness with increasing discharge is seen, although scatter in the data indicates that roughness is not exclusively dependent on discharge. For one-dimensional models like ICEJAM, the roughness accounts for all energy losses and not just the roughness, and in the case of ice jams must lump in the effects of seepage as well (when this is not explicitly considered).

Since Mannings roughness is not exclusively dependent on discharge, it is not appropriate to try and define an analytical relationship for Mannings roughness based solely on discharge. Therefore, the data presented in Figure 4.65 is presented "as is" with no attempt to represent the data by a single equation (or line) or to quantify the data using standard statistical methods.

#### **4.7.3 Validity of Beltaos' Mannings Approximation**

Figure 4.66 illustrates the comparison between the calibrated roughness values obtained from ICEJAM's Mannings equation to Beltaos' approximation. The open symbols represent  $c$  values calibrated by the ICEJAM model, and the filled symbols represent  $c$  values calibrated using RIVJAM. Beltaos' (1989) theoretical relationship (equation [3.19]) is shown for comparison.

$$n_o = 0.10\sqrt{c} \quad [3.19]$$

Mannings roughnesses that were used for comparison were taken from calibrations using ICEJAM. The Beltaos' Mannings approximation roughnesses (represented by

the  $c$  values) that were used for comparison. were taken from calibrations using the ICEJAM model, as well as from calibrations using the RIVJAM model where toe thickness data was provided. Since the equivalency between the models had already been established, the ICEJAM model was used to calibrate values for Beltaos' Mannings approximation because only the roughness required adjustment for calibration. The RIVJAM model was used to calibrate addition values of  $c$  for cases where the thickness at the toe could be fixed to match observed data and only the roughness,  $c$ , was calibrated. The square root of the calibrated  $c$  values were then plotted against the calibrated values of Mannings roughness obtained using the ICEJAM model.

As the figure shows, Beltaos' Mannings approximation generally suggests an  $n_o$  that is lower than that which is obtained using equation [3.19]. It was expected that the relationship described in equation [3.19] would not be exact as Beltaos' Mannings approximation is a function of the depth of flow.

Also, during RIVJAM calibrations, it was found that when Beltaos' Mannings roughness was set to a value that corresponded to the Mannings roughness computed using ICEJAM (through the use of equation [3.19]), the computed water surface profile consistently underestimated that computed by ICEJAM using Mannings equation (see results for RUN 5). These results supported the observations found in Figure 4.66.

#### **4.7.4 The Impact of Seepage on Roughness**

Since the plot in Figure 4.65 indicated that the scatter in the roughness versus discharge relationship was considerable when seepage was neglected, it was considered desirable to determine whether the effects of seepage were responsible for some of this scatter. This comparison was done using the Beltaos friction factor rather than Mannings roughness for two reasons. First, Mannings equation is not explicitly included in the RIVJAM model, and as Figure 4.66 has shown this

relationship has scatter as well. Second, Mannings roughness varies within a much more limited range than the Beltaos' friction factor, and so some sensitivity might have been missed in this case.

Figure 4.67 and Figure 4.68 present the calibrated roughness values required to compute coincident ice jam profiles where the seepage,  $\lambda$ , was set to 0 m/s (represented by  $c_{\lambda=0}$  m/s) and where seepage was set to 1.75 m/s (represented by  $c_{\lambda=1.75}$  m/s). By including seepage the roughness consistently decreased, and as shown in Figure 4.67 this effect increased as grounding increased. This is physically reasonable as when the seepage velocity,  $\lambda$ , is set to zero the flow under the ice cover effectively increases, and to maintain the same water level associated with the smaller discharge, the roughness must decrease.

Figure 4.68 illustrates the comparison between calibrated roughnesses (both with and without seepage) and the discharge under the accumulation. Figure 4.68(a) represents the calibrated roughnesses where seepage,  $\lambda$ , is set to zero m/s and Figure 4.68(b) represents the calibrated roughnesses where the seepage was set to zero. It was anticipated that the when seepage was included, the calibrated roughnesses would be represented by a narrower band of values than those calibrated without seepage. However, no such trend was indicated, and Figure 4.68 suggests that the reverse may have been indicated. This indicated that, although seepage is an important consideration, it is not a major factor in the scatter observed in the roughness versus discharge relationship.

#### 4.7.5 Velocity at the Toe

The average velocity under the ice at the toe,  $V_f$ , was also reported in Table 4.15 for each RIVJAM run done with Beltaos' friction factor using a seepage velocity,  $\lambda$ , of 1.75 m/s. It was found that the average velocities under the toe ranged between 0.24 and 1.95 m/s. In comparison, erosion velocities calibrated during the ICEJAM runs ranged from 1.00 to 2.25 m/s. It is evident that both models computed, or

calibrated, average velocities at the toe that may be considered high enough to cause erosion of the bed. However, the RIVJAM model generally computed lower average velocities at the toe than the calibrated erosion velocities for ICEJAM.

#### 4.7.6 Comparison of Computed Data to Equilibrium Theory

By definition, uniform flow cannot occur in natural channels, although in a manner analogous to open channel flow, we have seen that even for these non-prismatic channels reaches, sections within the computed ice jam profile exhibited equilibrium-like profiles (i.e. near constant thickness and water surface slope). It was decided to compare the results computed by the models (which are based on a gradually varied flow analysis) to equilibrium ice jam theory (which assumes uniform flow).

##### 4.7.6.1 Equilibrium Formulation for Beltaos' friction factor

For equilibrium conditions, a direct solution to the jam stability equation can be obtained because, by definition of equilibrium conditions, the rate change in thickness in the streamwise,  $x$ , direction is zero. The non-dimensional depth versus discharge relationships for equilibrium conditions developed by Beltaos (1983) is:

$$\eta = 0.63 f_o^{1/3} \xi_B + \frac{5.75}{\mu} \left[ 1 + \sqrt{1 + 0.11 \mu f_o^{1/3} \left( \frac{f_i}{f_o} \right) \xi_B} \right] \quad [4.1]$$

where  $\eta$  and  $\xi_B$  represent non-dimensional depth and discharge, respectively, and are defined as follows:

$$\eta = \frac{H}{BS_f} \quad [4.2]$$

$$\xi_B = \frac{\left(\frac{q^2}{gS_f}\right)^{1/3}}{BS_f} \quad [4.3]$$

and where:

$H$  is the depth from the water surface to the bed (equal to the depth of flow below the ice cover,  $h$ , plus the submerged ice thickness,  $t_s$ ).

In the RIVJAM model, Beltaos (1993) used the friction factor ratio defined previously in equation [3.3] as:

$$\beta_2 = \frac{f_i}{2f_o} \quad [3.3]$$

Substitution into equation [4.1] gives:

$$\eta = 0.63 f_o^{1/3} \xi_B + \frac{5.75}{\mu} \left[ 1 + \sqrt{1 + 0.11 \mu f_o^{1/3} (2\beta_2) \xi_B} \right] \quad [4.4]$$

#### 4.7.6.2 *Equilibrium Formulation for Roughness Height*

Gerard (1988) also presented a non-dimensional depth versus discharge relationship. However, in this case, it was based on roughness height and was presented only graphically. The analytical version of that relationship, later presented by Hicks, Steffler, and Gerard (1992), is as follows:

$$\eta = 0.38 \xi_G + \frac{5.75}{\mu} \left[ 1 + \sqrt{1 + 0.07 \mu \xi_G \left(\frac{k_i}{k_o}\right)^{1/4}} \right] \quad [4.5]$$

where:



$$\xi_G = \frac{\left( \frac{qk_o^{1/6}}{\sqrt{gS_f}} \right)^{3.5}}{BS_f} \quad [4.5]$$

#### 4.7.6.3 Comparison of Beltaos' Friction Factor to Calibrated Case Studies

Of the fourteen ice jam events investigated, eight exhibited equilibrium sections. Table 4.17 summarizes the roughness, geometric, and hydraulic data calculated within these sections, indicating the station where the channel properties were calculated. Using this data, the non-dimensional depth versus discharge for these events was calculated and plotted along with the theoretical depth versus discharge relationships defined in equations [4.1] and [4.4].

Figure 4.69(a) presents the non-dimensional depth,  $\eta$ , versus discharge,  $\xi_B$ , for Beltaos' friction factor. It was noted that the friction factor does not appear in the non-dimensional discharge term, so theoretical lines representing a range of friction factors (selected to represent the range of calibrated friction factors) were included on the plot. The data obtained from the case studies appears to fit the theoretical curves well within the range of roughnesses obtained during the calibrations.

Since the data fit the analytical relationships well, the sensitivity of ice cover to composite roughness ratio,  $\beta_2$ , could be investigated more thoroughly using the analytical equation [4.4]. Figure 4.69(b) indicates that thickness and depth of flow for equilibrium ice jams are not very sensitive to changes in the ice cover to composite roughness ratio, where the range of ratios presented encompass the range of values suggested by Beltaos (1997). As reported earlier, it was found during the analysis of non-equilibrium ice jams (for both a prismatic and natural channel case) that the computed ice jam profiles were not sensitive to changes in the composite roughness ratio. It is concluded that it would be reasonable to set the friction factor ratio,  $\beta_2$ , to 0.5 for practical applications of the RIVJAM model.

Table 4.17(a) Summary of Mannings roughness, discharge, and channel properties for ice jams with equilibrium sections.

| Event                           | Station<br>(m) | $n_0$ | * $k_0$<br>(m) | $t_s$<br>(m) | hydraulic<br>depth (m) | $S_f$   | B<br>(m) | Q<br>(m <sup>3</sup> /s) | q<br>(m <sup>2</sup> /s) |
|---------------------------------|----------------|-------|----------------|--------------|------------------------|---------|----------|--------------------------|--------------------------|
| Athabasca River, April 19, 1978 | 306275         | 0.045 | 2.8            | 6.0          | 3.13                   | 0.00098 | 408      | 1200                     | 2.94                     |
| Athabasca River, April 20, 1978 | 304781         | 0.040 | 1.4            | 5.3          | 2.70                   | 0.00092 | 402      | 1000                     | 2.49                     |
| Athabasca River, April 21, 1978 | 304283         | 0.040 | 1.4            | 5.0          | 2.59                   | 0.00088 | 399      | 900                      | 2.26                     |
| Athabasca River, 1979           | 288012         | 0.050 | 5.2            | 4.1          | 3.49                   | 0.00041 | 558      | 1150                     | 2.06                     |
| Athabasca River, April 14, 1985 | 318915         | 0.030 | 0.2            | 5.2          | 2.79                   | 0.00071 | 452      | 1400                     | 3.10                     |
| Athabasca River, April 16, 1985 | 318915         | 0.045 | 2.8            | 4.4          | 2.26                   | 0.00065 | 446      | 620                      | 1.39                     |
| Hay River, 1992                 | 5700           | 0.045 | 2.8            | 2.6          | 3.44                   | 0.00055 | 269      | 605                      | 2.25                     |
| <i>Restigouche River, 1988</i>  | 22420          | 0.070 | 39             | 3            | 3.02                   | 0.00079 | 212      | 330                      | 1.56                     |
| <i>Restigouche River, 1988</i>  | 23590          | 0.070 | 39             | 3            | 3.47                   | 0.00084 | 160      | 330                      | 2.06                     |
| <i>Restigouche River, 1988</i>  | 24460          | 0.070 | 39             | 3            | 3.19                   | 0.00096 | 172      | 330                      | 1.92                     |
| <i>Restigouche River, 1988</i>  | 25740          | 0.070 | 39             | 3            | 3.24                   | 0.00079 | 187      | 330                      | 1.76                     |
| Restigouche River, 1988         | averaged       | 0.070 | 39             | 3            | 3.23                   | 0.00085 | 183      | 330                      | 1.83                     |

\*calculated from Beliaos' friction factor equation [3.19]

Table 4.17 (b) Summary of Beltaos' friction factor, discharge, and channel properties for ice jams with equilibrium sections.

| Event                           | Station<br>(m) | * $f_0$<br>(m) | c    | $t_s$<br>(m) | hydraulic<br>depth (m) | $S_f$   | B<br>(m) | Q<br>(m <sup>3</sup> /s) | q<br>(m <sup>2</sup> /s) |
|---------------------------------|----------------|----------------|------|--------------|------------------------|---------|----------|--------------------------|--------------------------|
| Athabasca River, April 19, 1978 | 306275         | 0.26           | 0.16 | 5.73         | 3.58                   | 0.00098 | 413      | 1200                     | 2.91                     |
| Athabasca River, April 20, 1978 | 304781         | 0.20           | 0.12 | 4.98         | 3.03                   | 0.00088 | 405      | 1000                     | 2.47                     |
| Athabasca River, April 21, 1978 | 304283         | 0.23           | 0.15 | 4.63         | 3.03                   | 0.00083 | 403      | 900                      | 2.23                     |
| Athabasca River, 1979           | 288012         | 0.35           | 0.35 | 4.12         | 4.07                   | 0.00040 | 551      | 1150                     | 2.09                     |
| Athabasca River, April 14, 1985 | 318915         | 0.14           | 0.10 | 4.80         | 3.54                   | 0.00066 | 459      | 1400                     | 3.05                     |
| Athabasca River, April 16, 1985 | 318915         | 0.57           | 0.50 | 3.88         | 3.40                   | 0.00055 | 458      | 620                      | 1.35                     |
| Hay River, 1992                 | 5700           | 0.20           | 0.30 | 2.36         | 3.61                   | 0.00058 | 248      | 605                      | 2.44                     |
| Restigouche River, 1988         | 22420          | 0.55           | 0.64 | 2.77         | 3.22                   | 0.00084 | 212      | 330                      | 1.56                     |
| Restigouche River, 1988         | 23590          | 0.47           | 0.64 | 2.78         | 3.77                   | 0.00080 | 163      | 330                      | 2.02                     |
| Restigouche River, 1988         | 24460          | 0.51           | 0.64 | 2.83         | 3.52                   | 0.00089 | 175      | 330                      | 1.89                     |
| Restigouche River, 1988         | 25740          | 0.49           | 0.64 | 2.62         | 3.44                   | 0.00081 | 188      | 330                      | 1.76                     |
| Restigouche River, 1988         | averaged       | 0.50           | 0.64 | 2.75         | 3.49                   | 0.00084 | 185      | 330                      | 1.81                     |

\*calculated from Beltaos' friction factor equation [3.19]

#### ***4.7.6.3 Comparison of Roughness Height to Calibrated Case Studies***

By converting the Mannings roughness values obtained during model calibration to roughness heights using Strickler's equation (Henderson, 1965), this data could be applied to the non-dimensional depth versus discharge relationship presented by Hicks, *et al* (1992). Figure 4.70(a) shows the non-dimensional depth versus discharge relationship described by equation [4.5]. It is noted that the non-dimensional discharge term corresponding to equation [4.5] includes roughness, and that this helped to reduce the scatter compared to that seen in Figure 4.69(a). Analytical lines were plotted for  $\mu = 0.8, 1.0, \text{ and } 1.2$  to illustrate the sensitivity of the analytical solutions to changes in the jam strength parameter,  $\mu$ . These lines indicate that for equilibrium ice jams the non-dimensional depth is not very sensitive to changes in  $\mu$ , in particular for discharges within the range of the selected case studies and greater. Based on these results for the equilibrium case, it is concluded that for practical applications, the jam strength parameter,  $\mu$ , can be set to 1.0.

Figure 4.70(b) illustrates the impact of the roughness ratio on the analytical solution for equilibrium ice jams and it again appears that this ratio is insensitive for equilibrium ice jams.

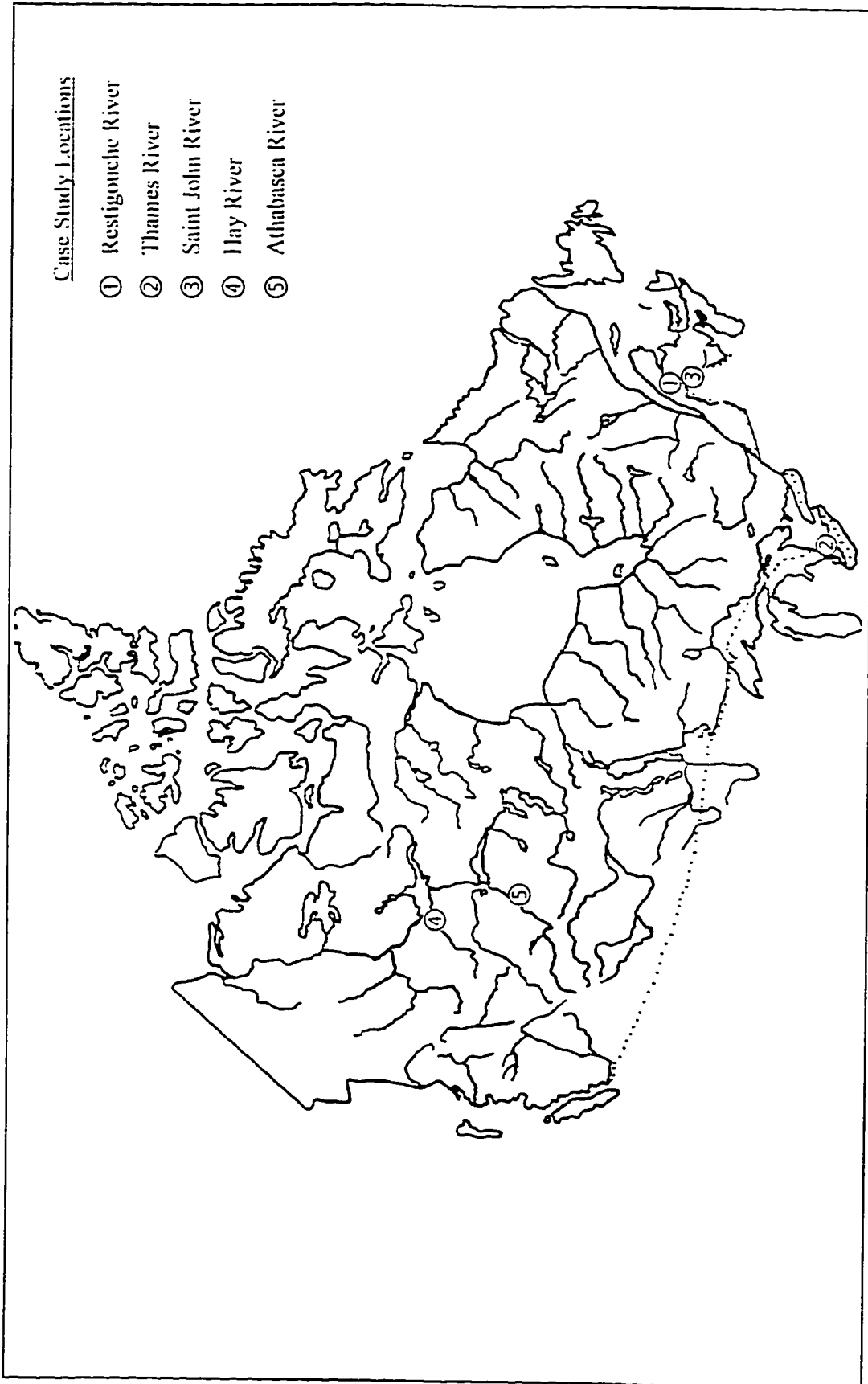


Figure 4.1. Case Study Locations.

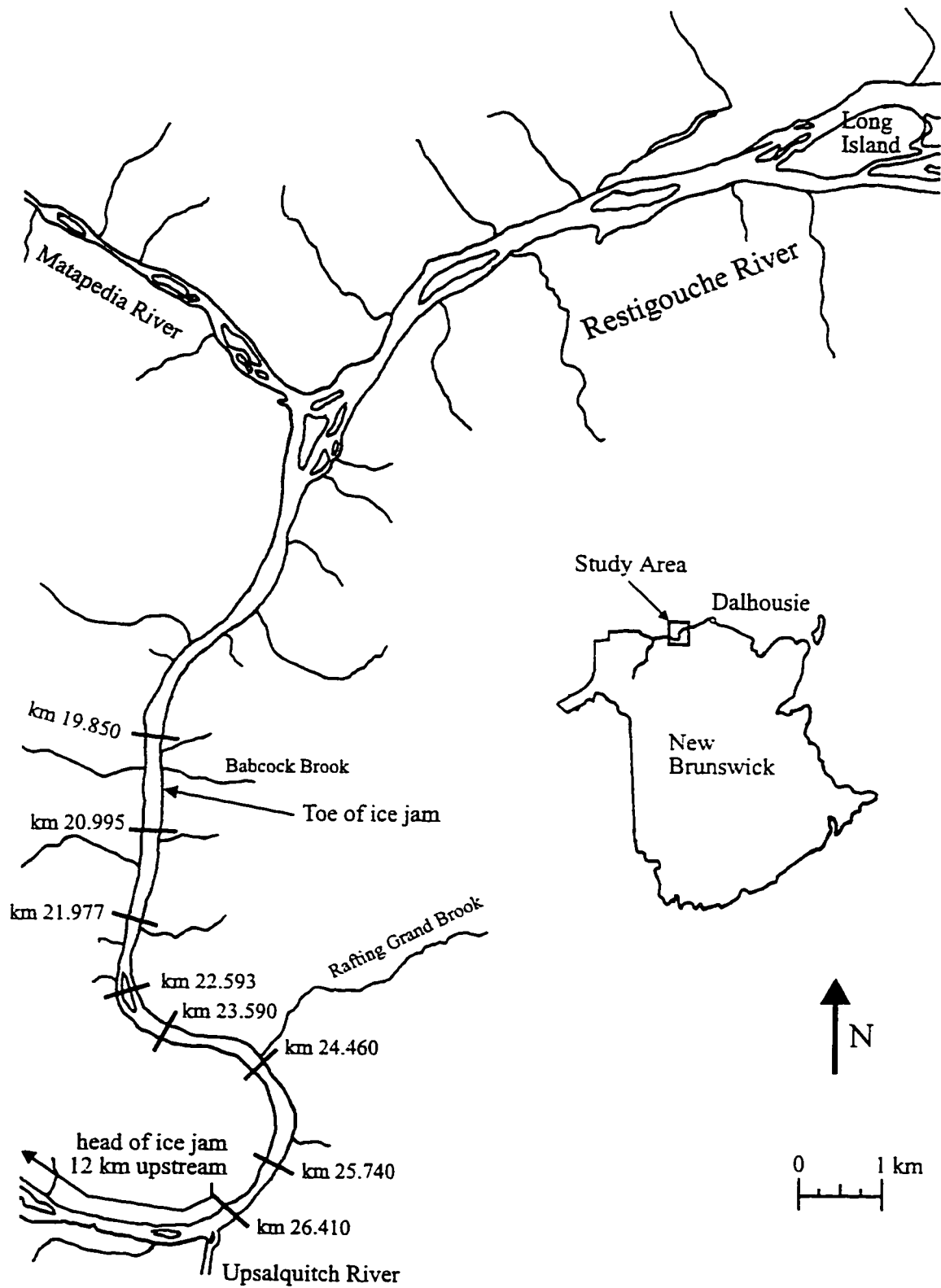


Figure 4.2. Extent of ice jam and cross section locations for the 1988 Restigouche River ice jam event.

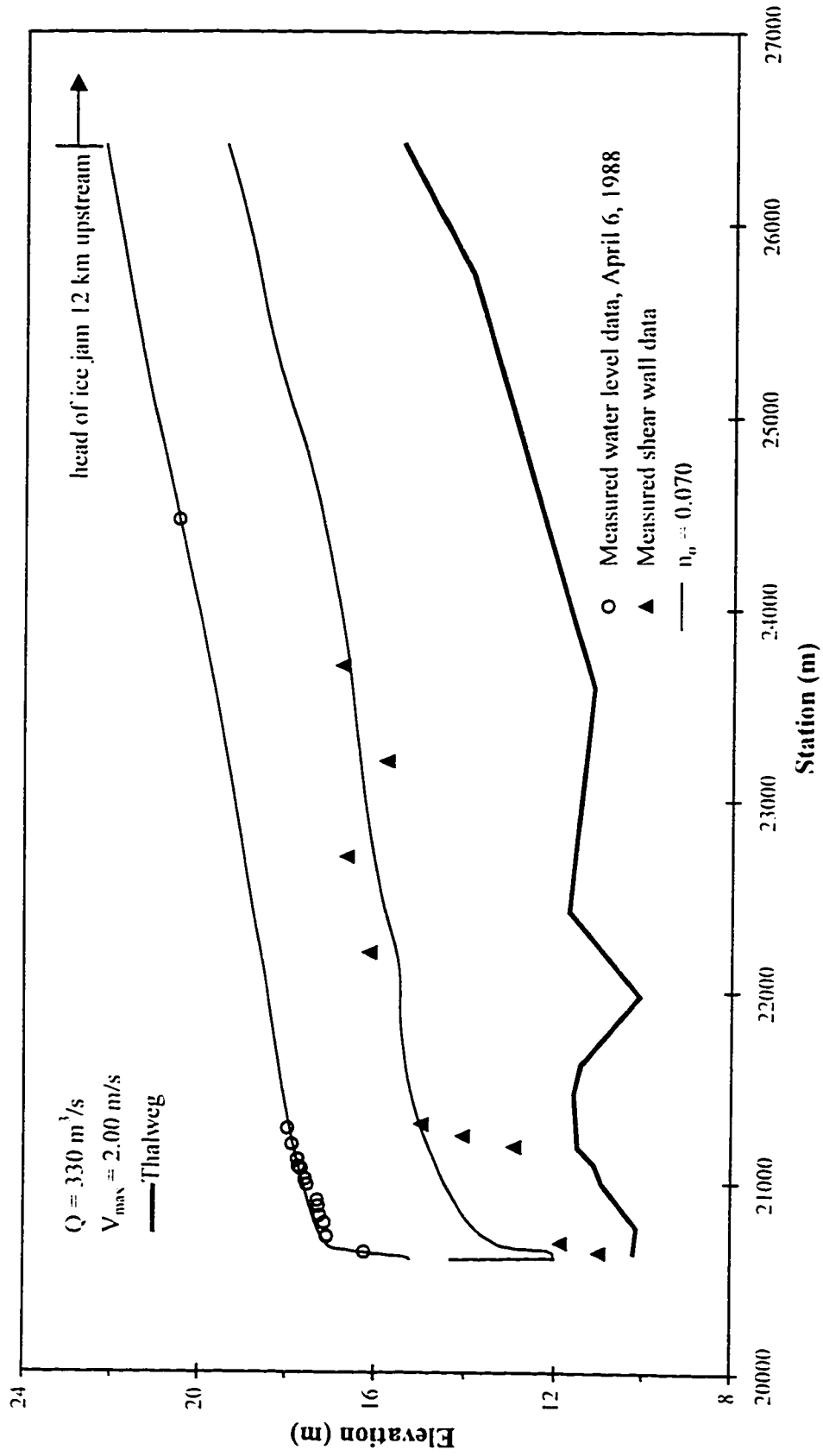


Figure 4.3. 1988 Restigouche River ice jam as predicted by ICEJAM using Mannings roughness.

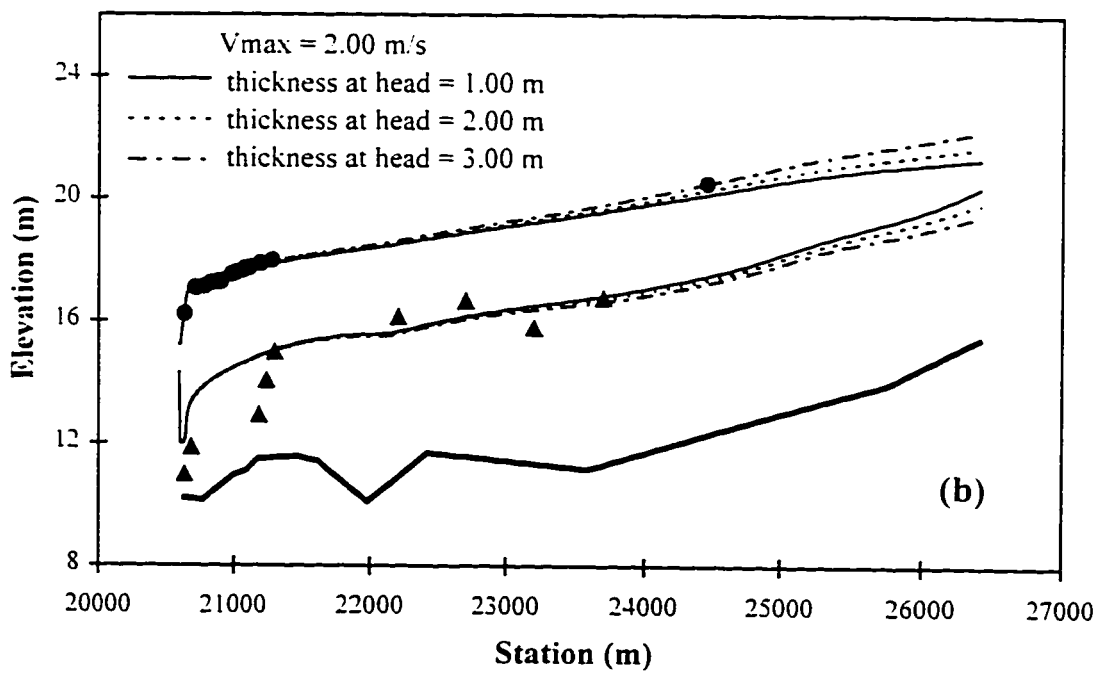
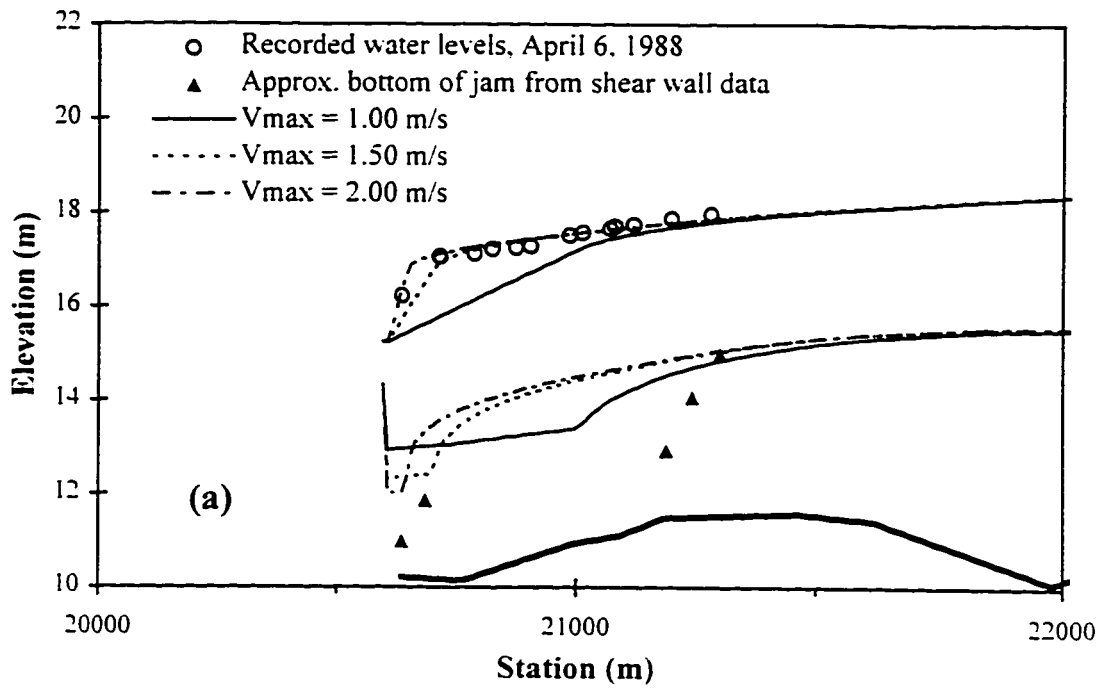


Figure 4.4. 1988 Restigouche River ice jam as predicted by ICEJAM using Mannings roughness, illustrating variation in (a) erosion velocity and (b) thickness at the head.



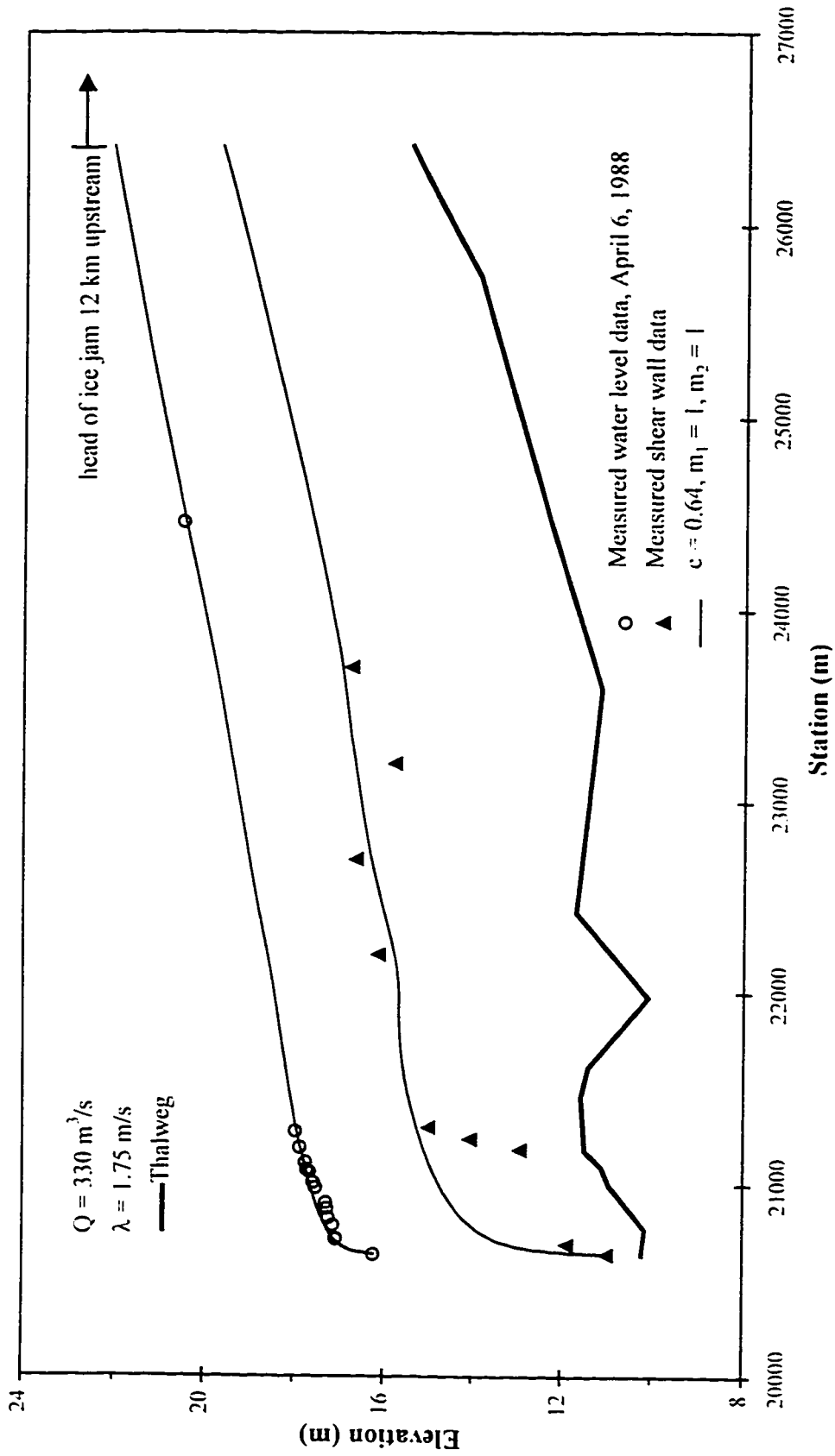


Figure 4.5. 1988 Restigouche River ice jam as predicted by RIVJAM using Beltaos' friction factor.

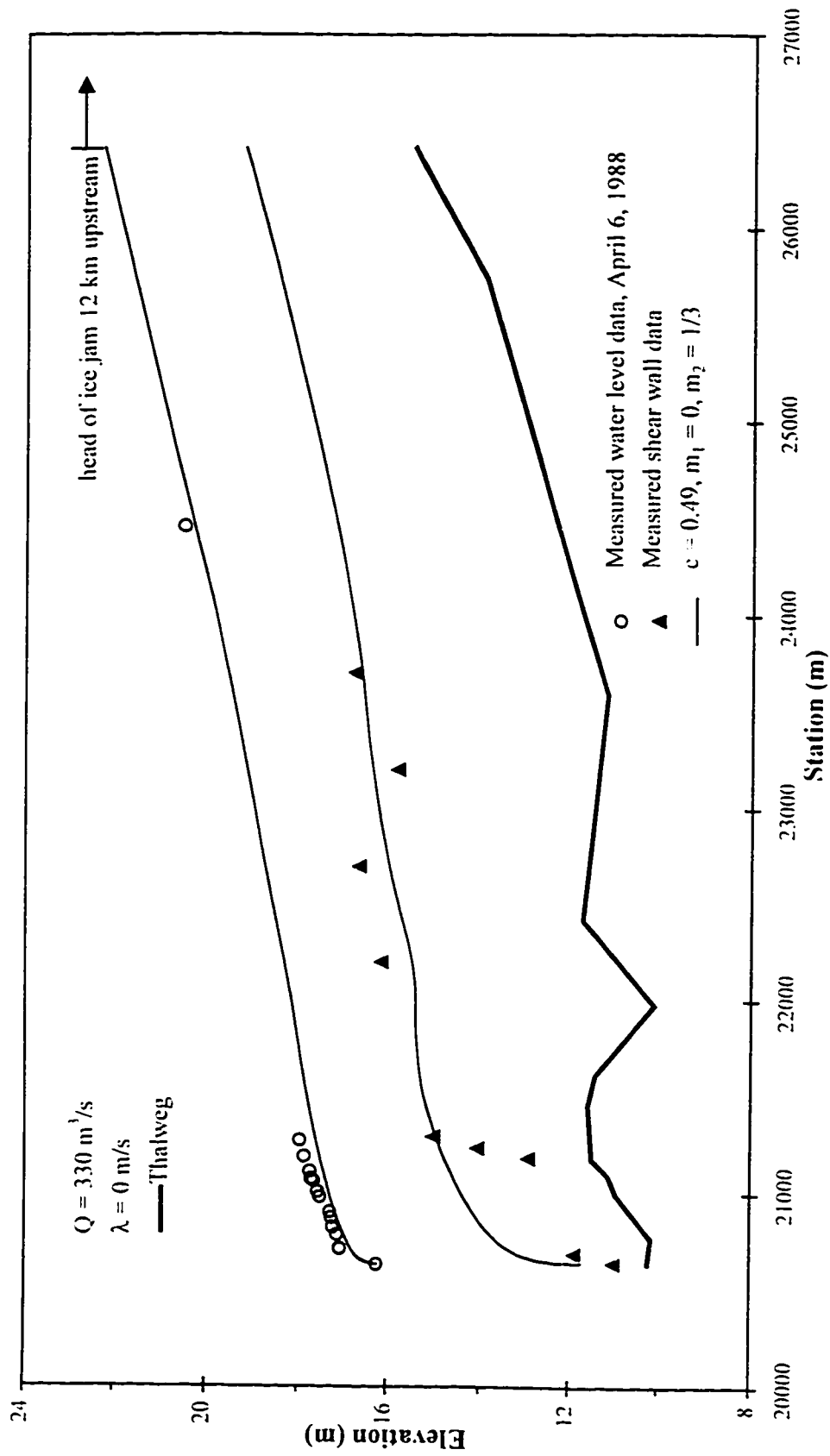


Figure 4.6(a). 1988 Restigouche River ice jam event as predicted by RIVIAM using Beltaos' Mannings approximation where  $c$  is set to match Mannings  $n = 0.070$  using equation [3.19].

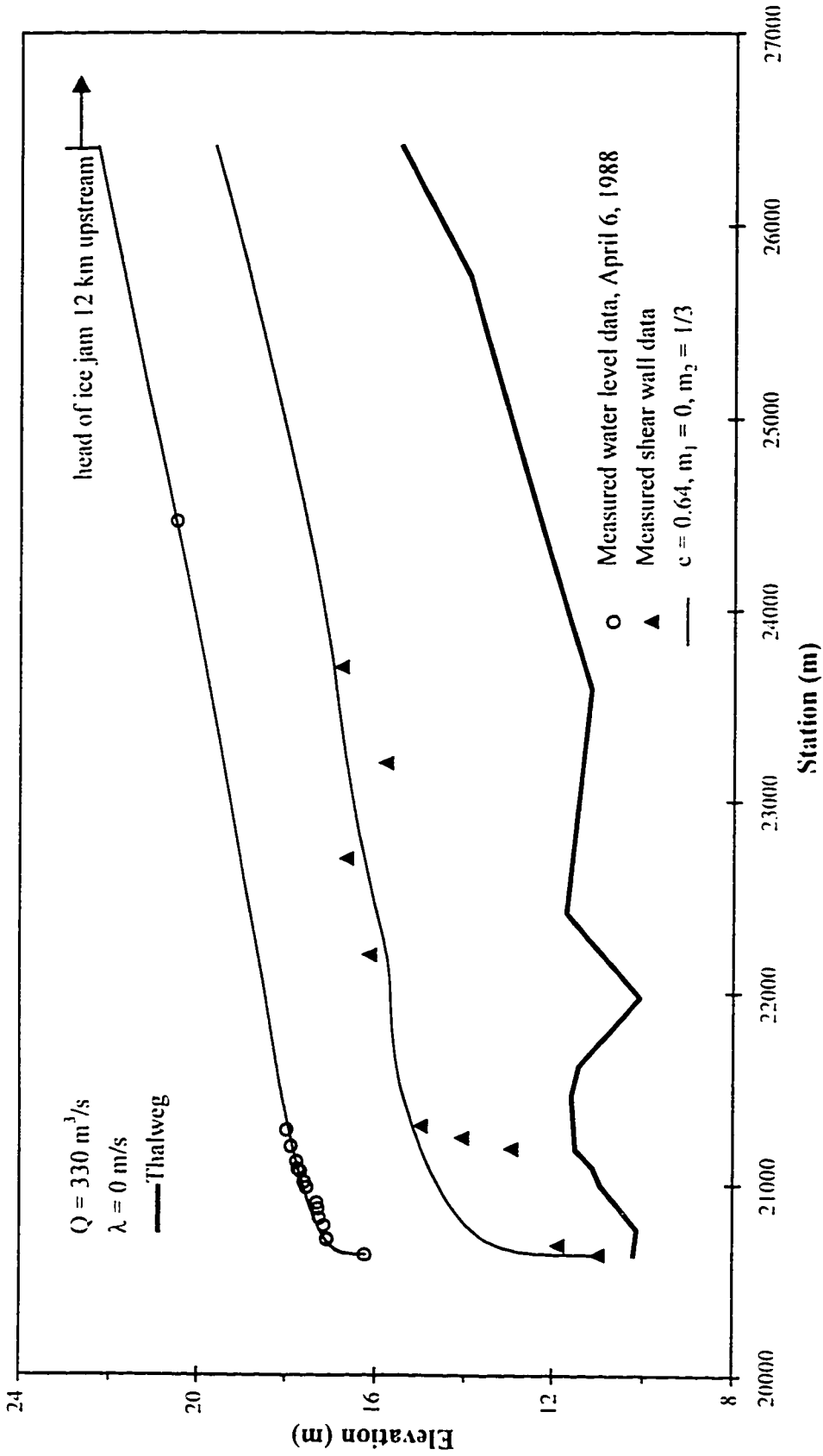


Figure 4.6(b). 1988 Restigouche River ice jam event as predicted by RIVJAM using Beltaos' Mannings approximation where thickness is set to match the observed data.

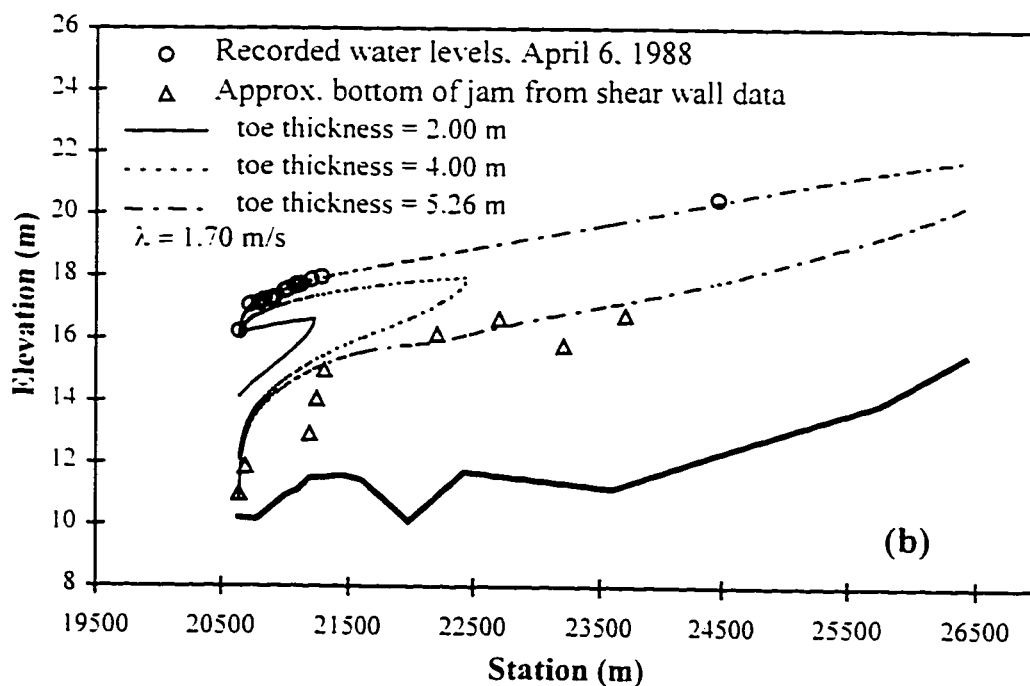
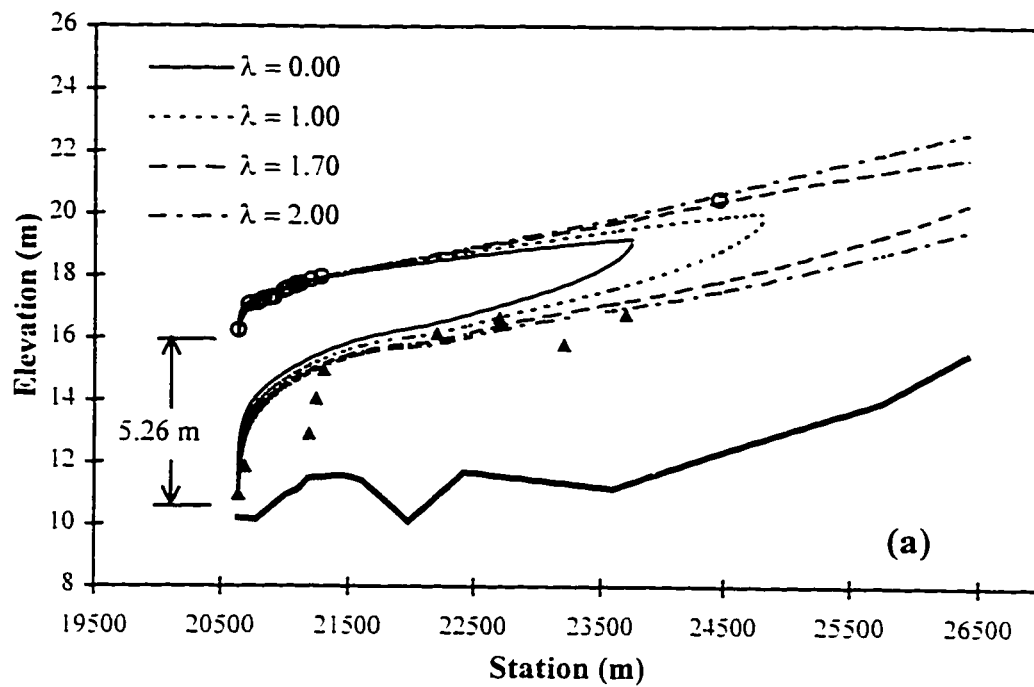


Figure 4.7. 1988 Restigouche ice jam as predicted by RIVJAM using Beltaos' Mannings approximation, illustrating the variation in (a) seepage velocity and (b) toe thickness.

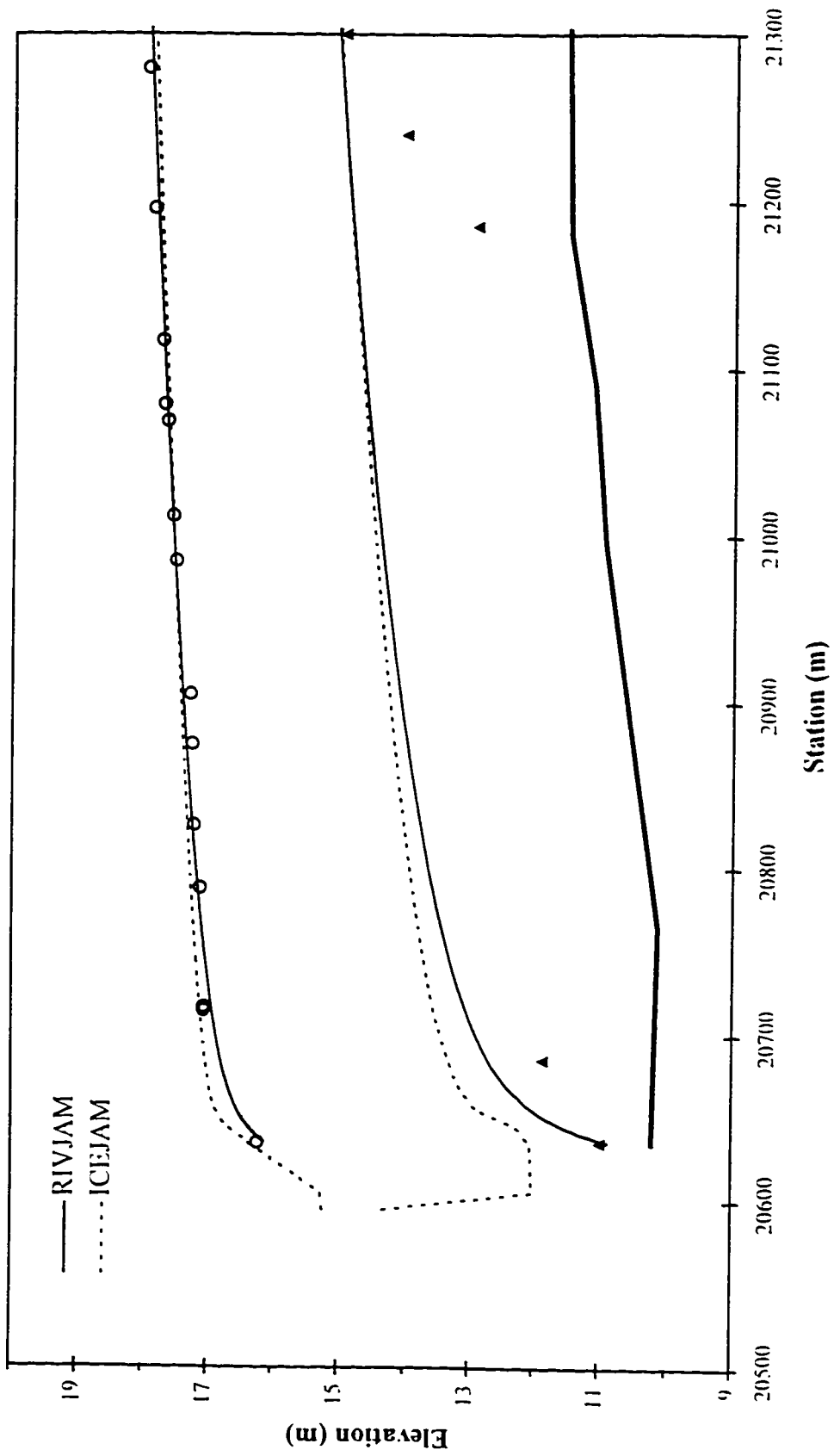


Figure 4.8. Comparison of predicted ice jam profiles computed by RIVJAM using Beltaos' Mannings approximation and by ICEJAM using Mannings equation.

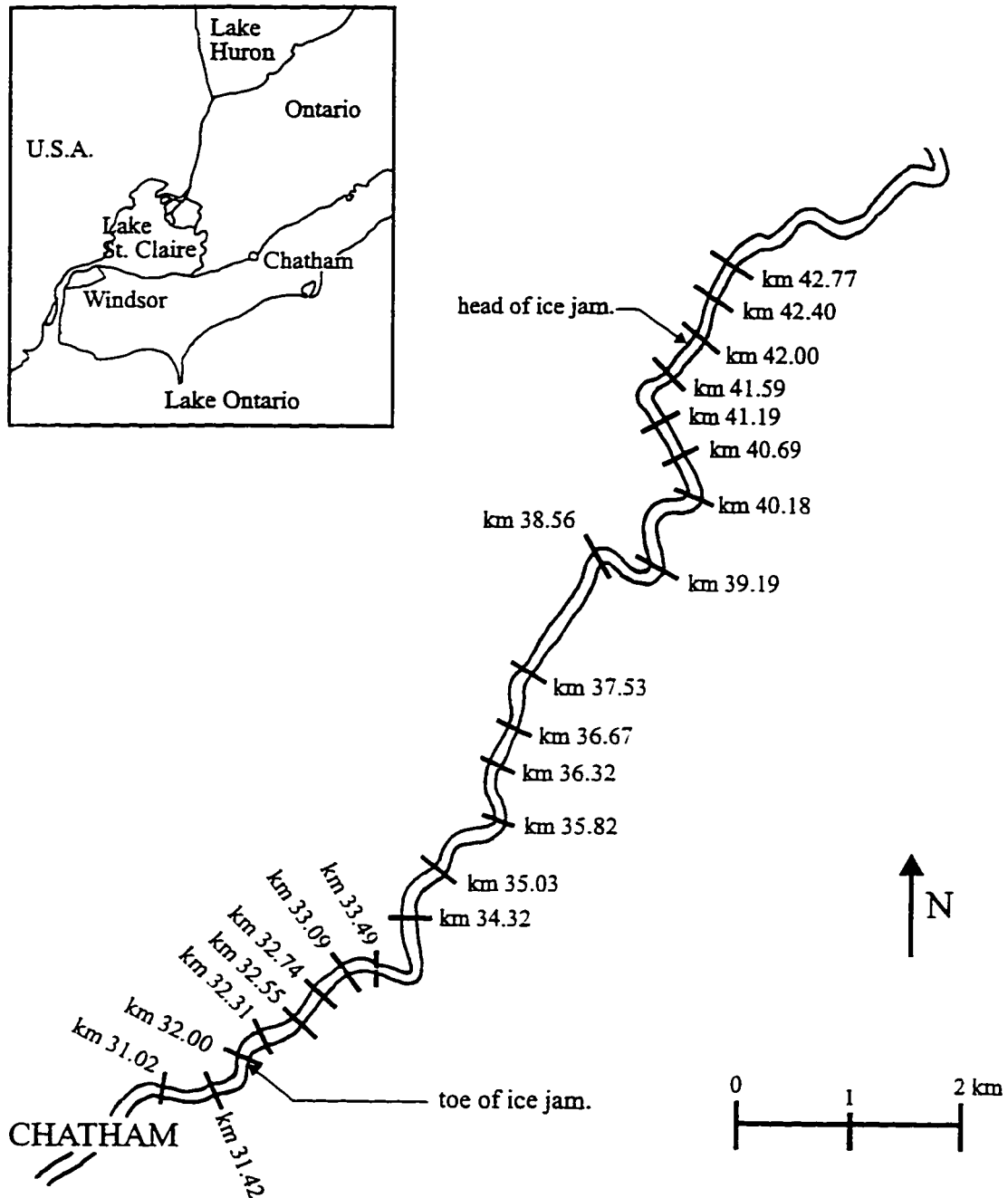


Figure 4.9. Extent of ice jam and cross section locations for the 1986 Thames River ice jam event.

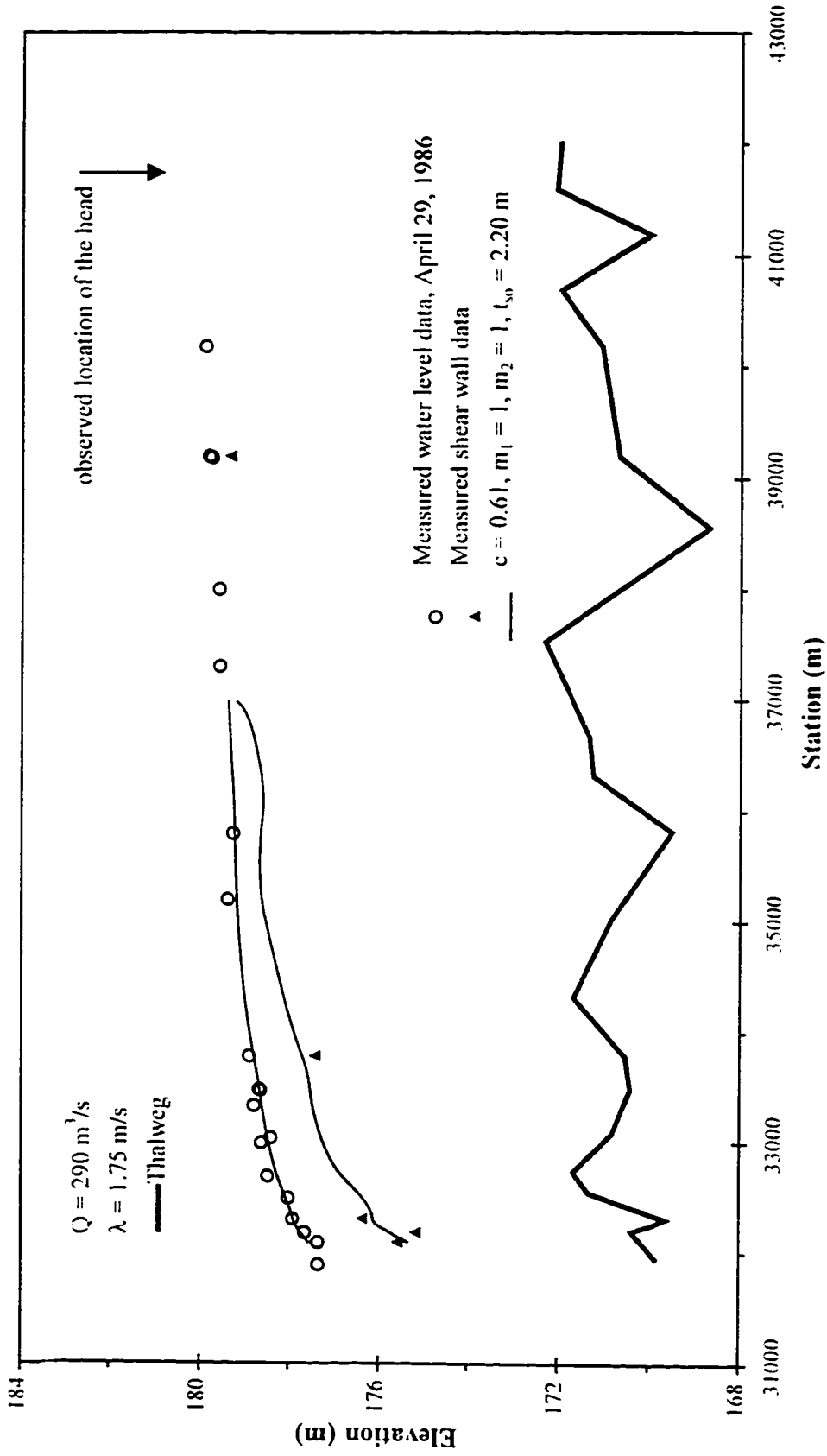


Figure 4.10(a). 1986 Thames River ice jam as predicted by RIVJAM using Bellaos' friction factor ( $c=0.61$ ).

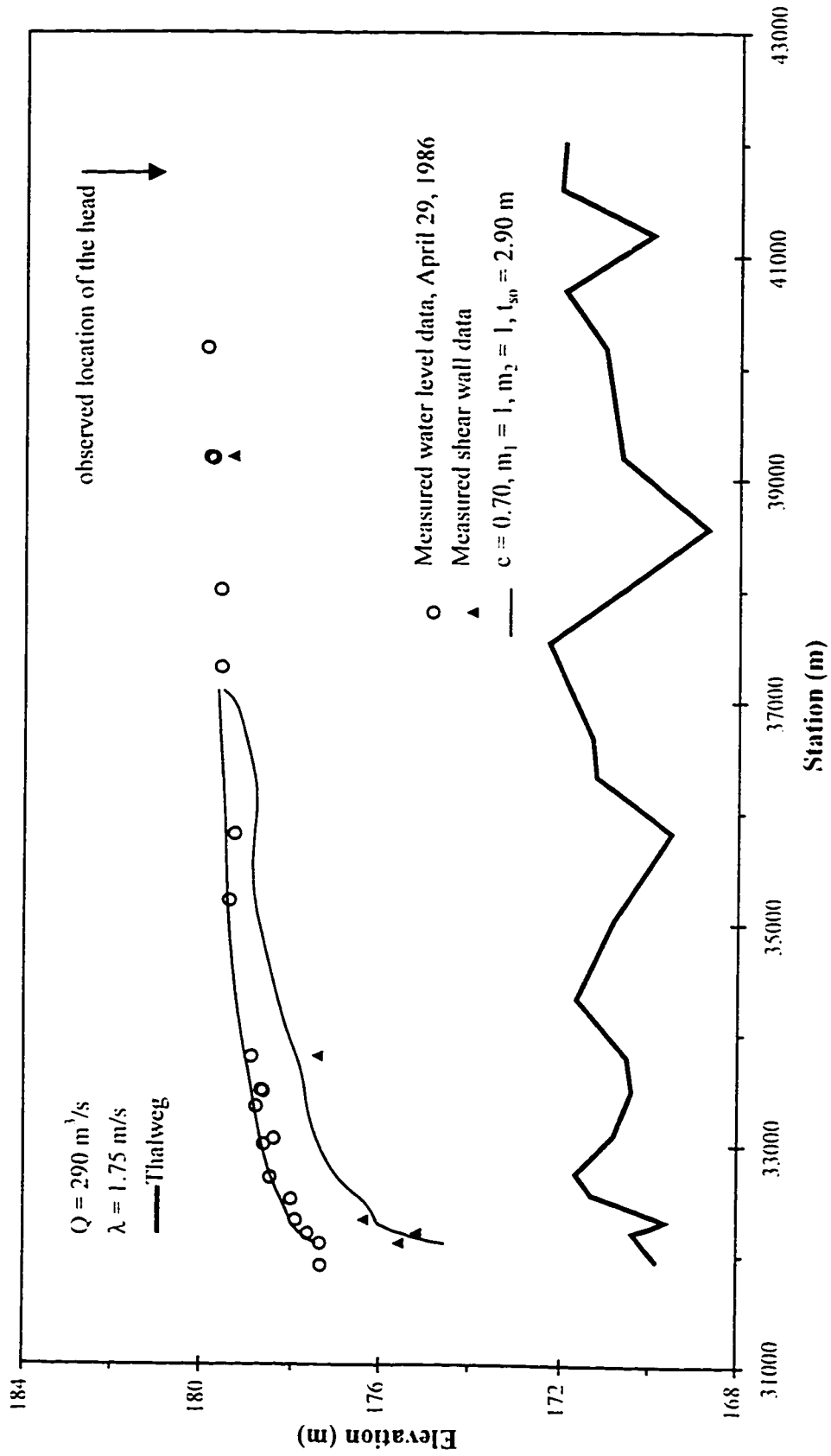


Figure 4.10(b). 1986 Thames River ice jam as predicted by RIV.IAM using Beltaos' friction factor ( $c=0.70$ ).



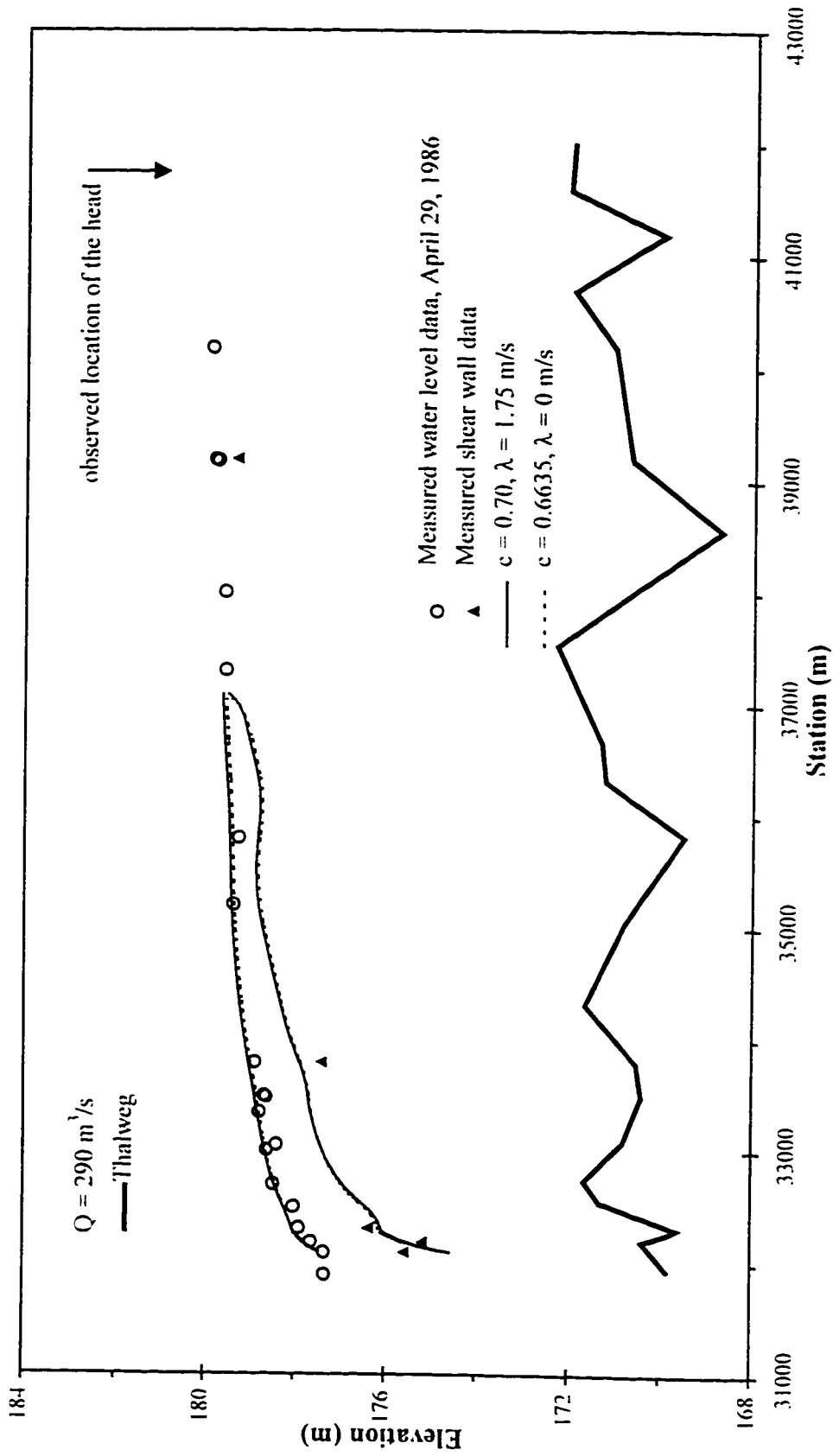


Figure 4.12(b). 1986 Thames River ice jam as predicted by RIVJAM using Beltaos' friction factor, illustrating the effect of seepage where the toe thickness is varied to achieve a jam of comparable length.

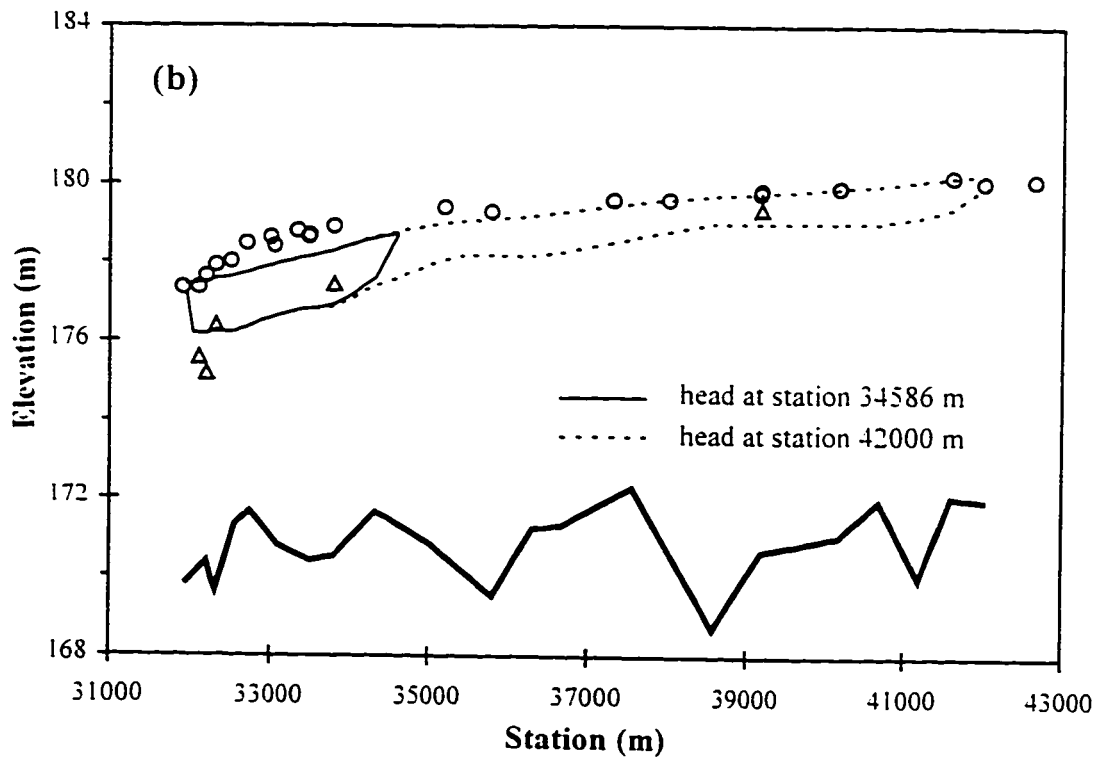
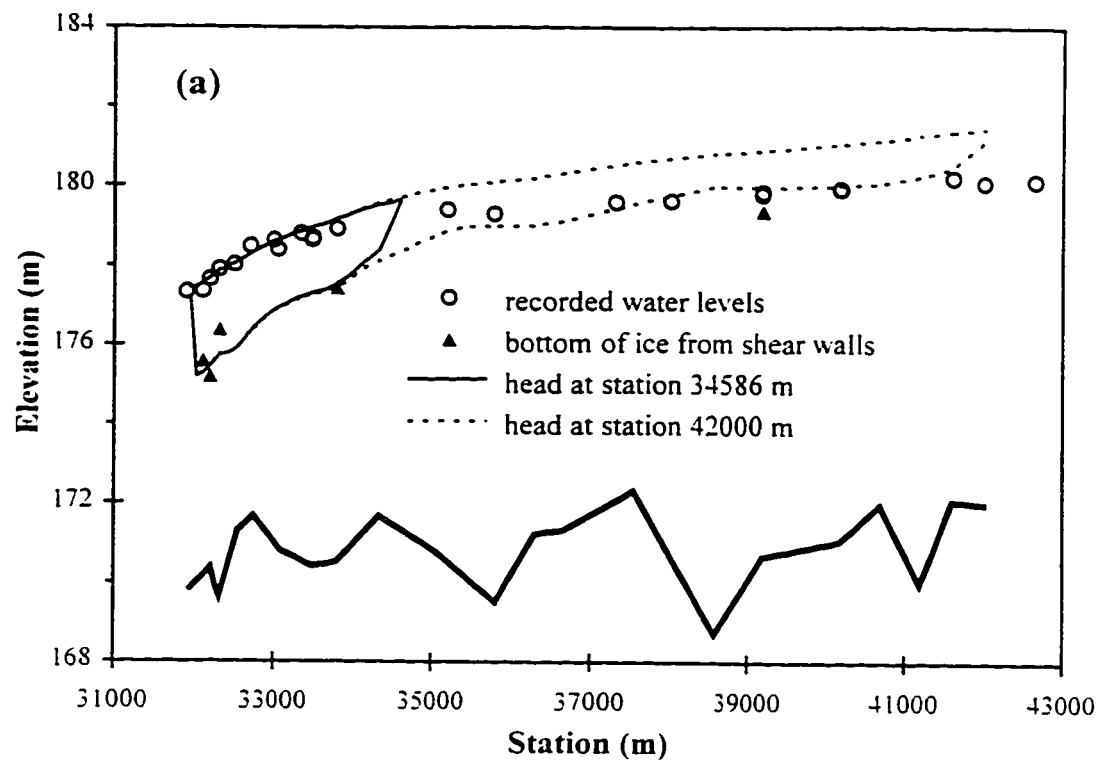


Figure 4.13. 1986 Thames River ice jam as predicted by ICEJAM for both long and short jam scenarios for Mannings roughness of (a) 0.070 and (b) 0.055.

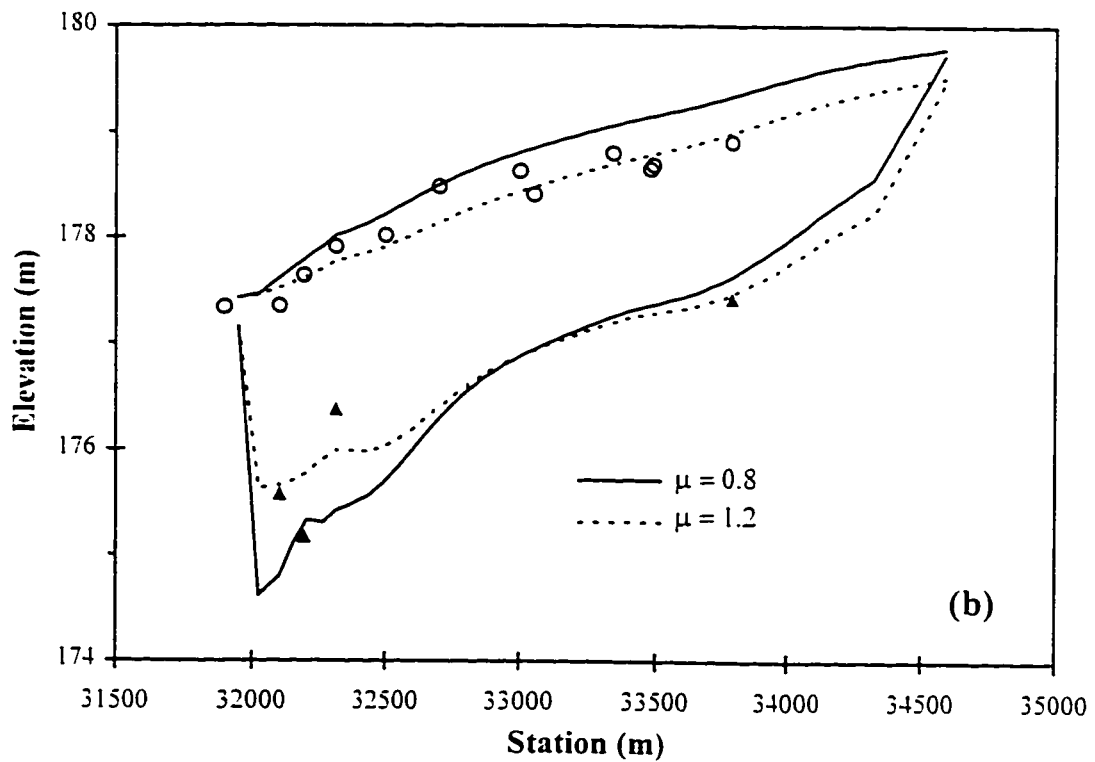
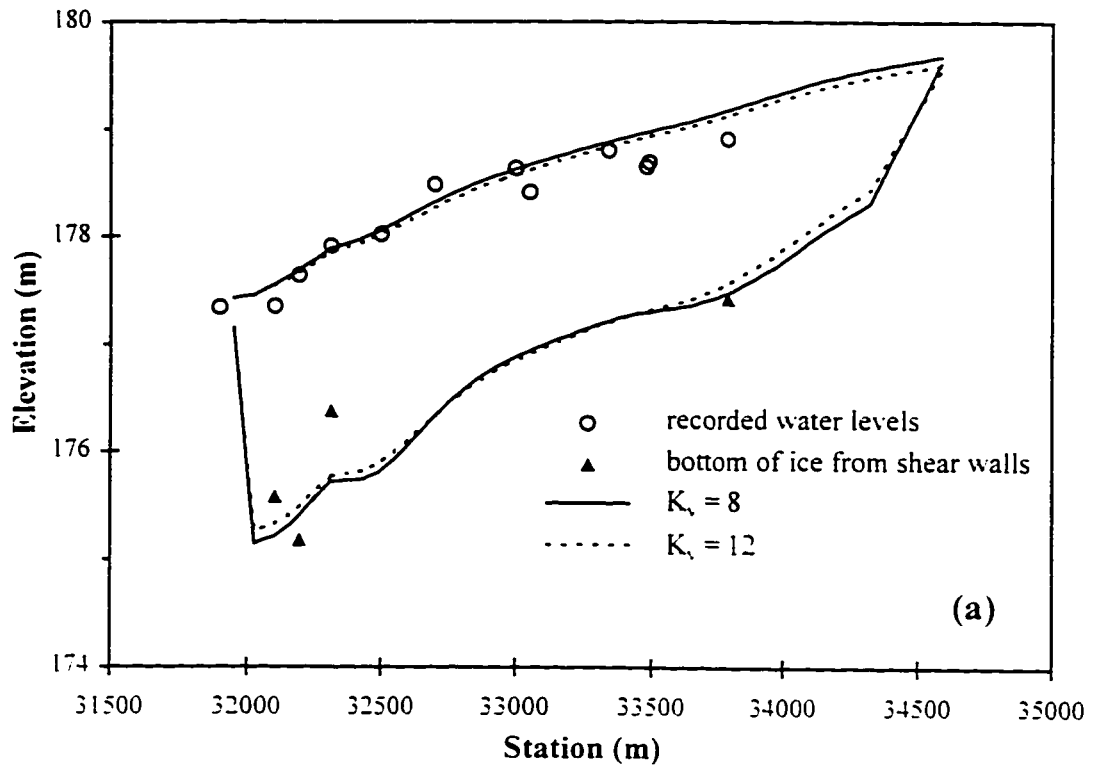


Figure 4.14. 1986 Thames River ice jam as predicted by ICEJAM illustrating sensitivity to (a)  $K_v$  and (b)  $\mu$ .

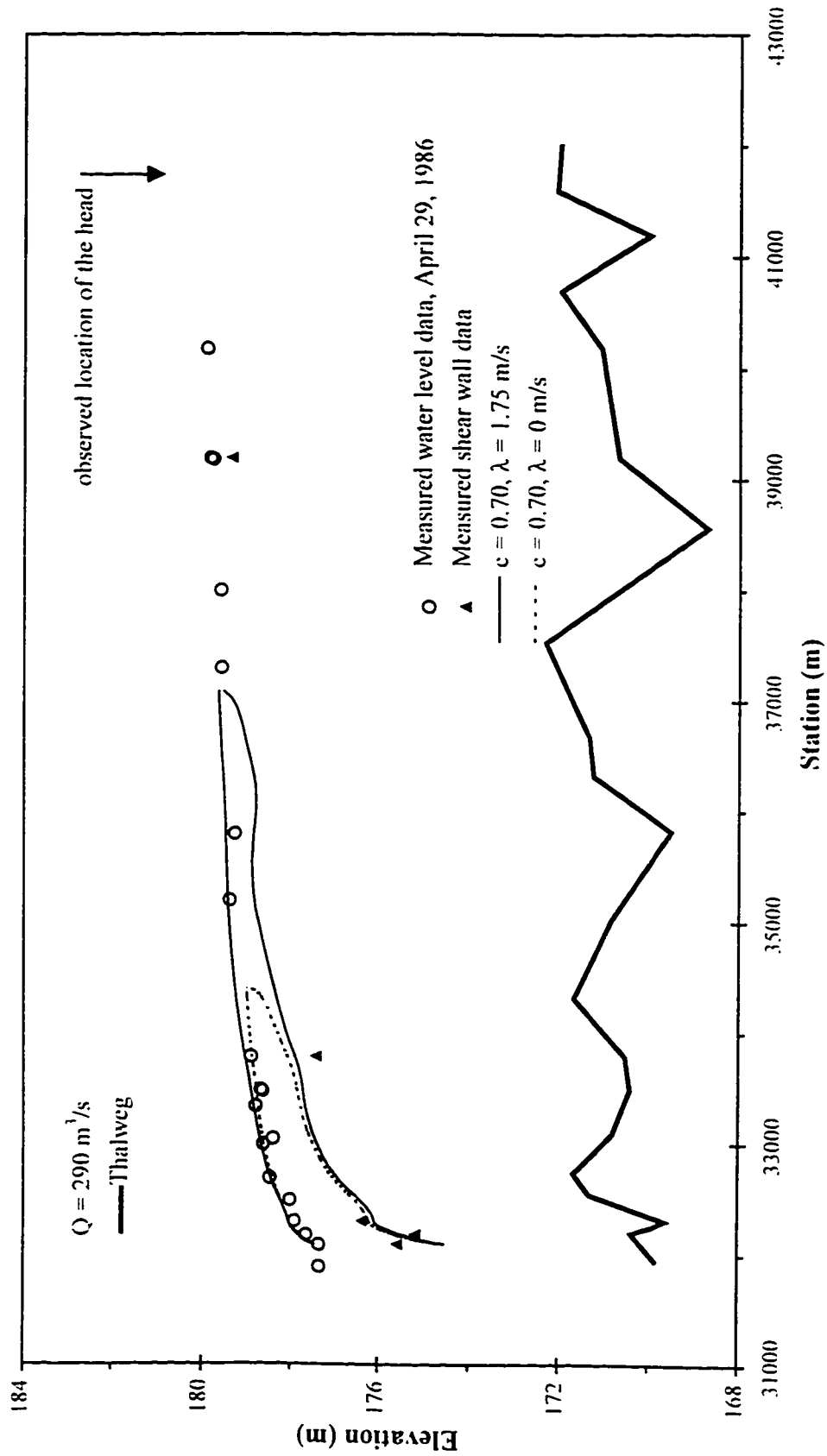


Figure 4.12(a). 1986 Thames River ice jam as predicted by RIVJAM using Beltaos' friction factor, illustrating the effect of seepage where the toe thickness is held constant.

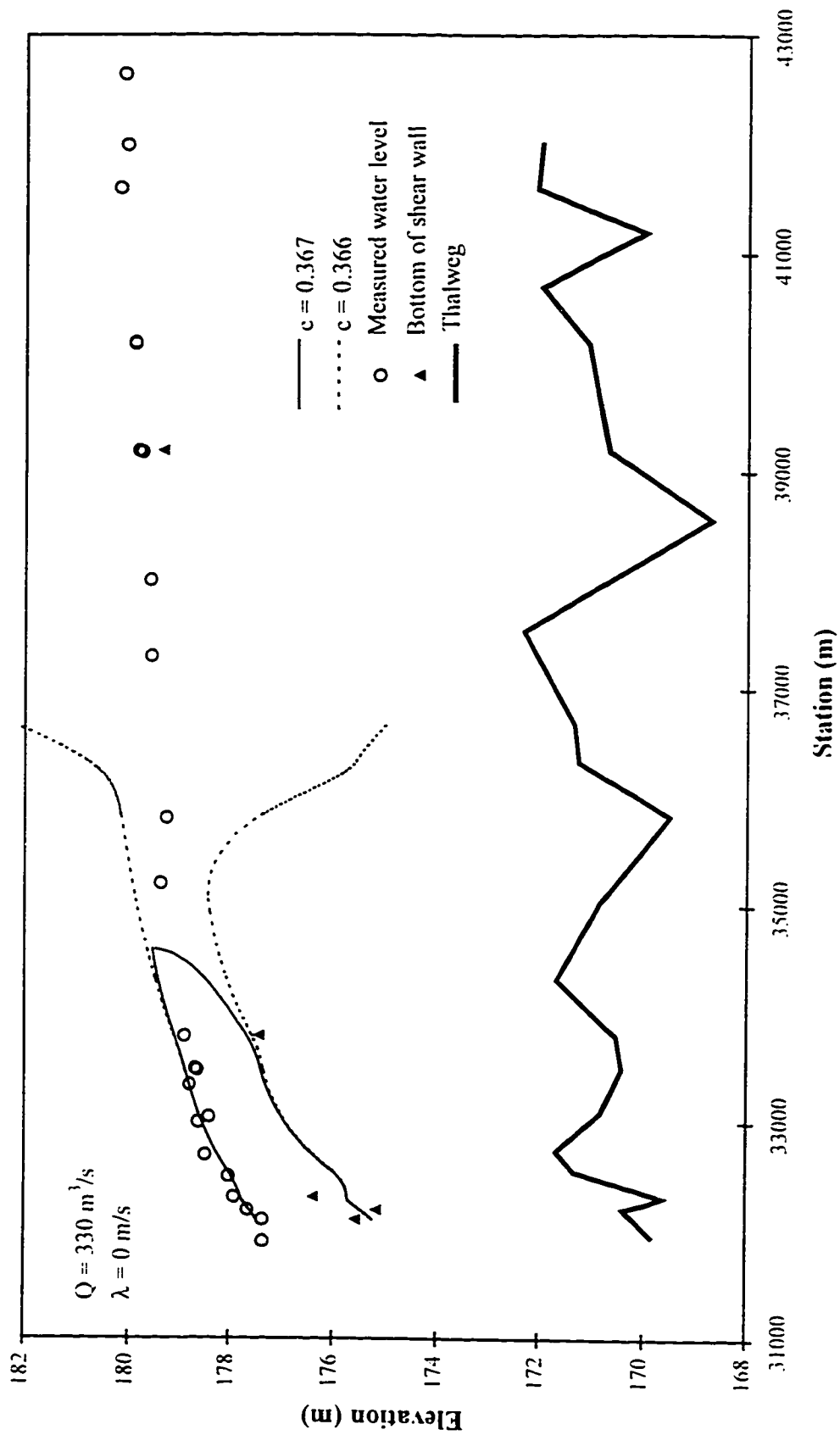


Figure 4.11. 1986 Thames River ice jam as predicted by RIVIAM using Beltaos' Mannings approximation, illustrating limiting value of roughness coefficient,  $c$ .

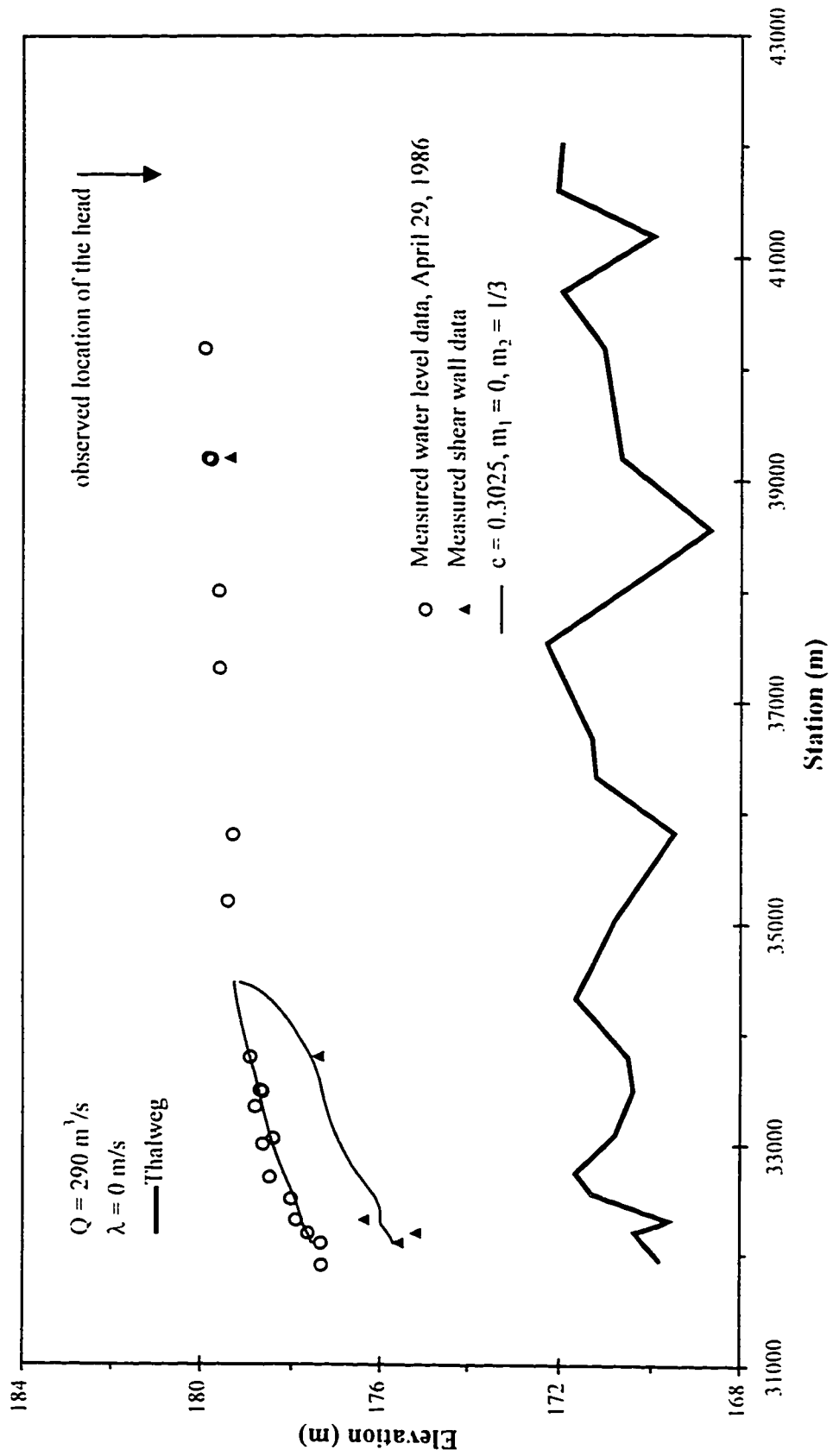


Figure 4.15. 1986 Thames River ice jam as predicted by RIVJAM using Beltaos' Mannings approximation.

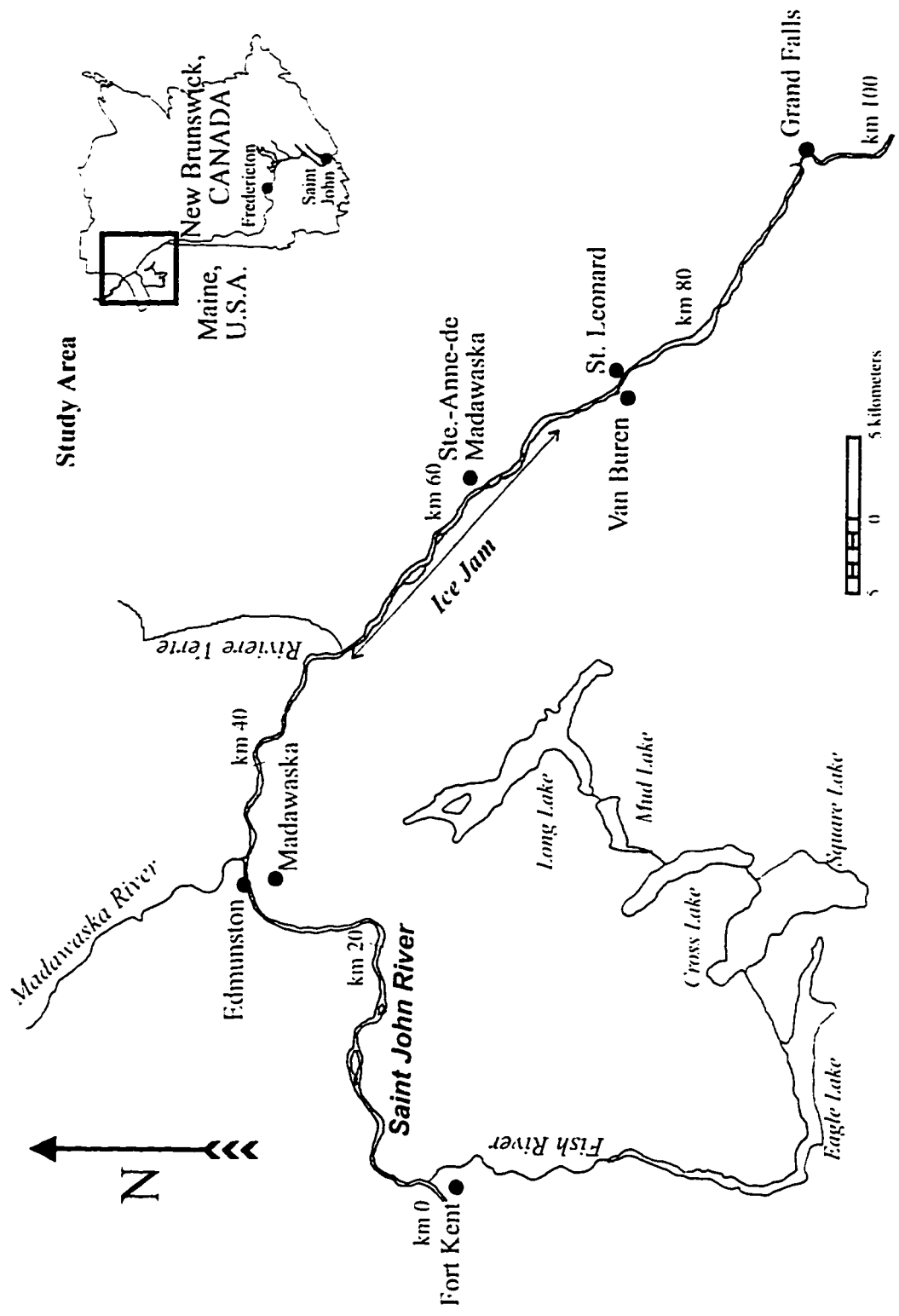


Figure 4.16. Extent of ice jam for the 1993 Saint John River ice jam event.

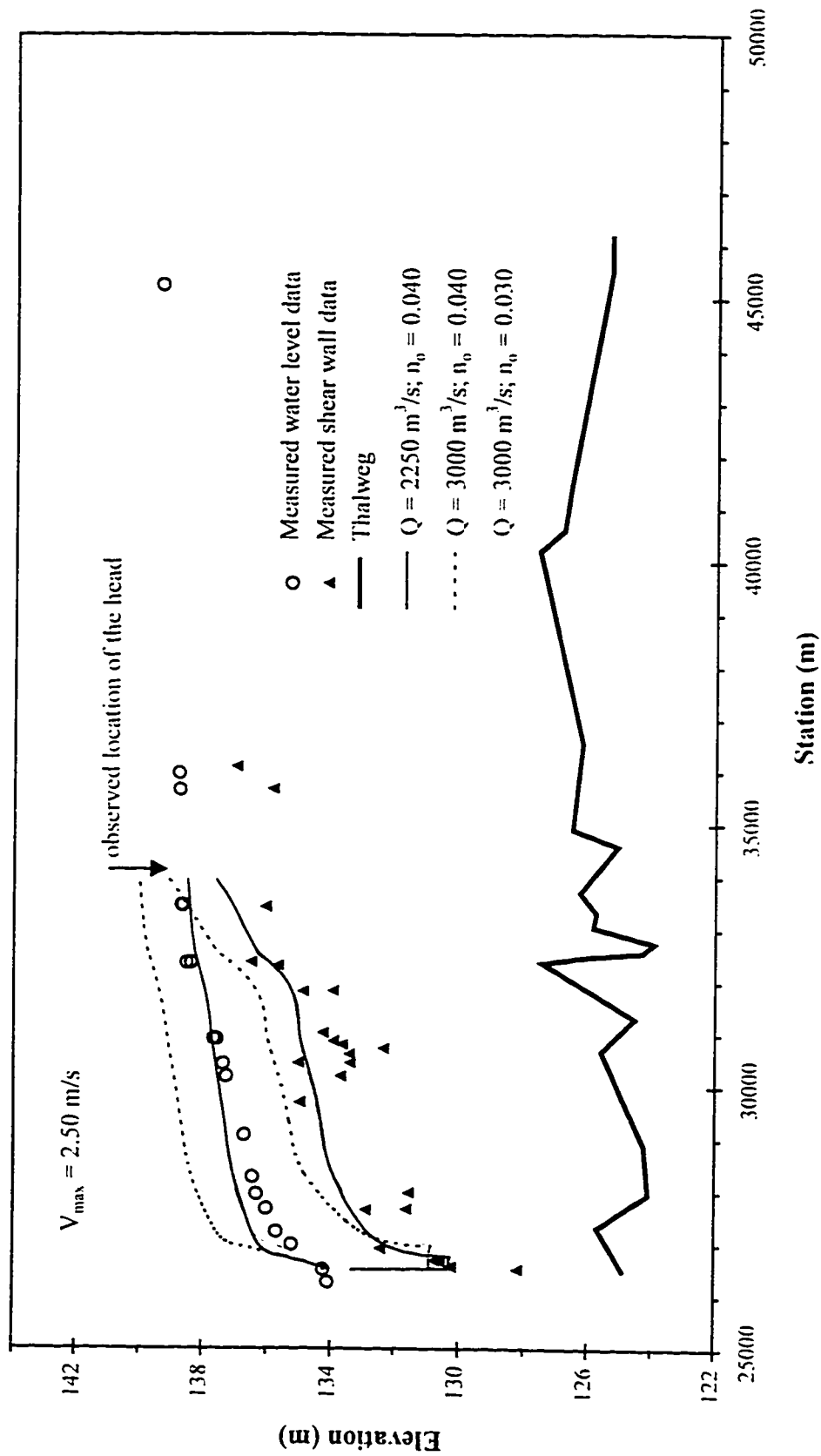


Figure 4.17. 1993 Saint John River ice jam as predicted by ICEJAM illustrating sensitivity to two different estimated carrier discharges.



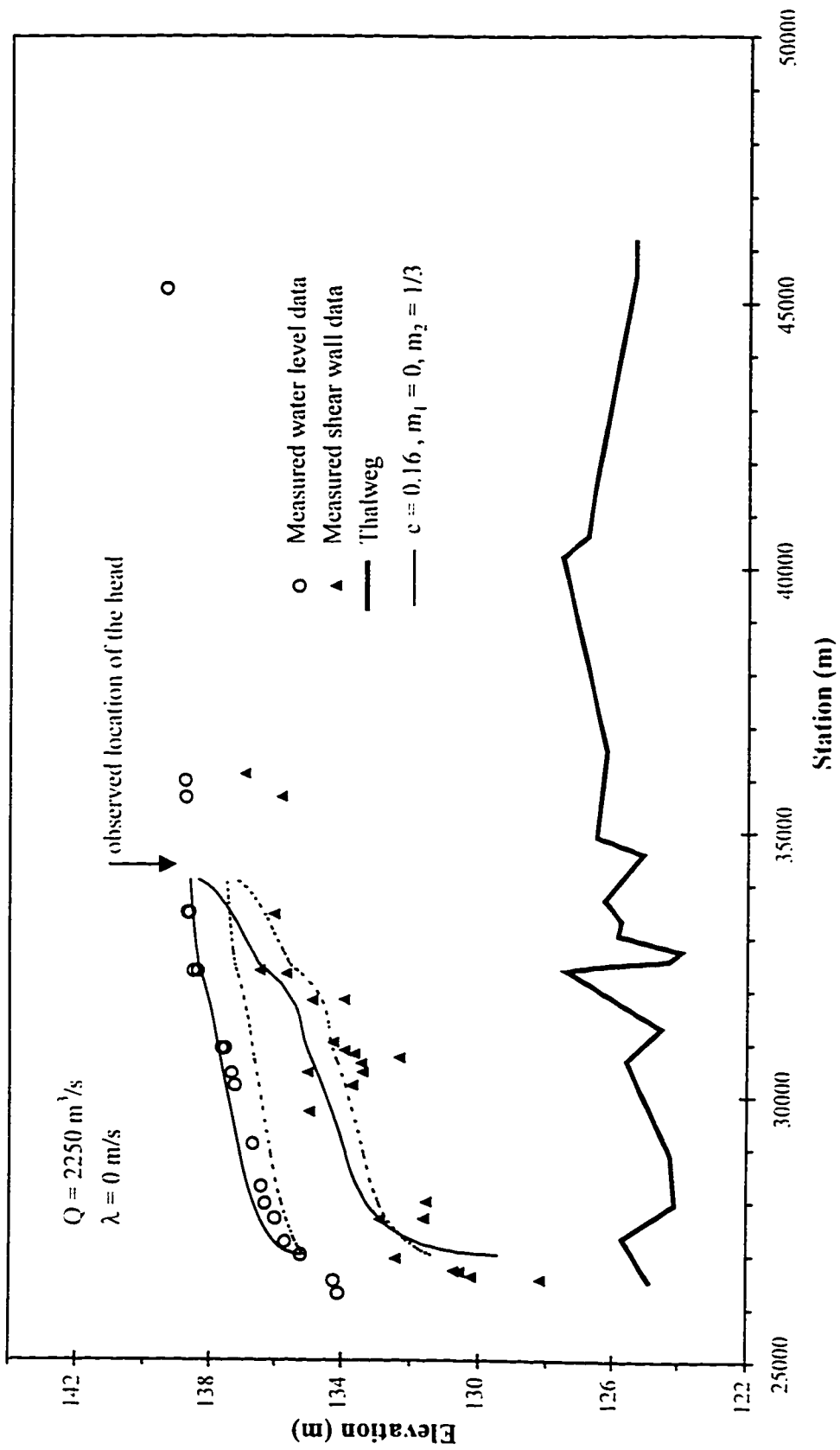


Figure 4.18. 1993 Saint John River ice jam as predicted by RIVJAM using Beltaos' Mannings' approximation.

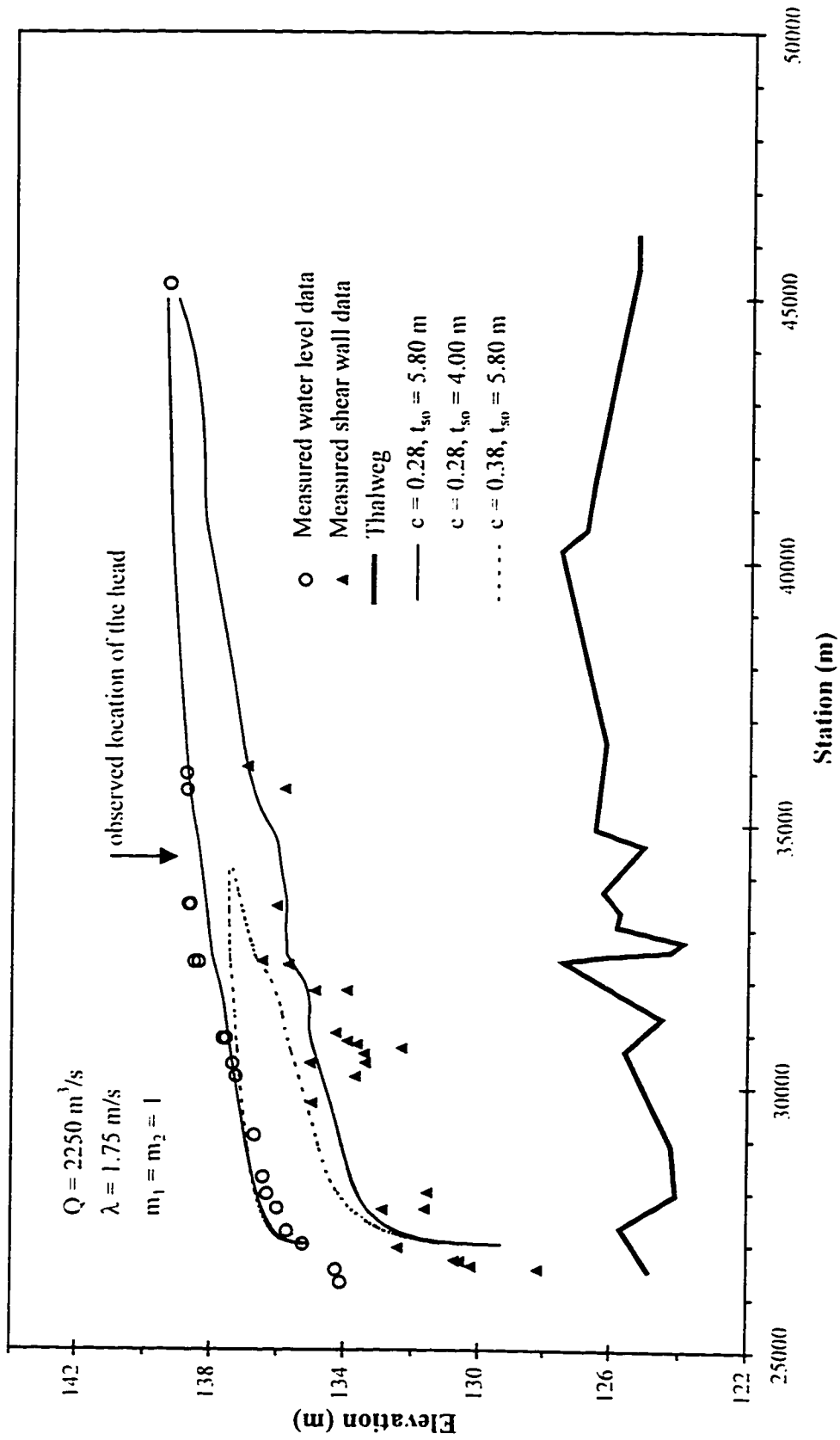


Figure 4.19. 1993 Saint John River ice jam as predicted by RIVJAM using Beltaos' friction factor.

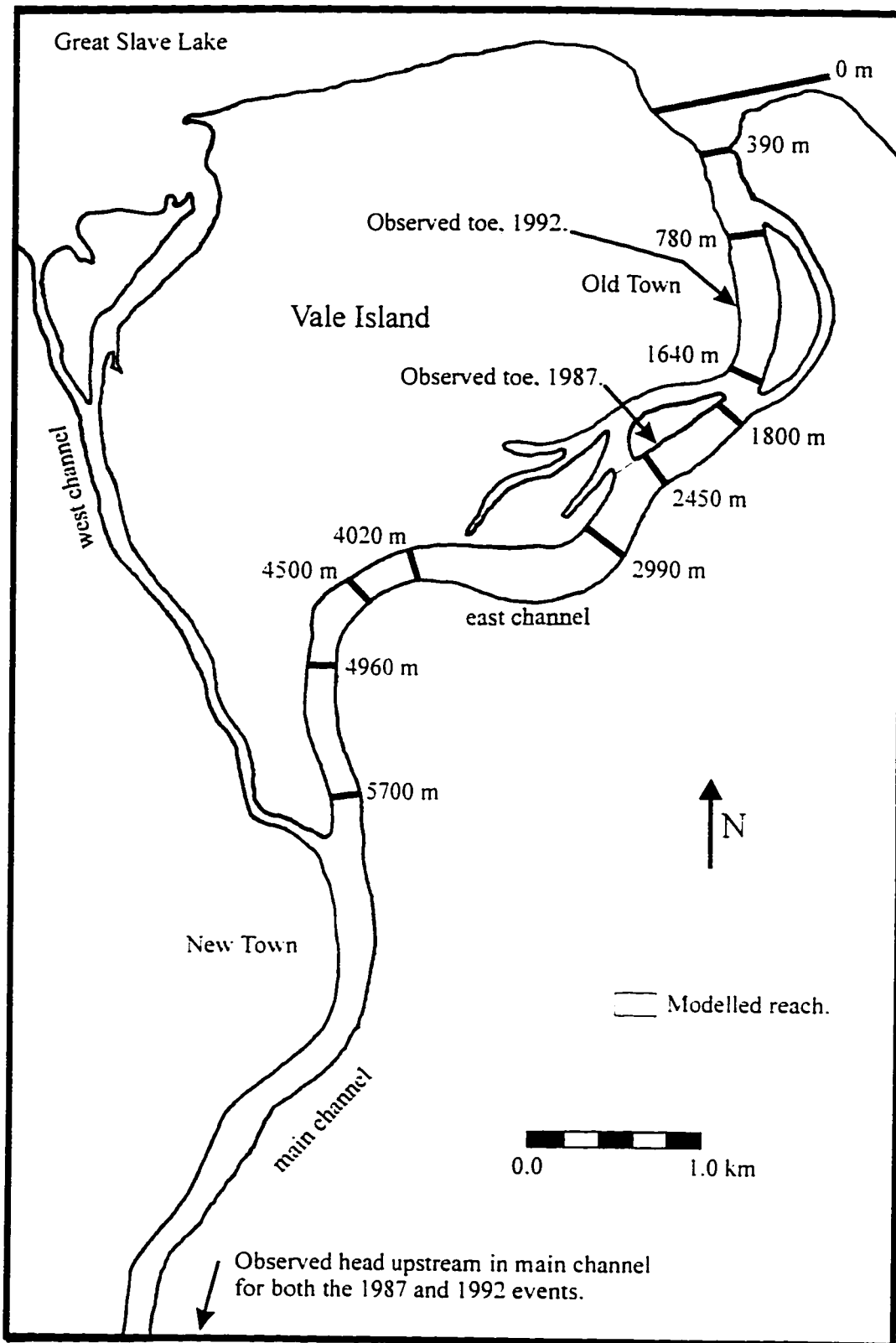


Figure 4.20. Extent of the 1987 and 1992 Hay River ice jams and cross section locations.

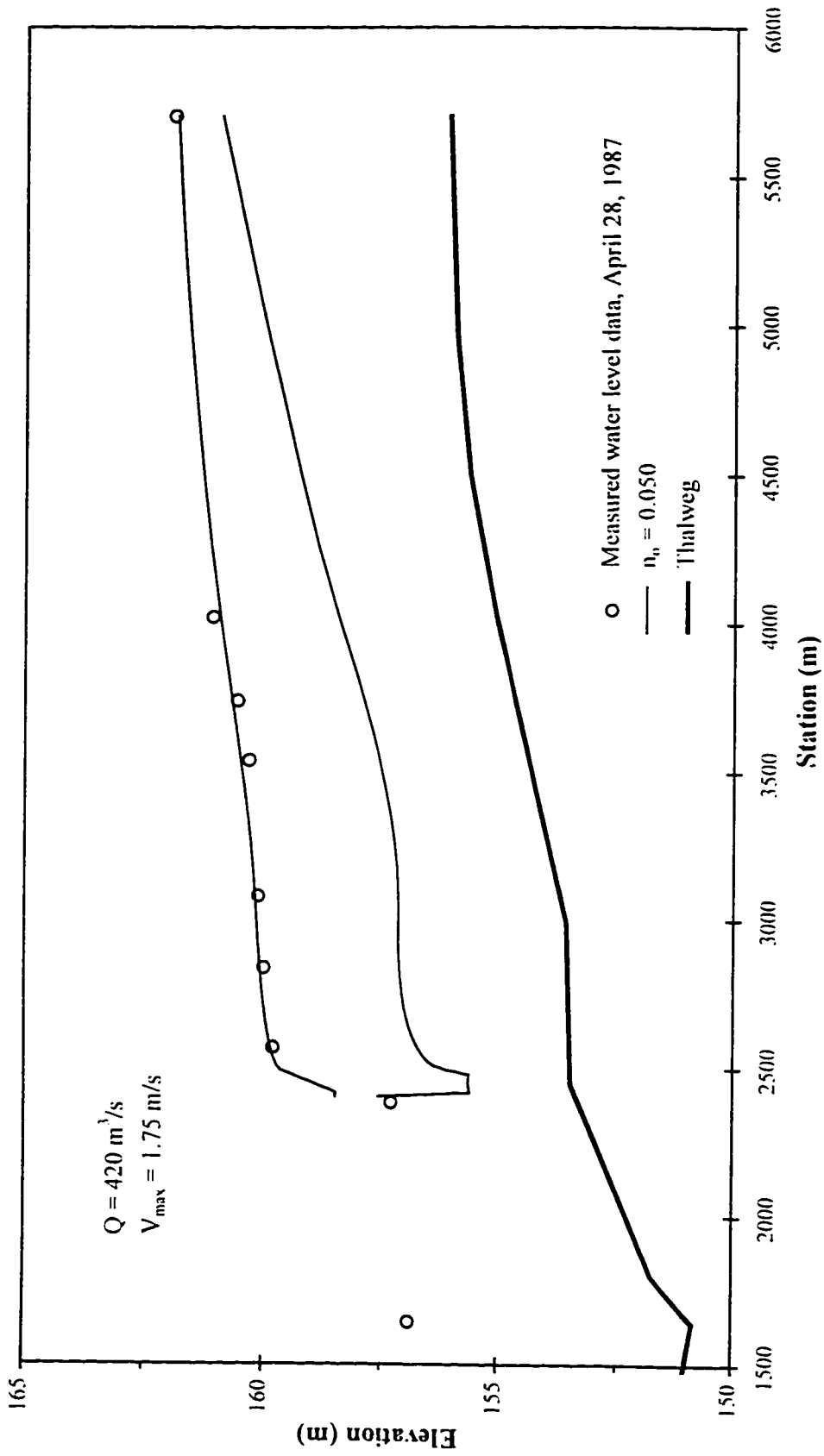


Figure 4.21. 1987 Hay River ice jam as predicted by ICEJAM using Mannings equation.

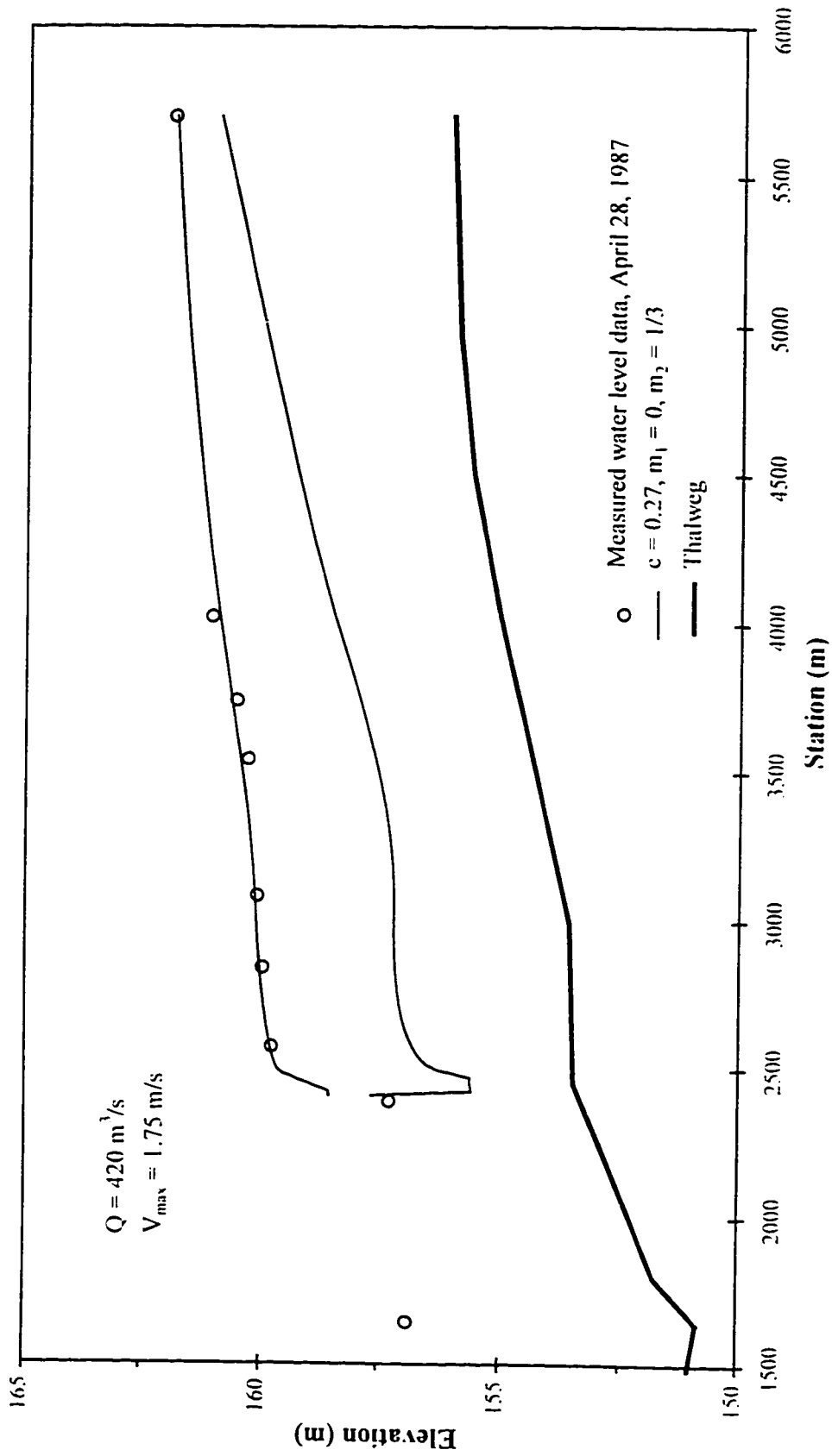


Figure 4.22. 1987 Hay River ice jam as predicted by ICEJAM using Beltaos' Mannings approximation.

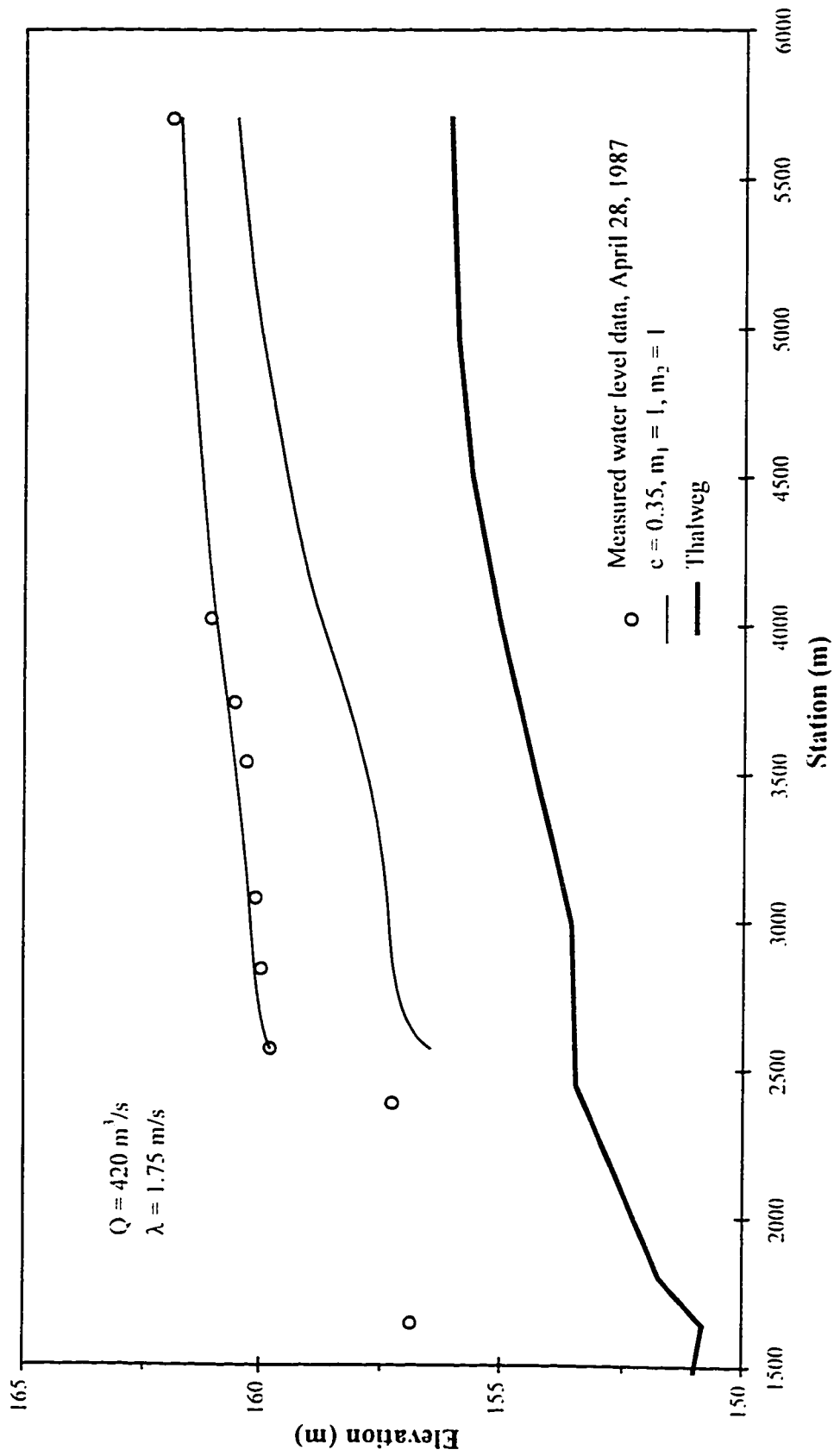


Figure 4.23. 1987 Hay River ice jam as predicted by RIVJAM using Beltaos' friction factor.

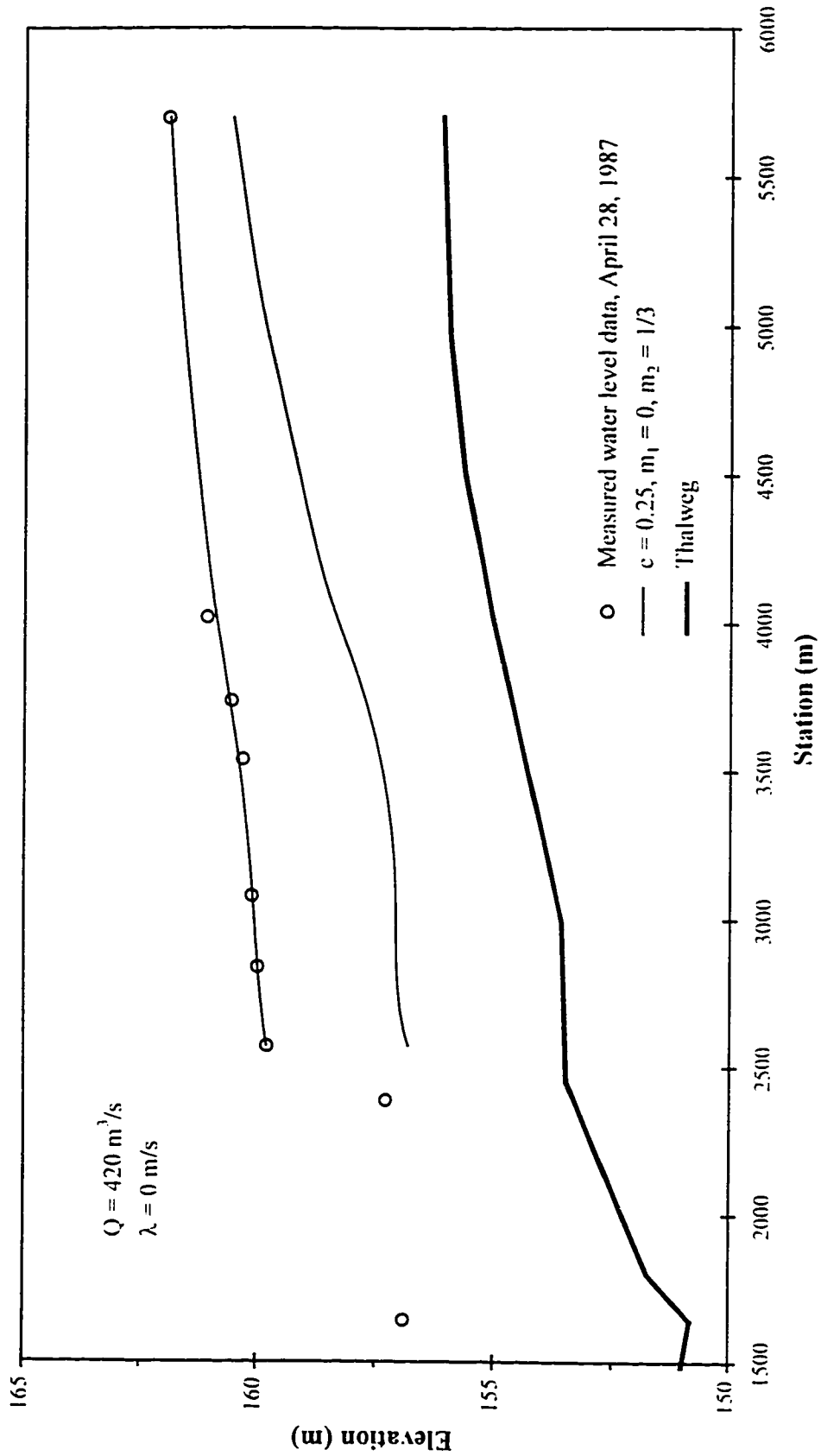


Figure 4.24. 1987 Hay River ice jam as predicted by RIVJAM using Beltaos' Mannings approximation.

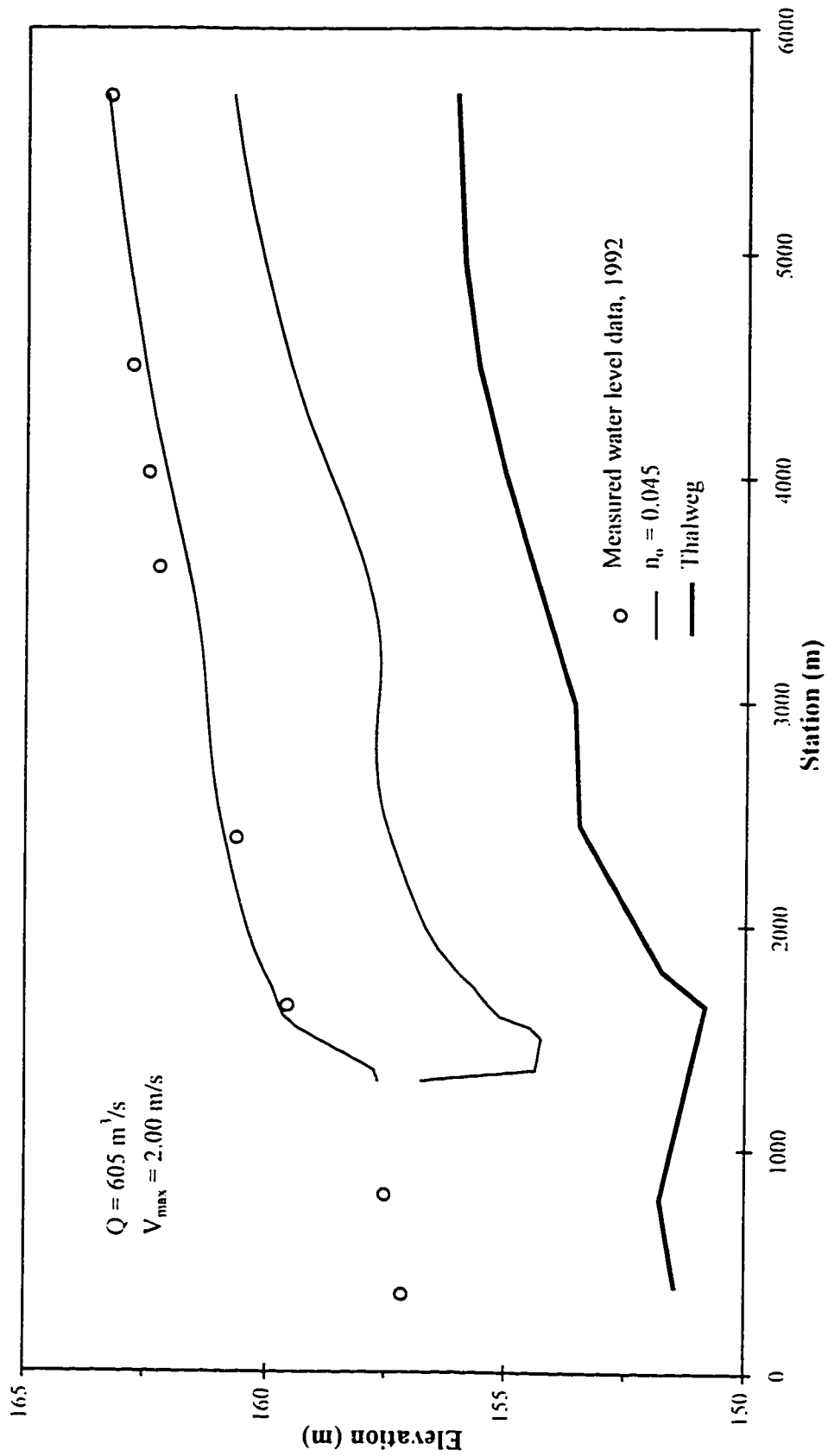


Figure 4.25. 1992 Hay River ice jam as predicted by ICEJAM using Mannings roughness.



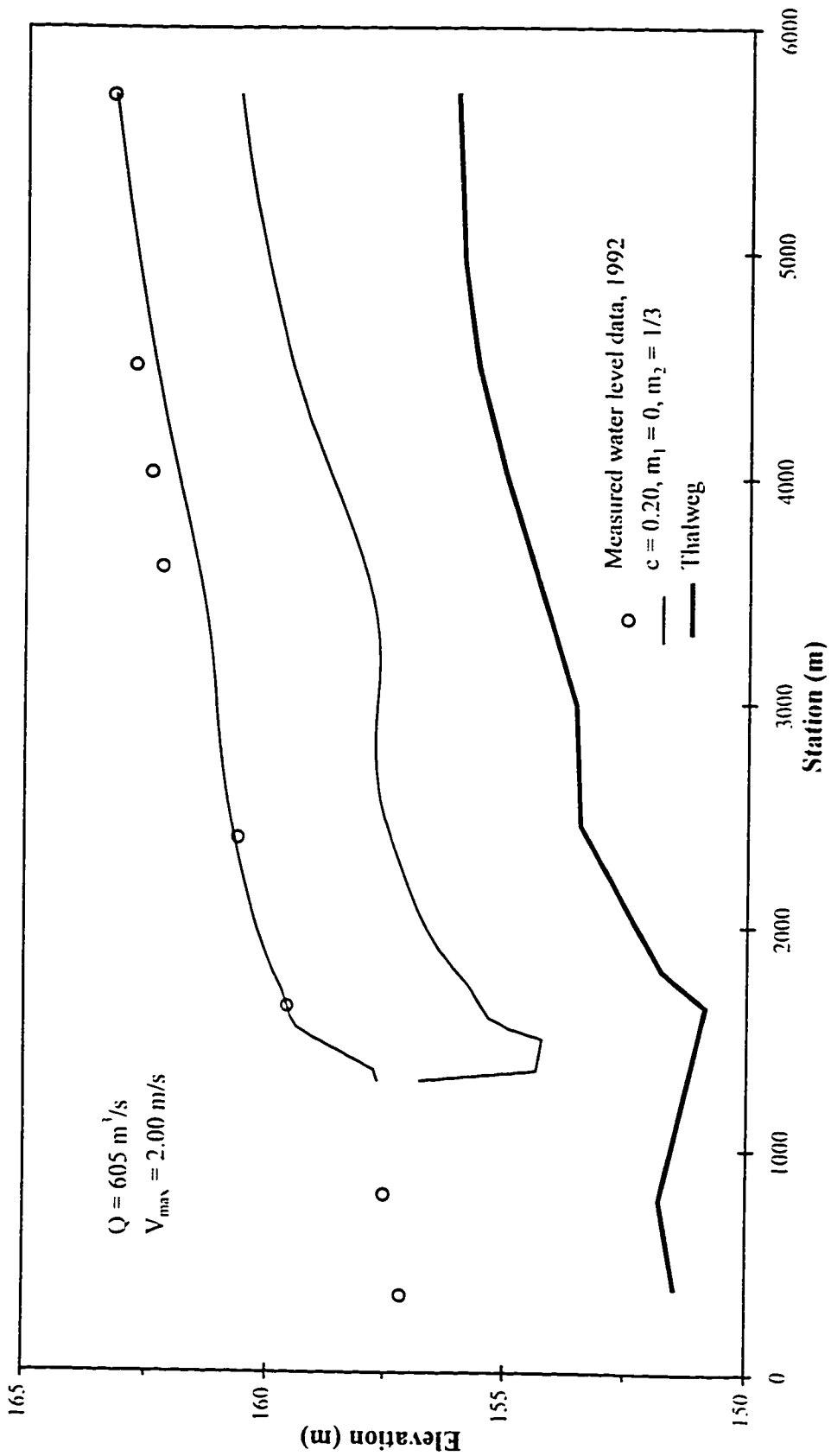


Figure 4.26. 1992 Hay River ice jam as predicted by ICIJAM using Beltaos' Mannings approximation.

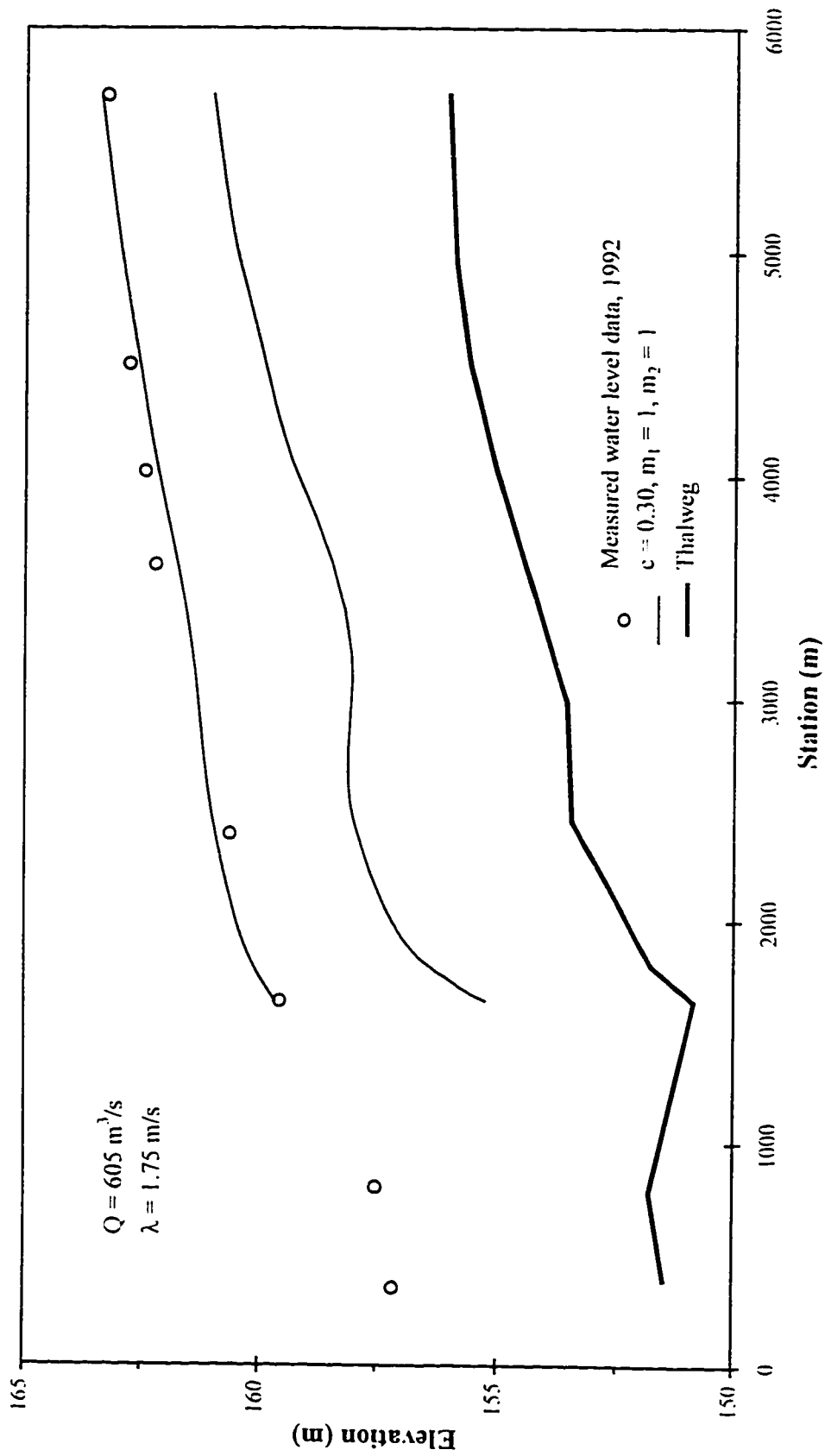


Figure 4.27. 1992 Hay River ice jam as predicted by RIVJAM using Beltaos' friction factor.

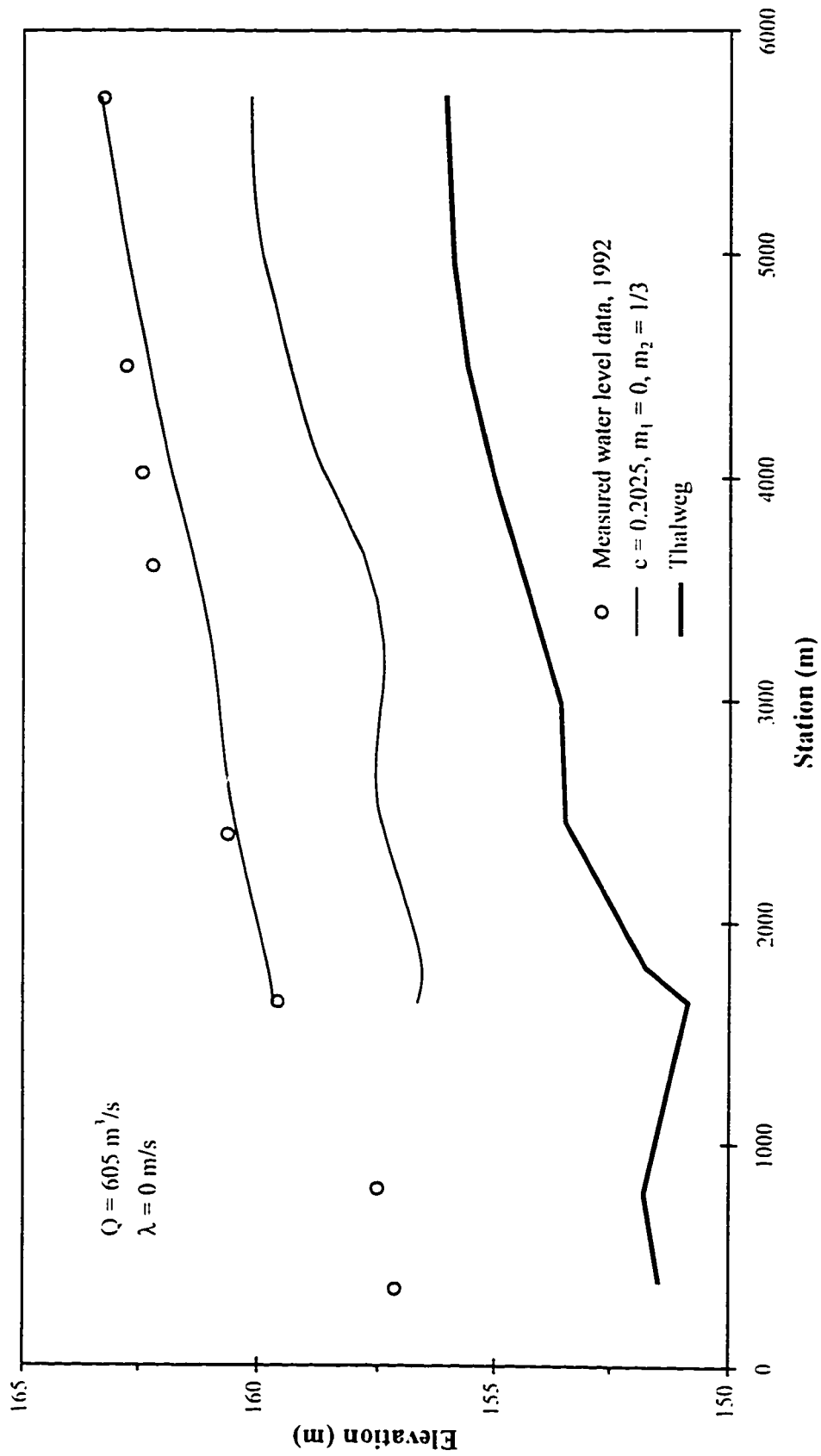
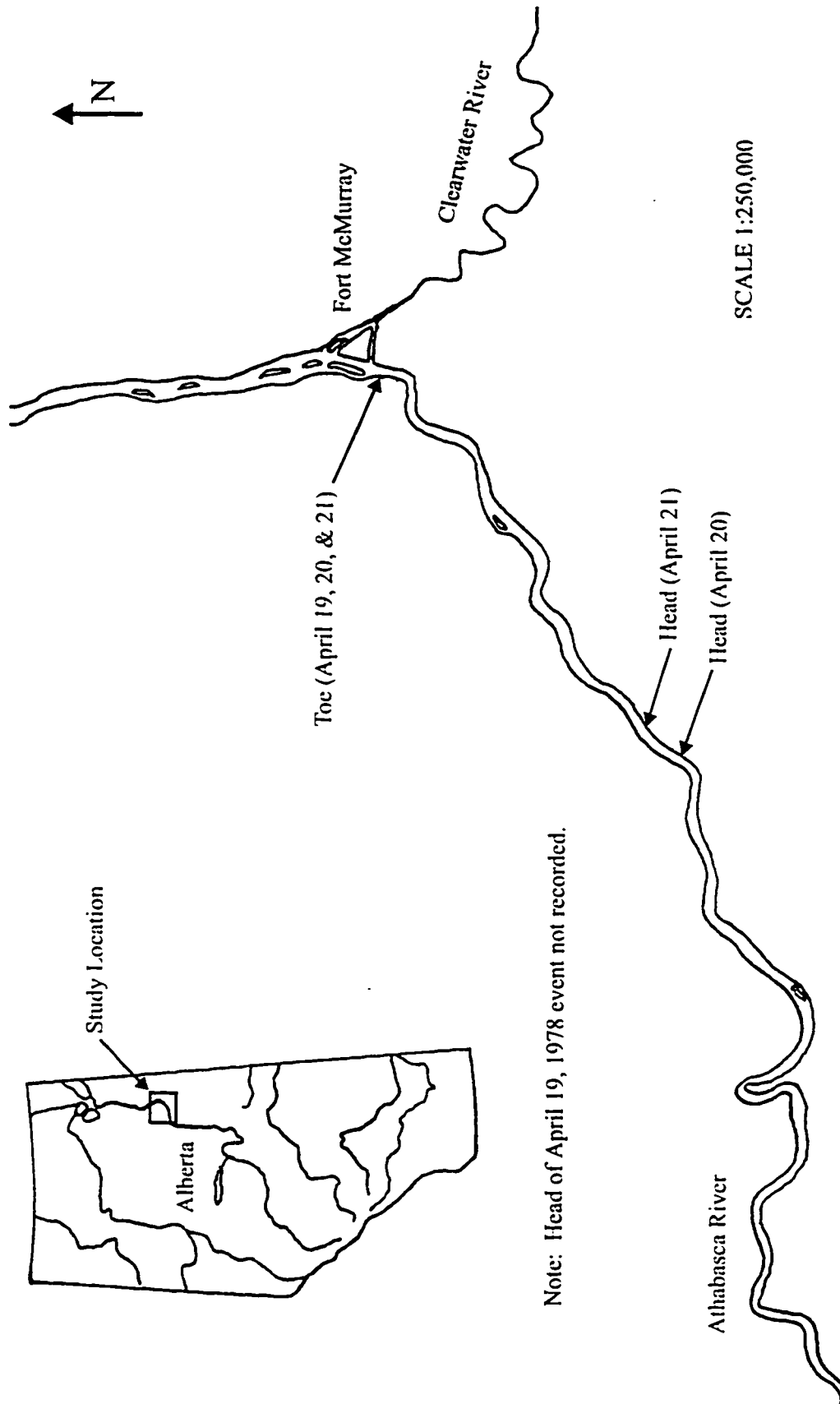


Figure 4.28. 1992 Hay River ice jam as predicted by RIVJAM using Beltaos' Mannings approximation with roughness fixed to correspond to the Mannings roughness calibrated by ICEJAM.



Note: Head of April 19, 1978 event not recorded.

Figure 4.29(a). Extent of the 1978 Athabasca River recorded ice jam events.

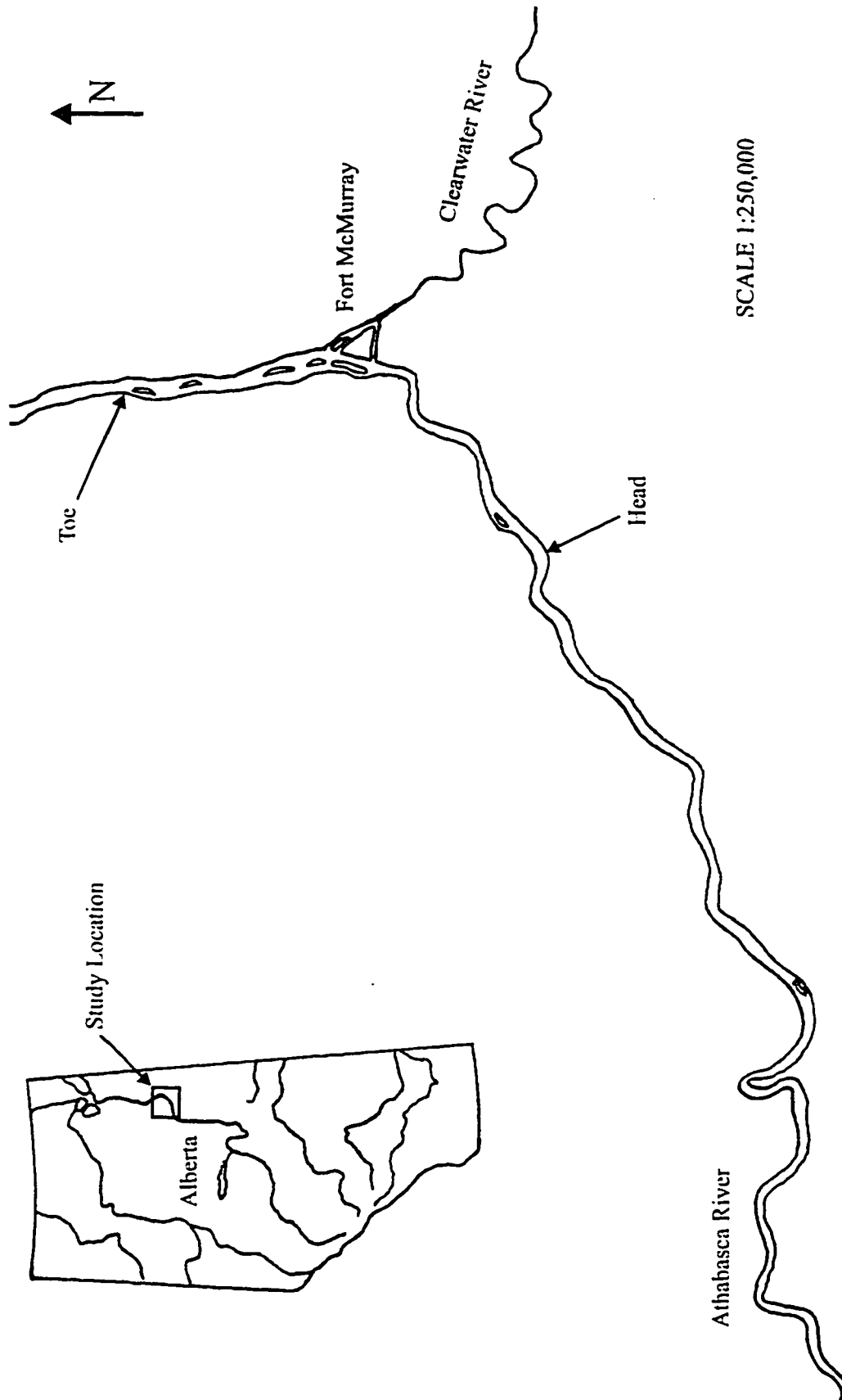


Figure 4.29(b). Extent of the 1979 Athabasca River recorded ice jam event.

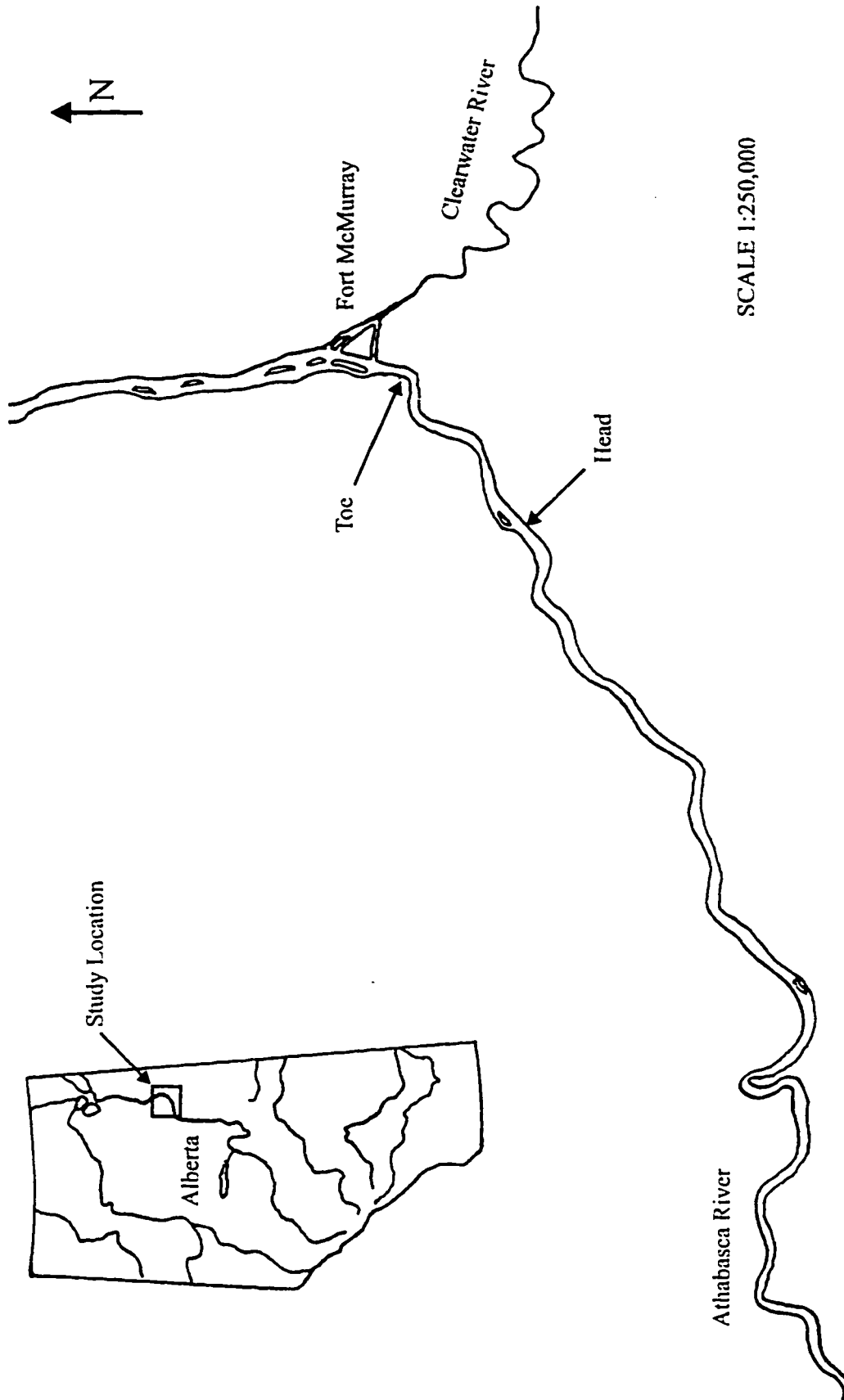


Figure 4.29(c). Extent of the 1984 Athabasca River recorded ice jam event.

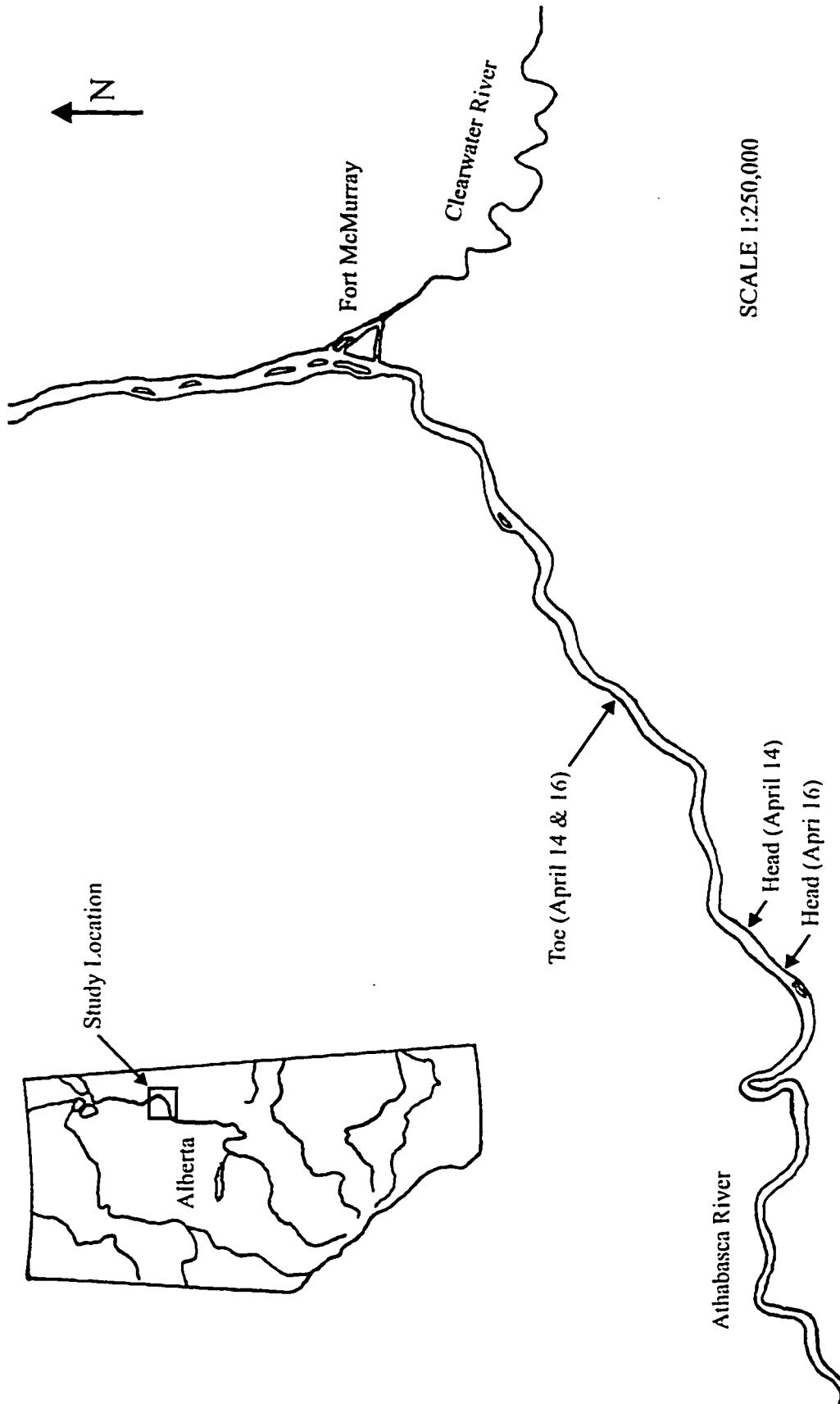


Figure 4.29(d). Extent of the 1985 Athabasca River recorded ice jam events.

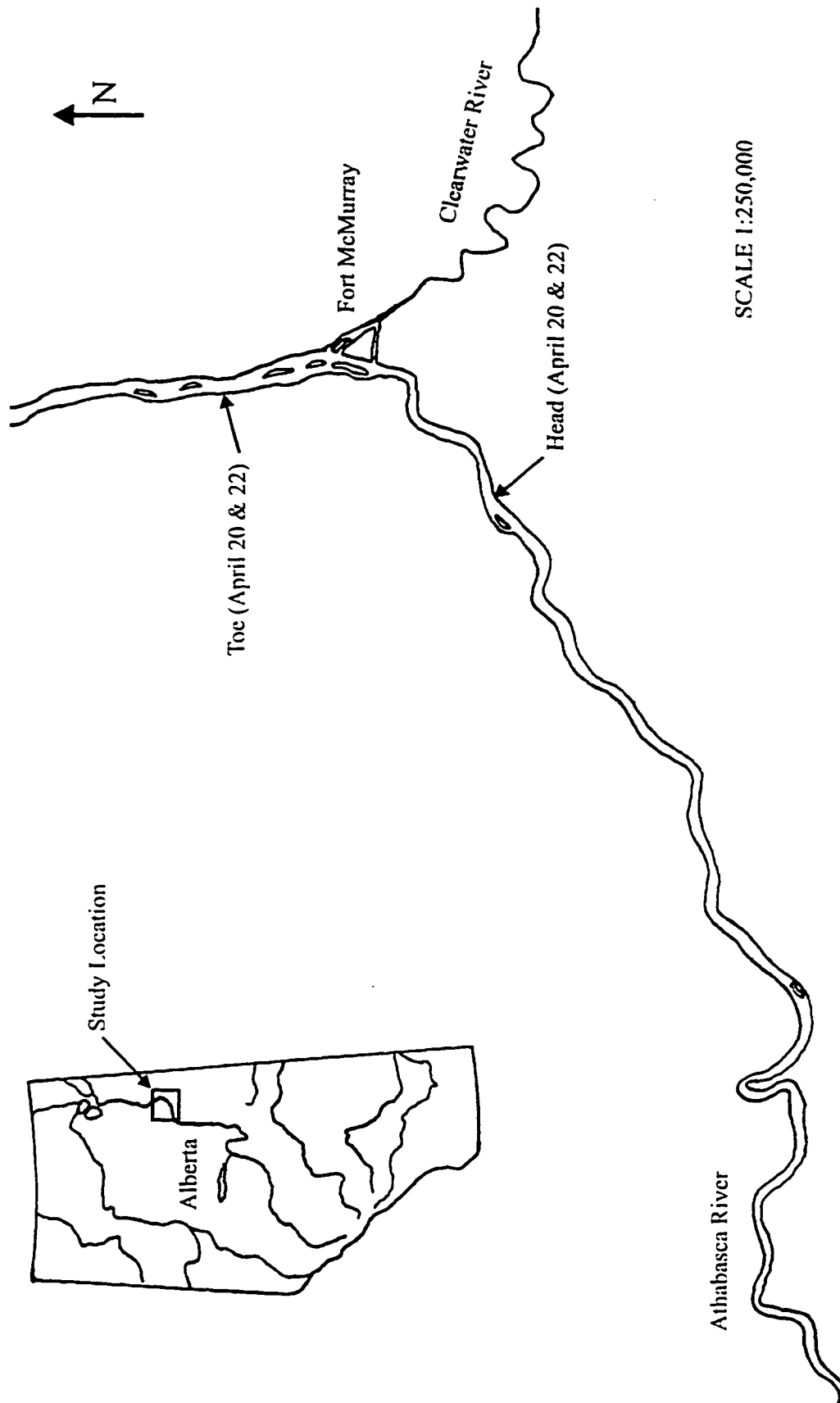


Figure 4.29(e). Extent of the 1986 Athabasca River recorded ice jam events.



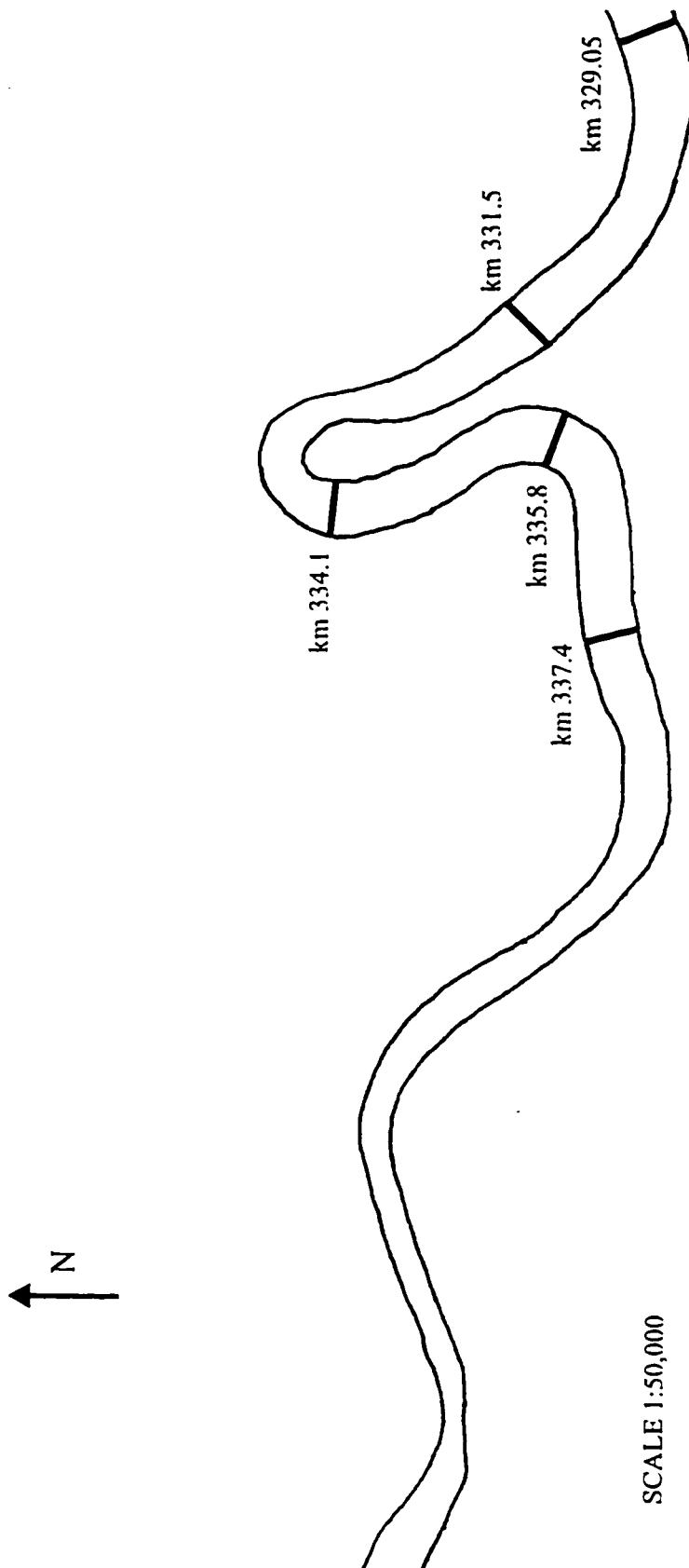


Figure 4.30. Approximate cross section locations along the Athabasca River.

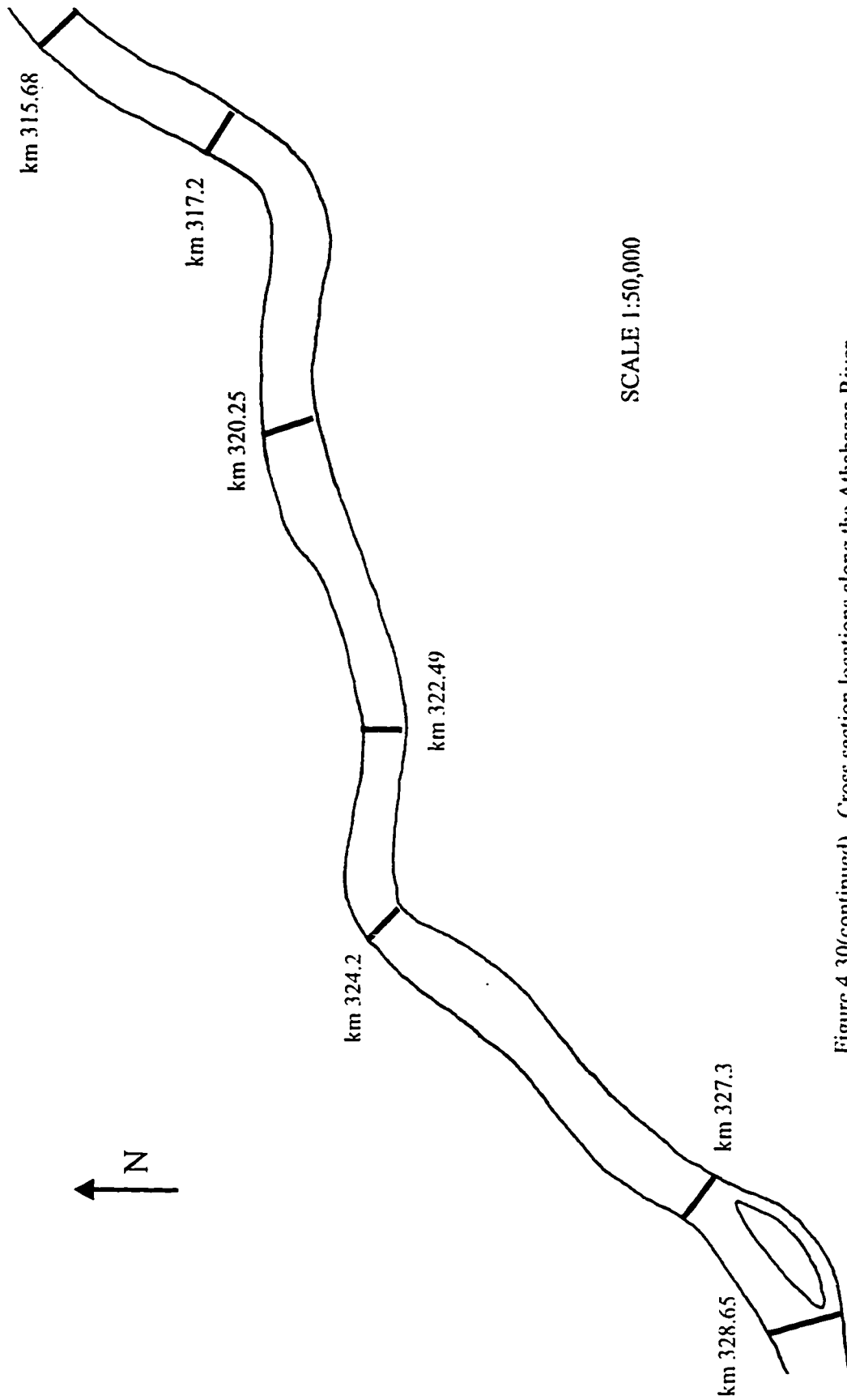


Figure 4.30(continued). Cross section locations along the Athabasca River.

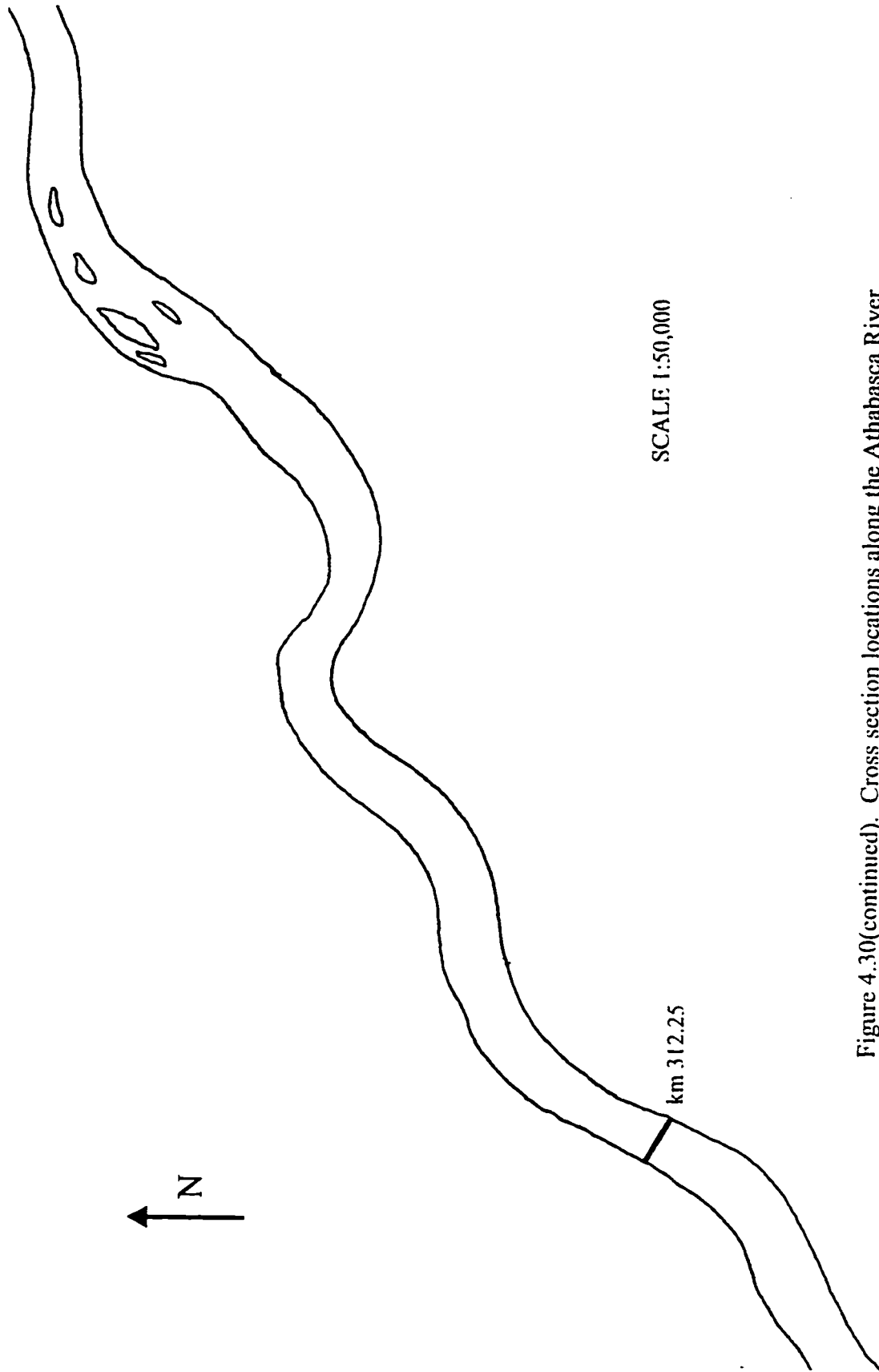


Figure 4.30(continued). Cross section locations along the Athabasca River.

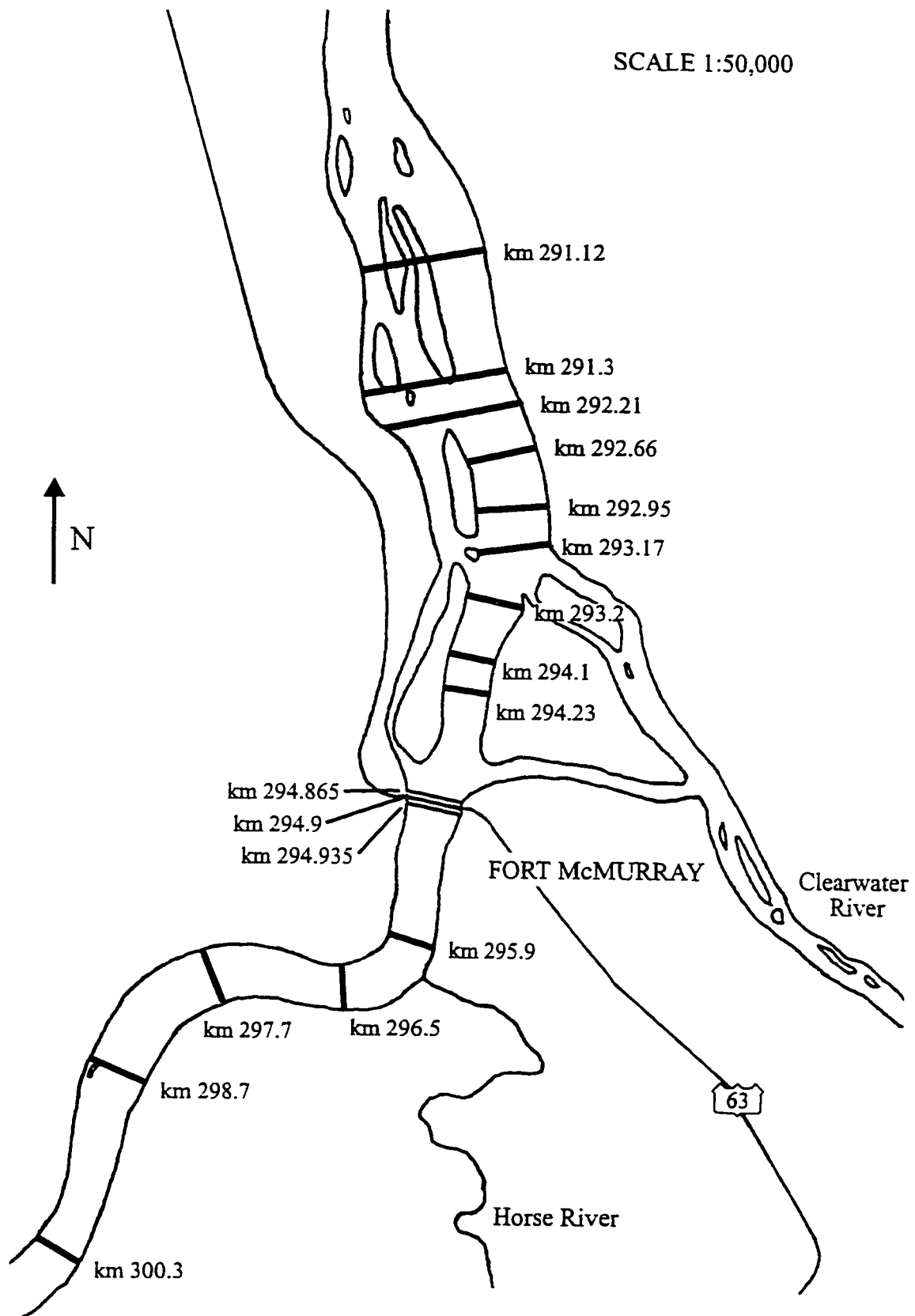


Figure 4.30 (continued). Cross section locations along the Athabasca River.

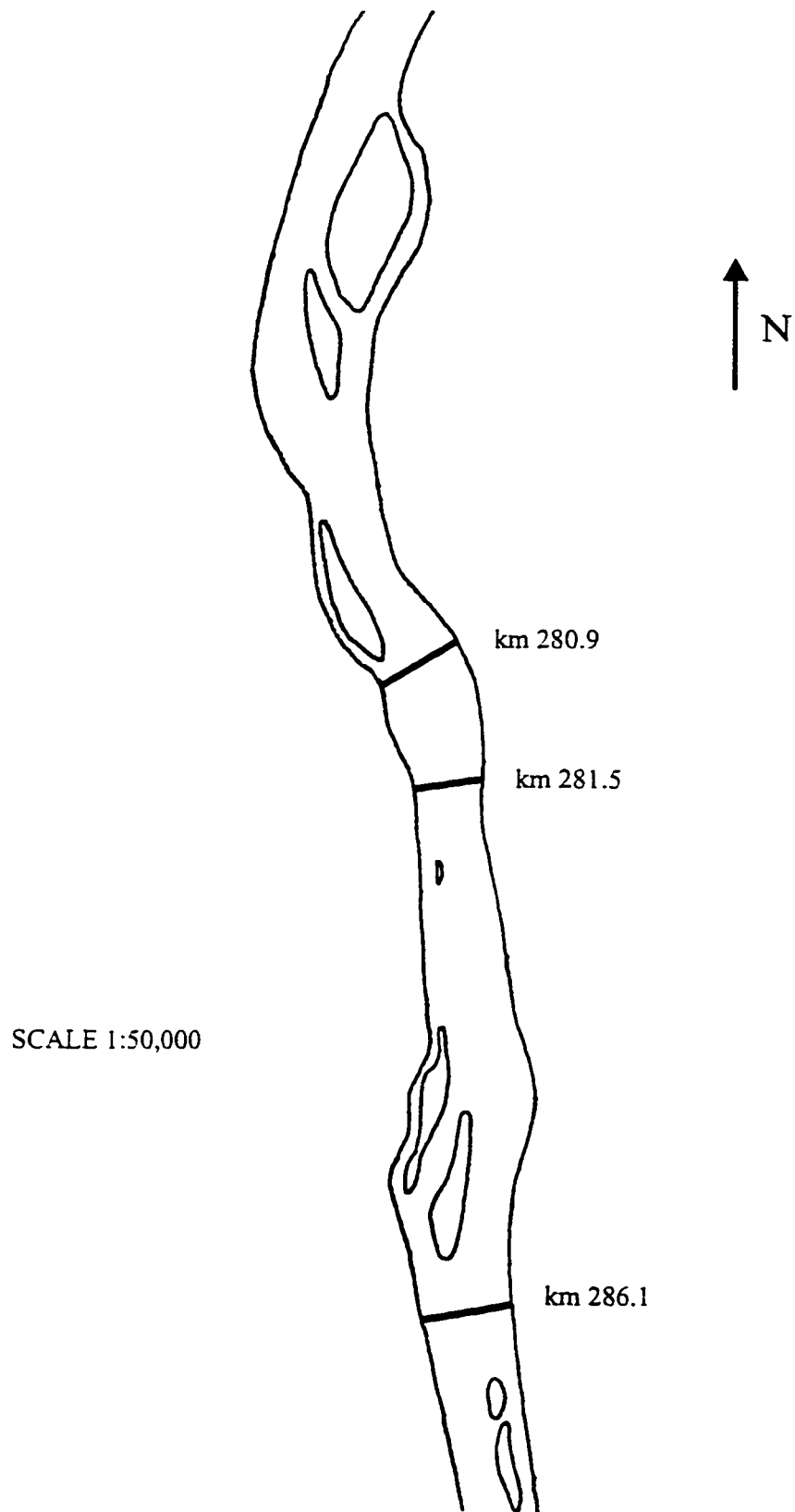


Figure 4.30(continued). Cross section locations along the Athabasca River.

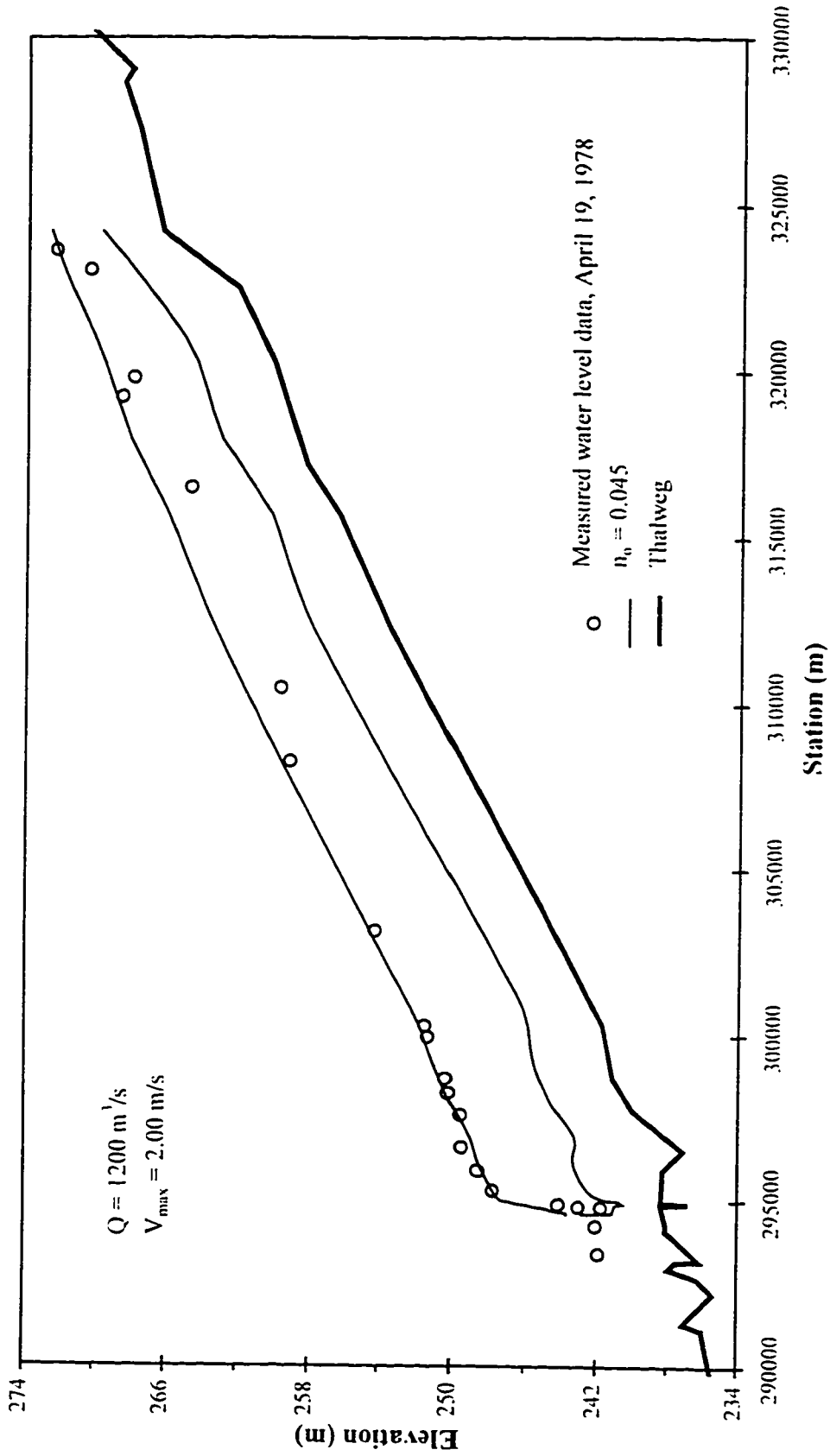


Figure 4.31. April 19, 1978 Athabasca River ice jam as predicted by ICEJAM using Mannings equation.

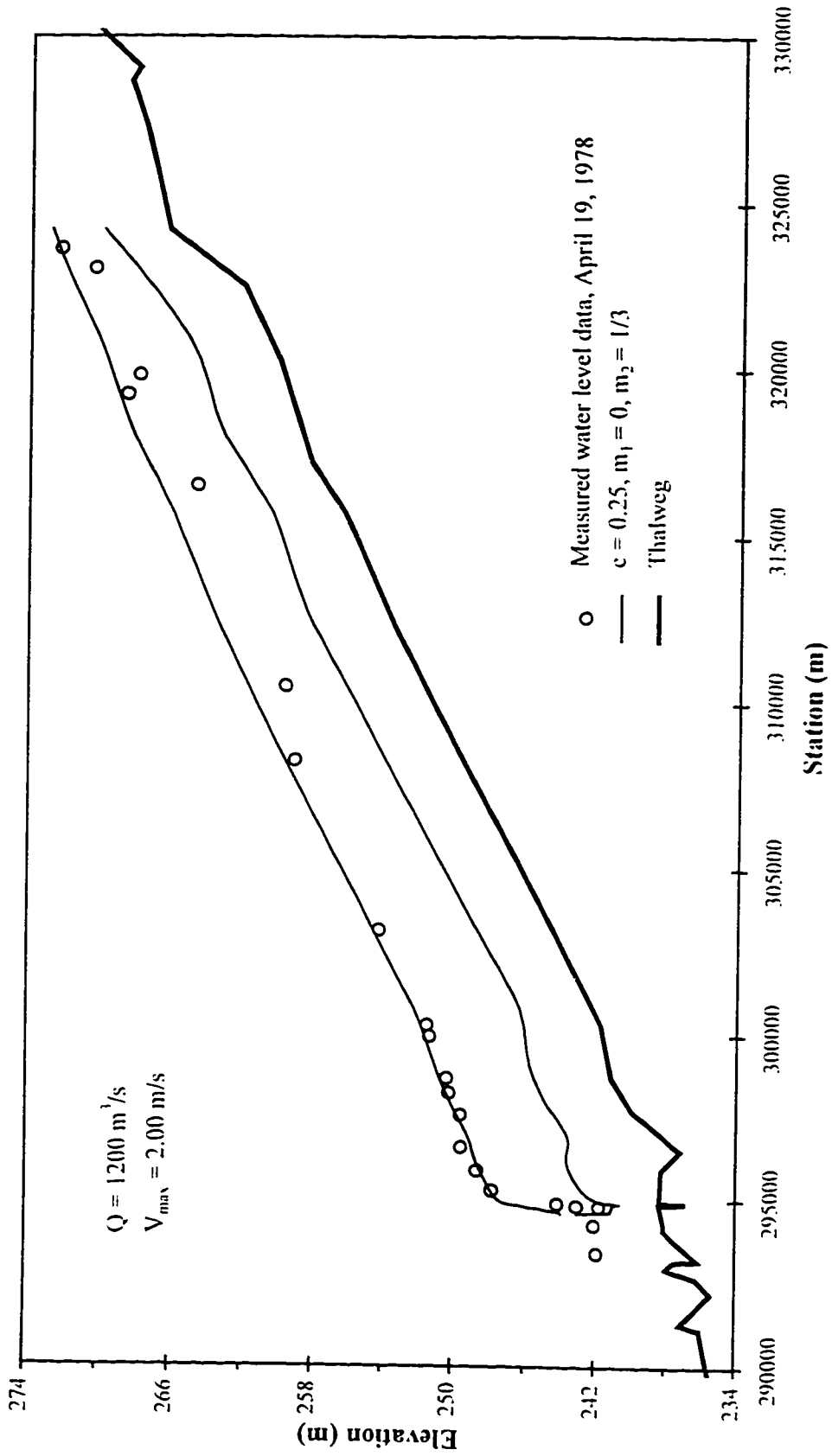


Figure 4.32. April 19, 1978 Athabasca River ice jam as predicted by ICEJAM using Beltaos' Mannings approximation.

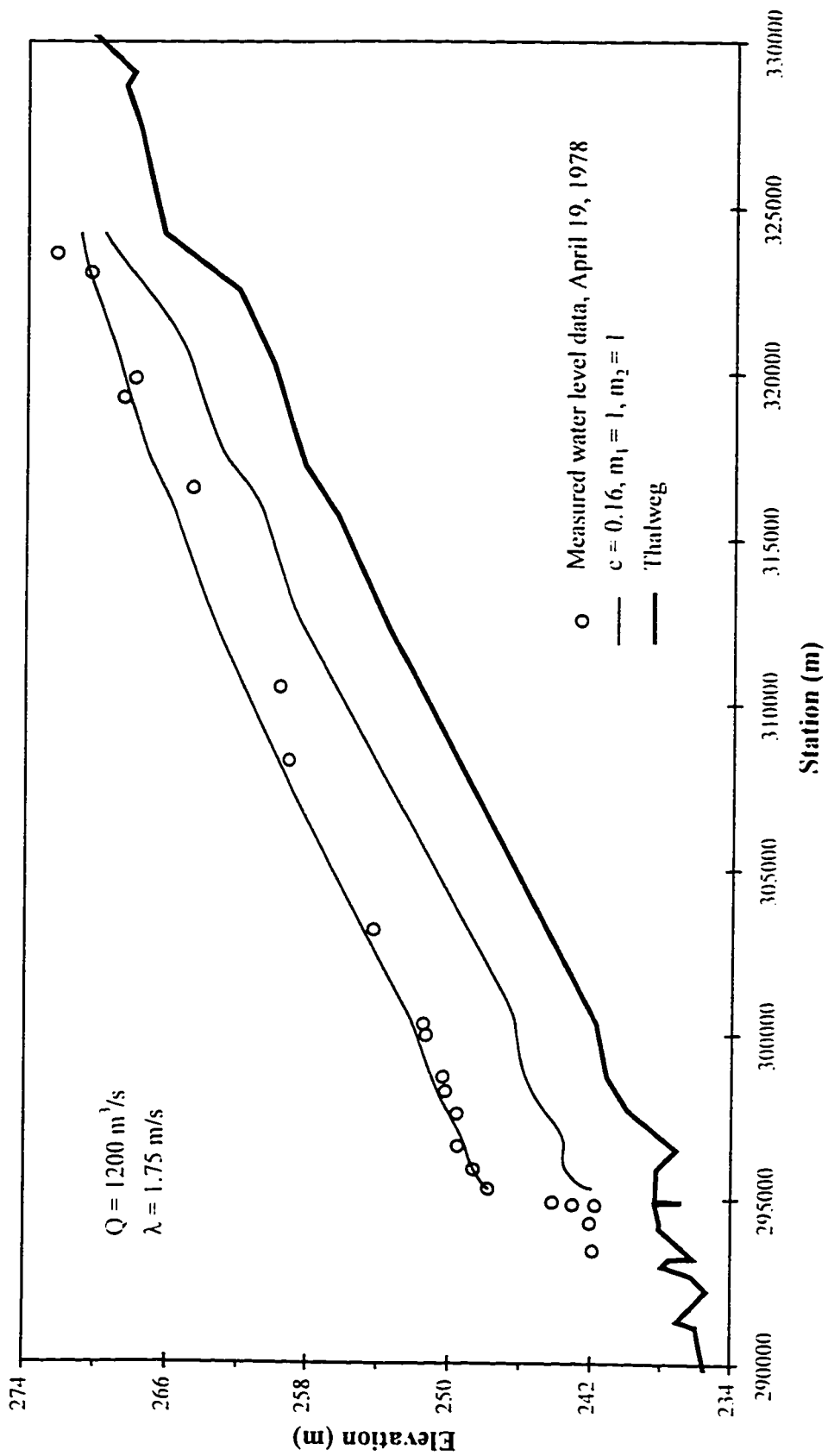


Figure 4.33. April 19, 1978 Athabasca River ice jam as predicted by RIVJAM using Beltaos' friction factor.



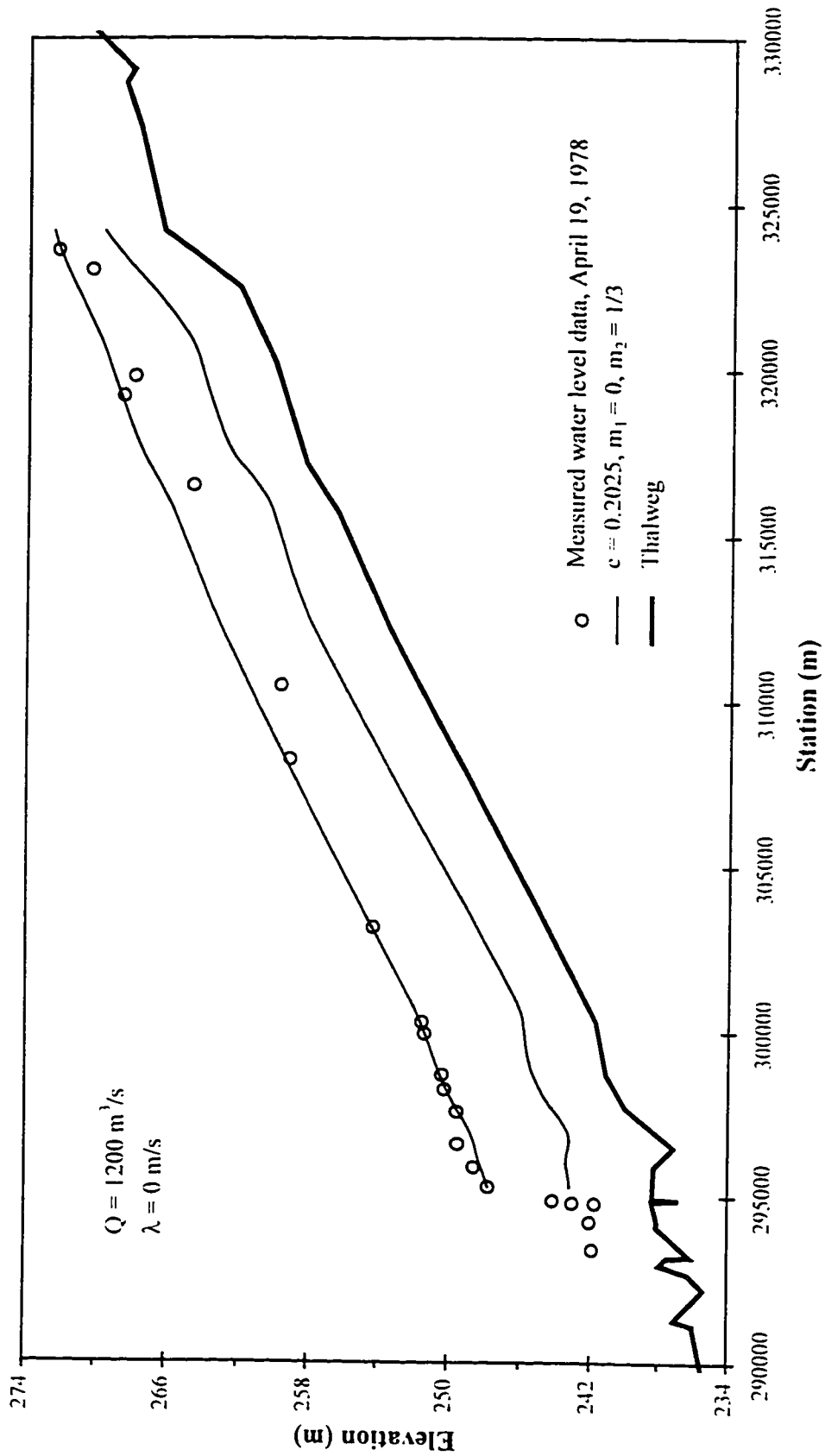


Figure 4.34. April 19, 1978 Athabasca River ice jam as predicted by RIVJAM using Beltaos' Mannings approximation.

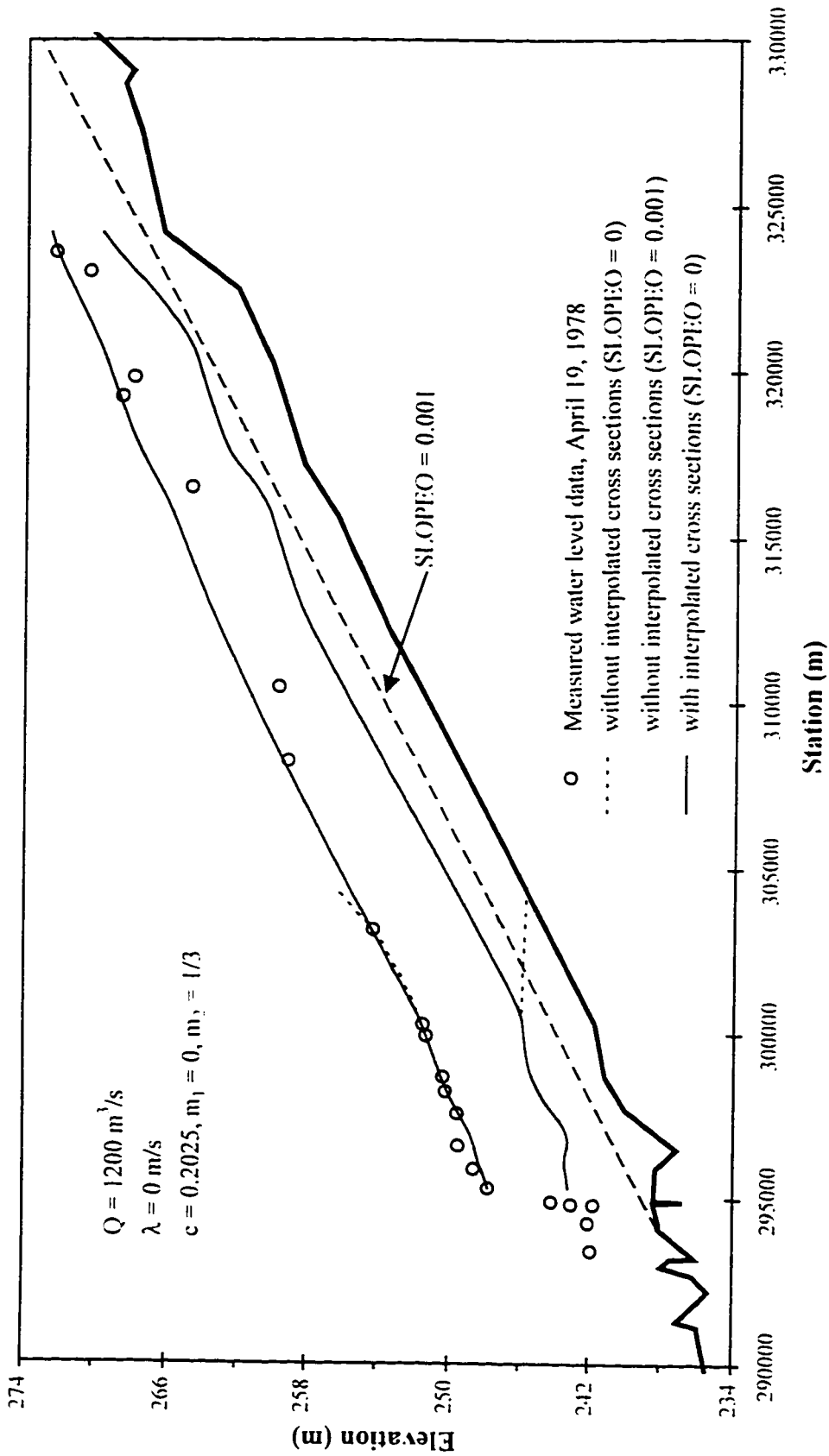


Figure 4.35. April 19, 1978 Athabasca River ice jam as predicted by RIVJAM using Beltaos' Mannings approximation, illustrating sensitivity to slope-line slope (SLOPEO).

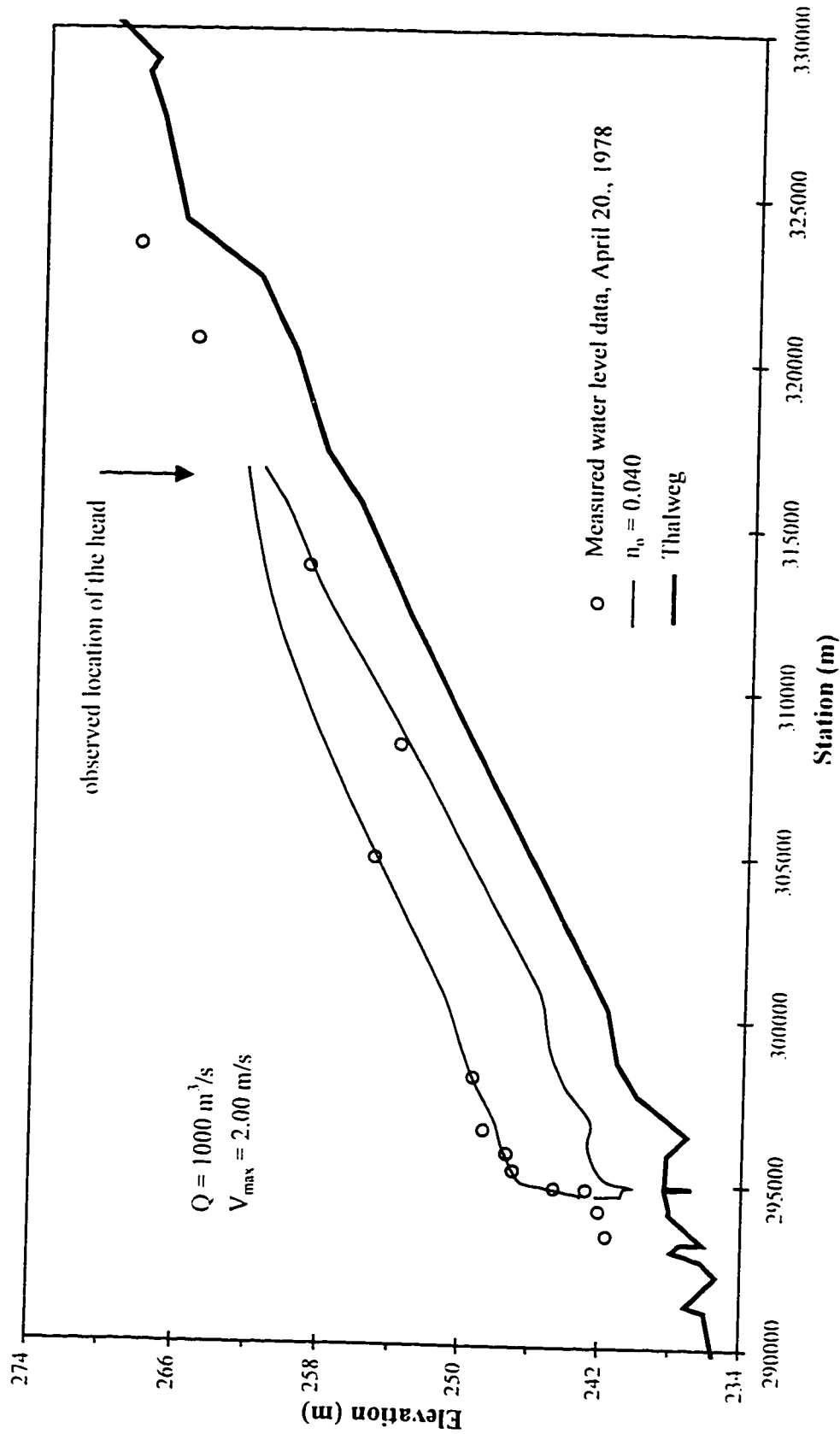


Figure 4.36. April 20, 1978 Athabasca River ice jam as predicted by ICEJAM using Mannings equation.

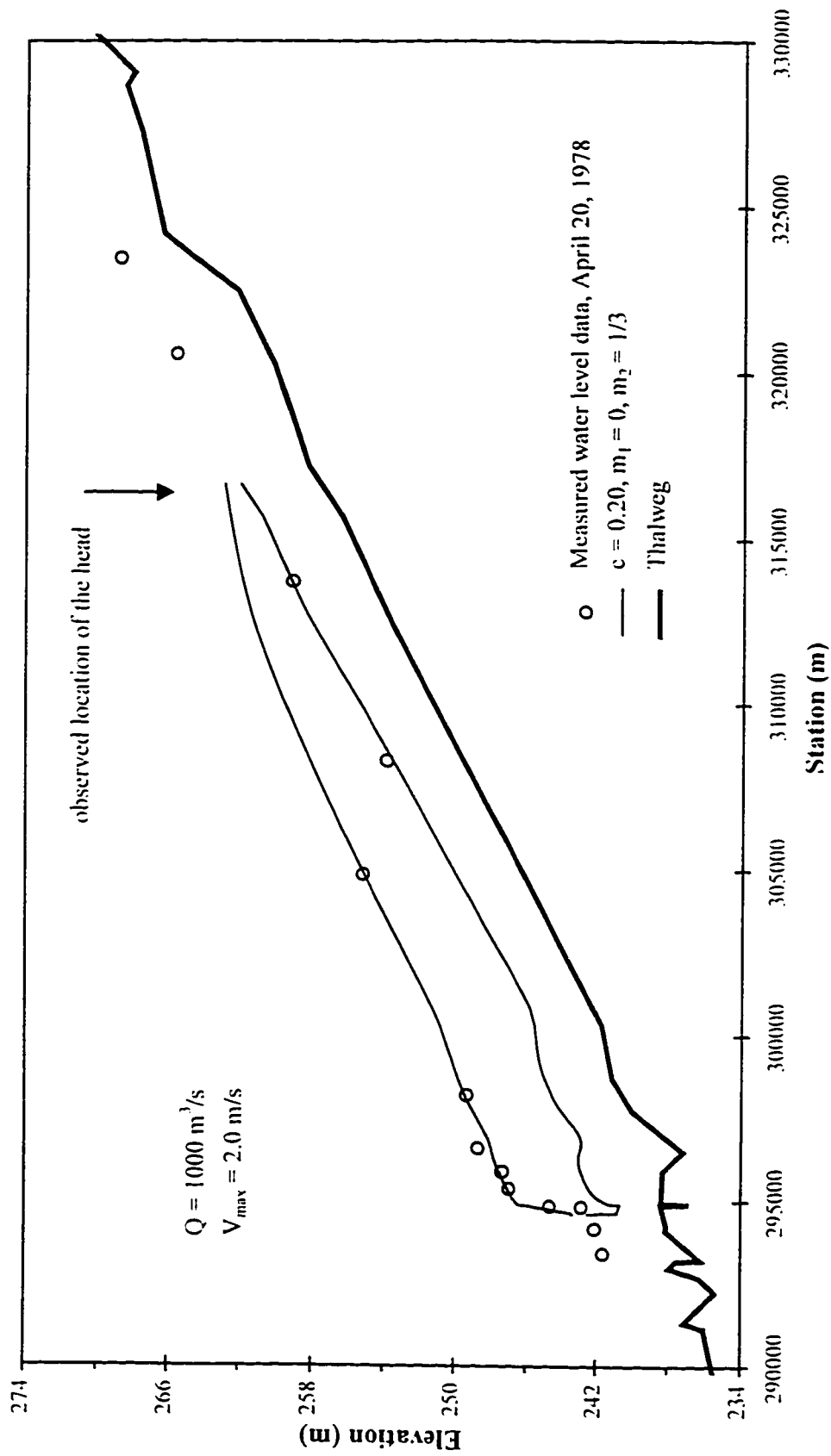


Figure 4.37. April 20, 1978 Athabasca River ice jam as predicted by ICF:JAM using Beltaos' Mannings approximation.

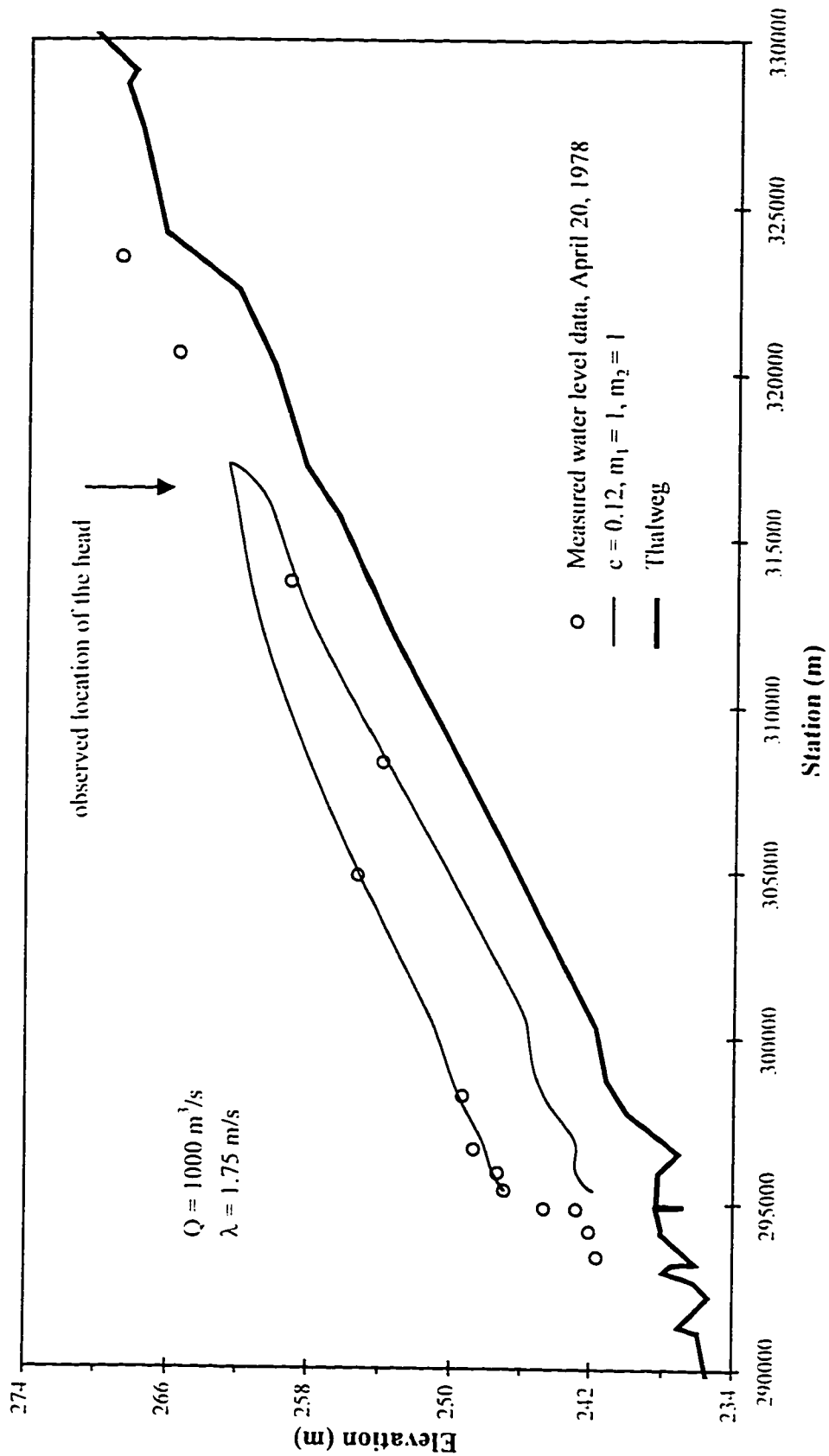


Figure 4.38. April 20, 1978 Athabasca River ice jam as predicted by RIVIAM using Beltaos' friction factor.

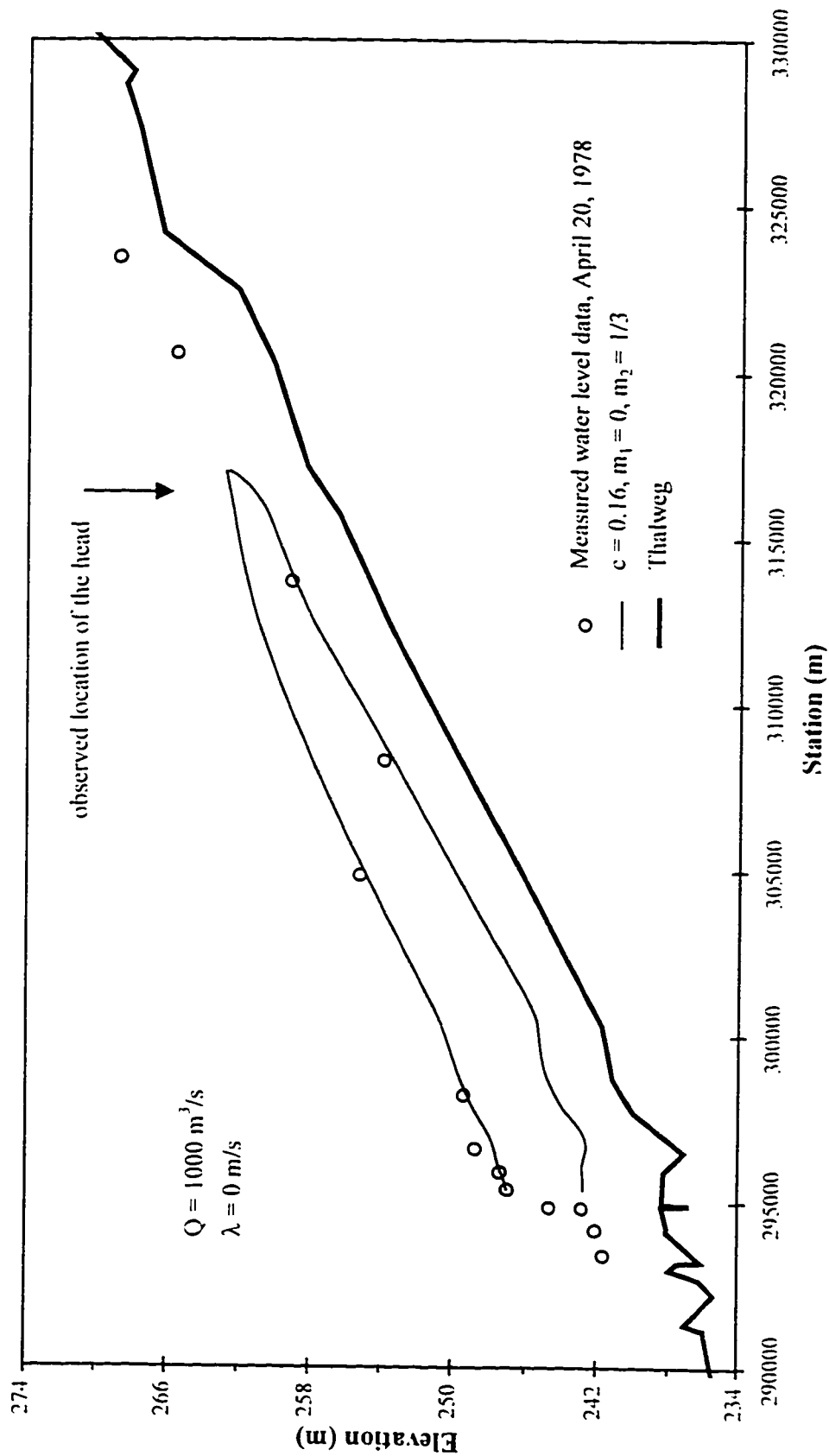


Figure 4.39. April 20, 1978 Athabasca River ice jam as predicted by RIVJAM using Beltaos' Mannings approximation.

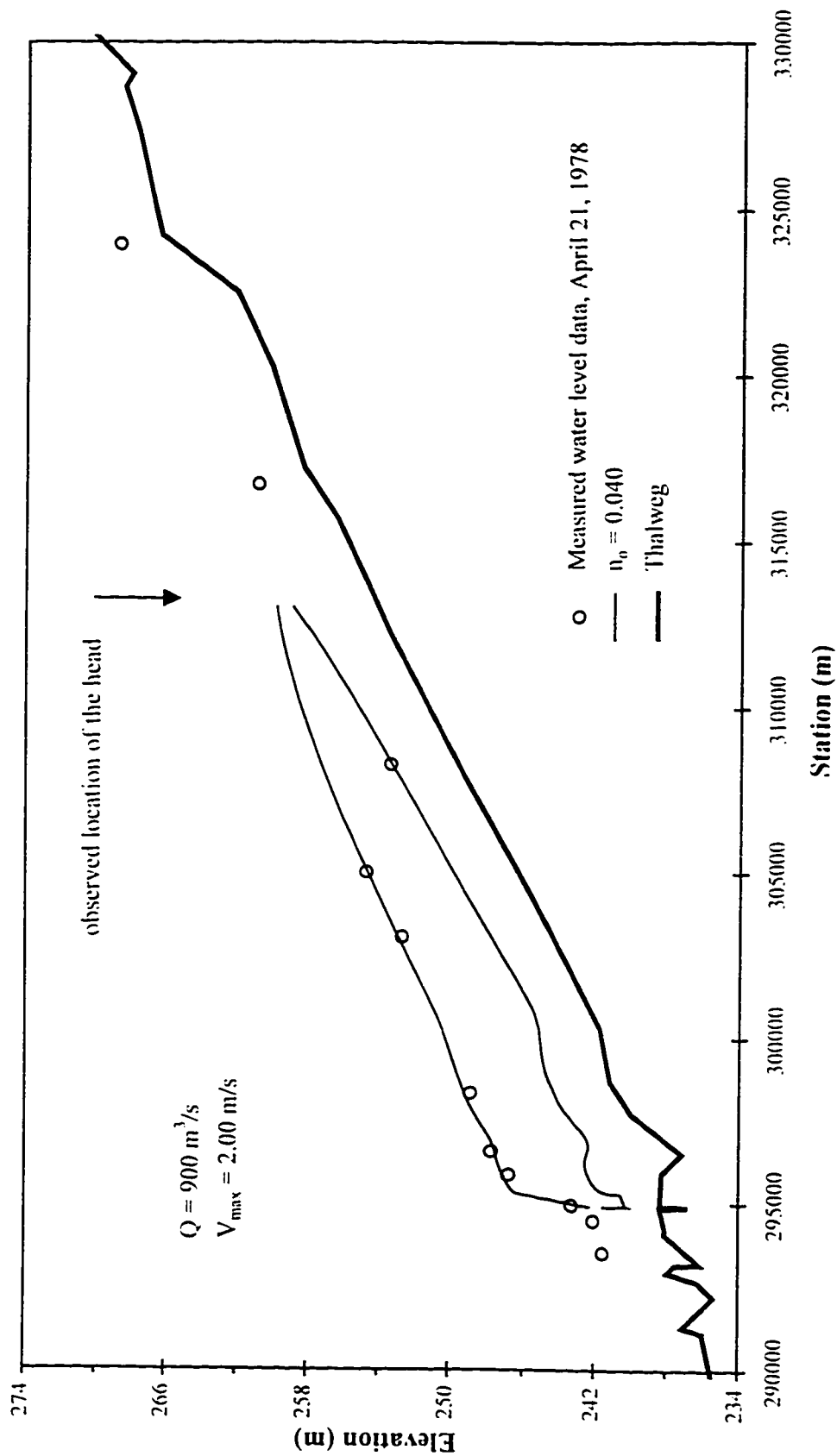


Figure 4.40. April 21, 1978 Athabasca River ice jam as predicted by ICEJAM using Mannings equation.

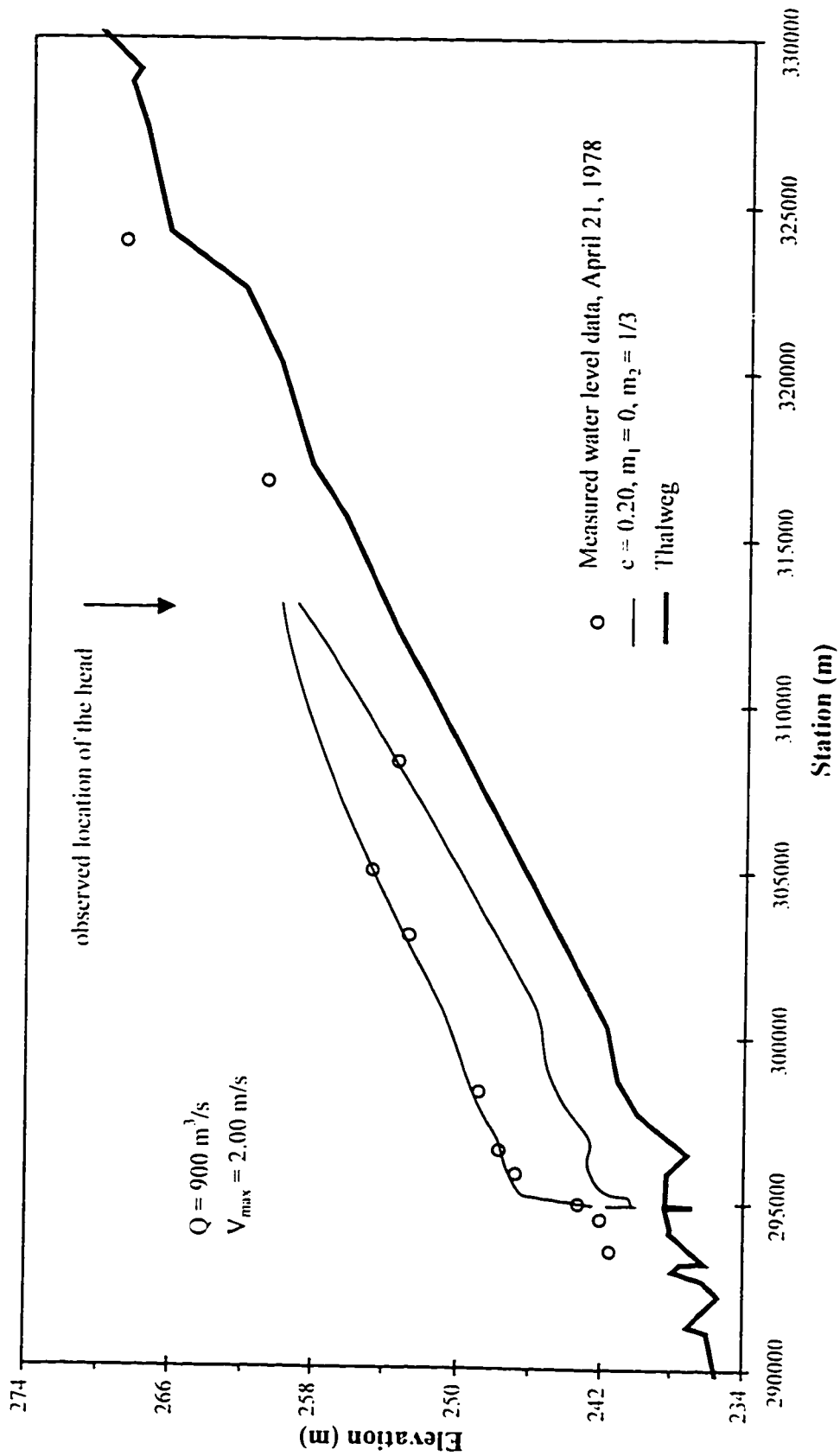


Figure 4.41. April 21, 1978 Athabasca River ice jam as predicted by ICF:JAM using Beltaos' Mannings approximation.



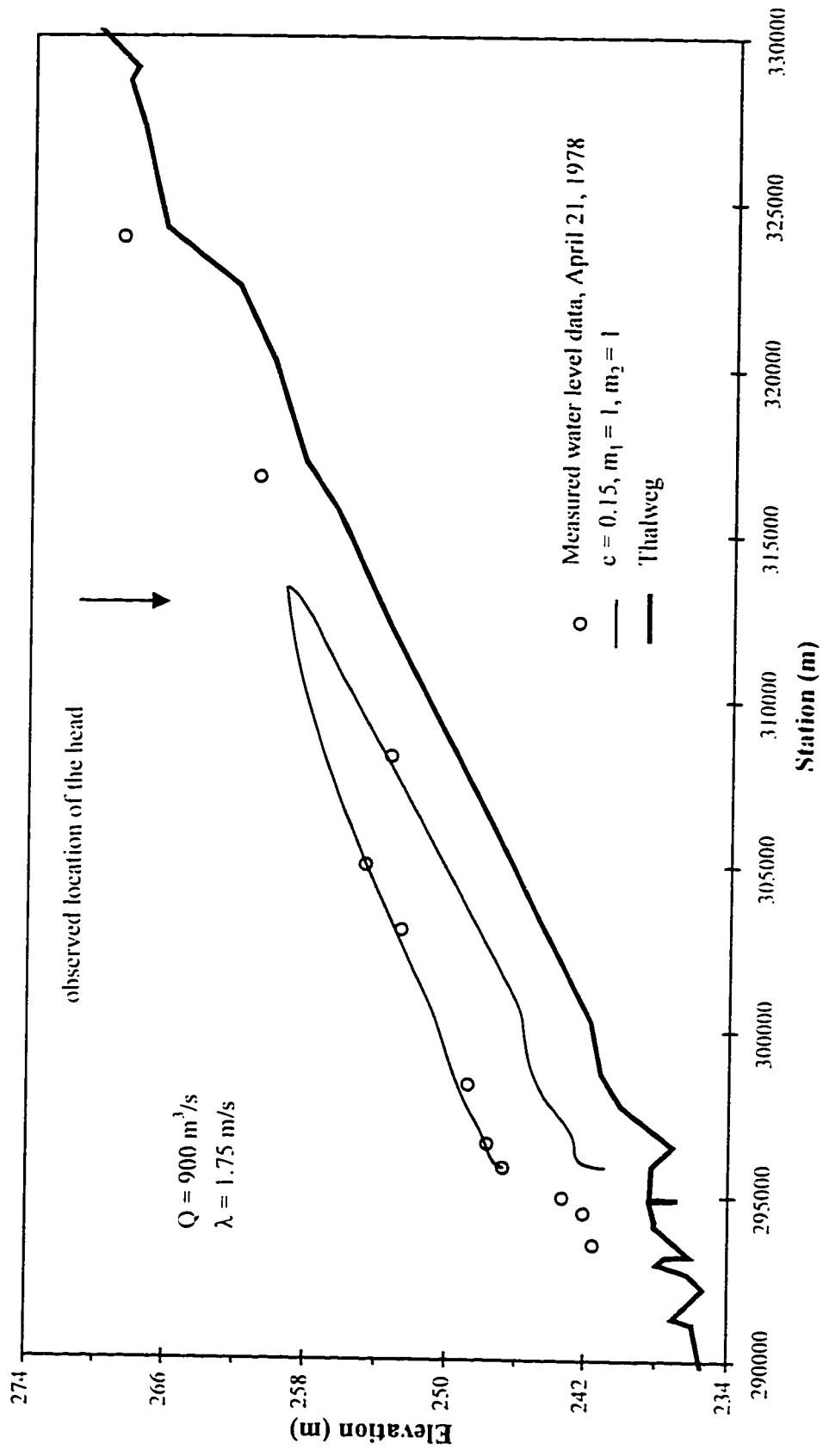


Figure 4.42. April 21, 1978 Athabasca River ice jam as predicted by RIVJAM using Bellaos' friction factor.

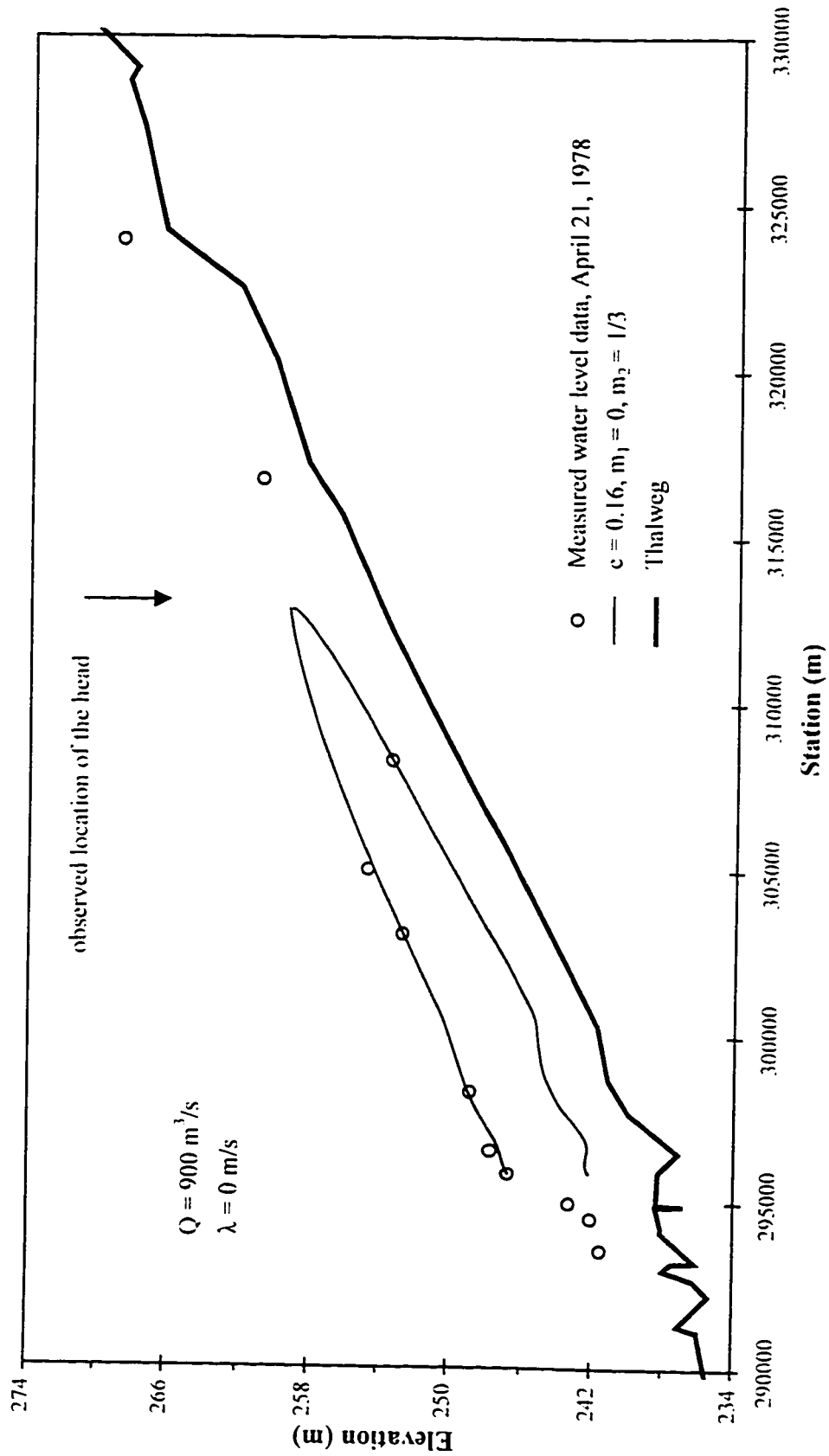


Figure 4.43. April 21, 1978 Athabasca River ice jam as predicted by RIVJAM using Beltaos' Mannings approximation.

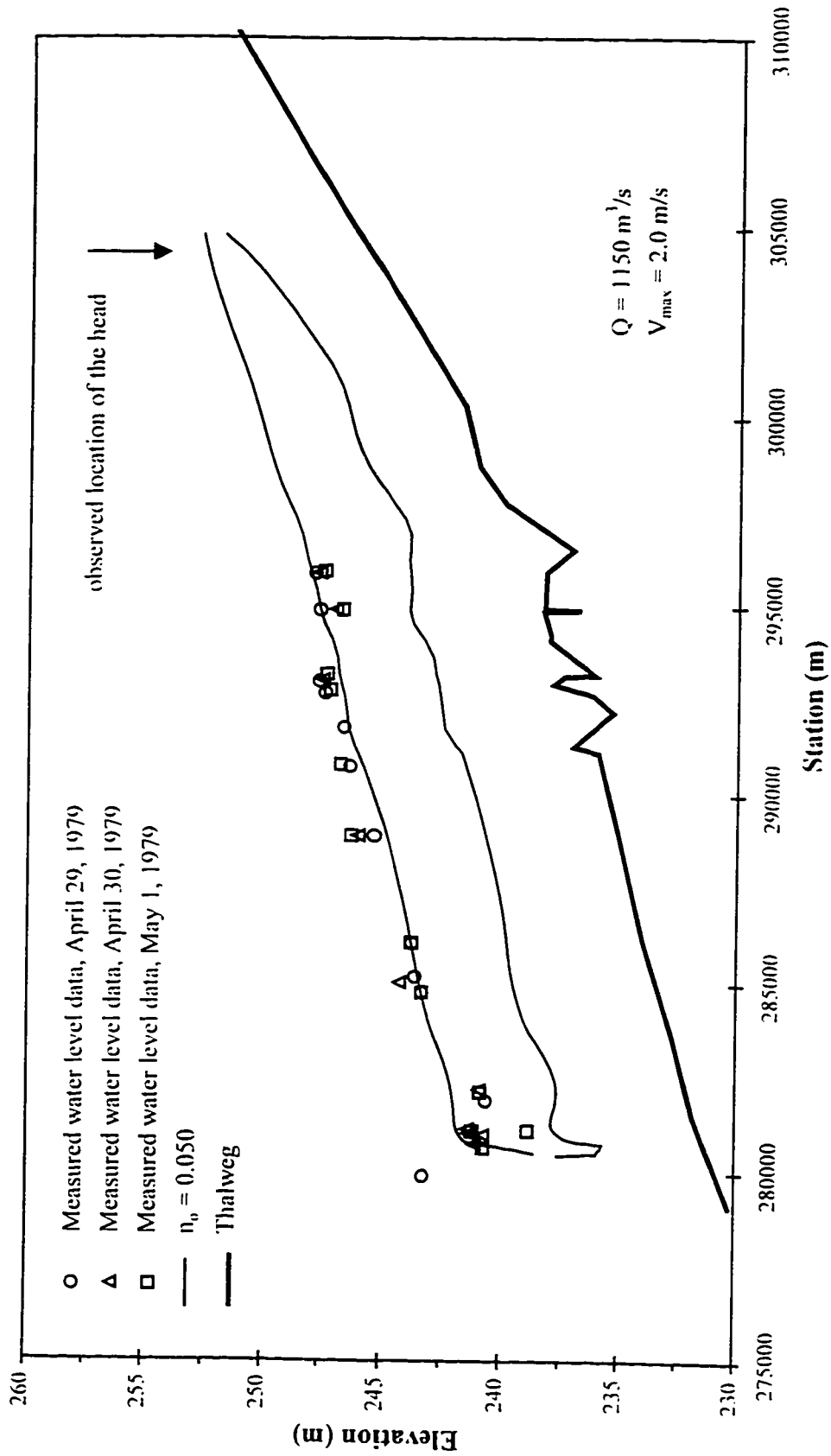


Figure 4.44. 1979 Athabasca River ice jam as predicted by ICJAM using Mannings equation.

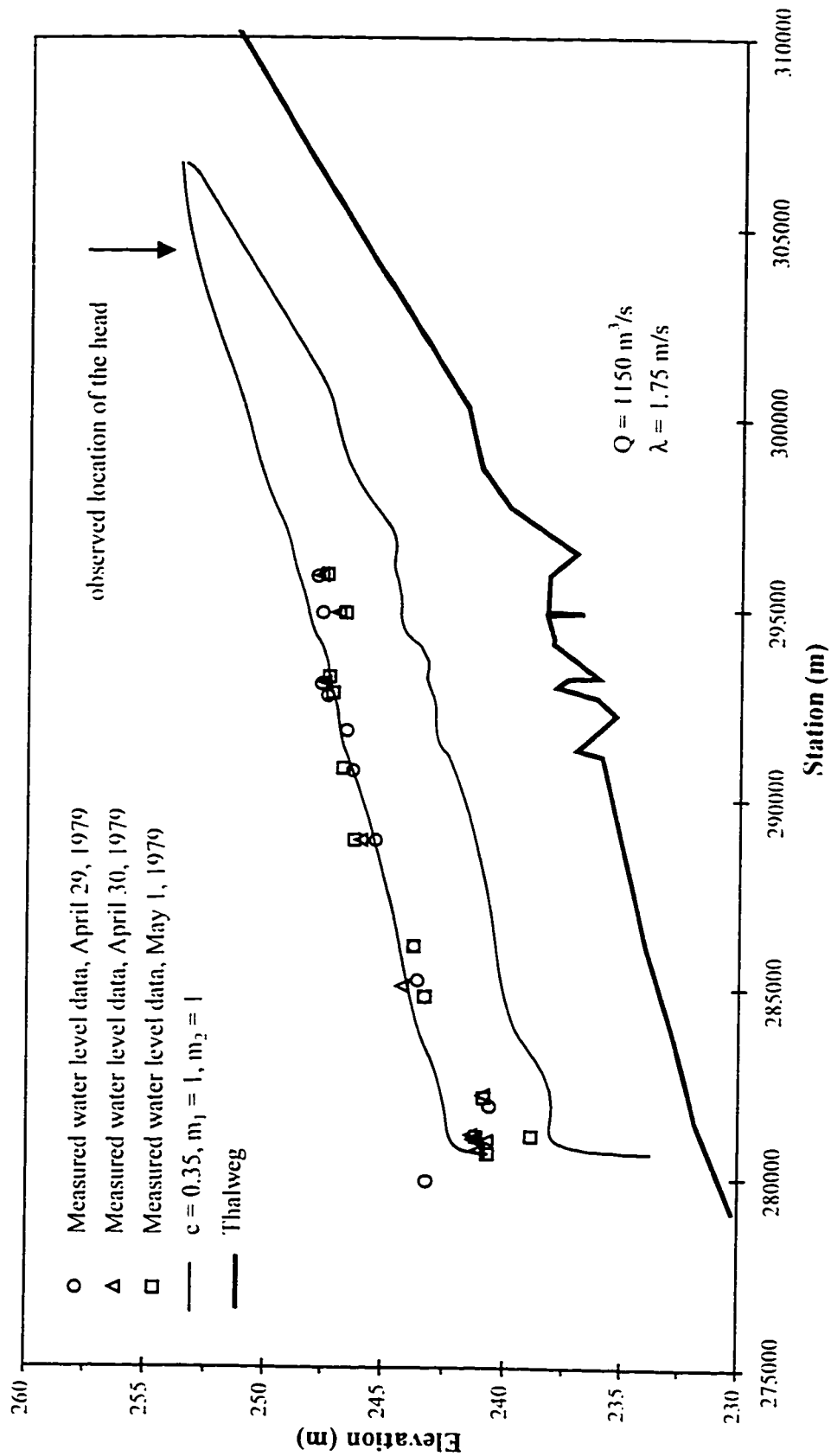


Figure 4.45. 1979 Athabasca River ice jam as predicted by RIVJAM using Betaos' friction factor.

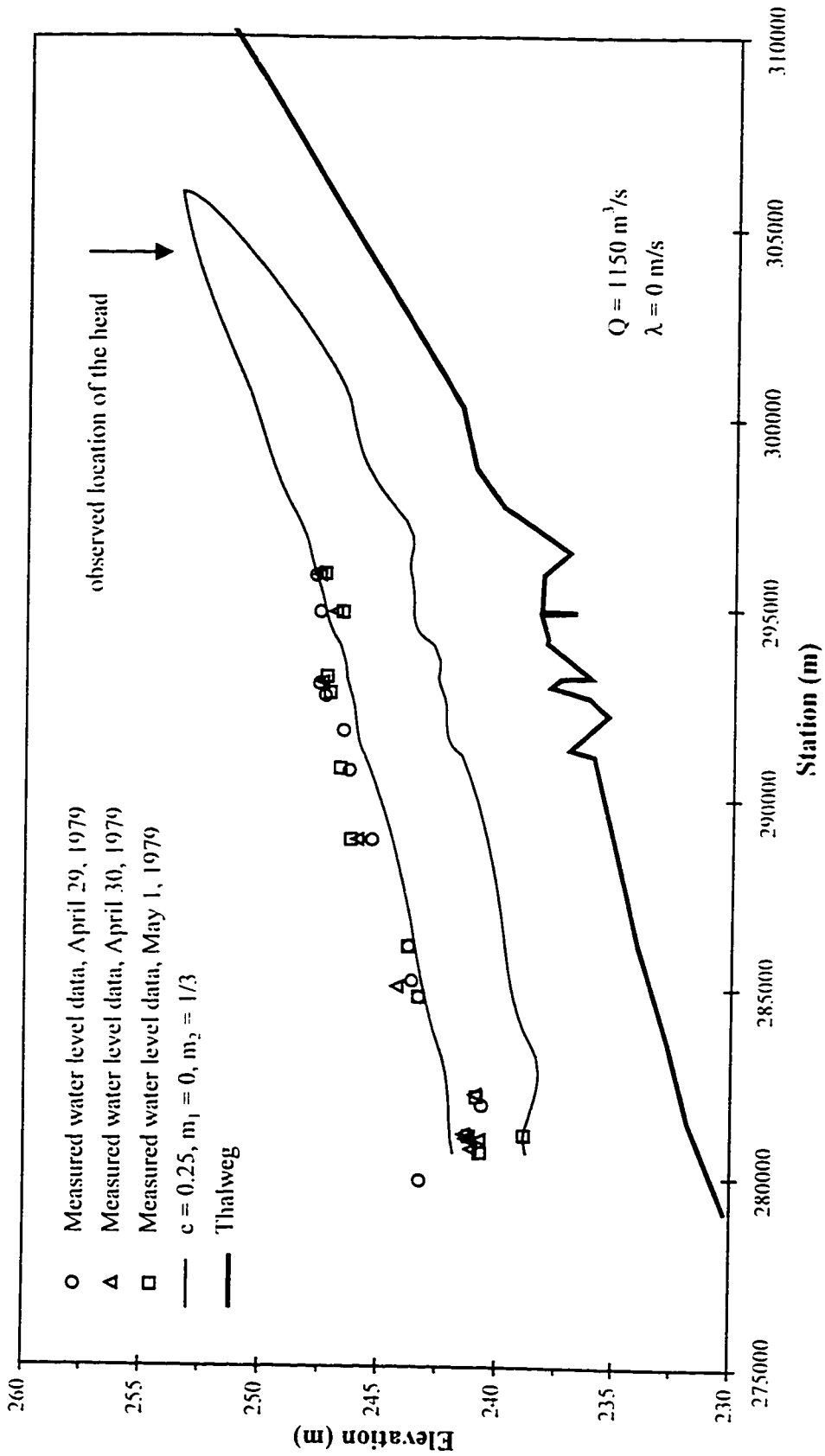


Figure 4.46. 1979 Athabasca River ice jam as predicted by RIVJAM using Beltaos' Mannings approximation.

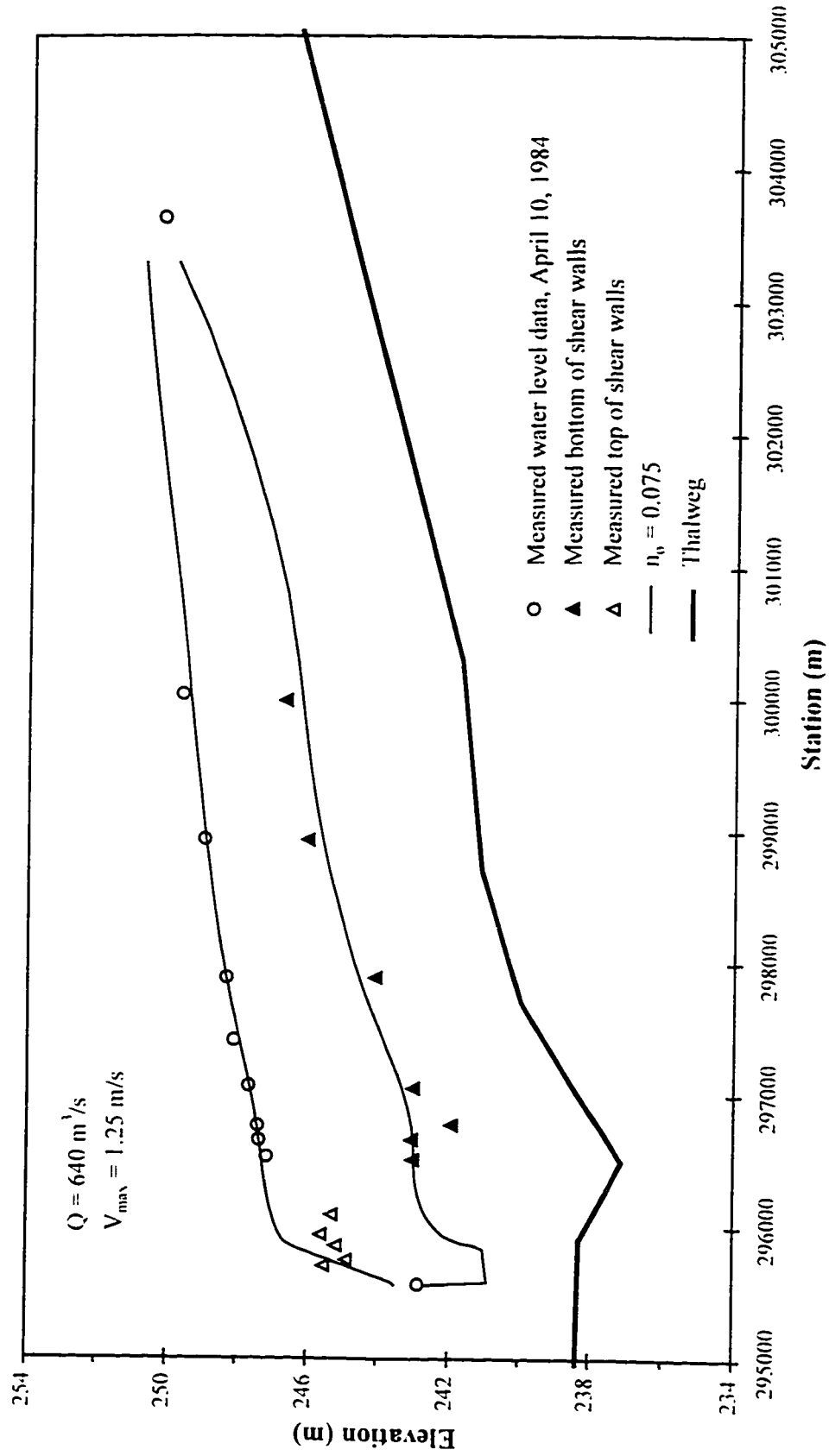


Figure 4.47. 1984 Athabasca River ice jam event as predicted by ICEJAM using Mannings equation.

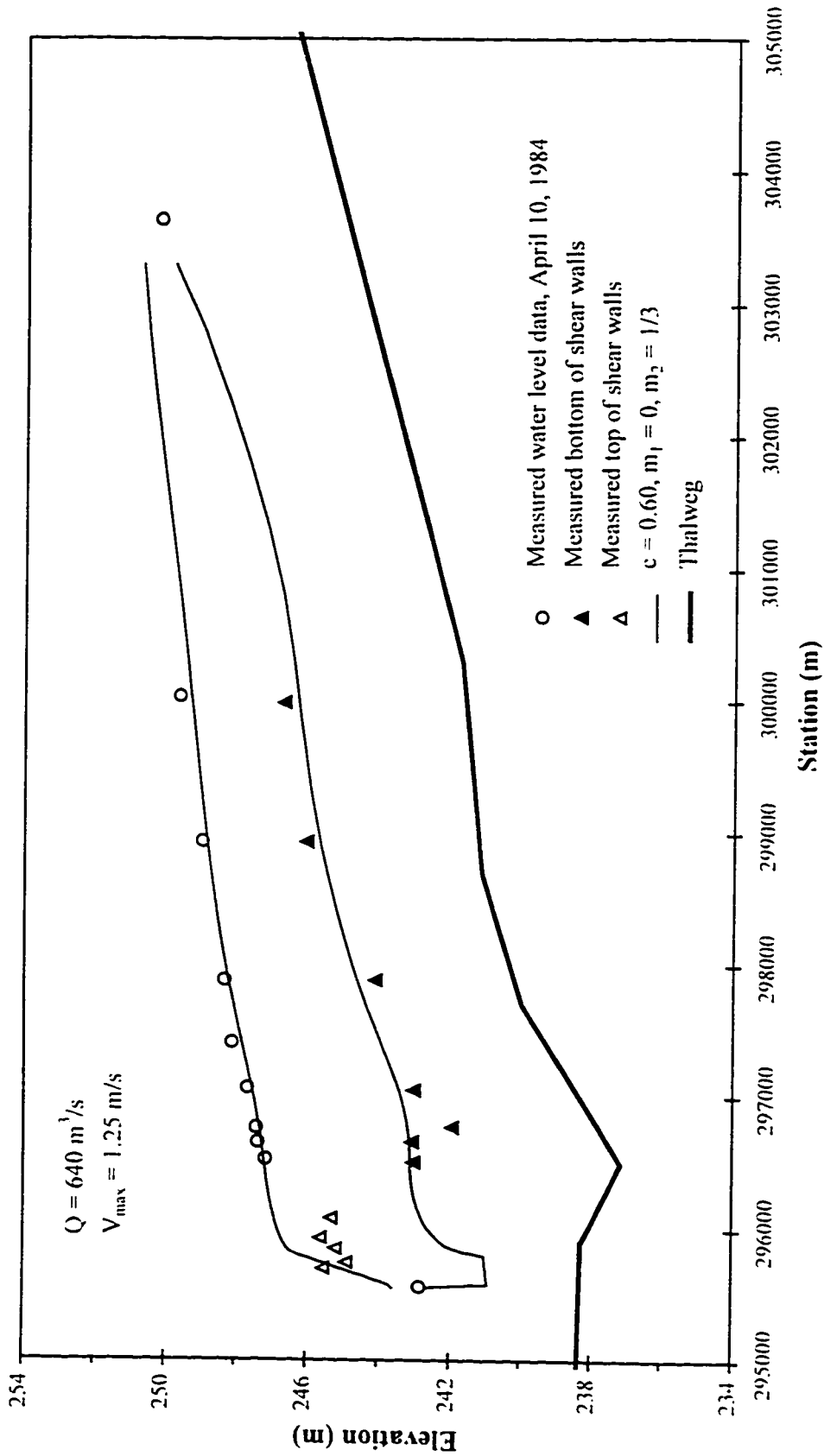


Figure 4.48. 1984 Athabasca River ice jam event as predicted by ICF-IAM using Beltaos' Mannings approximation.

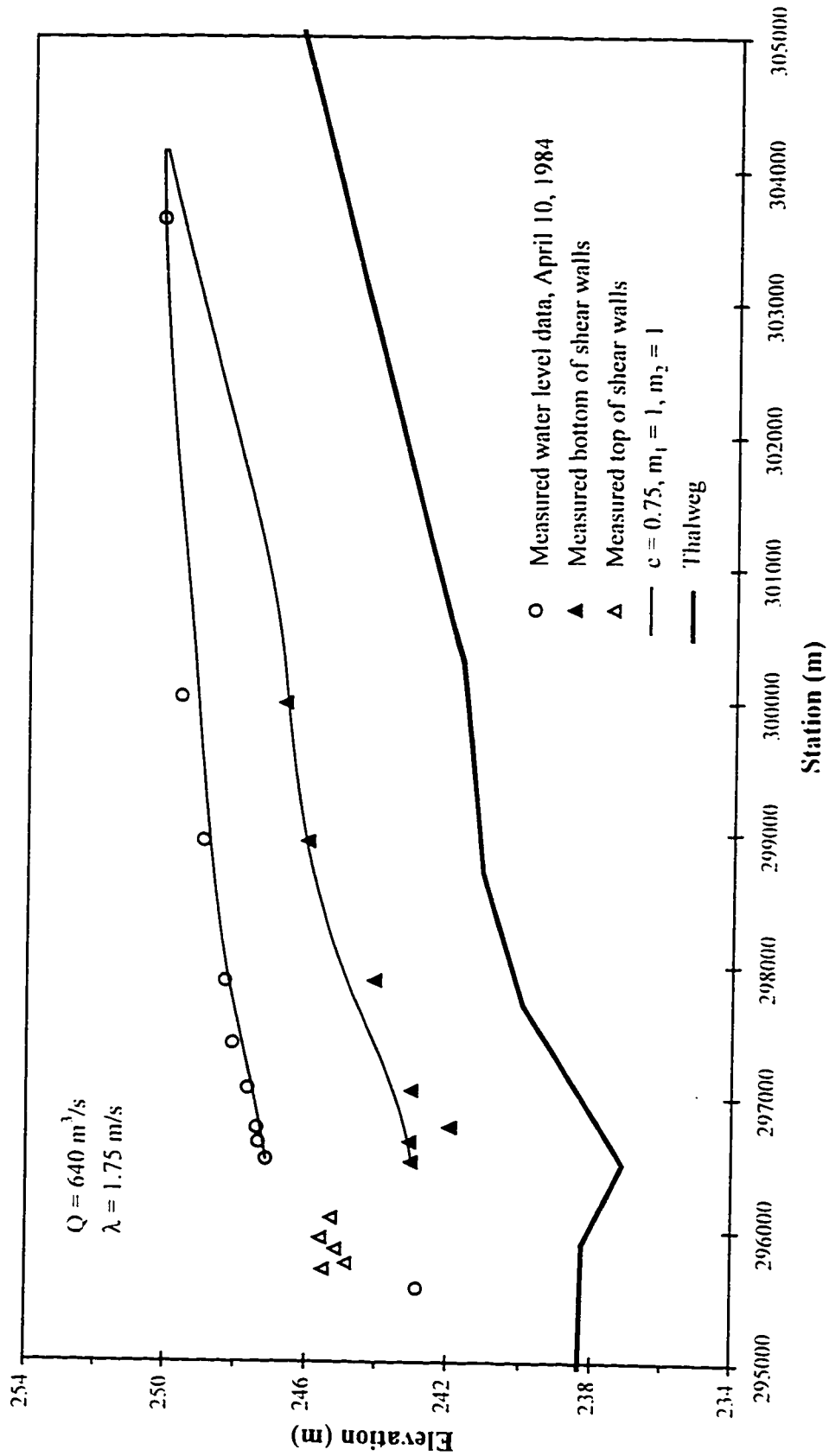


Figure 4.49. 1984 Athabasca River ice jam as predicted by RIVJAM using Beltaos' friction factor.



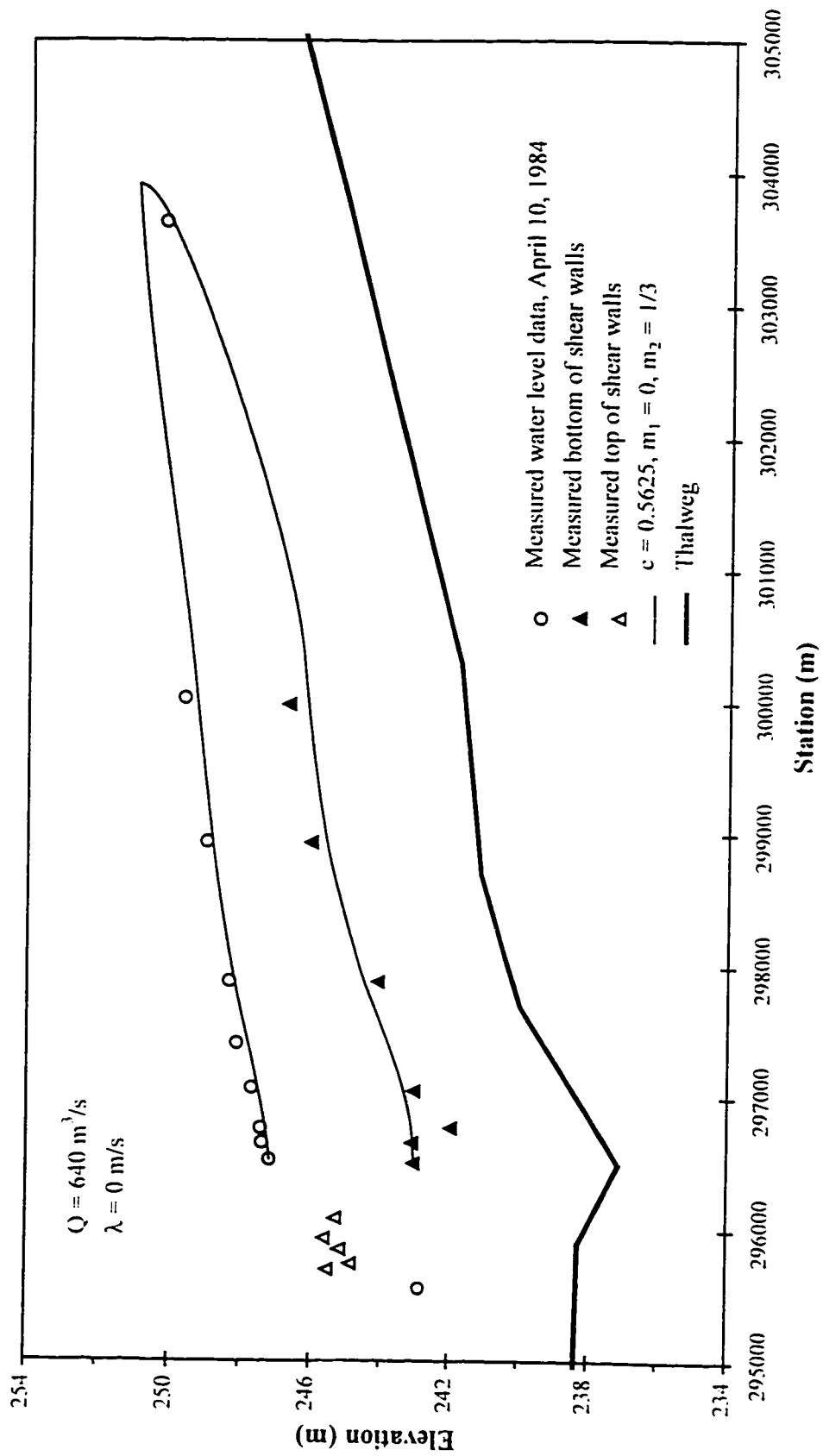


Figure 4.50. 1984 Athabasca River ice jam as predicted by RIVJAM using Beltaos' Mannings approximation.

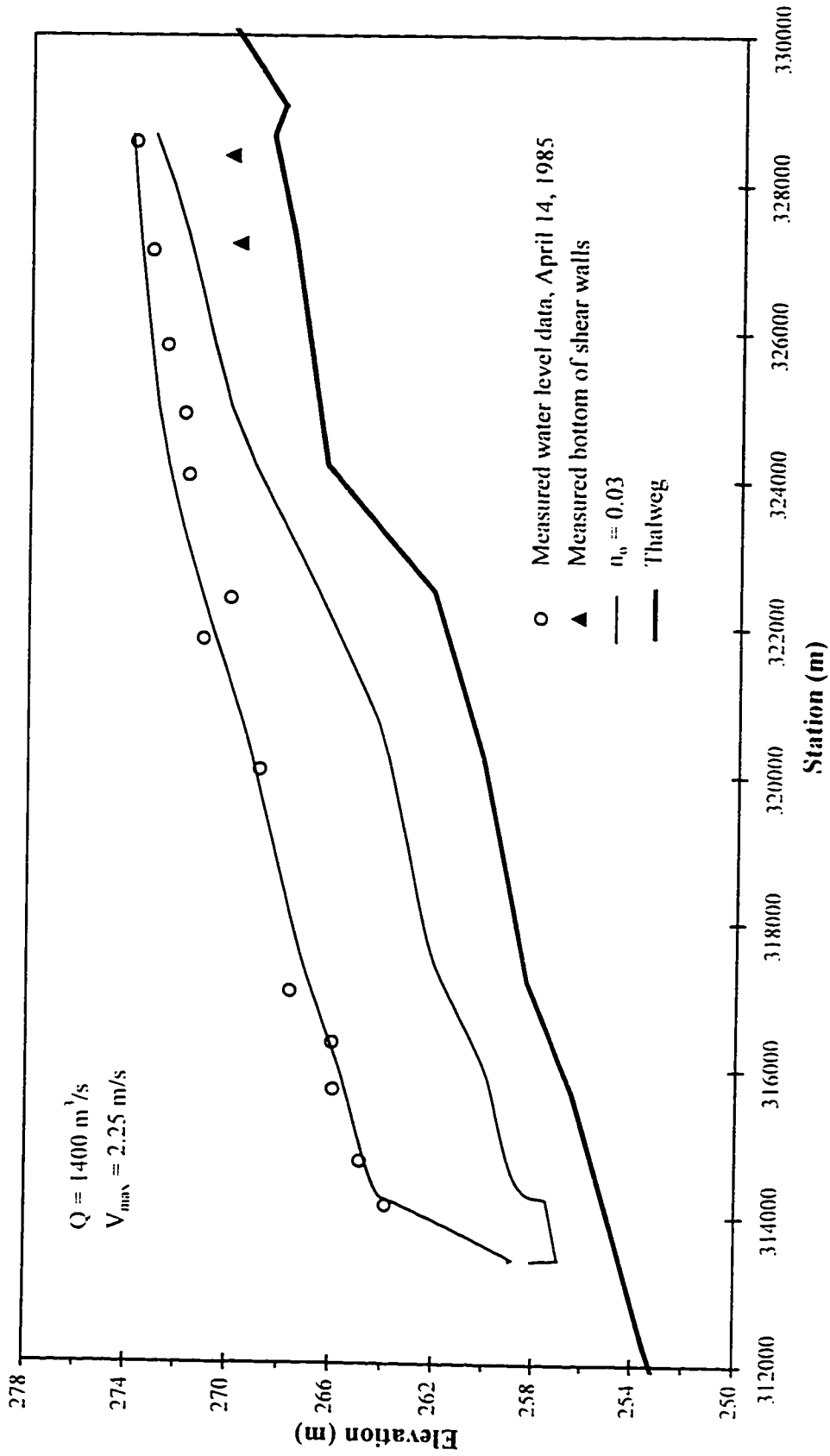


Figure 4.51. April 14, 1985 Athabasca River ice jam as predicted by ICEJAM using Mannings equation.

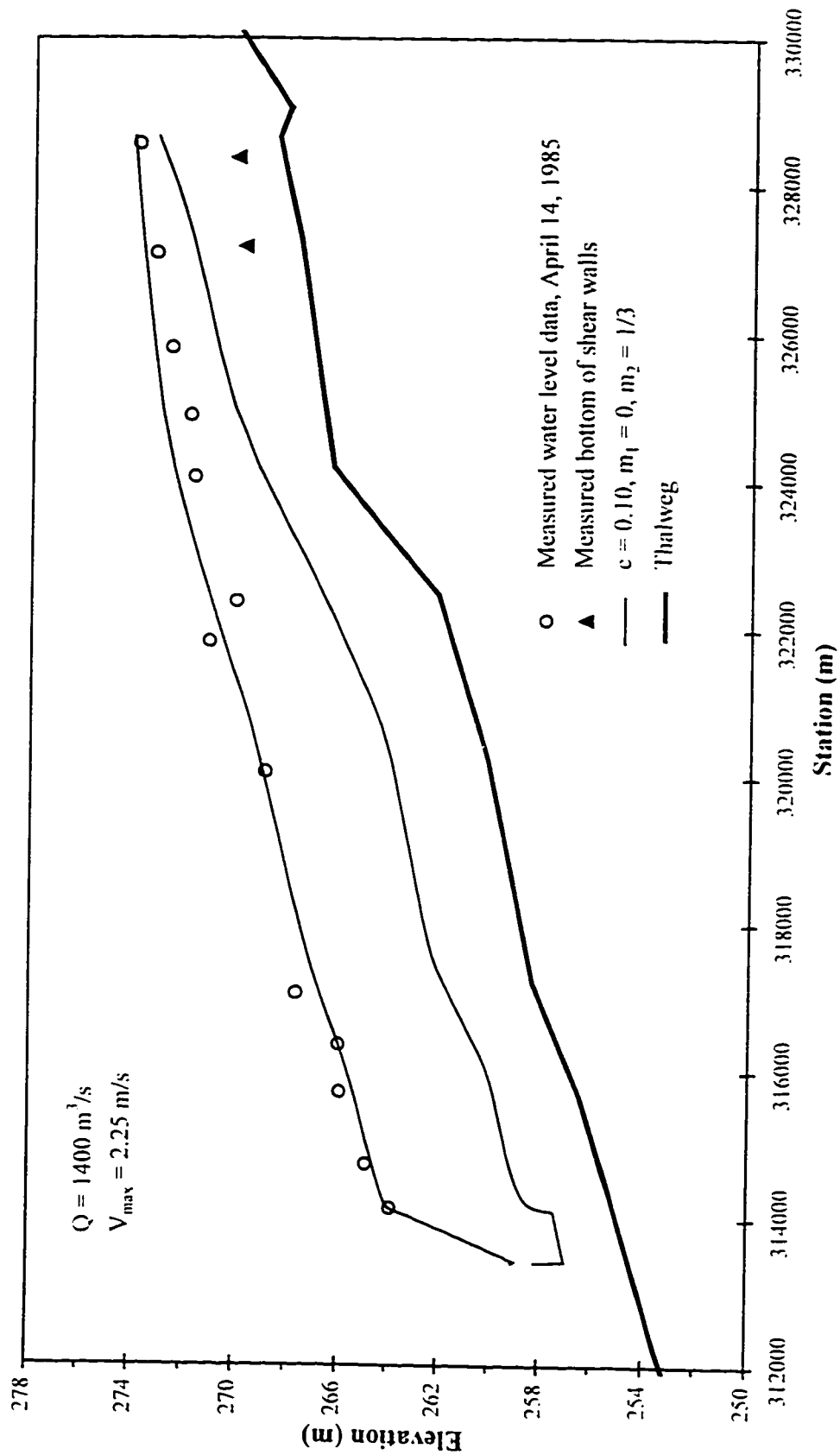


Figure 4.52. April 14, 1985 Athabasca River ice jam as predicted by ICEJAM using Beltraos' Mannings approximation.

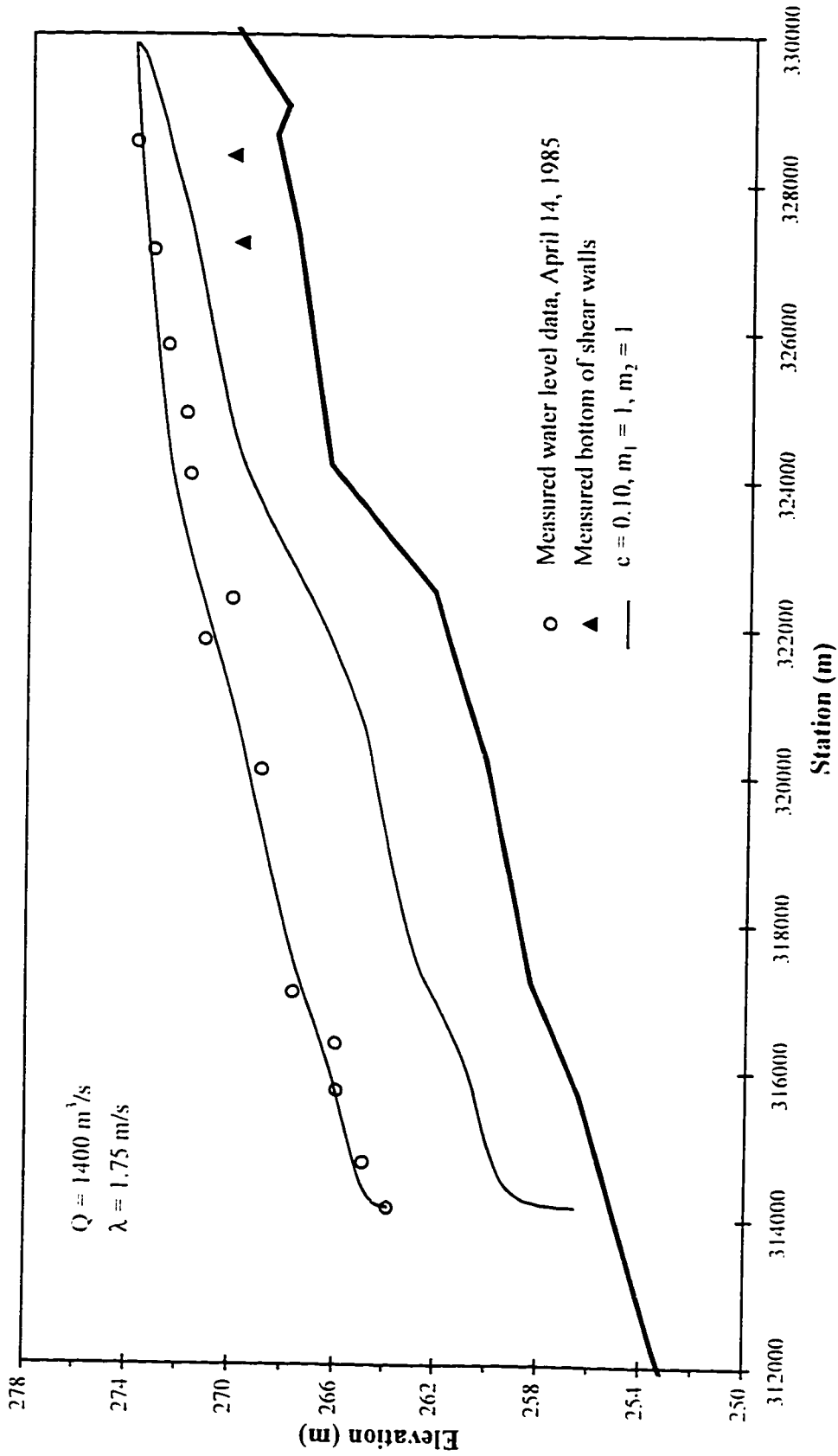


Figure 4.53. April 14, 1985 Athabasca River ice jam as predicted by RIVJAM using Beltaos' friction factor.

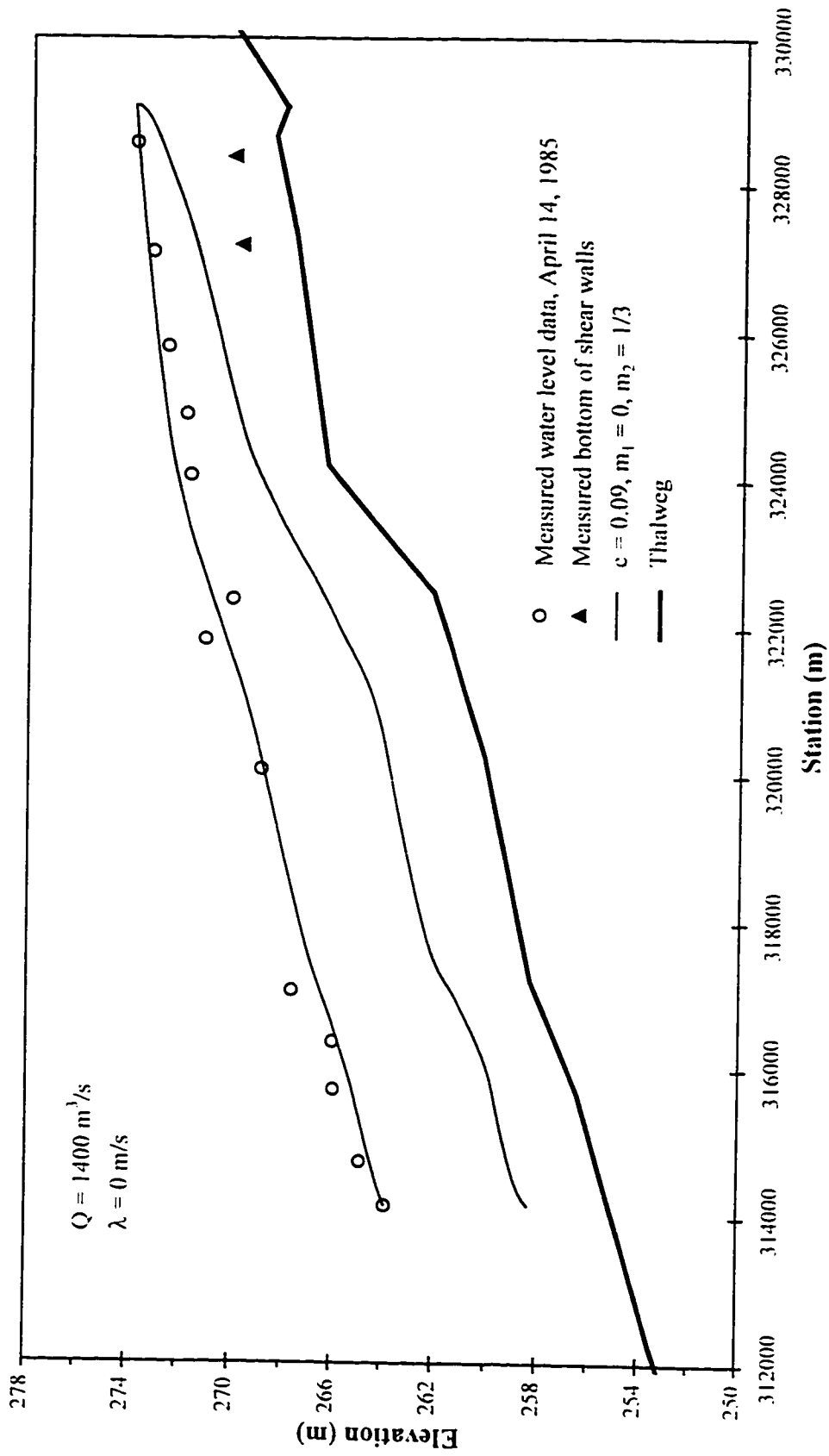


Figure 4.54. April 14, 1985 Athabasca River ice jam as predicted by RIVIAM using Beltaos' Mannings approximation.

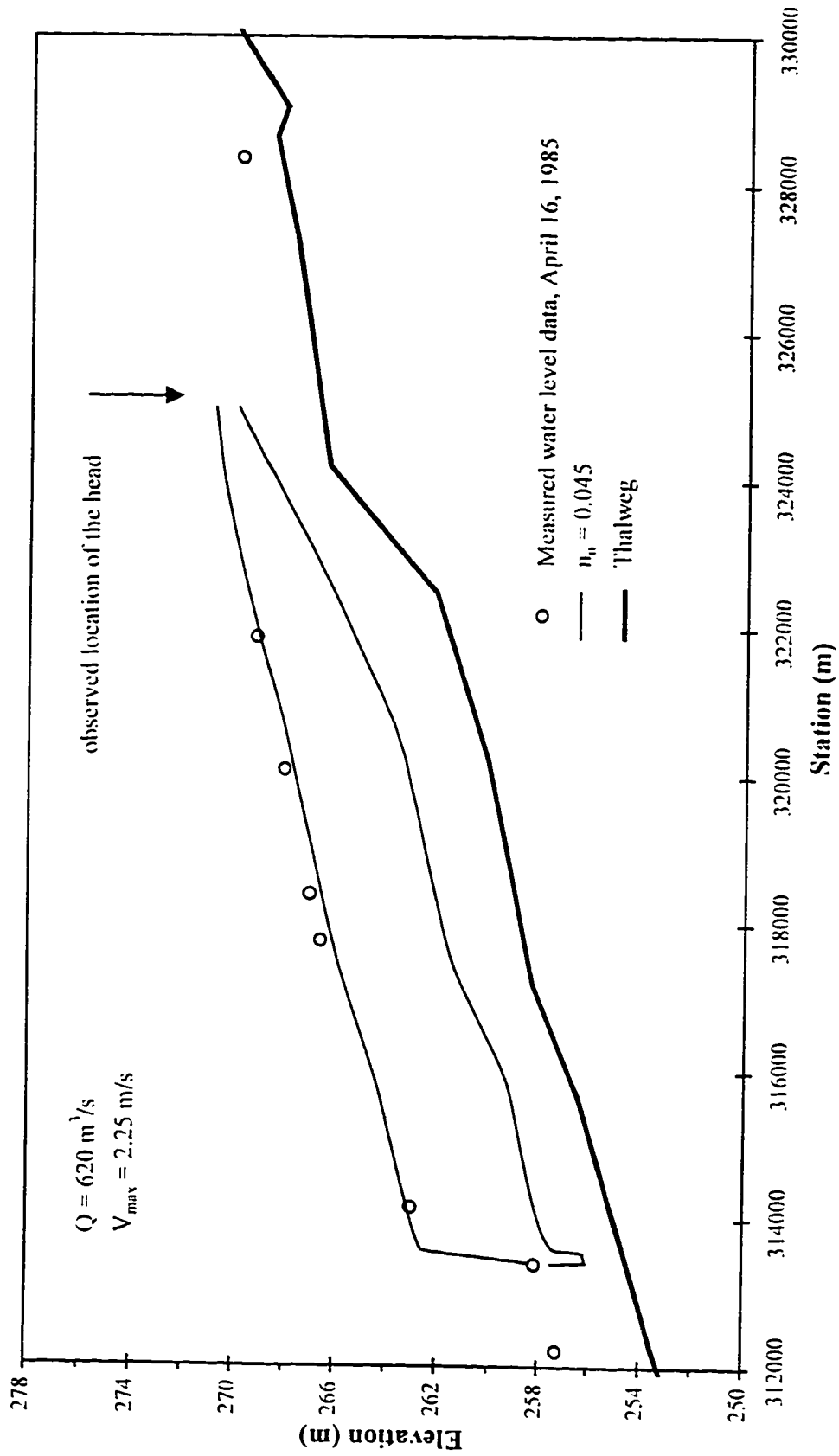


Figure 4.55. April 16, 1985 Athabasca River ice jam as predicted by ICF:JAM using Mannings equation.

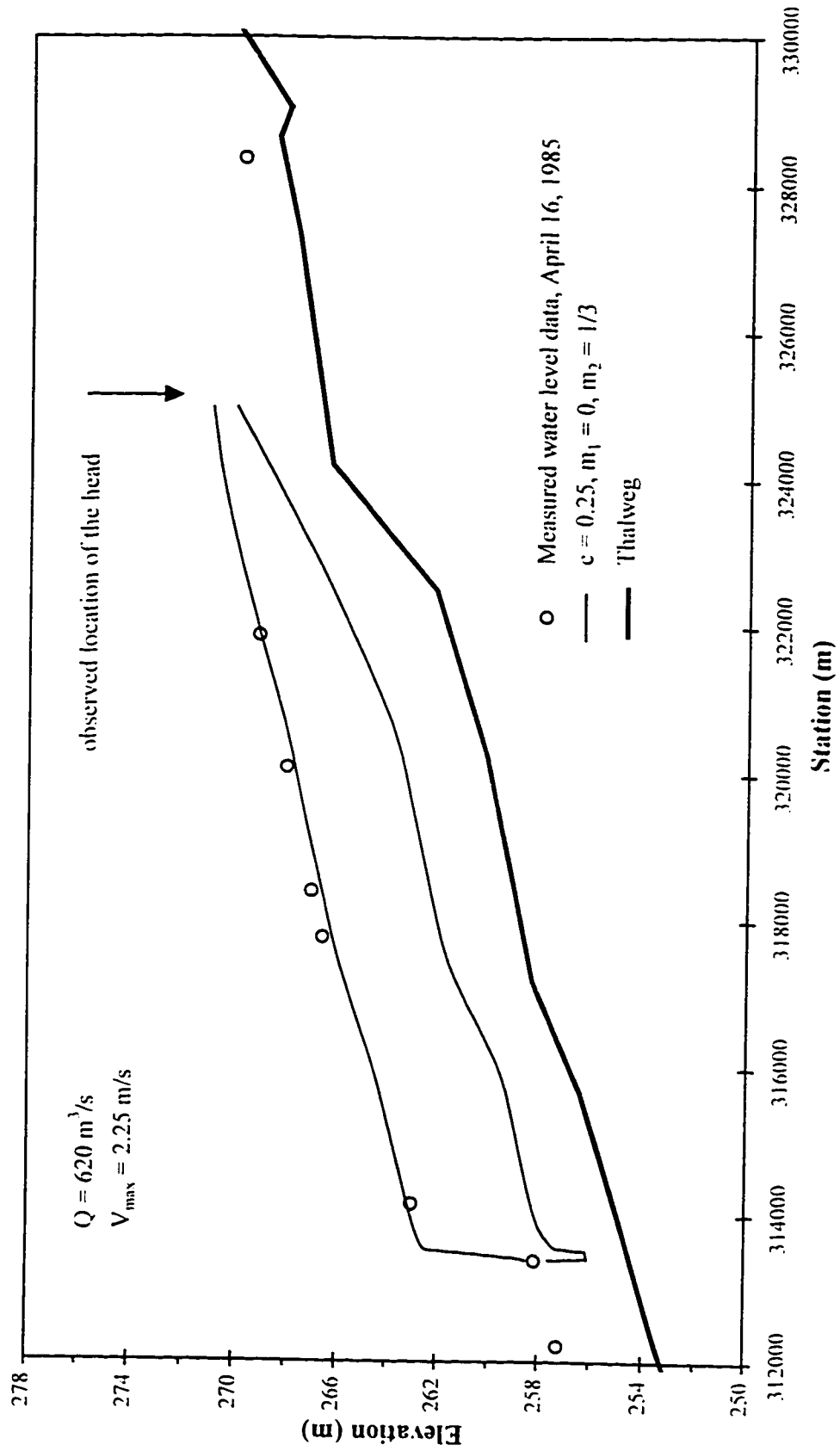


Figure 4.56. April 16, 1985 Athabasca River ice jam as predicted by ICEJAM using Beltaos' Mannings approximation.

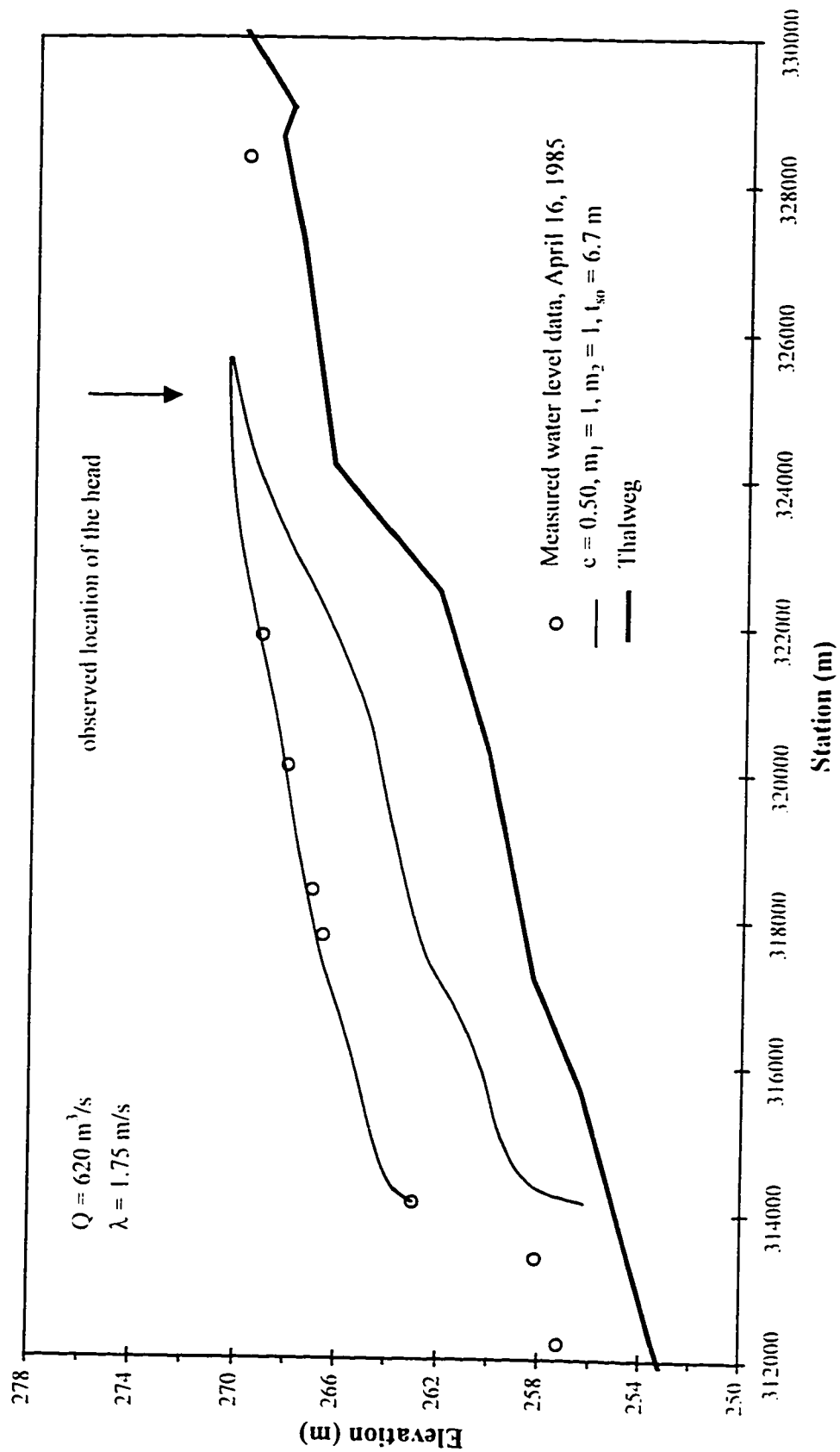


Figure 4.57. April 16, 1985 Alhabasca River ice jam as predicted by RIVJAM using Beltaos' friction factor.



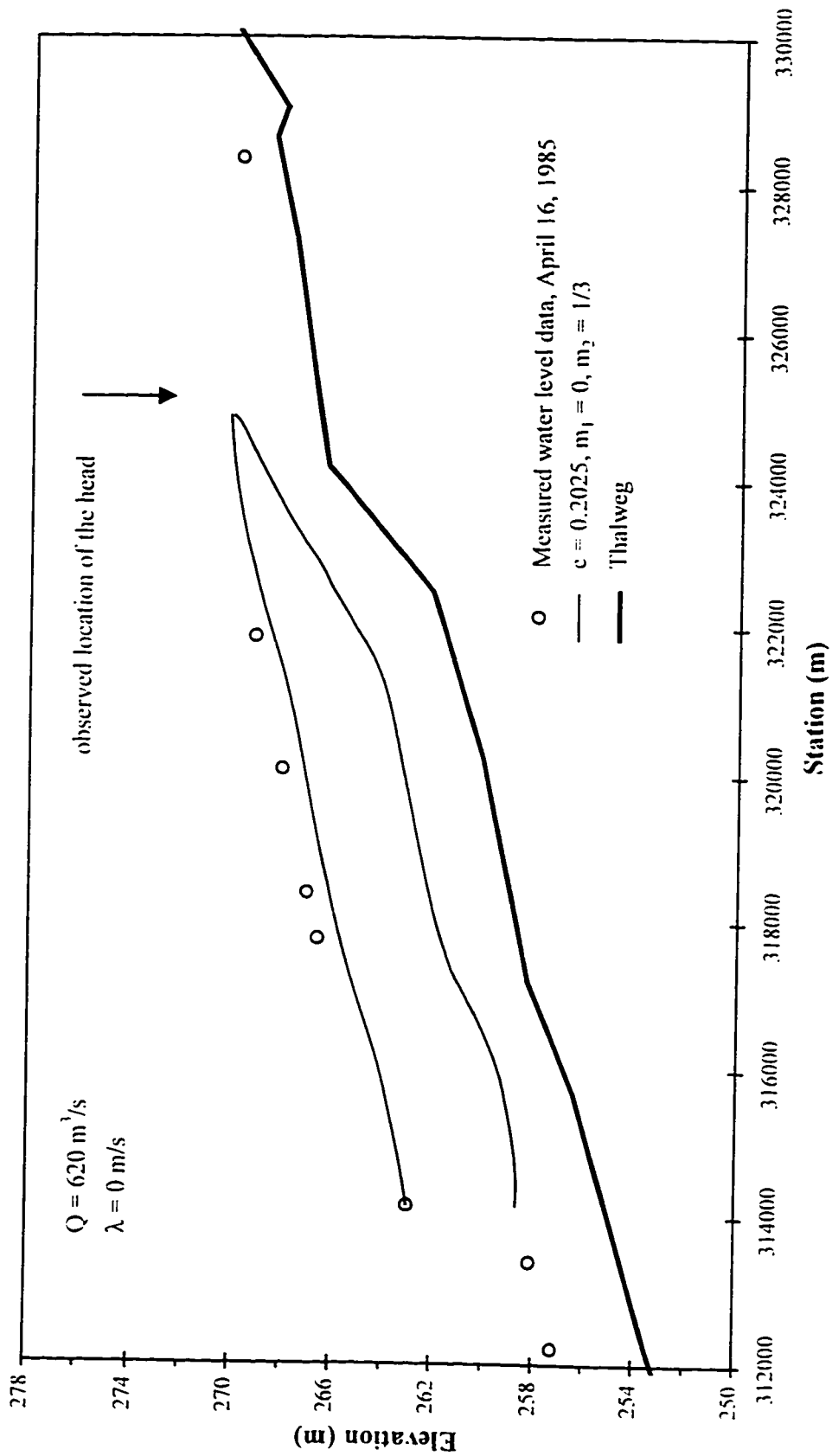


Figure 4.58. April 16, 1985 Athabasca River ice jam as predicted by RIVJAM using Beltaos' Mannings approximation.

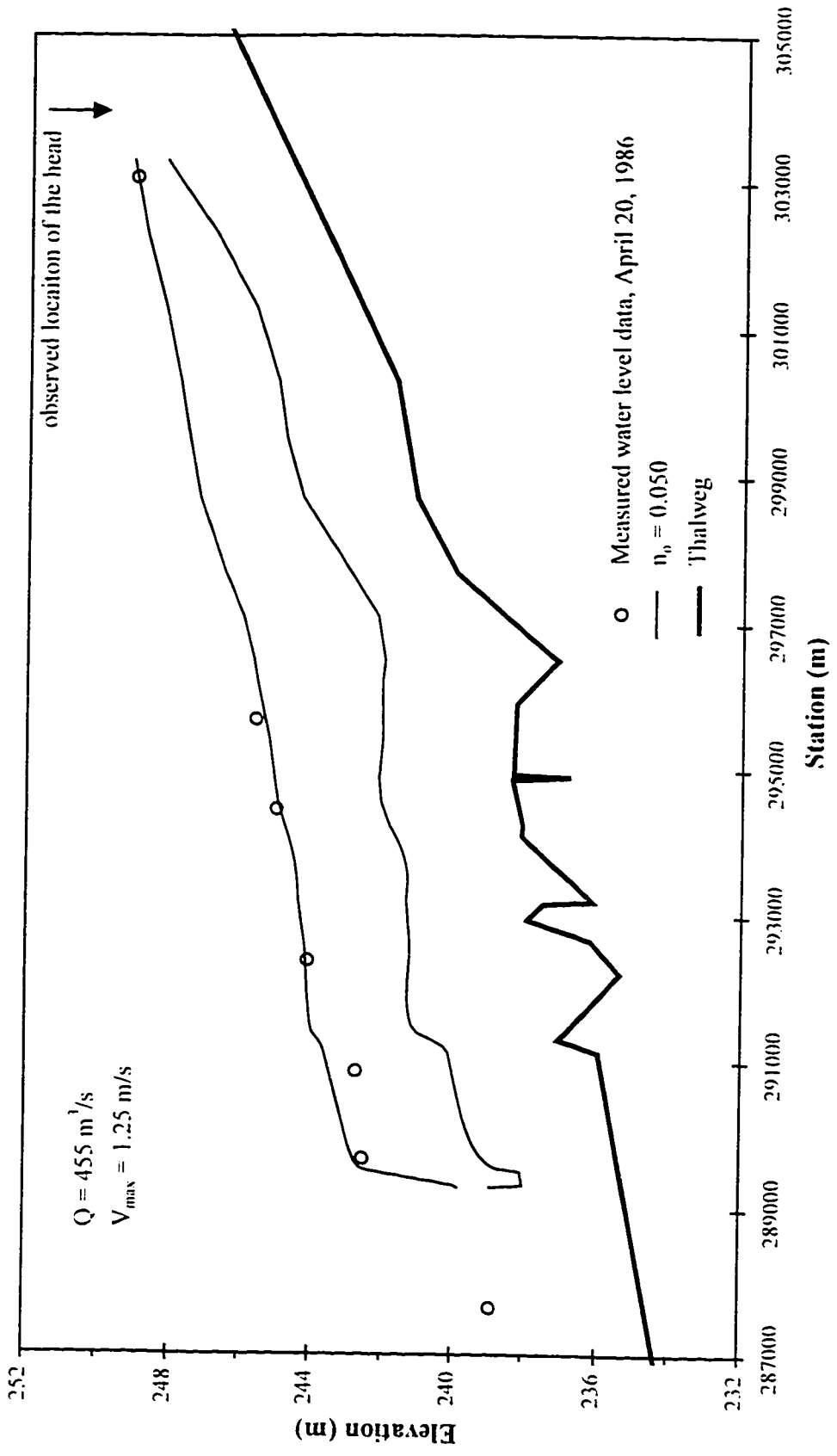


Figure 4.59. April 20, 1986 Athabasca River ice jam as predicted by ICEJAM using Mannings equation.

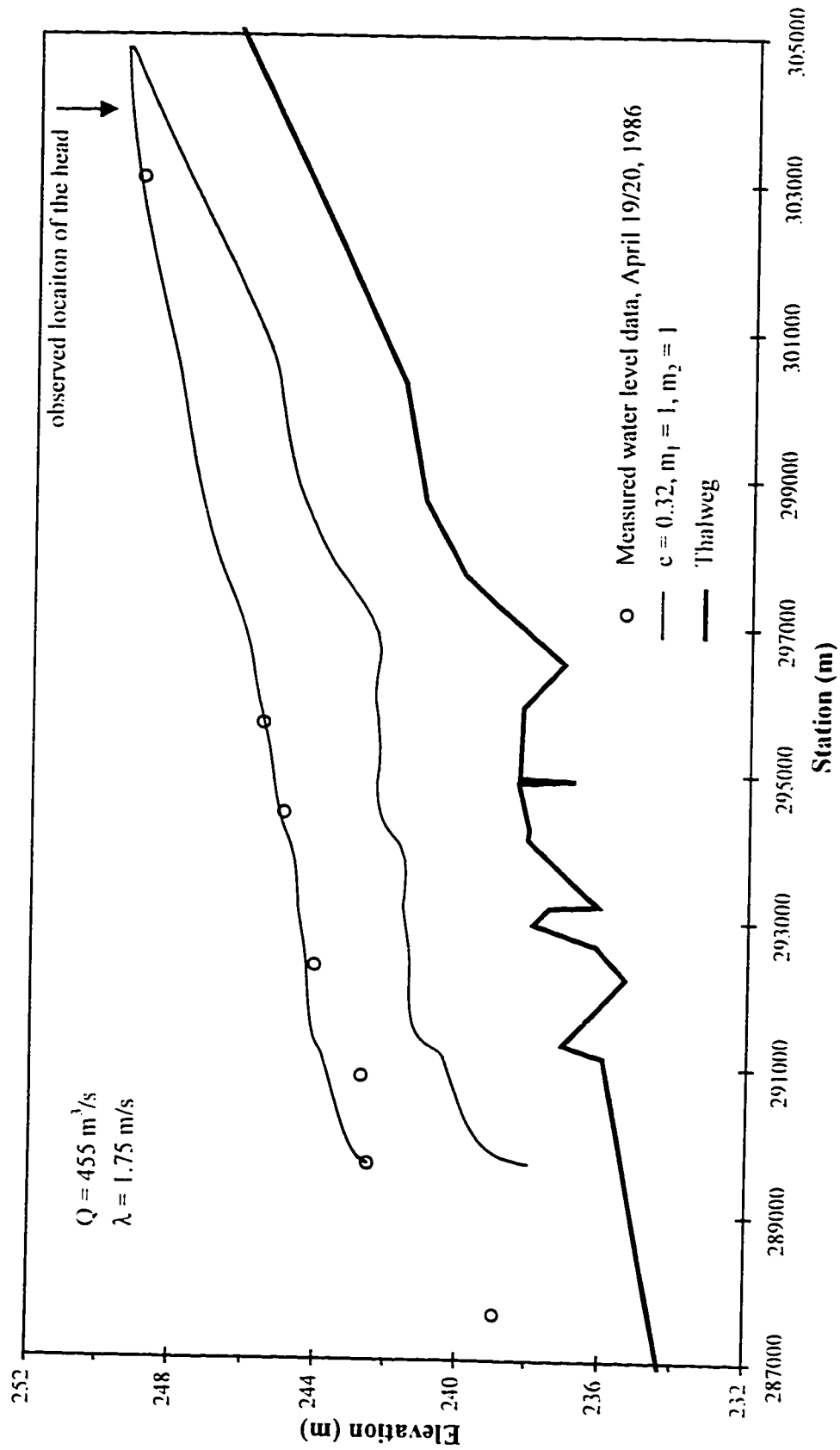


Figure 4.60. April 20, 1986 Athabasca River ice jam as predicted by RIVJAM using Beltaos' friction factor.

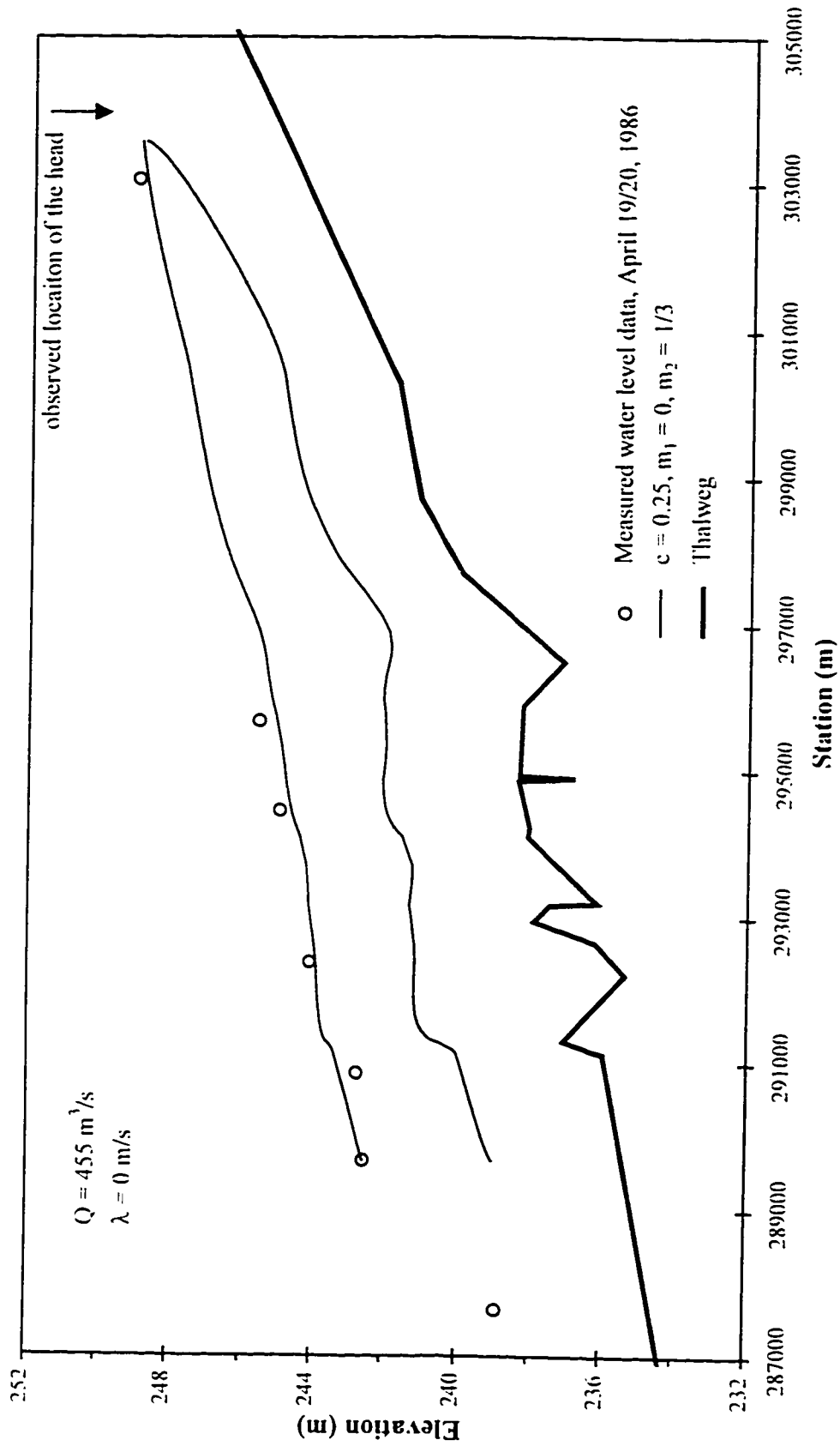


Figure 4.61. April 20, 1986 Athabasca River ice jam as predicted by RIVJAM using Beltaos' Mannings approximation.

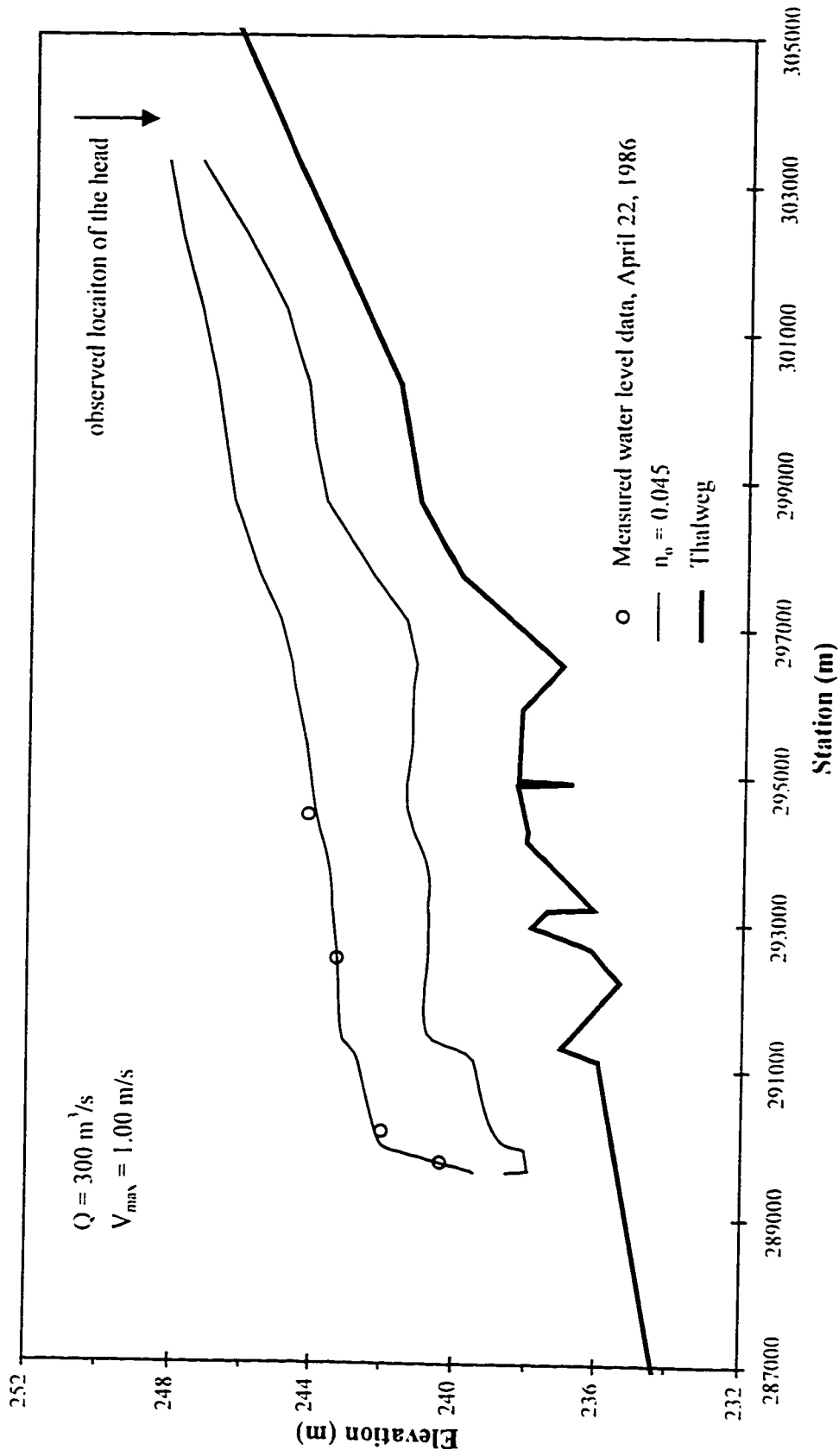


Figure 4.62. April 22, 1986 Athabasca River ice jam as predicted by ICJAM using Mannings equation.

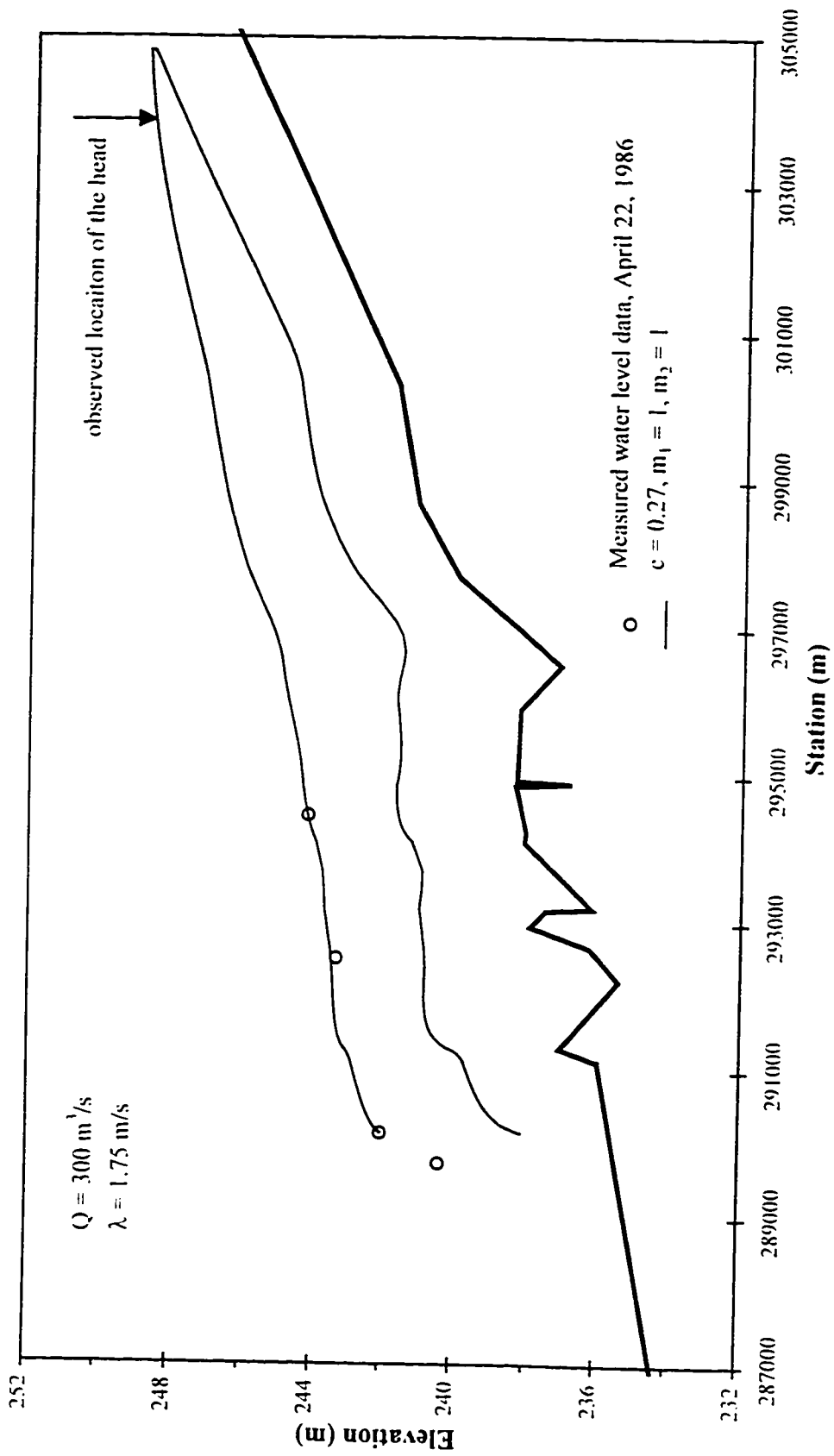


Figure 4.63. April 22, 1986 Athabasca River ice jam as predicted by RIVJAM using Bellaos' friction factor.

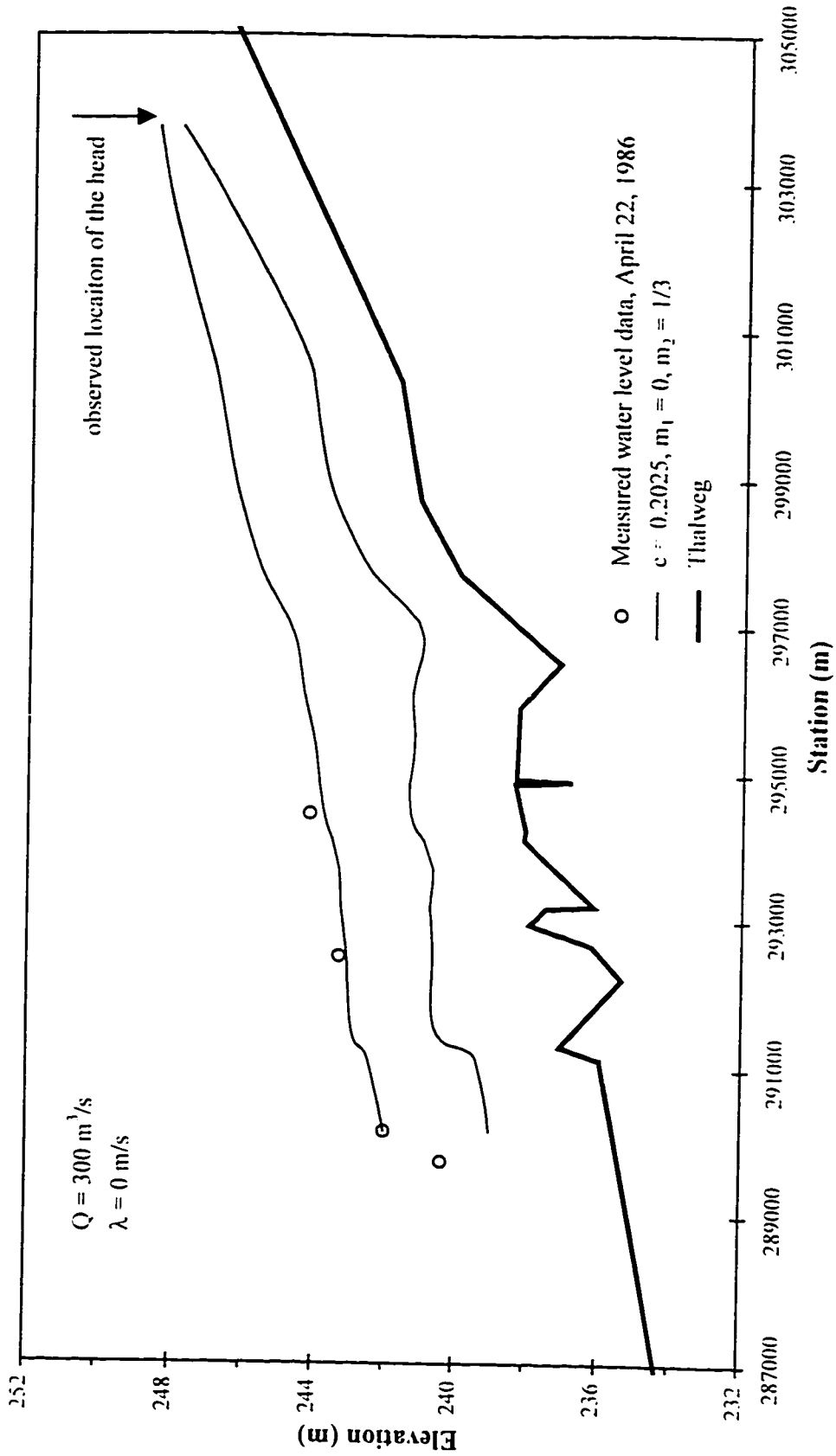


Figure 4.64. April 22, 1986 Athabasca River ice jam as predicted by RIVJAM using Beltaos' Mannings approximation.

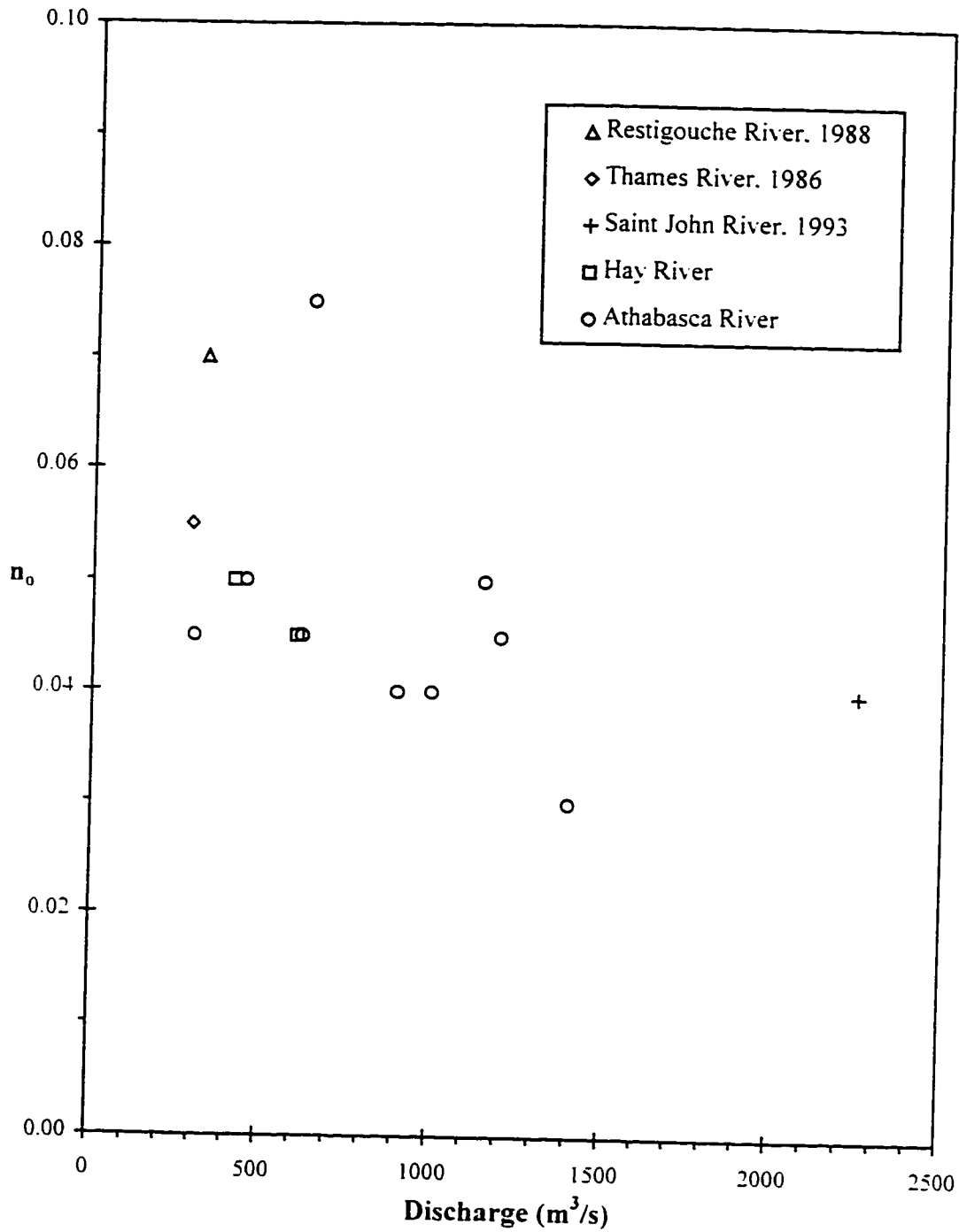


Figure 4.65. Discharge versus calibrated composite roughness.



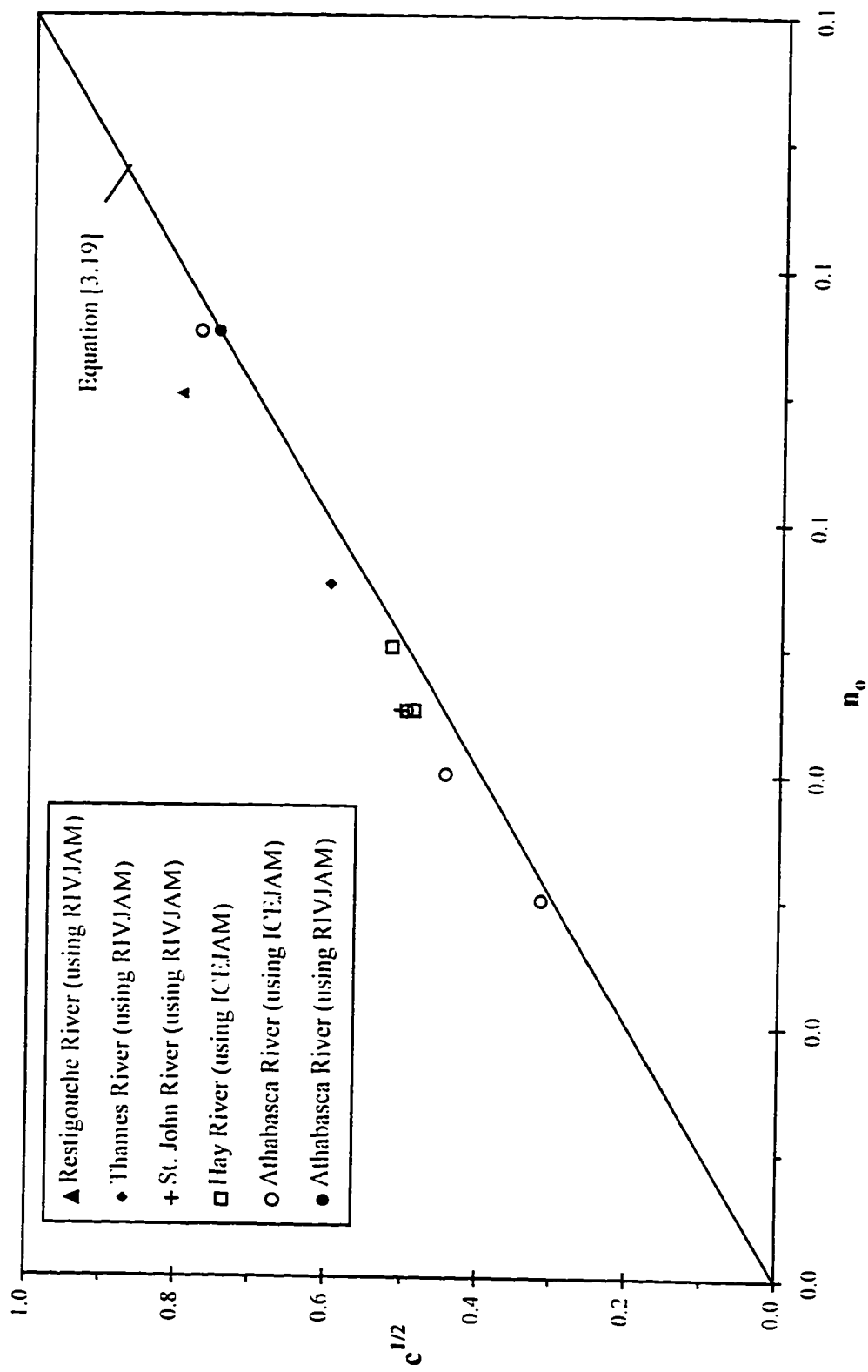


Figure 4.66 Comparison of Mannings  $n_0$  to Beltaos' friction factor equivalent to Mannings  $n_0$ .

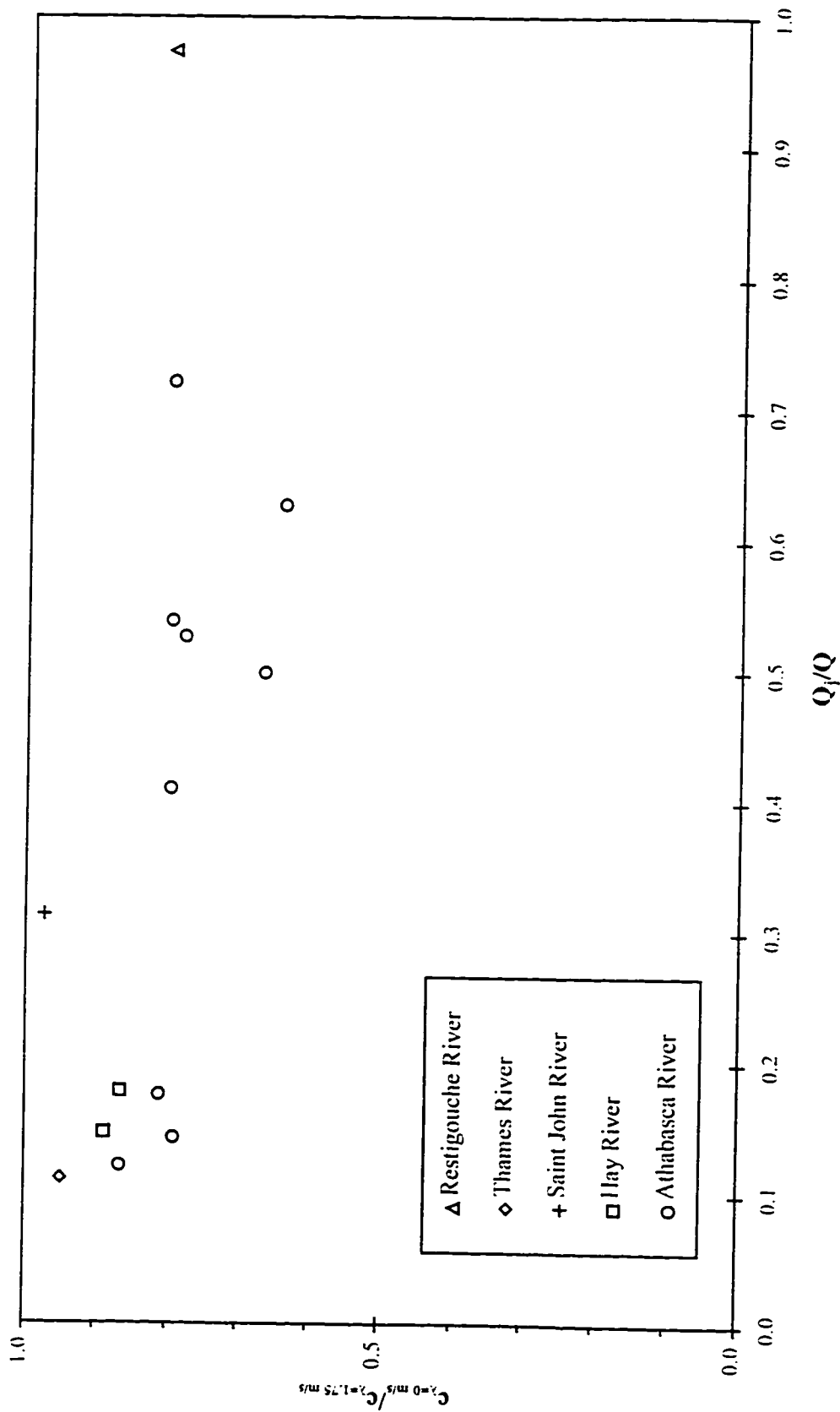


Figure 4.67 Ratio of the flow through interstices versus roughness ratio.

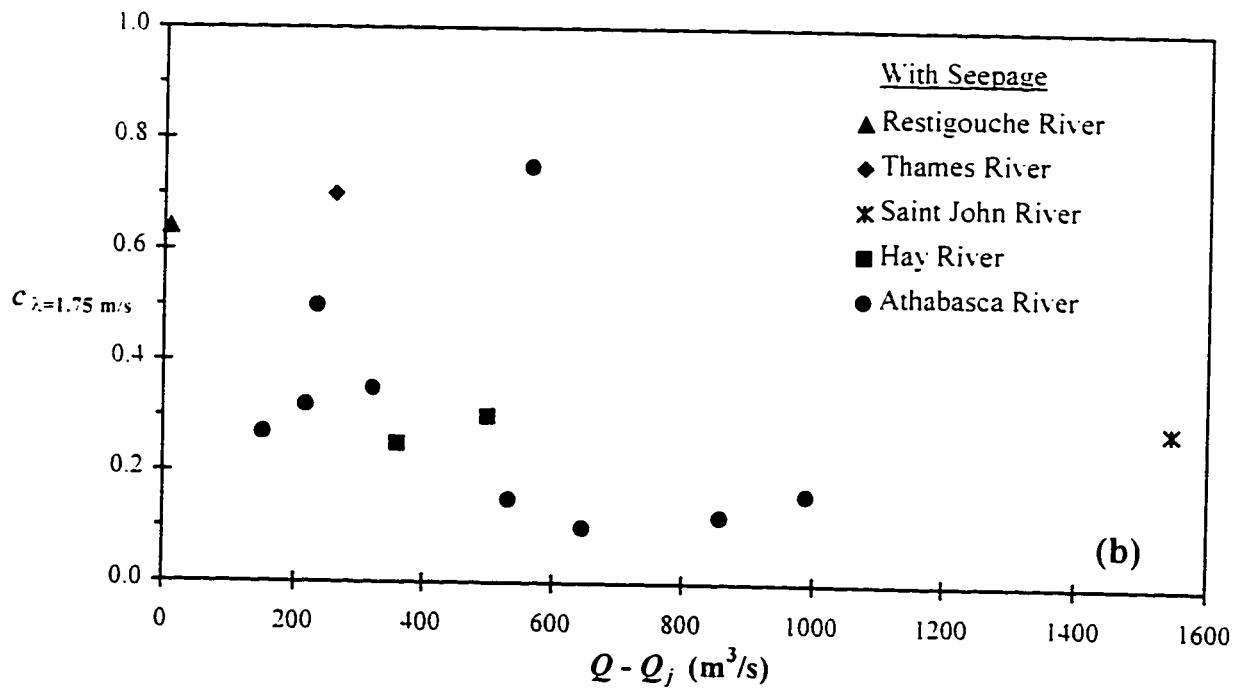
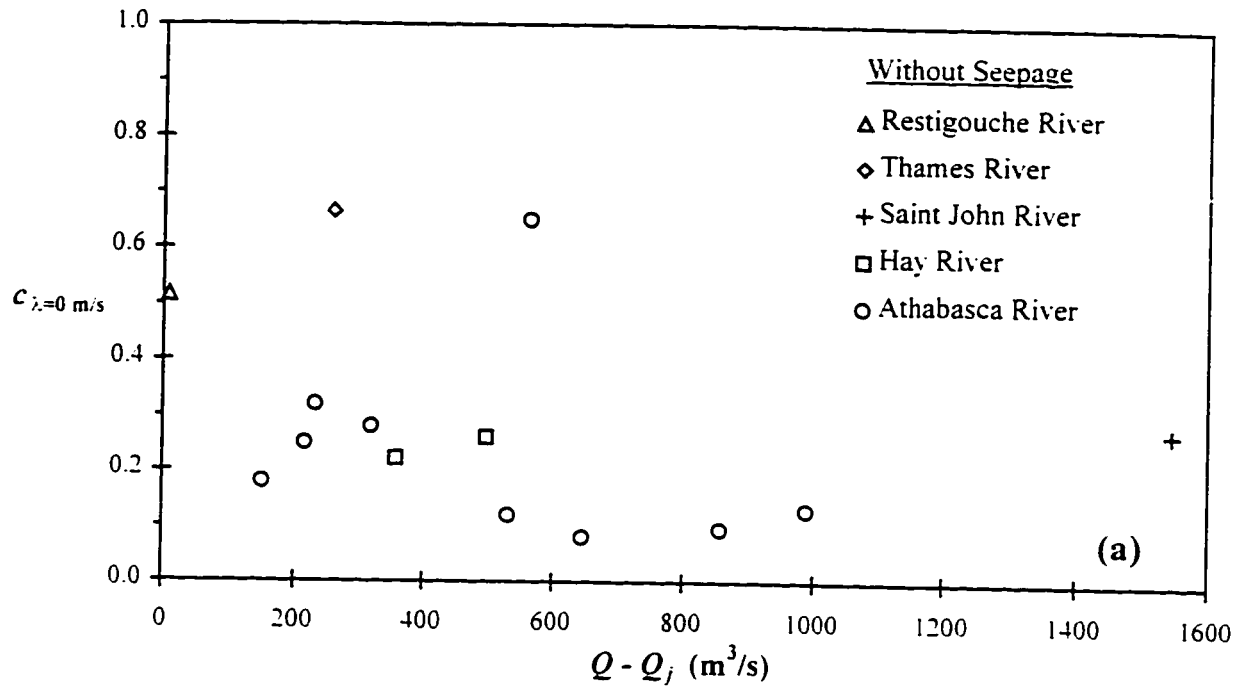


Figure 4.68. Variation in Beltaos' friction factor,  $c$ , where (a) seepage is neglected, and (b) seepage is included.

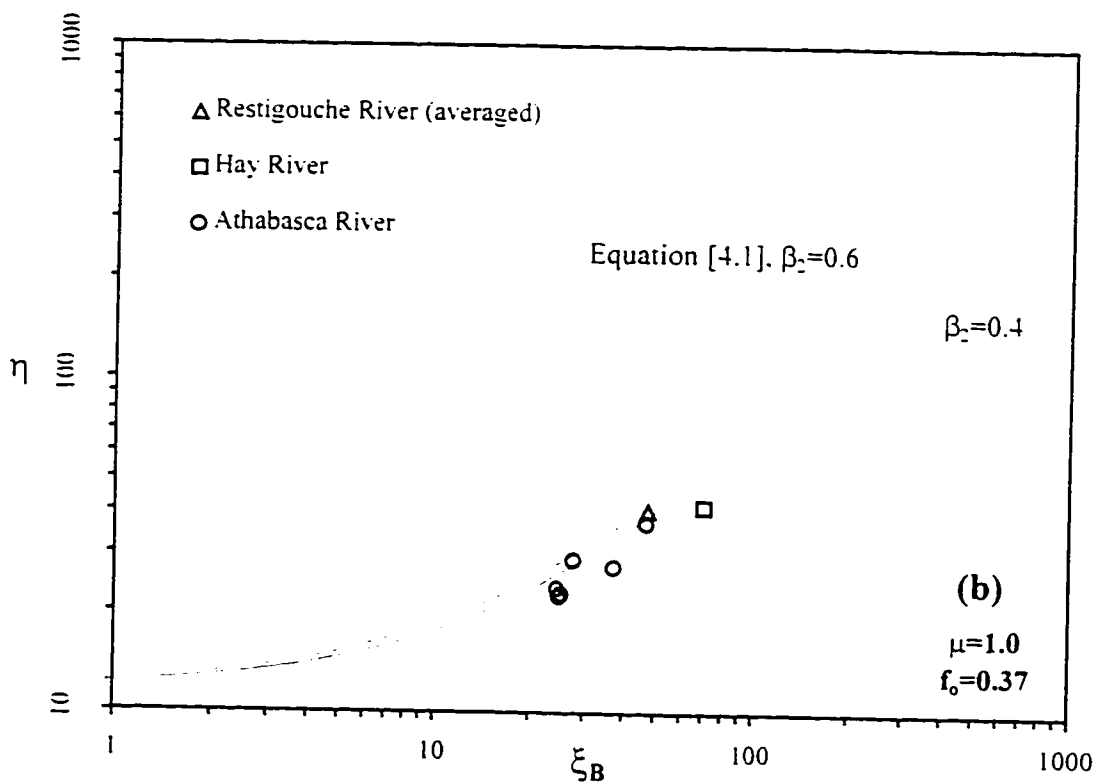
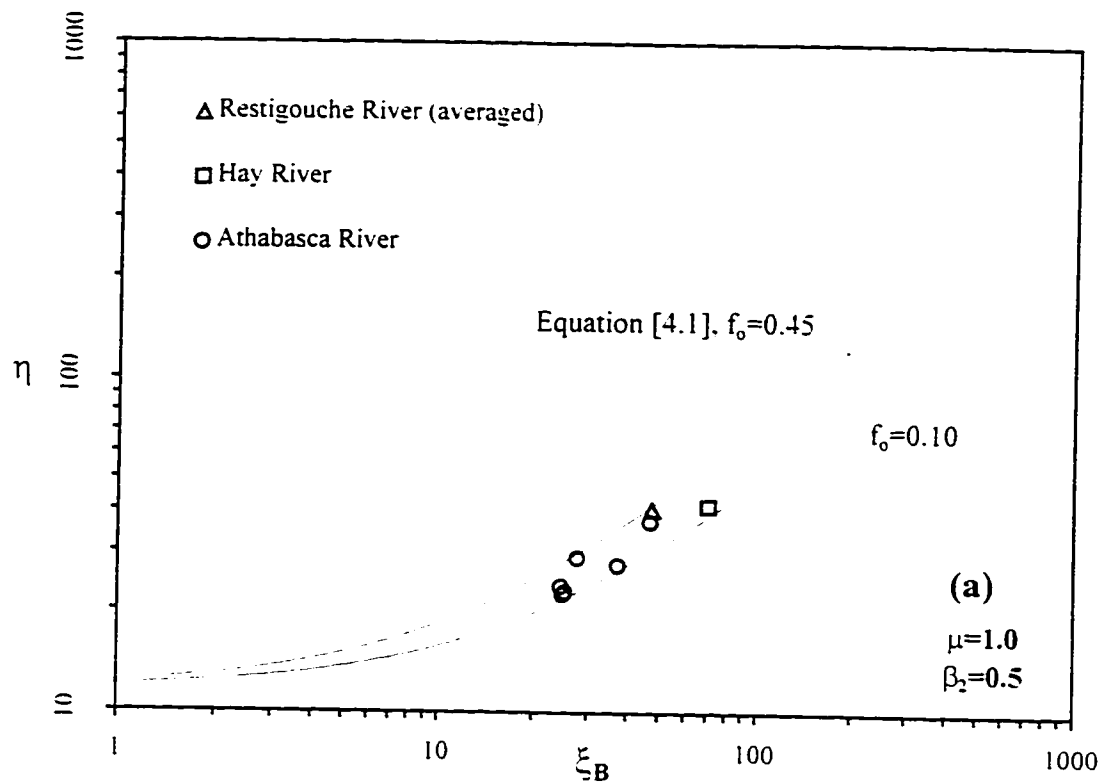


Figure 4.69. Non-dimensional depth versus discharge for (a) Beltaos' friction factor and (b) variation in under ice to composite roughness.

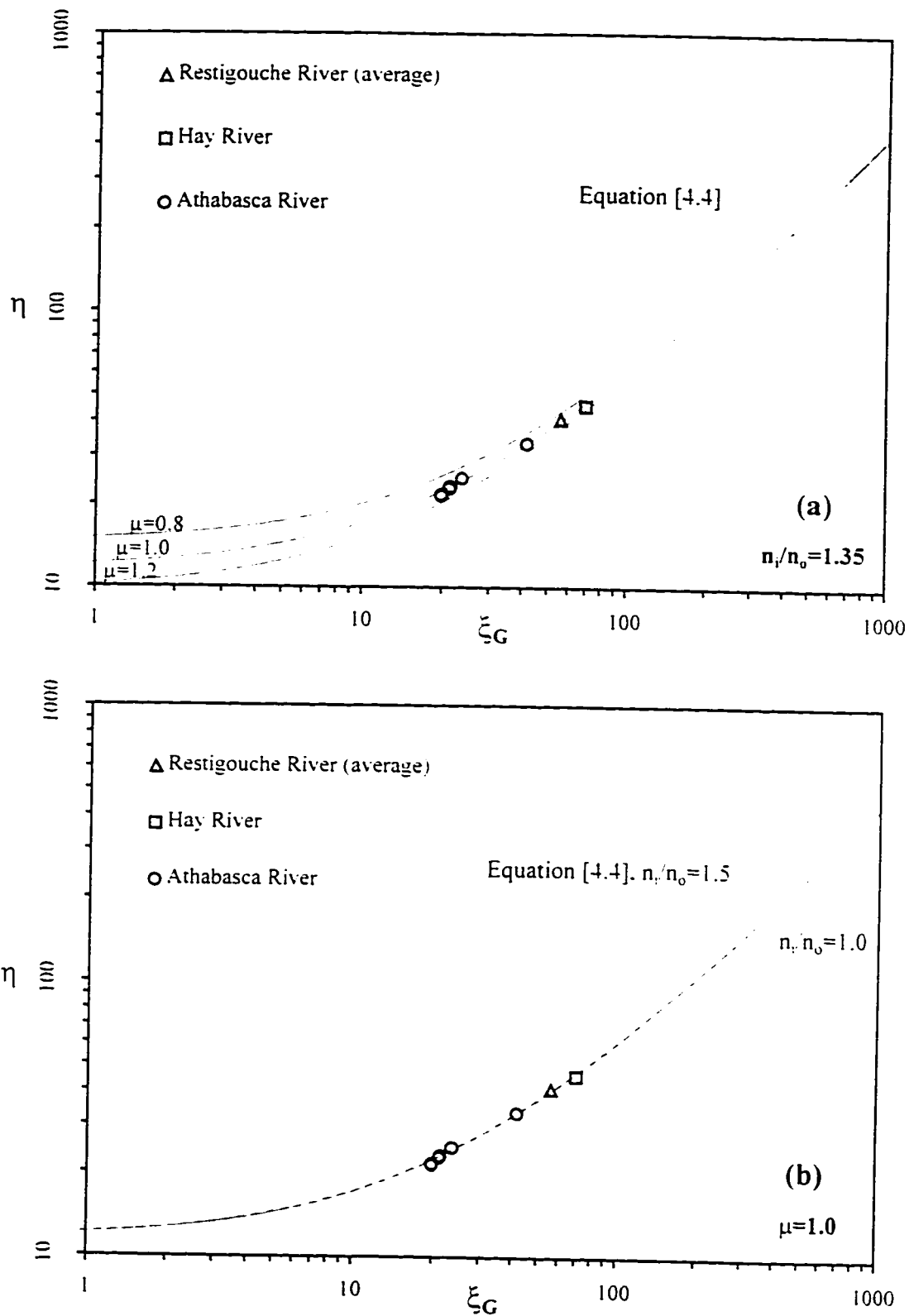


Figure 4.70. Non-dimensional depth versus discharge for (a) Mannings roughnes and (b) variation in under ice to composite roughness.

## CHAPTER 5.0 CONCLUSIONS AND RECOMMENDATIONS

The objectives of this study were to compare the RIVJAM and ICEJAM models and explore their suitability as tools to assist in the determination of flood levels that may be expected under ice jam conditions and to aid in the study of ice jam characteristics. In order to assess the ability of the models to meet these objectives, their formulations and implementation techniques were compared both analytically, and empirically (through the application to idealized and natural channels). The intent was to present the relative merits and limitations of these models in a practical manner and also to provide advice on the efficient use. Through the analysis of these models the following conclusions and recommendations were drawn.

### **5.1 VERIFICATION OF THE PHYSICS DESCRIBING ICE JAM MECHANICS**

Both models computed ice jam profiles which closely resembled those documented in the field. Therefore the jam stability equation coupled with a gradually varied flow approximation adequately described the shape of ice jams under steady state conditions. The primary assumption inherent in the derivation of the jam stability equation that a breakup ice jam can be treated as a cohesionless granular mass is supported, which facilitates the application of basic soil mechanics theory to ice jam analysis.

## 5.2 IMPORTANCE OF CARRIER DISCHARGE

Carrier discharge is commonly used to represent the discharge through an ice jam that is assumed to be under steady state conditions. It is difficult to obtain accurate estimates of the carrier discharge because of safety and logistical issues. However, good discharge estimates are essential for successful application of the ICEJAM and RIVJAM models, because as was illustrated in the Saint John River case study, both models were found to compute very different ice jam profiles for variable discharges. Discharge had a noticeable impact on the values of calibrated composite roughnesses obtained with these models.

## 5.3 PRACTICAL APPLICATION OF RIVJAM AND ICEJAM

With current technology, it is not possible to collect data on ice jam strength characteristics (which describe shear strength, internal friction, and porosity) directly in the field. Therefore, models like ICEJAM and RIVJAM provide the only means for investigating these ice jam characteristics.

Techniques for the practical application of these models were developed. In addition to the standardized modelling procedure outlined by the calibration protocols, the following salient observations should provide assistance to users of these models.

1. During the sensitivity analysis for a prismatic channel, the rigorous analysis of a natural channel, and the analysis of equilibrium ice jams, the computed, or calculated thickness and depth of flow appeared to be relatively insensitive to the jam strength coefficient  $\mu$  within the ranges suggested in the literature (i.e.  $\mu = 0.8$  to 1.2). For practical application of the models, this coefficient can be set to the average of the range of suggested values in the literature (i.e.  $\mu = 1.0$ ).
2. During the sensitivity analysis for a prismatic channel and in the analysis for equilibrium ice jams, the calculated thickness and depth of flow were shown to be

relatively insensitive to the ratio of ice cover to composite roughness ratio,  $\beta_2$ , within the ranges suggested in the literature (i.e.  $\beta_2 = 0.4$  to  $0.6$ ). For practical application of the models, this coefficient can be set to the average of the range of suggested values in the literature (i.e.  $\beta_2 = 0.5$ ).

3. During the sensitivity analysis for a prismatic channel, and the rigorous analysis of a natural channel, the computed ice jam thickness and depth of flow appeared to be relatively insensitive to the Mohr Coulomb internal strength coefficients,  $K_x$  (for RIVJAM) and  $K_v$  (for ICEJAM), within the ranges suggested in the literature (i.e.,  $K_x$  or  $K_v = 8$  to  $12$ ). For practical application of the models, this coefficient can be set to the average of the range of suggested values in the literature (i.e.  $K_x = K_v = 10$ ).
4. In the absence of ice jam toe thickness data, the specified thickness at the downstream boundary becomes an important calibration parameter in the RIVJAM model. The ICEJAM model is less sensitive to estimates of the specified thickness boundary condition (at the head of the accumulation) as gradients in the solution are typically much larger near the toe than near the head.
5. Although the assumed toe configuration used in the ICEJAM model expedites the transition to the jam stability equation, the resulting shape is not entirely consistent with field observations of natural occurrences, particularly when the toe is grounded.
6. Inspection of Beltaos' friction factor indicated that for equilibrium jams, the roughness coefficient becomes a constant (since the depth of flow and ice thickness remain constant). Beltaos (1997) indicated that for ice thicknesses greater than approximately 3 m, the roughness no longer varies with the jam thickness. This effect was illustrated during the Restigouche River case study.



## 5.4 RECOMMENDATIONS

More complete data describing the thickness profiles of ice jams would assist in the quantification of ice jam characteristics. However, with current field techniques the ability to improve the quality and quantity of such data seems unlikely. Therefore, it is recommended that new technologies for measuring ice jam thickness data be pursued.

Prior knowledge of the length of the jam associated with the "wide" channel jam defined by Pariset, *et al.* (1966) was required for successful calibration of these models. Therefore, during field investigations of ice jams the mode of formation must be documented in greater detail (i.e. beyond simply noting the point at which the upstream limit of the ice accumulation meets open water). If it is not possible to identify the mode of formation under current techniques, then it is recommended that as a minimum, the appearance of the surface of the ice accumulation be documented in detail, using a standardized terminology. This may lead to improved methods for determining the mode of formation.

As both models were found to be very sensitive to variations in discharge, it is recommended that the models not be used to determine discharge through a calibration process since roughness and all other ice jam parameters are also unknown in such cases. Discharge estimates should be based on data collected in the field during the recorded event and it is recommended that at least two discharge estimates be obtained by separate methods to better quantify the quality of the discharge estimates.

No attempts to describe the physics of the toe region of an ice jam are expressed in the literature. For the reasons discussed earlier, this region does not behave (physically) like the upstream floating accumulation of ice (which is adequately represented by basic principles of soil mechanics). Therefore it is recommended that

future research effort be directed towards a better understanding of the physics of the toe region.

It is recommended that new or improved versions of the existing models which include unsteady effects combined with the already well established ice jam stability relationships be explored. In addition, the development of two dimensional models would handle the effects of channel topography explicitly (which for one-dimensional models are "lumped" into roughness), and facilitate the study of documented ice jam events which occur in reaches with islands.

Finally, the RIVJAM model is preferred over the ICEJAM model for the following three reasons:

1. The RIVJAM model includes seepage which is known to occur in ice jams (particularly for grounded ice accumulations) and if ice jam models are to be used to explore ice jam characteristics, then models describing more ice jam processes should be preferred.
2. In contrast to the ICEJAM model, the length of the computed ice jam is not forced by the RIVJAM model to a specific value prior to computation. It is essentially an output parameter, and this feature of the RIVJAM model can be used to explore potential locations of the upstream limit of the ice jam exhibiting "wide" channel behaviour where this location is unknown.
3. The RIVJAM model is supported by the Federal government and its continued development is expected. The RIVJAM model is intended for practical application, and has been tested against a variety of case studies and the results of these tests in addition to other supported information has been documented. In contrast, there is limited documentation on the ICEJAM model which was primarily developed as a research tool and no further enhancements are expected.

## REFERENCES

- Andres, D.D. 1996. Review of WSC Border gauge discharge estimates. Consulting Engineering Report, Trillium Engineering and Hydrographics Inc., 23 p.
- Andres, D.D., and Rickert, H.A. 1985a. Observations of breakup in the Athabasca River upstram of Fort McMurray, Alberta, 1984. Alberta Research Council, Report No. SWE 85-09.
- Andres, D.D., and Rickert, H.A. 1985b. Observations of the 1985 breakup in the Athabasca River upstram of Fort McMurray, Alberta, 1985. Alberta Research Council, Report No. SWE 85-10.
- Ashton, G.D. 1986. River and lake ice engineering. Water Resources Publications, Littleton, Colorado, 485 p.
- Beltaos, S. 1978. Field investigation of river ice jams. IAHR Symposium on Ice Problems, Lulea, Sweden, pp. 355-371.
- Beltaos, S. 1979. Flow resistance of fragmented ice covers (ice jams). Canadian Hydrology Symposium, Vancouver, Canada (NRCC No. 17834), pp. 93-126.
- Beltaos, S. 1983. River ice jams: theory, case studies, and applications. ASCE Journal of Hydraulic Engineering, 109(10): 1338-1359.
- Beltaos, S. 1988. Configuration and properties of a breakup jam. Canadian Journal of Civil Engineering, 15(4): 685-697.
- Beltaos, S. 1989. Quasi user's guide to the RIVJAM model. National Water Research Institute, Burlington, Ontario, 15 p.

- Beltaos, S. 1993. Numerical computation of river ice jams. *Canadian Journal of Civil Engineering*, 20(1): 88-99.
- Beltaos, S. 1995. River ice jams. Water Resources Publications, LLC, Highlands Ranch, Colorado, p. 372.
- Beltaos, S. 1997. Users guide for the RIVJAM model. National Water Research Institute, Burlington, Ontario (in press).
- Beltaos, S., and Burrell, B.C. 1990. Ice breakup and jamming in the Restigouche River, New Brunswick: 1987-1988 observations. National Water Research Institute, NWRI Contribution 90-169, 25 p.
- Beltaos, S., and Burrell, B.C. 1996. Case study of a grounded jam: Restigouche River, New Brunswick. *Northern Hydrology: Selected Perspectives*, NHRI Symposium No. 6, pp. 1-15.
- Beltaos, S., and Moody, W.J. 1986. Measurements on the configuration of a breakup jam. National Water Research Institute, NWRI Contribution 86-123, 37 p.
- Beltaos, S., and Wong, J. 1986. Downstream transition of river ice jams. *ASCE Journal of Hydraulic Engineering*, 112(2): 91-110.
- Beltaos, S., Burrell, C., Ismail, S. 1994. Ice sedimentation processes in the Saint John River, Canada. *IAHR Symposium, Trondheim 1994*, pp. 11-21.
- Calkins, D.J. 1983. Ice jams in shallow rivers with floodplain flow. *Canadian Journal of Civil Engineering*, 10(2): 538-548.
- Cheng, S.T., and Tatincluax, J.C. 1977. Compressive and shear strengths of fragmented ice cover: a laboratory study. *IIHR Report No. 206*, 82 p.
- Craig, R.F. 1992. *Soil Mechanics*. Fifth Edition. Chapman and Hall, New York, 427 p.

- Demuth, M.N., Hicks, F.E., Prowse, T.D., and McKay, K. 1988. A numerical modelling analysis of ice jam flooding on the Peace/Slave River. Peace-Athabasca Delta. Peace Athabasca Delta Technical Studies Sub-component of Task F.2: Ice Studies, May 1996.
- Doyle, P.F., and Andres, D.D. 1978. 1978 breakup in the vicinity of Ft. McMurray and investigation of two Athabasca River ice jams. Alberta Research Council. Report No. SWE 78-5.
- Doyle, P.F., and Andres, D.D. 1979. 1979 spring breakup and ice jamming on the Athabasca River near Ft. McMurray. Alberta Research Council. Report No. SWE 79-05.
- Flato, G. 1988. Calculation of ice jam profiles. M.Sc. thesis submitted to the Department of Civil Engineering, University of Alberta, Canada. 176 p.
- Flato, G., and Gerard, R. 1986. Calculation of ice jam thickness profiles. Proceedings of Fourth Workshop on Hydraulics of River Ice. Montreal. pp. C3.1-C-3.25.
- Gerard, R. Stanley, S. 1988. Ice jams and flood forecasting. Hay River, N.W.T. Department of Civil Engineering, University of Alberta. Report 88-6. 175 p.
- Gerard, R. 1975. Preliminary observations of spring ice jams in Alberta. IAHR Symposium on Ice Problems. Hanover, pp. 261-273.
- Henderson, F.M. 1965. Open channel flow. The Macmillan Company, New York.
- Hicks, F., McKay, K., and Shabayek, S. 1997. Modelling an ice jam release surge on the Saint John River. New Brunswick. 9th Workshop on River Ice, Fredericton, September, 1997 (in press).

- Hicks, F.E., Steffler, P.M., and Gerard, R. 1992. Finite element modeling of surge propagation and an application to the Hay River, N.W.T. *Canadian Journal of Civil Engineering*, 19(3): 99-113.
- Holtz, R.D., and Kovacs, W.D. 1981. *An introduction to geotechnical engineering*. Prentice Hall, Inc., Englewood Cliffs, New Jersey, 733 p.
- IAHR Working Group on River Ice Hydraulics. 1986. *River ice jams: a state-of-the-art report*. IAHR Ice Symposium, Iowa City, pp. 561-594.
- International Mathematical and Statistical libraries Inc. 1980. *The IMSL Library*. Vol. 3. Houston, Texas.
- Ismail, S., and Davis, J.L. 1992. Ice jam thickness profiling on the Saint John River, New Brunswick. IAHR 11th Symposium, Banff, pp. 383-394.
- Janssen, H.A. 1974. Versuche uber getreidruck in silozellen. *Z. Ver. Dt. Ing.*, pp. 1045-1050.
- Kellerhals, R., Neill, C.R., and Bray, D.I. 1972. Hydraulic and geomorphic characteristics of rivers in Alberta. Research Council of Alberta, *River Engineering and Surface Hydrology*. Report No.72-1.
- Kennedy, J.F. 1975. Ice-jam mechanics. IAHR Symposium on Ice Problems, Hanover, pp. 143-164.
- Kennedy, R.J. 1958. Forces involved in pulpwood holding grounds. *Engineering Journal*. Vol. 41: 58-68.
- Kennedy, R.J. 1962. The forces involved in pulpwood holding grounds. Pulp and Paper Research Institute of Canada, Technical Reports Series, No. 292, 207 p.

- Malcovish, C.D., Andres, D.D., and Mostert, P. 1988. Observations of breakup on the Athabasca River near Fort McMurray, 1986 and 1987. Alberta Research Council. Report No. SWE 88-12.
- Michel, B. 1978. Ice accumulations at freeze-up or break-up. IAHR Symposium on Ice Problems, Lulea, Sweden. Part 2, pp. 301-317.
- Moberly, H.J., and Cameron, W.B. 1929. When fur was king. J.M. Dent and Sons Ltd., Toronto, Canada, p. 151.
- Neil, C.R., and Andres, D.D. 1984. Freeze-up flood stages associated with fluctuating reservoir releases. Cold Regions Engineering Specialty Conference, Edmonton, Alberta, Canadian Society for Civil Engineering, Montreal, Canada, pp. 249-264.
- Nezhikhovskiy, R.A. 1964. Coefficients of roughness of bottom surface on slush-ice cover. Soviet Hydrology, Selected Papers, Washington, American Geographical Union, pp. 127-150.
- Pariset, E., and Hausser, R. 1961. Formation and evolution of ice covers in rivers. Transactions of the EIC, Vol.5(1): 41-49.
- Pariset, E., Hausser, R., and Gagnon, A. 1966. Formation of ice covers and ice jams in rivers. Journal of the Hydraulics Division, 92(HY6): 1-24.
- Stanley, S.J. 1988. Ice jam analysis in a complex reach: a case study. M.Sc. thesis presented to the Department of Civil Engineering, University of Alberta, Canada, 248 p.
- Tatinclaux, J.C. 1977. Equilibrium thickness of ice jams. Journal of the Hydraulics Division, 103(HY9): 959-974.
- Tatinclaux, J.C., and Cheng S.T. 1978. Characteristics of river ice jams. IAHR Symposium on Ice Problems, Lulea, Sweden, Part 2, pp. 461-475.

- Uzner, M.S., and Kennedy, J.F. 1974. Hydraulics and mechanics of river ice jams. IIHR, Report No. 161, 158 p.
- Uzner, M.S., Kennedy, J.F. 1976. Theoretical model of river ice jams. Journal of the Hydraulics Division, 102(HY9): 1365-1383.
- Uzuner, M.S. 1975. The composite roughness of ice covered streams. Journal of Hydraulic Research, 13(1): 79-102.
- Van Der Vinne, G., Prowse, T.D., and Andres, D. 1996. Economic impact of river ice jams in Canada. Northern Hydrology: Selected Perspectives, pp. 333-352.
- Wong, J., and Beltaos, S. 1985. Preliminary study of grounded ice accumulations. National Water Research Institute Contribution, Burlington, Ontario. pp. 8-09.
- Wong, J., Beltaos, S., and Krishnappan, B.G. 1985. Seepage flow through simulated grounded ice jam. Canadian Journal of Civil Engineering, 12(4): 926-929.
- Zufelt, E. 1996. Ice jam dynamics. Ph.D. thesis submitted to the Department of Civil and Environmental Engineering, University of Iowa. 203 p.



## **APPENDIX A**

Cross-section Interpolation Program

(INTERPO.FOR)

developed by:

Dan Healy,

Water Resources Engineering

University of Alberta

July, 1996.

## CONTENTS OF APPENDIX A

|   |     |
|---|-----|
| A-1.0 INTERPO.FOR - Cross-section Interpolation Program ..... | 255 |
| A-2.0 Interpolation Scheme .....                              | 255 |
| A-2.1 Approximating Surveyed Sections .....                   | 256 |
| A-2.2 Interpolating New Cross-sections .....                  | 256 |
| A-3.0 Input/Output File Formats .....                         | 257 |
| A-3.1 HEC2 File Format .....                                  | 257 |
| A-4.0 Parameter Description.....                              | 259 |
| Sample HEC2 Data File.....                                    | 262 |
| Source Code (FORTRAN).....                                    | 264 |

## A-1.0 INTERPO.FOR - Cross-section Interpolation Program

The cross-section interpolation program described herein was developed to provide an automatic means of generating cross-sections between surveyed or "known" cross-sections. Through interpolation between known cross-sections, based on a maximum spacing specified by the user, the effective number of computational nodes available for modelling is increased. The method of interpolation and a detailed description of the interpolation program (INTERPO.FOR) is described below. In addition, required input file formats will be outlined.

## A-2.0 Interpolation Scheme

Surveyed cross-sections typically provide a suitable number of x and y coordinates to adequately describe the channel section. The number of points describing a channel section varies for each surveyed cross-section. Cross-sections with equal number of points facilitate the ease of interpolation between the two cross-sections.

Furthermore, the points used for interpolation between sections should describe similar features of a cross-section. More specifically, a point should not be interpolated between a point in a *channel* from one cross-section and a point in the *floodplain* from another cross-section. To avoid this complication the surveyed cross-sections are first approximated by 46 points. 10 points for left overbank, 10 points for right overbank, and 25 points describe the channel section, and one point for closure.

Top of left and right bank locations are provided as input. Once the surveyed sections have been approximated, a simple linear interpolation between sections is carried out based on a user specified cross-section spacing. Details of the interpolation process are described below.

### **A-2.1 Approximating Surveyed Sections**

The first step in the interpolation scheme is to approximate the surveyed sections by the 46 points as mentioned above. Each of the floodplains (left and right) are divided into 10 equal spaces in the transverse direction. Elevations corresponding to these new locations are then assigned through linear interpolation between the surveyed points. In a similar manner the channel section is approximated by 25 evenly spaced points. Figure A-1 illustrates this process.

### **A-2.2 Interpolating New Cross-sections**

Once the surveyed sections have been approximated, new cross-sections are generated between the known cross-sections based on a user specified maximum spacing. The program determines the distance between “known” cross-sections from station data provided in the input file. Evenly spaced cross-sections are then generated between the “known” cross-sections whilst respecting the “maximum spacing” provided by the user. The generated cross-sections are obtained through direct interpolation between

the "known" cross-sections on a point by point basis (i.e. points 1 through 46).

(Figure A-2)

### A-3.0 Input/Output File Formats

INTERPO.FOR recognizes X1 and GR cards (HEC2 file format) as input. Similarly the output file generated by INTERPO.FOR is in a HEC2 file format. Parametric data and any other cards other than X1 and GR cards must be removed from the input file prior to running INTERPO.FOR. More details on the HEC2 file format are discussed below.

#### A-3.1 HEC2 File Format

Prior to interpolation, HEC2 files must be edited so that only cross-sectional data is included. In addition, each cross-section must be described by only one X1 card followed by the appropriate number of GR cards required to describe the cross-section. The program will recognize the same line formats used in HEC2 - that is (a2.f6.0.9f8.0). INTERPO.FOR reads in the data in a similar format, (t3,f6.0.9f8.0), ignoring the X1 and GR line descriptors. However, the X1 and GR descriptors are included when a HEC2 output file is written ('GR',t3,f6.2,9f8.2). The program reads only the first four entries in the X1 card corresponding to station identification, number of points in cross-section, x-coordinate of left bank, and x-coordinate of right

bank. Any entries in the X1 card beyond the fourth entry need not be removed however they will be ignored by INTERPO.FOR. Output files will only include the first four entries of the X1 card.

NOTE: Station identification will be interpreted to be the station (in metres) for that cross-section.

Sample X1 Card

|       |       |    |      |          |        |        |        |       |       |
|-------|-------|----|------|----------|--------|--------|--------|-------|-------|
|       |       |    |      |          |        |        |        |       |       |
| 0     | 1     | 2  | 3    | 4        | 5      | 6      | 7      | 8     | 9     |
|       |       |    |      | Column   |        |        |        |       |       |
|       |       |    |      | Location |        |        |        |       |       |
| <hr/> |       |    |      |          |        |        |        |       |       |
| X1    | 50000 | 23 | 0.00 | 764.32   | 500.00 | 500.00 | 500.00 | 00.00 | 00.00 |
|       |       |    |      |          |        |        |        |       |       |

Sample GR Card

|       |        |      |        |      |        |       |        |       |        |
|-------|--------|------|--------|------|--------|-------|--------|-------|--------|
|       |        |      |        |      |        |       |        |       |        |
| 0     | 1      | 2    | 3      | 4    | 5      | 6     | 7      | 8     | 9      |
| <hr/> |        |      |        |      |        |       |        |       |        |
| GR    | 240.00 | 0.00 | 214.36 | 1.00 | 214.07 | 24.73 | 205.78 | 48.43 | 204.25 |
|       |        |      |        |      |        |       |        |       |        |

A sample input file (HEC.DAT) is included in Appendix A.

## A-4.0 Parameter Description

A brief description of each parameter used in the program is described below.

| Parameter(s)    | Description   |
|-----------------|---|
| i,j,k,l         | counters used in loops  |
| input, output   | input and output file names   |
| infile,outfile  | identify input and output file types (eg. infile=1 for HEC2 format) |
| nxsec           | total number of cross-sections in data file                         |
| totxsec         | counts total cross-sections. including generated sections           |
| npts            | number of points in a cross-section                                 |
| sta             | station value in metres   |
| x,y             | x and y coordinates of a point in the cross-section                 |
| xint, yint      | x and y coordinates of approximated (interpolated) cross-sections   |
| xl,xr           | x coordinate of the left and right bank respectively                |
| lwidth, rwidth, | left overbank, right overbank, and channel widths respectively      |
| chwidth         |   |
| lspace, rspace, | left overbank, right overbank, and channel spacing respectively     |
| chspace         |   |
| dxmax           | user specified maximum spacing between cross-sections in metres     |
| dx              | actual spacing between cross-sections ( $dx \leq dxmax$ ) in metres |
| ndx             | number of equal spaces between two cross-sections                   |
| stadist         | distance between two stations used for interpolation                |
| rmdr            | remainder of stadist/dxmax (used for determining spacing, dx)       |
| known           | known value used when interpolating                                 |
| unknown         | value solving for when interpolating                                |
| xx.yy.xxl.xxr   | temporary values used for interpolation                             |

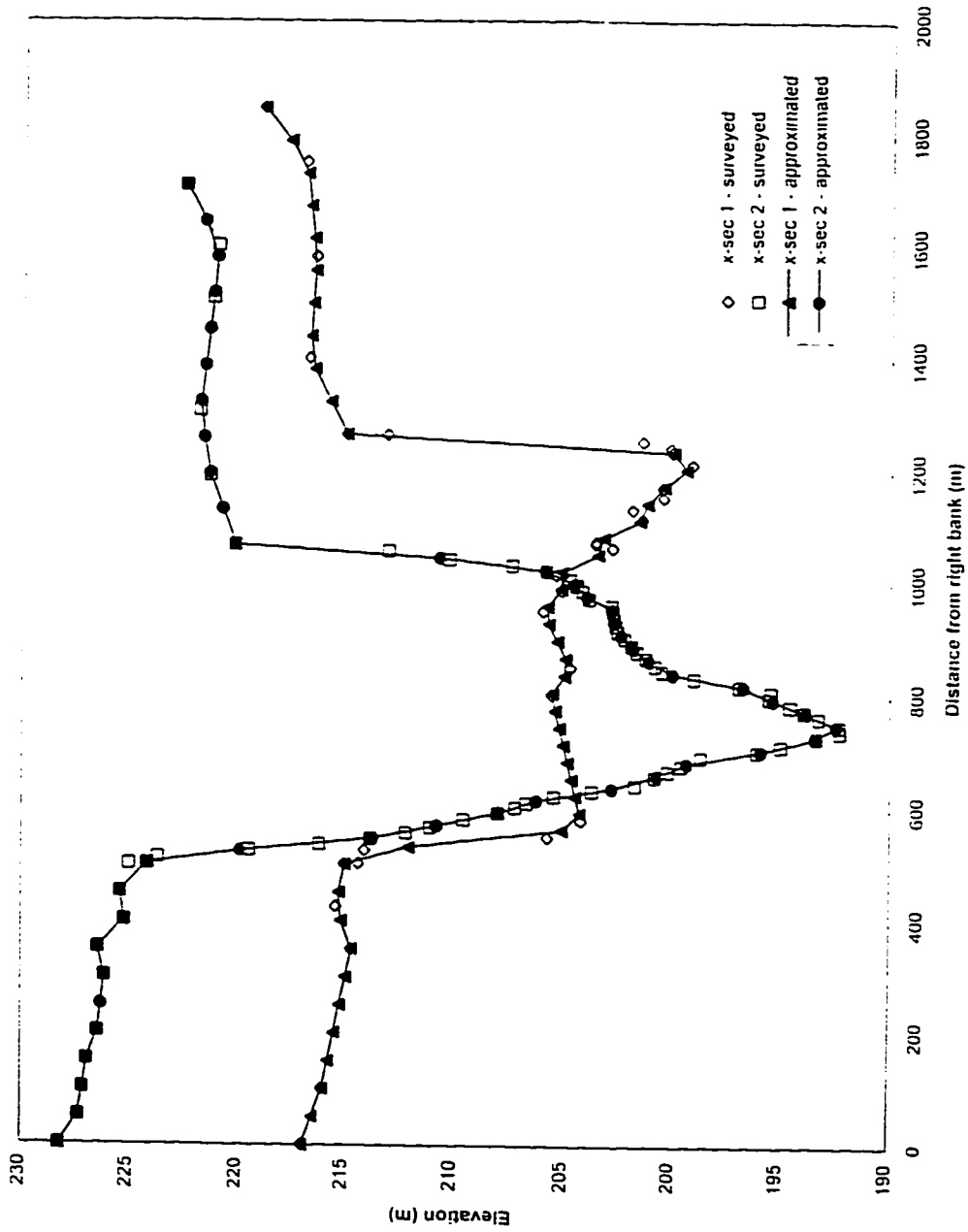


Figure A-1 Approximated surveyed sections.



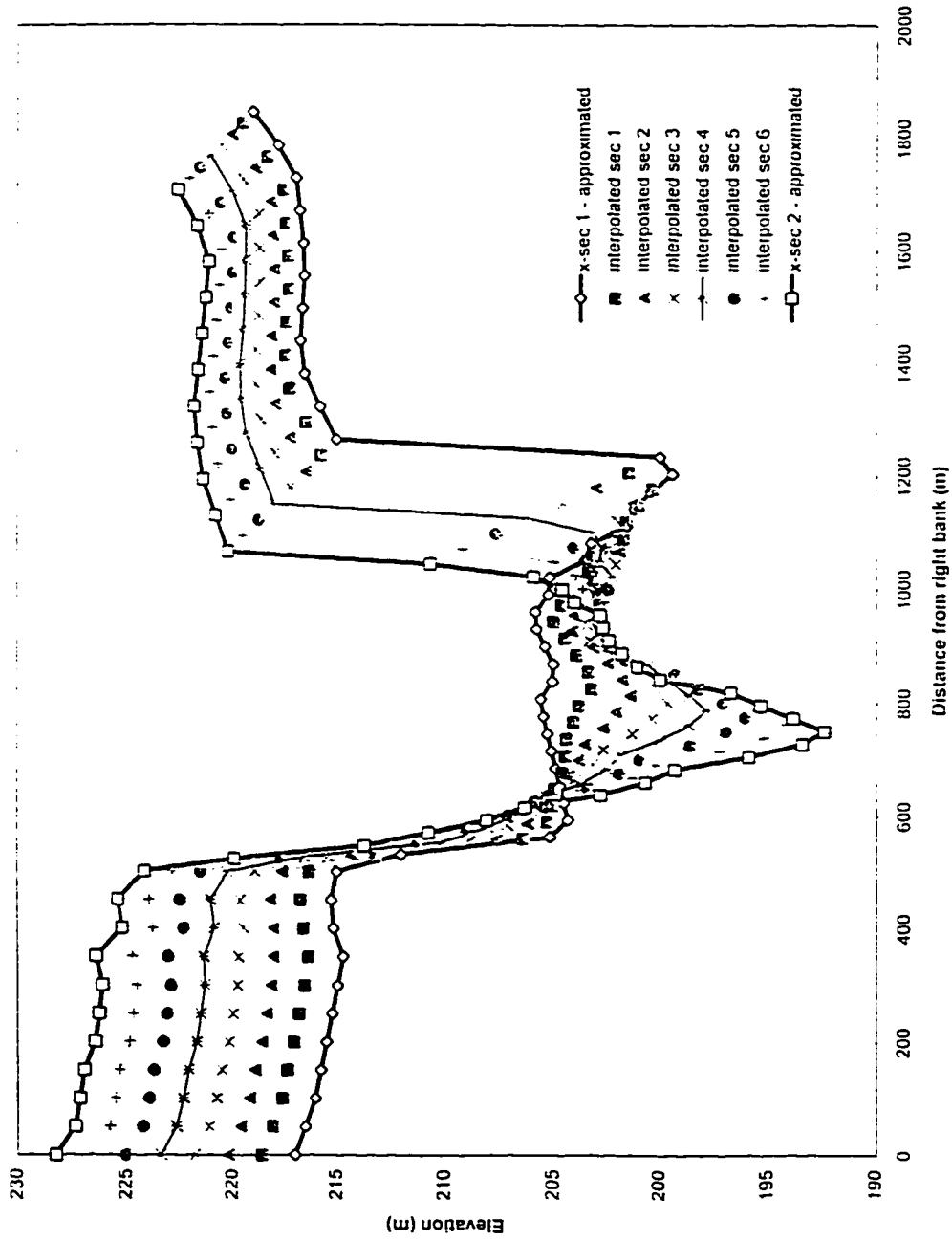


Figure A-2 Interpolated cross sections.

## Sample HEC2 Data File

XI 49000 30 0.00 470.00  
 GR240.00 0.00 215.00 1.00 206.00 20.00 205.00 24.00 203.00 50.00  
 GR203.00 69.00 201.00 92.00 202.00 101.00 202.00 147.00 203.00 161.00  
 GR202.00 190.00 203.00 201.00 203.00 211.00 202.00 217.00 204.00 239.00  
 GR203.00 247.00 203.00 266.00 205.00 291.00 205.00 310.00 203.00 330.00  
 GR206.00 346.00 207.00 358.00 208.00 373.00 207.00 394.00 203.00 412.00  
 GR205.00 431.00 207.00 448.00 210.00 465.00 214.00 469.00 240.00 470.00  
 XI 50000 23 0.00 764.32  
 GR240.00 0.00 214.36 1.00 214.07 24.73 205.78 48.43 204.25 78.85  
 GR205.62 303.38 204.79 350.72 206.04 449.20 205.18 486.34 205.43 514.55  
 GR202.87 562.98 203.62 569.59 203.62 574.26 201.46 613.55 201.92 631.94  
 GR200.47 653.16 200.50 670.14 199.12 711.98 200.03 734.94 200.11 741.98  
 GR201.46 752.95 213.10 763.32 240.00 764.32  
 XI 54000 51 0.00 566.57  
 GR240.00 0.00 224.16 1.00 223.71 11.18 219.51 24.91 216.20 35.59  
 GR213.79 45.77 212.16 55.94 211.05 66.10 209.57 79.83 208.02 91.53  
 GR207.24 101.70 206.74 109.84 205.49 121.96 203.76 132.07 201.74 142.17  
 GR200.81 157.33 200.19 167.43 199.57 177.54 198.64 192.70 196.04 202.80  
 GR194.96 212.90 193.35 228.06 192.27 238.16 192.31 248.27 193.25 262.92  
 GR193.93 273.53 194.57 283.63 195.48 297.79 195.41 308.90 196.87 319.00  
 GR198.98 332.65 200.48 344.27 200.82 354.37 201.26 367.51 201.67 379.63  
 GR201.93 389.73 202.27 402.37 202.60 414.99 202.69 425.10 202.76 437.23  
 GR202.83 450.36 202.88 460.46 203.95 472.09 204.24 485.73 204.50 495.83  
 GR204.84 506.95 205.87 521.09 207.45 531.20 210.26 541.81 213.03 556.46  
 GR240.21 566.57  
 XI 55900 52 0.00 550.00  
 GR240.00 0.00 210.62 1.00 210.52 7.21 210.18 18.86 209.68 28.30  
 GR208.90 37.74 207.88 48.28 206.04 59.96 204.39 71.37 203.21 82.78  
 GR204.12 94.19 205.56 105.61 206.77 117.02 207.28 128.43 207.74 139.73  
 GR207.68 150.11 207.12 160.52 205.86 170.89 204.85 181.30 203.85 191.68  
 GR202.79 202.73 202.39 214.15 202.05 225.32 201.67 236.73 201.28 248.14  
 GR200.90 259.56 200.51 270.97 200.13 282.38 199.38 293.80 199.05 305.21  
 GR197.91 316.37 198.68 326.75 198.13 337.16 197.63 347.53 197.77 357.94  
 GR197.95 368.32 197.82 379.51 197.70 390.92 197.57 402.34 197.48 413.75  
 GR197.62 425.16 197.75 436.57 197.80 447.99 197.51 459.40 197.22 470.81  
 GR197.57 481.98 198.88 493.01 201.56 503.42 204.43 513.80 211.06 524.20  
 GR213.70 534.58 240.00 550.00

## Source Code (FORTRAN)

```

*****Cross-section interpolation program.
*****Dan Healy. Water Resources. UofA. June, 1996.
*****NOTE:Parametric data at beginning of a file must
*****be ommitted prior to automatic interpolation.
*****Input data format similar to RJVJAM format with
*****the inclusion of left bank and right bank identification
*
*****define variables*****
*****
character infile*10,outfile*10
dimension npts(100),sta(100),x(100,100),y(100,100)
integer i,k,nxsec,xsec,npts.totxsec
real sta,x,y
dimension xl(100),xr(100),lwidth(100),chwidth(100),rwidth(100)
real xl,xr,lwidth,chwidth,rwidth
dimension lspace(100),chspace(100),
l rspace(100)
real lspace,chspace,rspace
dimension xint(100,100),yint(100,100)
real xint,yint
*
*
*****open the appropriate files*****
*****
print*
print*
print*.'Input file?'
print*.'(include single quotation marks)'
read*.infile
print*.'Output file?'
print*.'(include single quotation marks)'
read*.outfile
*
open(unit=7,file=infile,status='unknown')
open(unit=8,file=outfile,status='unknown')
open(unit=9,file='temp.gen'.status='unknown')
*
*****
*****main program*****
*****
totxsec=0
*
*
*****read the x-sectional data file*****
*
c print*.'Input File?'
c read*.input
c print*.'Output File?'
c read*.output
print*.'Number of x-sections?'
read*.nxsec
call readhec(nxsec,npts,sta,x,y,xl,xr,id)
print*.'input data file read...'

```

```

*
*
c  write(8.*) 'surveyed x-sectional data'
c  write(8.*) '-----'
c  do 410 i=1,nxsec,1
c    write(8.*) 'x-section number',i
c    write(8.22)
c    do 400 j=1,npts(i),1
c      write(8.11) x(j,i),y(j,i)
c400  continue
c410  continue

*
*
*
*****find approximated surveyed x-sections to be used for*****
*****interpolation (10 points each flood plain, 25 for channel)*****
*
  call approximate(npts,xsec,nxsec,x,xl,xr,xint,y,yint,
  l  lwidth,chwidth,rwidth,lspace,ospace,rspace)
  print*, 'surveyed x-sections approximated...'
*
*
c  write(8.*) 'interpolated x-sectional data'
c  write(8.*) '-----'
c  do 430 i=1,nxsec
c    write(8.*) 'x-section number',i
c    write(8.22)
c    do 420 j=1,46,1
c      write(8.11) xint(j,i),yint(j,i)
c420  continue
c430  continue
c11  format(t5,f8.2,t15,f8.2)
c22  format(t5,'x',t15,'elv.')
*
*
*****generate xsections between surveyed sections based*****
*****on a maximum allowable spacing, dxmax*****
*
  call genxsec(totxsec,nxsec,sta,xint,yint,xl,xr)
  print*, 'interpolated x-sections generated'
*
*
*****return xsectional data from temp.gen file to a usable*****
*****x-sectional data file (HEC2 format)*****
*
  print*, 'rewind file 9'
  rewind 9
  do 30 k=1,totxsec,1
    read(9.*) sta(k),xl(k),xr(k)
    do 20 i=1,46
      read(9.*) x(i,k),y(i,k)
      npts(k)=46
20  continue

```

```

30  continue
    print*, 'file 9 read'
    call writehec(totxsec.npts.sta.x.y,xl.xr)
*
*
    stop
    end
*
*
*
*****subroutines*****
*****
*
*
*****interpolation subroutine*****
*****
* (a,b) is point of interest
* a is known
* b is unknown
* a1,b1 are known lower bounds corresponding to a,b
* a2,b2 are known upper bounds corresponding to a,b
*
subroutine interpolate(a,a1,a2,b,b1,b2)
real a,a1,a2,b,b1,b2
    b=-((b1-b2)/(a1-a2)*(a1-a)-b1)
return
end
*
*
*****approximate surveyed x-section subroutine*****
*****
subroutine approximate(npts,xsec,nxsec,x,xl.xr,xint,y,yint,
    l lwidth,chwidth,rwidth,lspace,ospace,ospace)
integer i,j,xsec,nxsec,npts
dimension x(100,100),xl(100),xr(100),xint(100,100),y(100,100),
    l yint(100,100),lwidth(100),chwidth(100),rwidth(100),
    l lspace(100),ospace(100),ospace(100),npts(100)
real x,xl.xr,xint,y,yint,lwidth,chwidth,rwidth,
    l lspace,ospace,ospace
*
do 140 xsec=1,nxsec,1
print*, 'processing x-section',xsec
*
* determine width of each section
lwidth(xsec)=abs(x(1,xsec)-xl(xsec))
c write(8,*) 'lwidth',lwidth(xsec)
*
chwidth(xsec)=abs(xl(xsec)-xr(xsec))
c write(8,*) 'chwidth',chwidth(xsec)
*
rwidth(xsec)=abs(xr(xsec)-x(npts(xsec),xsec))
c write(8,*) 'rwidth',rwidth(xsec)
*

```

```

*   determine interpolation spacing for each section
  lspace(xsec)=lwidth(xsec)/10
  chspace(xsec)=chwidth(xsec)/25
  rspace(xsec)=rwidth(xsec)/10
c   write(8,*) 'lspace',lspace(xsec)
c   write(8,*) 'chspace',chspace(xsec)
c   write(8,*) 'rspace',rspace(xsec)
*
*   determine x-coord. for interpolated points in each section
  xint(1,xsec)=x(1,xsec)
c   write(8,*) 'xint 1=',xint(1,xsec)
  do 100 i=2,11,1
    xint(i,xsec)=xint(i-1,xsec)+lspace(xsec)
c   write(8,*) 'xint'.i.'=',xint(i,xsec)
100 continue
  do 110 i=12,36,1
    xint(i,xsec)=xint(i-1,xsec)+chspace(xsec)
c   write(8,*) 'xint'.i.'=',xint(i,xsec)
110 continue
  do 120 i=37,46,1
    xint(i,xsec)=xint(i-1,xsec)+rspace(xsec)
c   write(8,*) 'xint'.i.'=',xint(i,xsec)
120 continue
*
*   determine y-coord. for interpolated points in each section
*   starting at left bank for each section
  yint(1,xsec)=y(1,xsec)
c   write(8,*) 'yint 1=',yint(1,xsec)
  j=1
  do 130 i=1,46
    while(xint(i,xsec).ge.x(j,xsec) .and. j.lt.npts(xsec))do
      j=j+1
    endwhile
    call interpolate(xint(i,xsec),x(j-1,xsec),x(j,xsec),
1      yint(i,xsec),y(j-1,xsec),y(j,xsec))
c   write(8,*) 'x(j-1)',x(j-1,xsec),'y(j-1)',y(j-1,xsec)
c   write(8,*) 'xint'.i.'=',xint(i,xsec)
c   write(8,*) 'yint'.i.'=',yint(i,xsec)
c   write(8,*) 'x(j)',x(j,xsec),'y(j)',y(j,xsec)
*
130 continue
140 continue
  return
  end
*
*
*****generate interior x-sections between surveyed x-sections*****
*****
subroutine genxsec(totxsec,nxsec,sta,xint,yint,xl,xr)
integer nxsec,i,k,nspaces,totxsec
dimension sta(100),xint(100,100),yint(100,100),xl(100),xr(100)
real sta,xint,yint,dxmax,ndx,stadist,dx,rmdr,xl,xr
*
print*, 'Maximum spacing in metres?'

```



```

    read*. dxmax
    do 210 k=1,nxsec-1,1
*   write out the kth surveyed xsection to temp.gen
    write(9,*) sta(k),xl(k),xr(k)
    do 200 i=1,46,1
    write(9,*) xint(i,k),yint(i,k)
200  continue
*
    totxsec=totxsec+1
*
*   find distance between station k and station k+1
    stadist=sta(k+1)-sta(k)
*   find the number of spaces between surveyed sections k & k+1
    ndx=abs(stadist/dxmax)
*   find remainder of ndx/1
    rmdr=amod(ndx,1.0)
    if(rmdr.eq.0)then
        dx=dxmax
        nspaces=int(ndx)
    else
        nspaces=int(ndx)-1
        dx=stadist/nspaces
    endif
c   write(8,*) 'station'.k.'dx=',dx

*
*   generate interior x-sections between sta(k) & sta(k+1)
    call subxsec(totxsec,k,sta,xint,yint,nspaces,dx,xl,xr)
210  continue
*   write out the last surveyed xsection to temp.gen
    write(9,*) sta(k),xl(k),xr(k)
    do 220 i=1,46,1
    write(9,*) xint(i,k),yint(i,k)
220  continue
*
    totxsec=totxsec+1
*
    return
end
*
*
*****generate interior x-sections between two stations (k & k+1)****
*****
subroutine subxsec(totxsec,k,sta,xint,yint,nspaces,dx,xl,xr)
integer i,j,k,nspaces,totxsec
dimension sta(100),xint(100,100),yint(100,100),xx(100),yy(100),
1 xl(100),xr(100)
real sta,xint,yint,xx,yy,dx,known,unknown,xl,xr,xxl,xxr
*
do 320 j=1,nspaces-1,1
    known=sta(k)+dx*j
*   determine x and y coords. for the jth subsection
    do 300 i=1,46,1
*   determine x-coords.

```

```

        call interpolate(known.sta(k),sta(k+1),
1          unknown.xint(i,k),xint(i,k+1))
        xx(i)=unknown
*       determine y-coords.
        call interpolate(known.sta(k),sta(k+1),
1          unknown.yint(i,k),yint(i,k+1))
        yy(i)=unknown
*       determine xl-coord.
        call interpolate(known.sta(k),sta(k+1),
1          unknown.xl(k),xl(k+1))
        xxl=unknown
*       determine xr-coord.
        call interpolate(known.sta(k),sta(k+1),
1          unknown.xr(k),xr(k+1))
        xxr=unknown
300    continue
*       write the generated subsections to temp.gen
        write(9,*) known,xxl,xxr
        do 310 i=1,46,1
            write(9,*) xx(i),yy(i)
310    continue
*
        totxsec=totxsec-1
*
320    continue
*
        return
        end
*
*
*****read hec2 file format*****
*****
subroutine readhec(nxsec,npts,sta,x,y,xl,xr)
*
integer i,j,k,l,nxsec,npts
real sta,x,y,xl,xr,pts
dimension npts(100),sta(100),x(100,100),y(100,100),xl(100),
1    xr(100),pts(100)
*
do 510 l=1,nxsec,1
    read(7,511) sta(l),pts(l),xl(l),xr(l)
    npts(l)=int(pts(l))
    i=int((pts(l)-.1)/5)
    do 500 k=1,i+1
        j=k*5-4
        read(7,511) y(j,l),x(j,l),y(j+1,l),x(j+1,l),
1    y(j+2,l),x(j+2,l),y(j+3,l),x(j+3,l),y(j+4,l),x(j+4,l)
500    continue
510    continue
*
511    format(t3,f6.0,9f8.0)
*
        return
        end

```

```

*
*
*****write hec2 file format*****
*****
subroutine writehec(nxsec,npts,sta,x,y,xl,xr)
*
integer i,j,k,l,nxsec,npts
real sta,x,y,xl,xr,pts
dimension npts(100),sta(100),x(100.100),y(100.100),xl(100),
l xr(100),pts(100)
*
do 530 l=1,nxsec,l
write(8,512) sta(l),npts(l),xl(l),xr(l)
pts(l)=npts(l)
i=int((pts(l)-.1)/5)
do 520 k=1,i
j=k*5-4
write(8,513) y(j,l),x(j,l),y(j+1,l),x(j+1,l),
l y(j+2,l),x(j+2,l),y(j+3,l),x(j+3,l),y(j+4,l),x(j+4,l)
520 continue
j=k*5-4
if(npts(l)-i*5.eq.1)then
write(8,522) y(j,l),x(j,l)
elseif(npts(l)-i*5.eq.2)then
write(8,533) y(j,l),x(j,l),y(j-1,l),x(j-1,l)
elseif(npts(l)-i*5.eq.3)then
write(8,544) y(j,l),x(j,l),y(j-1,l),x(j-1,l),
l y(j-2,l),x(j-2,l)
elseif(npts(l)-i*5.eq.4)then
write(8,555) y(j,l),x(j,l),y(j+1,l),x(j+1,l),
l y(j-2,l),x(j-2,l),y(j+3,l),x(j+3,l)
elseif(npts(l)-i*5.eq.5)then
write(8,513) y(j,l),x(j,l),y(j+1,l),x(j+1,l),
l y(j-2,l),x(j-2,l),y(j+3,l),x(j+3,l),y(j+4,l),x(j+4,l)
else
endif
530 continue
*
512 format('X1',t3,f6.0,i8.2f8.2)
513 format('GR',t3,f6.2,9f8.2)
522 format('GR',t3,f6.2,1f8.2)
533 format('GR',t3,f6.2,3f8.2)
544 format('GR',t3,f6.2,5f8.2)
555 format('GR',t3,f6.2,7f8.2)
*
return
end
*
*

```